

CHARACTERISATION AND PREDICTION OF
PARTICLE ATTRITION IN LEAN PHASE PNEUMATIC
CONVEYORS: THE INFLUENCE OF PARTICLE
CONCENTRATION

BENJAMIN ANDREW KOTZUR

A thesis submitted in partial fulfilment of the
requirements of the University of Greenwich for the
Degree of Doctor of Philosophy

This research programme has been carried out in
collaboration with BASF SE

March 2018

VOLUME 1

DECLARATION

I certify that the work contained in this thesis, or any part of it, has not been accepted in substance for any previous degree awarded to me, and is not concurrently being submitted for any degree other than that of Doctor of Philosophy being studied at the University of Greenwich. I also declare that this work is the result of my own investigations, except where otherwise identified by references and that the contents are not the outcome of any form of research misconduct.

Signed,

Benjamin Kotzur, Candidate

Date

Professor Michael Bradley, First Supervisor

Date

Dr Robert Berry, Second Supervisor

Date

ACKNOWLEDGEMENTS

This research could not have been possible without the key contributions from a number of people.

Firstly, the contributions of Michael Bradley (First Supervisor) are gratefully acknowledged in the form of useful conversations, advice, and for performing the experiments on the Industrial Scale Pneumatic Conveying Facility at the Wolfson Centre.

Many thanks go to Robert Berry (Second Supervisor) for the many hours of conversations, guiding the research, and many more in reviewing the research output from this programme.

To BASF SE for sponsoring the research. In particular, to Kristina Eger, Hanno Wolf and Miguel Angel Romero for provisions of materials, external Industrial Scale Pneumatic Conveying Data, CFD-DEM Simulation Data, and particle density data, in addition to the many hours of useful conversation.

To the staff of the Wolfson Centre: Jon Larkin for numerous hours of technical support and time spend teaching the practical skills required to complete this work; Richard Farnish for the hours of stimulating conversation and valuable design input; and Caroline Chapman, for all of her administrative support and without whom nothing would be possible.

To the many people who provided data and analysis to the research: Francois Neuville for testing of Carbolux SK (QPM) and preparation of the Carbolux SK size fractions; Darren Oxborrow for breakage data of sucrose (QPM); Ana Carolina de Mello Santos e Silva and Gustavo Castilho Dias for biomass pellet length attrition data (LSPAT); Pablo Garcia Trinanes for useful conversations, acquisition and subdivision of Spent FCC Catalyst samples and reviewing research outputs; Amit Gupta for particle attrition data of Carbolux SK (Wolfson Industrial System); Lahiru Lulbadda Waduge for assistance in photography.

To my Spanish family; Pedro, Constanza, Luis e Isa. Muchas gracias por todo lo que habéis hecho por mí. Nunca podré pagar vuestra bondad.

To Mum, Dad, and Jess; thank you all for your unconditional support. I could not have ridden the rollercoaster without your calls, care packages and words of reassurance. I hope that what lays within these pages makes you proud.

Finally, to my dear Raquel. You have been through the frustrations and triumphs, every step of the way with me. Your patience, and kind words over these last years have been invaluable, and will never be forgotten. In seeing this work, I hope you feel your efforts worthwhile.

ABSTRACT

This thesis aimed to determine the influence of particle concentration on the magnitude of measured particle attrition within horizontal, homogeneous lean phase pneumatic conveying systems. Furthermore, to propose a characterisation method for predicting the magnitude of particle attrition in such pneumatic conveying systems.

After conducting an extensive literature review, no conclusive research which quantitatively described the relationship between particle concentration and the magnitude of particle attrition inflicted within lean phase pneumatic conveying was found. Additionally, there was no generally accepted model to predict the magnitude of particle attrition caused by such systems.

Two test facilities were designed, constructed, commissioned and employed for the experimental programme:

- A 'centrifugal accelerator style' particle impact tester; for characterisation of particle attrition behaviour under closely controlled impact velocities and angles.
- A pilot scale vacuum pressure pneumatic conveying system containing a single bend; to study the influence of geometric and conveying variables, on particle attrition.

From experiments with the above test facilities, no indication that particle concentration affected the magnitude of particle attrition could be discerned. However, experimentation using industrially-sized pneumatic conveyors, found increasing particle concentration reduced attrition. For the industrial systems it was proposed that reduced attrition was due to their geometrical features which influenced the relationship between the particle velocity distribution and particle concentration.

The centrifugal impact tester was used to carry out factorial experiments to determine the individual influences of particle impact velocity, angle, and particle size. An interpolation method was proposed, to reduce the number of experiments required to characterise particle attrition behaviour. Through evaluating different techniques for calculating the mean particle impact angle at the bend in the pilot scale vacuum conveyor, the particle attrition behaviour was reconciled to that measured in the centrifugal impact tester. This enabled the prediction of particle attrition within such lean phase pneumatic conveying systems, based on a bench scale characterisation technique.

NOMENCLATURE

Symbol	Definition	Pages
<i>Arabic Symbols</i>		
A	Ore impact breakage parameter (-)	33
	Area (m ²)	184-185
	Projected area of particle (m ²)	245
A_0	Initial contact area (m ²)	26
A_1	Post-impact contact area (m ²)	26
A_F	Empirically obtained model parameter	30-31
A_p	Projected impact area of particle stream (m ²)	229
A_r	Archimedes number (-)	249, 255
b	Ore impact breakage parameter (-)	33
	Material-specific, empirically-determined constant (-)	272, 279
B	Breakage matrix (-)	66
B_F	Empirically obtained model parameter	30-31
c	Curve fit parameter (-)	61-62
	Distance to the point farthest from the neutral axis (m)	160
	Material-specific, empirically-determined constant (-)	272, 279
C_D	Coefficient of drag (-)	245-246, 249
C_p	Particle impact velocity (m/s)	62
d	Particle diameter (m)	254-255
	Material-specific, empirically-determined constant (-)	272, 279
d_i	Mean size of the size fraction correlating to w_i (mm)	66-67
d_{mean}	Particle mean sieve diameter (mm)	30-31
d_p	Particle diameter (m)	249

D	Pipe diameter (m)	237, 249, 254
D_d	Diameter of the spinning disc (m)	94
D_F	Empirically obtained model parameter	30-31
D_n^*	Damage sustained by a particle on the n^{th} impact (-)	44
e	Euler's number (-)	279
E_{cs}	Specific comminution energy (kW h/t)	33
$E_{k,n}$	Kinetic energy of a striker at the n^{th} impact per unit mass of the particle (J/kg)	44
E_{min}	Specific comminution energy threshold (kW h/t)	33
E_{n-1}	Energy required to completely disintegrate the particle, per unit mass of the particle in the previous impact event (J/kg)	44
f	Coefficient of friction (-)	249
f_{Mat}^*	Adjusted material parameter (kg/Jm)	30
F_c	Crushing force (N)	30-31
F_D	Drag force (N)	245
g	Acceleration due to gravity (m/s ²)	250, 254-255
\dot{G}	Mass flow rate of solids (kg/s)	254
i	Input particle size distribution column matrix (-)	66
I	Second moment of area (mm ⁴)	160
I_c	Second moment of area of a circle (mm ⁴)	160
k	Number of impacts (-)	30
L_{acc}	Particle acceleration length (m)	255
L_{accel}	Acceleration length of the solid phase (m)	254
m	Curve fit parameter (-)	61-62
\dot{m}_g	Mass flow rate of the gas phase (kg/s)	184-185
\dot{m}_s	Mass flow rate of the solid phase (kg/s)	184-185

M_f	Mass feed rate of particles (kg/s)	228-229
M_{flux}	Mass flux of particles at the target face (kg/m ² /s)	228-229
M_{sample}	Mass of total test sample (kg)	132-133
M_{sieve}	Mass retained on sieve (kg)	132-133, 261
M_y	Yield moment (Nm)	160
n	Constant (-)	238
	Coefficient to account for flow over a layer of particles (-)	249
N	Number of compression cycles (-)	43-44
N_0	Number of unbroken particles (-)	61-62
o	Output particle size distribution column matrix (-)	66
P^*	Dimensionless number (-)	43-44
P_1	Dimensionless group (-)	43-44
	Percent mass retained on the sieve in question for virgin sample (-)	132-133
P_2	Dimensionless group (-)	43-44
	Percent mass retained on the sieve in question for post-test sample (-)	132-133
P_3	Dimensionless group (-)	43-44
$P(\theta)$	Probability density function of particle impact angle (-)	288-289
P_m	Particle compressive strength (Pa)	43-44
P'_m	Particle fatigue compressive strength (Pa)	43-44
r	Radius of a circle (m)	160
r_b	Radius of pipe bend centreline (m)	286
r_p	Radius of the internal wall of a pipe bend (m)	286
	Pipe thickness (m)	288-289

R	Radius of pipe (m)	238
	Distance from pipe radius to pipe outer surface (m)	288-289
R^2	Coefficient of determination (-)	266, 293
R_b	Distance from pipe radius to pipe centreline (m)	288-289
R_e	Reynolds number of a fluid flowing in a pipe (-)	237
R_p	Particle Reynolds number (-)	246
R_t	Radius of accelerating tube (m)	228
S	Section modulus (m ³)	160
S_F	Breakage probability under specific force (-)	30-31
t_n	The cumulative mass fraction passing 1/n th of the parent particle size (-)	31
u	Fluid velocity at position of calculation (m/s)	238
u_{max}	Maximum fluid velocity in the pipe cross section (m/s)	238
U	Impact Velocity (m/s)	26
$U_{pu,calculated}$	Calculated minimum pickup velocity (m/s)	249
v_s	Velocity of the solid phase (m/s)	184-185
V	Fluid velocity (m/s)	245
V_{avg}	Average velocity of fluid in a pipe (m/s)	237
V_i	Particle impact velocity (m/s)	94
\dot{V}_g	Volumetric flow rate of the gas phase (m ³ /s)	184-185
V_m	Model velocity (m/s)	263, 272, 293
V_n	Normal component of impact velocity (m/s)	263
V_p	Particle velocity under experimental conditions (m/s)	263, 272
\dot{V}_s	Volumetric flow rate of the solid phase (m ³ /s)	184-185
V_t	Tangential component of impact velocity (m/s)	263
w_i	Fraction of material retained on a given sieve size (-)	66-67

$W_{m,min}^*$	Adjusted mass-specific threshold energy (J/kg)	30
$W_{m,eff}^*$	Mass-specific effective impact energy (J/kg)	30
x	Particle size (m)	30
X_c	Distance from the spinning disc centre to the centre of the target (m)	228
X_d	Particle flight distance (m)	228
X_h	Harmonic mean particle size (mm)	66-67
y	Distance from pipe wall (m)	238
Y	Dynamic Yield Stress (Pa)	26

Greek Symbols

α	Material characteristic (-)	31
	Percent change criterion (-)	206, 261, 272, 279, 293
β	Velocity combination ratio, $0 < \beta < 1$, (-)	263, 79
γ	Damage accumulation constant (-)	44
$\Delta\%$	Magnitude of Deviation (-)	132-133, 261
ε	Summed with the Velocity Combination Ratio, β , to form unity (-)	263, 279
θ	Particle impact angle under experimental conditions (degrees)	263, 272
	Particle impact angle under experimental conditions (radians)	288-289
θ_c	Centreline impact angle (radians)	288-289
θ_d	Particle jet dispersion angle (degrees)	228
θ_e	Exit angle of the particle stream from the spinning disc (degrees)	94
θ_m	Pipe centreline impact angle (radians)	286

θ_{max}	Maximum particle impact angle (radians)	288-289
μ	Fluid viscosity (Pa s)	237
μ_f	Fluid viscosity (kg/m s)	249
μ_θ	Mean particle impact angle (radians)	289
ν	Kinematic viscosity of the fluid (m ² /s)	255
π	The mathematical number, Pi (-)	286
ϱ	Gas density (kg/m ³)	254
ϱ_p	Particle density (kg/m ³)	254
ρ	Density (kg/m ³)	26
	Density of the fluid (kg/m ³)	237, 245, 249
ρ_f	Fluid density (kg/m ³)	255
ρ_p	Particle density (kg/m ³)	255
ρ_s	Density of the solid phase (kg/m ³)	184-185
σ^*	Dimensionless number (-)	43-44
σ_y	Yield stress (N/m ²)	160
φ	Sphericity (-)	249
ω_d	Rotational velocity of the spinning disc (RPM)	94

GLOSSARY OF TERMS

Term	Meaning	Page Reference
BSPAT	Bench Scale Particle Attrition Tester	95
ECT	Electrical Capacitance Tomography	16
ID	Internal diameter	104
LSPAT	Large Scale Particle Attrition Tester	100
Magnitude of Deviation	The algebraic difference between the percent mass retained on a given size fraction before and after an attrition test. Positive values indicate material has entered the size fraction; negative values indicate material has left the size fraction.	132-133
MVR	Mass Volume Ratio (Particle concentration on a mass/volume basis)	184-185
NB	Nominal Bore	111
NPS	Nominal Pipe Size	104
OD	Outer diameter	104
PEPT	Positron Emission Particle Tracking	18
PIV	Particle Image Velocimetry	17
PP	Pilot Plant	131
PVC	Polyvinyl Chloride	104
r/D	Bend radius over pipe diameter ratio	14-15
SBAT	Single Bend Attrition Tester	103
SLR	Solids Loading Ratio (Particle concentration on a mass/mass basis)	184-185

SVR	Spatial Volumetric Ratio (Particle concentration on a volume/absolute volume basis)	184-185
UFLC	Ultrafast Load Cell	44
VLR	Volumetric Loading Ratio (Particle concentration on a volume/volume basis)	184-185

CONTENTS

DECLARATION.....	i
ACKNOWLEDGEMENTS.....	ii
ABSTRACT	iv
NOMENCLATURE	v
GLOSSARY OF TERMS	xi
CHAPTER 1: Introduction.....	1
1.1 Introduction to Pneumatic Conveying within the Industrial Context and the Issue of Particle Attrition	1
1.2 The Influence of Particle Concentration on Particle Attrition	2
1.3 Prediction of Particle Attrition as a Design Tool	3
1.4 Preview of the Thesis.....	4
CHAPTER 2: Literature Review	6
2.1 Introduction	6
2.2 Acknowledgement of Previous Review Works and Objectives of the Present Work	7
2.3 Particle Attrition within Lean-Phase Pneumatic Conveying	9
2.3.1 Velocity and Acceleration	9
2.3.2 Particle Concentration	15
2.3.3 Concluding Remarks on the Process Factor	20
2.4 Influence of Physical Particle Properties on Attrition Behaviour	23
2.4.1 Particle Material Characteristics	23
2.4.2 Particle Geometry	31
2.4.3 Particle Fracture	34
2.4.4 Particle Attrition Mechanisms	35
2.4.5 Experimental Techniques for Measuring Particle Attrition	45
2.4.6 Concluding Remarks on the Material Factor.....	56
2.5 Modelling of Particle Attrition in Lean Phase Pneumatic Conveying	57
2.5.1 Numerical Modelling Approaches	57

2.5.2	Empirical Modelling Approaches.....	61
2.5.3	Concluding Remarks on Modelling Approaches	69
2.6	Experimental Method Considerations.....	72
2.6.1	Sampling of Particulate Materials	72
2.6.2	Particle Size Measurement.....	73
2.7	Conclusions of the Review	75
CHAPTER 3: Research Approach and Scope.....		77
3.1	Aims of the Present Research.....	77
3.2	Breakdown of the Subject Area	78
3.3	Scope of the Present Work	81
3.4	Approach to the Problem.....	83
3.4.1	Material Factor.....	83
3.4.2	Process Factor.....	84
3.4.3	Modelling	85
3.5	Research Objectives	85
CHAPTER 4: Description of Test Equipment, Method and Materials		87
4.1	Sample Preparation.....	87
4.2	Measurement of Particle Size Distribution.....	89
4.3	Particle Characterisation Devices	89
4.3.1	QPM Degradation Tester (QPM)	90
4.3.2	Bench Scale Particle Attrition Tester (BSPAT)	95
4.4	Large Scale Particle Attrition Testing	100
4.4.1	Large Scale Particle Attrition Tester (LSPAT).....	100
4.4.2	Single Bend Attrition Tester (SBAT)	103
4.4.3	Pilot Plant Test Facility	110
4.4.4	External Pilot Plant Test Facility	115
4.5	Particulate Materials.....	118
4.5.1	Sodium Chloride (Salt).....	119

4.5.2	Golden Breadcrumbs.....	120
4.5.3	Sucrose (Granulated Sugar).....	122
4.5.4	Biomass Pellets.....	124
4.5.5	Carbolux SK.....	125
4.5.6	Adipic Acid.....	127
4.5.7	Spent FCC Catalyst.....	128
4.5.8	Summary.....	130
CHAPTER 5: Results and Observations: Particulate Material Attrition Behaviour		
	Characterisation.....	132
5.1	BSPAT Testing.....	132
5.1.1	Influence of Impact Velocity.....	133
5.1.2	Influence of Impact Angle.....	137
5.1.3	Influence of Secondary Impacts.....	139
5.1.4	Influence of Sample Material.....	143
5.2	Supplementary Studies.....	157
5.2.1	Attrition of Biomass Pellets.....	158
5.2.2	Influence of Mass Feed Rate on the QPM and BSPAT Testers.....	166
5.2.3	Particle Attrition caused by Screw Feeding.....	170
5.2.4	Comparison of Centrifugal Accelerator Attrition Testers.....	172
5.3	Conclusions.....	181
CHAPTER 6: Results and Observations: Characterisation of Pipeline Geometry and		
Conveying Conditions with respect to Particle Attrition.....		
6.1	Characterisation of the Apparatus.....	187
6.1.1	Attrition Attributed to the Receiver.....	187
6.1.2	Flow Characterisation.....	189
6.1.3	Mass Flow Rate through the Orifice Plates.....	190
6.1.4	Slip Velocity Characterisation.....	192
6.2	Single Bend Attrition Tester Results.....	195
6.2.1	Influence of Particle Velocity on Measured Particle Attrition.....	204

6.2.2	Influence of Particle Concentration	205
6.2.3	Influence of Bend Radius.....	206
6.2.4	Influence of Particle Size Distribution	206
6.2.5	Influence of Material Type (FCC catalyst).....	208
6.3	Conclusions.....	210
CHAPTER 7: Results and Observations: Industrial Scale Pneumatic Conveying		212
7.1	Wolfson Centre Testing Facility.....	212
7.1.1	Conveying of Carbolux SK Type C	213
7.1.2	Conveying of Adipic Acid	217
7.2	External Industrial-Scale Pneumatic Testing Facility.....	223
7.3	Conclusions.....	226
CHAPTER 8: The Influence of Particle Concentration on Particle Attrition in Lean Phase Pneumatic Conveying Systems.....		227
8.1	Analysis of the Data collected from the BSPAT and the SBAT	227
8.2	Proposed Thought-Model of the Observed 'Shielding Effect'.....	230
8.2.1	Geometrical Considerations of the Wolfson Centre Industrial Pneumatic Conveyor	230
8.2.2	Geometrical Considerations of the External Industrial Pneumatic Conveyor.	251
8.3	Conclusions.....	257
CHAPTER 9: Optimisation of Particle Attrition Characterisation and Modelling		260
9.1	Optimisation of the Bench Scale Particle Attrition Test Programme.....	260
9.1.1	Conclusions	283
9.2	Modelling the Relationship between Particle Attrition Behaviour in the BSPAT and the SBAT.....	284
9.2.1	Pipe Centreline Particle Impact Angle	286
9.2.2	Straight Line Projection Mean Particle Impact Angle	288
9.2.3	Definition of Particle Impact Angle Distribution by CFD-DEM Simulation	290

9.2.4	Conclusions on the Method of Determining the Mean Particle Impact Angle	293
.....		
CHAPTER 10:	Conclusions and Further Work	295
10.1	Conclusions of the Research	295
10.2	Recommendations for Further Work	301
CHAPTER 11:	References	304

VOLUME 2

APPENDIX A:	List of Publications	A1-A18
APPENDIX B:	Bench Scale Particle Attrition Tester Design Drawings	B1-B37
APPENDIX C:	Particulate Material Safety Precautions	C1-C3
APPENDIX D:	Example of Single Bend Attrition Tester Data Processing	D1-D4
APPENDIX E:	Conveying Conditions Tested in the Single Bend Attrition Tester	E1-E3
APPENDIX F:	MATLAB Code for Breakage Map Generation	F1
APPENDIX G:	Industrial Scale Pneumatic Conveying Test Conditions	G1-G2
APPENDIX H:	Modelling Curves for Variation in the Value of β	H1-H27
APPENDIX I:	MATLAB Code for Curve Fit Optimisation	I1-I2
APPENDIX J:	Fitting Results for the Single Bend Attrition Tester Data	J1-J15
APPENDIX K:	Experimental Data – QPM Attrition Tester	K1-K28
APPENDIX L:	Experimental Data – Large Scale Particle Attrition Tester	L1-L44
APPENDIX M:	Experimental Data – Bench Scale Particle Attrition Tester	M1-M109
APPENDIX N:	Experimental Data – Single Bend Attrition Tester	N1-N51
APPENDIX O:	Experimental Data – Industrial Scale Pneumatic Conveying	O1-O23

CHAPTER 1: Introduction

1.1 Introduction to Pneumatic Conveying within the Industrial Context and the Issue of Particle Attrition

Pneumatic conveying is a method of transporting particulate materials which is widely used in the processing industry. This is where a gaseous medium (typically air) is used to carry a particulate material through a pipeline. This transportation process can be utilised between process steps, storage vessels, or bulk carrying facilities such as road tankers or ships.

Pneumatic conveying has a number of advantages over other conveying methods. These include, but are not limited to, hygiene through environmental separation, flexibility in routing, dust containment, minimisation of maintenance through use of minimal moving parts, and capability of vertical conveying. One of the disadvantages in using this method of conveying is the propensity for particle attrition throughout the pipeline. Some processes require a controlled level of particle attrition to occur, such as in the applications of husk removal of grains, comminution processes, and in achieving target particle size distributions for subsequent process steps such as mixing.

Conversely, particle attrition can pose a significant issue if it has not been accounted for (or expected to occur to a given degree) in the design of the materials storage and handling systems. Excess quantities of smaller particles within a sample may result in repercussions such as:

- Damage to customer perception if the product is not visually pleasing
- Reduced material flowability, resulting in blocked hopper outlets
- Variation in bulk density, resulting in dosing issues
- Alteration of particle surface area to volume ratio, resulting in changed reaction rates if used as a chemical feedstock
- Increased propensity for dust generation and subsequent settling on floor and work surfaces. This may increase the risk of worker slips and trips
- Increased chance of dust explosions due to increased dust generation
- Increased chance of worker health hazards due to particle inhalation

Pneumatic conveying systems can be operated under a number of different flow regimes, which have repercussions on the magnitude of particle attrition inflicted. In the simplest terms, three primary flow regimes can be defined:

1. Lean/dilute phase
2. Dense phase / slug flow
3. Transition Flow

Lean phase pneumatic conveying (1) is defined as the condition where all particles are suspended in the air flow (homogeneous lean-phase flow). This form of conveying typically requires high superficial air velocities, and low particle concentrations within the pipeline. Flow conditions where a strand of material is present on the pipe floor can also be described under the lean-phase conveying regime (strand flow). This strand can be stationary or dynamic in nature.

Dense phase pneumatic conveying (2) is characterised by particles populating the entire cross-section of the conveying pipe, and the material moving through the pipe in 'batches' or 'slugs' separated by air pockets, or through one continuous slug. This form of pneumatic conveying is generally achieved using low superficial air velocities and high particle concentrations.

Transition Flow (3) describes the intermediate flow conditions between Regime 1 and 2.

This thesis shall focus on homogeneous lean-phase flow within horizontal pneumatic conveying systems. The operating variables of such pneumatic conveying systems are wide and varied, and are summarised in Figure 3.1 and Figure 3.2 of Chapter 3. The influence of each variable requires characterisation before the phenomena of particle attrition within such systems can be comprehensively elucidated.

1.2 The Influence of Particle Concentration on Particle Attrition

Particle concentration can be measured in different ways, typically comparing the air and solids flowrates within the pipeline on either a volumetric or mass basis. It has been suggested in studies addressed in Section 2.3.2, that higher particle concentration results

in a 'shielding' effect, whereby a sliding bed of particles on the outer wall of a pipe bend cushions the impact of other particles; partially reducing the impact energy experienced and therefore the particle attrition observed. Such an effect has not been comprehensively studied, nor has it been specifically quantified.

1.3 Prediction of Particle Attrition as a Design Tool

While particle attrition may not be wholly prevented, it is desirable to be able to predict and control the levels of particle attrition that result from a bespoke pneumatic conveying process. In this way, the particle attrition expected to occur within the process can be accounted for in the design of the process itself.

Due to the complexity and diversity of particulate materials that can be pneumatically conveyed, a particle attrition model must be informed by particle attrition characterisation testing. Such testing should capture the full mechanism responsible for particle attrition within such systems. When a new process is to be implemented, it is possible that only a small sample of the material to be conveyed is available. This could also be the case for an existing process handling a high-value particulate material. It is therefore valuable to have the ability to characterise a particulate material from a small sample size.

The process of conveying particles pneumatically is a complex one; however, this process must be described in detail to inform a particle attrition model applied to such a system. Considering the flexibility of pneumatic conveying systems, the associated variables must be isolated to study them systematically.

Once the influences of the material and process have been defined, these can be used to comprehensively advise a particle attrition model. Such a model could be used to determine, for example, the quality of a product after passing through a pneumatic conveying system and appraise the designer of the system's appropriateness for the application. Additionally, such a predictive model could be used to troubleshoot an existing pneumatic conveying system, and dictate the alterations necessary to achieve an acceptable reduction of particle attrition.

1.4 Preview of the Thesis

Chapter 1 provides an introduction to the research area, touching on key aspects of importance to the present research.

Chapter 2 consists of a detailed review of the existing research in the literature, relevant to the present work. At the conclusion of this chapter, key gaps in knowledge requiring further research are identified.

Chapter 3 defines the aims and scope of the present work, as informed by the conclusions of Chapter 2. The research approach taken to address the key research questions is also described by breaking down the subject area, and mapping out the relationships between the studies undertaken.

Chapter 4 describes the experimental equipment used throughout the research programme, coupled with the methods used. The particulate materials are also identified along with key characterisation parameters.

Chapter 5 presents the results and observations of the material characterisation component of the experimental programme. These experiments were aimed at characterising the particle attrition behaviour of a range of materials in response to well-defined loading conditions.

Chapter 6 presents the results and observations of the process characterisation component of the experimental programme. These experiments measured the magnitude of particle attrition manifested in a closely controlled, well-defined, intermediate-scale pneumatic conveying system containing one bend in the pipeline.

Chapter 7 presents the results and observations of the industrial-scale pneumatic conveying component of the experimental programme. These pneumatic conveying systems were representative of the systems used in industry.

Chapter 8 contains the analysis of the data obtained in Chapter 5 and Chapter 6 with respect to the influence of particle concentration on the magnitude of particle attrition measured within a pneumatic conveying pipeline. Conclusions are drawn on the influence of particle concentration on the particle attrition behaviour within lean phase pneumatic conveying systems, and alternate explanations for the observations reported by other researchers are given.

Chapter 9 presents a model to interpolate for impact velocity and impact angle within the particle attrition characterisation tester. This is then applied to the impact scenario in a pneumatic conveying pipeline.

The conclusions of the research are presented in Chapter 10 with research areas requiring further work are identified in Chapter 11.

Finally, the references used in this research are detailed in Chapter 12, and the Appendices in Chapter 13.

This work formed the basis for a number of publications, the abstracts of which are available in Appendix A

CHAPTER 2: Literature Review

2.1 Introduction

The previous chapter described some of the requirements that industrial lean phase pneumatic conveying systems are required to provide. This chapter will systematically review each of the variables that influence the manifestation of particle attrition within such systems. The inter-relationships between these variables shall also be addressed to determine the state-of-the-art with respect to the subject area.

Previous review works (Section 2.2) on particle attrition and pneumatic conveying are presented first as a basis upon which the current review will build.

The subject is then divided into the process influences and the material influences affecting particle attrition. Process influences (Section 2.3) are those such as superficial air velocity, particle concentration, and pipeline geometry. Material influences (Section 2.4) are those including material hardness, particle morphology, and particle structure (i.e. Crystalline, agglomerate, etc). Reconciling the behaviour of the particulate material to the forces experienced in a pneumatic conveying line under lean phase conditions is a primary aim of this review, and fundamental to any attempt in explaining particle attrition within such systems.

Subsequently, research looking specifically at particle attrition in lean phase pneumatic conveying systems is reviewed. Each study was categorised as either numerical (Section 2.5.1) or empirical (Section 2.5.2) in nature. Having looked at these methods, the importance of sample preparation (Section 2.6.1) and particle size measurement (Section 2.6.2) are addressed and identified as key considerations when obtaining experimental data from particulate materials.

Key conclusions are drawn from the present review work, and finally the gap in knowledge to be addressed will be elucidated (Section 2.7).

2.2 Acknowledgement of Previous Review Works and Objectives of the Present Work

Previous key review works are summarised in this section to lay the foundation on which the present work will build.

Bemrose and Bridgwater [1] covered an extensive range of topics, broadly categorised under four themes: the nature and occurrence of particle attrition, particle attrition mechanisms, characterisation and assessment of particulate attrition, and attrition testing methods. Two key challenges were highlighted at the conclusion of their review:

1. Specification of a useful, useable and representative test method, in which the particle attrition mechanism is well understood, within a test environment that is simple and well-defined.
2. Specification of a reproducible and satisfactory method of assessing particle attrition in terms of its extent and nature.

Both of these challenges are defined within a test method that is ideally accelerated in order to maximise utility. Shear testing and impact testing are concluded to have clear importance; however the attrition mechanisms present in such tests require further correlation with the mechanisms present in lean phase pneumatic conveying. Furthermore, the number of loading scenarios contained within industrial processes are diverse, adding another dimension to the complexity in predicting attrition behaviour.

Hutchings [2] recognised that surface erosion and particulate attrition are both results of the same contact event. Abrasive and erosive wear of ductile and brittle surfaces were addressed. The mechanisms responsible for material removal vary significantly between the two surface material types. Material properties of fundamental importance were determined to be the fracture toughness, K_{IC} , and the hardness, H , of the surface material, and the hardness of the particles. In applying this to the concept of particle attrition, the results of a particle-wall contact may be viewed in terms of damage to either the particle or wall, or both, depending on the properties of each material and the method by which a contact takes place. Hutchings also notes the likelihood of a fundamental relationship between surface wear and particle attrition (or particle wear) in such scenarios.

Breakage of agglomerates within the granulation process is reviewed by Reynolds et al. [3]. Breakage is addressed at the process scale (bulk behaviour), and at the granule scale (particle behaviour), and how the variables in the granulation process affect these. The granule manufacturing method had a significant influence on its breakage behaviour. Factors to be considered include: properties of the binder (viscosity, surface tension, amount of binder added, and contact angle with primary particles), size and shape of the primary particles, and granulation process variables (such as agitation intensity, granulation time, and binder addition method). Furthermore, different agglomerate types were considered; containing different types of bonds between the primary particles. This review provides valuable insight into the complex particle structure of agglomerates, and subsequently, their specific failure mechanisms.

Previous reviews have addressed the subjects of particle attrition in the general sense [1], as well as contact events within pneumatic conveying systems [2] and attrition of specific particle types [3]. Each of these reviews contain elements that can be applied to particle attrition in lean phase pneumatic conveying systems, however the present work will adopt a more holistic approach.

2.3 Particle Attrition within Lean-Phase Pneumatic Conveying

The studies reviewed in this section will account for the loading conditions imposed on particles within lean phase pneumatic conveying systems. The relationship between the pipeline geometry and operating conditions, and the level of particle attrition measured, will be reviewed.

2.3.1 Velocity and Acceleration

Particle velocity during pneumatic conveying is the velocity at which a particle travels longitudinally along the pipeline using a global coordinate system as a frame of reference. The superficial air velocity is obtained by neglecting the presence of the solid particles within the pipeline, and is often used as an operating condition to define the system. To achieve a lean phase pneumatic conveying condition, superficial air velocities are typically in the range of 10 to 45 m/s [4–8]. It is therefore essential to understand the operating parameters which affect the particle velocity within the pipeline.

Salman et al. [9] tested approximately-spherical fertiliser particles, with diameters of 3.2, 5.15 and 7.1 mm, in a single-bend pneumatic conveying line. In all cases, it was concluded that increasing the superficial air velocity increased the amount of particle attrition. Additionally, it was found that each particle diameter had a particle velocity, below which, no breakage could be measured. The shortcoming of this study however, is that due to the 4.5 m acceleration zone, particles were not verified to be fully accelerated as the particle velocity was not measured.

Kalman and Goder [10] tested potassium sulfate particles (1.4-1.7 mm diameter) through a pneumatic conveying system consisting of six blind-T bends. Superficial air velocities of 10.8, 19.2, and 24.0 m/s were tested throughout 10 passes, with the percentage of broken particles recorded at the end of each pass. It was concluded that the amount of particle breakage increases with increasing superficial air velocity, and that this trend is magnified with successive passes.

If all other conveying variables are held constant, increasing superficial air velocity (and hence particle velocity) has been repeatedly shown to increase the magnitude of particle

attrition observed across a range of materials. It is widely accepted that in order to minimise the degree of particle attrition occurring within a pipeline, a superficial air velocity as close as is possible to the saltation velocity should be used [9].

As shall be demonstrated in Section 2.4, the particle response to the loading conditions (particle velocity inclusive) is specific to the particle material properties and morphology.

A number of different methods have been adopted by different researchers to measure particle velocity, including:

1. High speed photography / Particle Image Velocimetry (PIV) [11, 12].
2. Two photodiodes separated by a known distance [13–16]. Two photo detectors are placed on the pipeline separated by a known distance. When the light beam is interrupted, this is registered by each detector. The time delay between the two detectors is used in conjunction with the separation distance to calculate the velocity of particles. This method is only appropriate for detection of single particles in the stream, or very lean particle flows.
3. Photodiode coupled with a vibration transducer separated by a known distance* [17]. This method operates in a comparable way to method 2, however the second photodiode is replaced with a vibration transducer on an impact plate at the end of the pneumatic conveying pipe. The vibration transducer generates a signal when the particle impact on the plate is detected, and a time-distance calculation is performed. The drawback of using this method is that if the impact on the plate causes particle damage, and therefore can only be used on particle characterisation equipment.
4. Electrostatic sensing approaches [18, 19]. As particles interact with each and the walls of the pipe in a pneumatic conveying system, they can acquire an electrostatic charge. This charge is detected through conductive sensors (of varying geometry, for example a pin or a ring), and the signal is cross-correlated across successive sensors along the length of the pipe to determine mean or local particle velocity across the pipe cross-section (subject to sensor arrangement).
5. Laser Doppler Velocimetry [8, 20]. Two coherent, monochromatic laser beams are intersected in the conveying pipe volume. Light scattered from the solid phase is detected with photodetectors. The doppler shift between the incident light and the scattered light attributed to the particle velocity. If tracers are added to the gaseous

phase (such as smoke), the velocity of the gaseous phase can also be measured. One drawback is that the pipe section being measured must be optically clear. Fine particles adhering to the pipe wall will inhibit measurements.

6. Optical Fibre Probe [21]. A single probe, 1-2 mm in diameter is inserted into the pipe. The probe contains two bundles of optical fibres, with each fibre measuring 20 μm in diameter. The fibres are used to transmit light from a source to create a measurement zone within the pipe. Photoelectric detectors positioned at the end of the probe detect the light reflected by passing particles. Particle velocity is determined through cross-correlation signal processing of the signals received from each of the detectors. One drawback of this technique is that it is possible for the conveyed particles to become electrostatically attached to the probe and interfere with the photodetectors.

7. Radiometric Sensors [^] [22]

* Indicates use with particle characterisation apparatus only

[^] Description of method available in Section 2.3.2.1

2.3.1.1 Slip Velocity

The difference between the superficial air velocity and the particle velocity is known as the slip velocity. A number of works do not directly measure the particle velocity (for example, see [5, 23]). Mendies et al. [24] looked at the effect of suspension density on the acceleration of particles within a pipeline. Through studying the dilute flow of plastic particles with pin electrodes, the mean axial particle velocity was determined. The particle velocities were plotted against their corresponding air velocities, clearly showing the presence of a slip velocity (Figure 2-1). Furthermore, each of the materials tested exhibited a different slip ratio (particle velocity / superficial air velocity). It was demonstrated that the solids loading ratio had negligible effect on the fully expanded flow slip velocity of the particles (Figure 2-2). Additionally, slip velocity increased linearly with increase in superficial air velocity for all conditions tested, suggesting a constant slip ratio. With respect to the length of the acceleration zone, all materials tested required the full horizontal pipe length of 11 m to reach a steady-state flow.

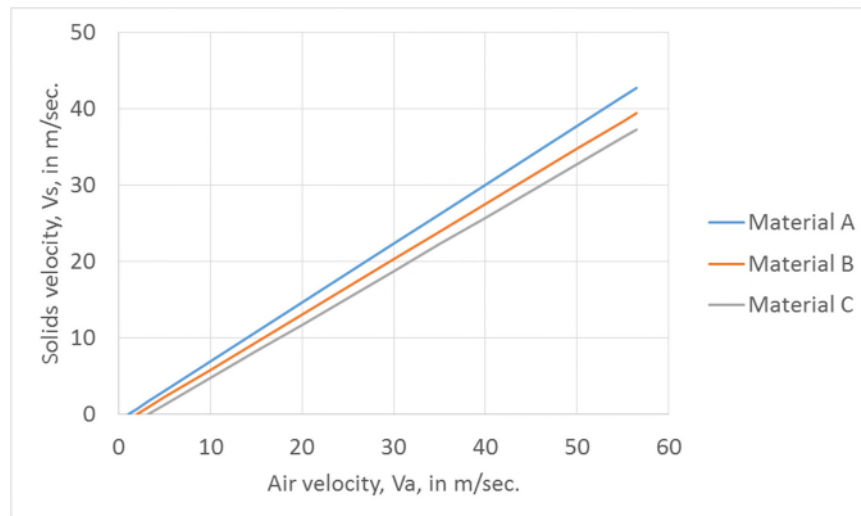


Figure 2-1: Particle Velocity plotted against Air Velocity for three Plastic Materials adapted from Mendies et al. [24].

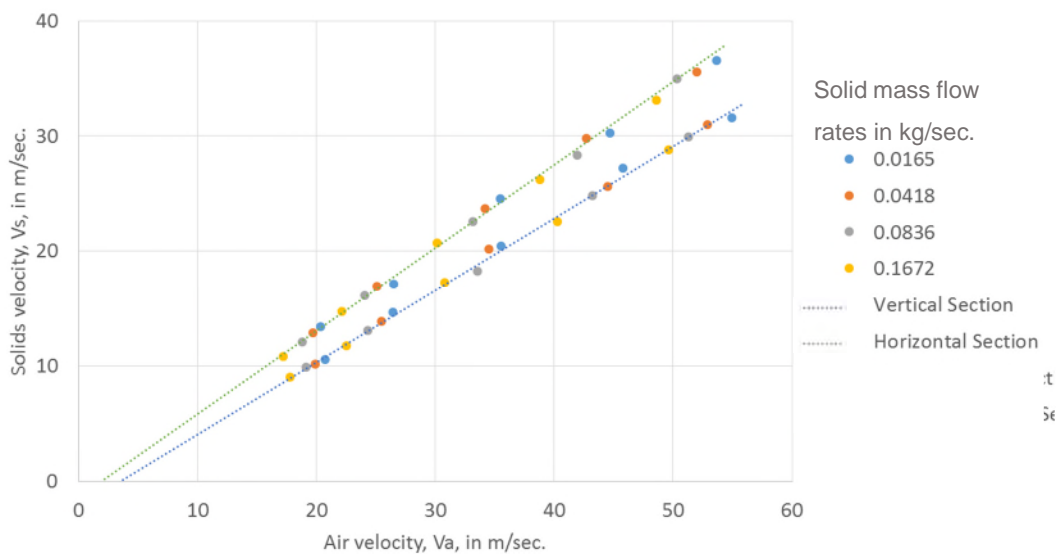


Figure 2-2: Particle Velocity vs Air Velocity across a range of Solids Loading Ratios for Vertical and Horizontal Sections adapted from Mendies et al.[24]

When considering a pipeline geometry where straight sections of pipe are insufficiently long to accommodate steady-state flow, the acceleration profile of the particulate material is required. A model to describe the acceleration of particles after a bend in lean phase pneumatic conveying systems was presented by Bradley et al. [25]. The calculation takes into account a moving bed of material (strand) which progressively loses mass to a clear

bore flow of air (Figure 2-3). The interaction between these two phases is governed by the shear force imposed across the face of the moving bed exposed to the clear bore. The force balance used in the calculation is also shown in Figure 2-3. This model demonstrated a reasonable correlation with experimental results (superficial air velocity range and suspension density range; 21-30 m/s, and 8-30 kg/m³ respectively), with a mean absolute error of 8%. Particle size and density were deemed to have minimal effect on the acceleration length.

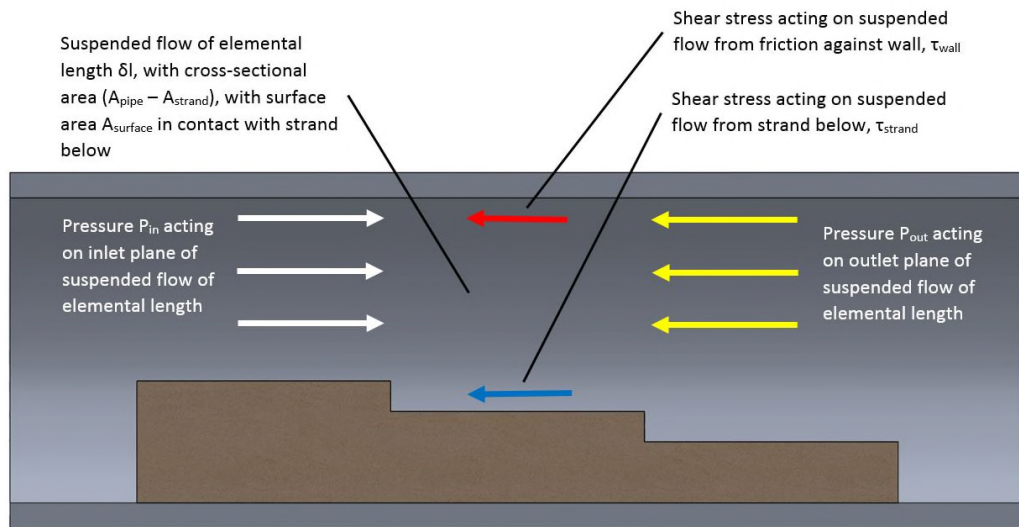


Figure 2-3: Strand Flow Force Balance adapted from the Acceleration Model by Bradley et al.[25]

It has been shown that to determine the particle velocity in the pipeline, the slip velocity and acceleration profile (for the case of non-steady-state flows) must be determined for each material. While generally, particle attrition increases with increased particle velocity, further detail is provided in Section 2.4 where the particle material response is addressed.

2.3.1.2 Pipeline Geometry

Pipeline geometry includes the internal diameter, material, internal finish quality, alignment, length of the straight sections of pneumatic conveying pipeline, and the geometry of the bends and couplings (these topics shall also be addressed with respect to particle concentration in Section 2.3.2, and consolidated in Section 2.3.3). The feeding arrangement or receiving arrangement shall not be addressed.

The pipe diameter used in the majority of studies is small, ranging from 0.75 to 2 inches [4, 6, 26], however some account for pipe bores as large as 4 inches in diameter [27]. One possibility for this trend is that an exponentially greater volumetric air flow rate is required to achieve the same conveying conditions with a larger bore size. Whilst use of small pipe diameters is more economically viable, a scale-up procedure is required to calculate the flow conditions expected in pipe systems of a larger bore size. Examples of scale-up models may be found within the works of Wypych and Arnold [28], Wypych [29], Ratnayake [30], and Bradley [27].

The length of straight sections of pipe is expected to inflict minimal damage on the conveyed particles by comparison with that occurring at the pipe bends [4, 9, 31], and therefore is acknowledged to cause little impact on attrition.

It has been demonstrated by Lagrangian simulation, that the wall roughness does alter the particle rebound behaviour following particle-wall contacts [32] for 50 μm and 100 μm spherical glass particles. Increasing wall roughness was found to reduce mean particle velocity (increase slip velocity), and reduction of 'particle-free zone' within the pipe cross section. Furthermore, these results were influenced by particle size. These results are supported by the experimental work of Sommerfeld and Kussin [33], albeit with a rectangular channel. The channel was 35 mm high and 350 mm wide with a length of 6 m. Surface roughness was tested across a 2 – 17 μm range, and mean particle sizes of 60 – 625 μm , at a conveying velocity of approximately 20 m/s. They concluded that when the surface roughness of the channel wall was increased, the particle distribution across the channel cross-section became more uniform. The same trend was observed with increasing particle size. The effect of wall roughness decreases with decreasing particle size. Finally, the measured slip velocity increased with increasing wall roughness. While there are no studies that link directly the effect of wall roughness on the attrition observed in lean phase pneumatic conveying systems, the aforementioned studies do yield valuable insight into the particle-wall contact conditions required for prediction of attrition.

The bends have been widely accepted to be the primary location of attrition within lean phase pneumatic conveying systems and a number of studies have been conducted into determining the influence of bend geometry on particle attrition behaviour [5, 16, 26, 34]. The variable of interest in these studies has been the bend r/D ratio (radius of the centreline of the bend divided by the diameter of the pipe). Many studies also refer to

short radius ($r/D \approx 3$ to 5) and long radius ($r/D \approx 9$ to 12). It is commonly reported that short radius bends produce more attrition [16, 26, 34]. The argument made in favour of increased degradation in long radius bends is that particles are expected to be subjected to a higher number of impacts. Conversely, higher impact angles are expected in short radius bends, theoretically resulting in increased particulate attrition. Particle shape can be a significant factor when considering particle-wall interaction, as demonstrated by Deng et al. [35]. These observations may contribute to an underlying relationship with the impact angle expected within different lean phase pneumatic conveying bend types.

2.3.2 Particle Concentration

Particle concentration measurement techniques shall first be considered, followed by acknowledgement of variation of the particle concentration across the conveying pipe cross-section. Finally, the influence of particle concentration on attrition shall be discussed in conjunction with the concept of particle shielding. The influence of particle concentration on particle attrition within lean phase pneumatic conveying systems is not thoroughly understood. Few studies have isolated this conveying condition while keeping all other variables constant.

2.3.2.1 *Measurement Techniques*

Several techniques have been developed to measure the particle concentration within pneumatic conveying pipelines. These are largely addressed in the review works of Zheng and Liu [36], and Yan [37], and therefore a selection of techniques shall be summarised here.

Averaged Measurement Methods

If the air mass flow rate and the solids mass flow rate are monitored, the particle concentration throughout the pipeline can be defined as a dimensionless ratio of mass flow rates (also known as the solids loading ratio or SLR). This approach has the

advantage of remaining constant along the length of the pipeline and has been widely used [5, 7, 33, 38, 39]. Measurement of this variable is facilitated with a loss-in-mass measurement of the feed hopper and air supply characteristics, and is typically between 0-15 for lean phase pneumatic conveying systems [40]. However, this criterion cannot be used to describe the conditions in a pipe bend in isolation, as the volume of the fluid phase changes along the length of the pipe, and the residence time of the solid phase is specific to the pipeline geometry and conveying conditions.

Additionally, the volumetric loading ratio (dimensionless ratio of volumetric flow rates of solids to gas phase) can be calculated along the pipeline, local to online pressure tappings [18, 41]. The value of this variable changes along the length of the pipeline to reflect the expansion of conveying air.

A hybrid of the previous two methods can also be adopted, whereby the ratio of the mass flow rate of solids to volumetric flow rate of the gas phase is used to characterise the particle concentration in the conveying line [42–44].

Electrical Capacitance Tomography (ECT)

Electrical Capacitance Tomography functions on the basis that as the amount of material in a pipeline increases, the measured capacitance across the pipe cross-sectional area will also increase. Sensing electrodes can take a number of forms including pins, rings and plates, mounted internally or externally (on insulated pipe) on the pipeline [37]. Whilst the resources required to implement this technique are relatively cheap, it is necessary to evaluate the influence of baseline drift, temperature of the conveyed phases, and moisture content of the conveyed phases, as in the work of Hu et al. [45]. Moreover, it is essential that the operator is aware of build-up of the solids phase in the sensing volume of the pipeline as this too will affect the readings obtained. Sensor structure is a key consideration in how two-phase flows are characterised. This is exemplified in the work of Yang and Xu [46], who compared two twin-array capacitance sensors: one with 4 electrodes and the other with 6. It was concluded that while the 4-electrode sensor offers a higher data acquisition speed (making it suitable for high-velocity flows), the 6-electrode sensor can detect more complex flow patterns.

Radiometric Sensors

This method of particle concentration measurement can use sources including low-energy gamma rays (such as Am-241) [37], or x-ray point sources [47] to inspect the entire pipe cross section. While there is only a weak effect of moisture content of the conveyed medium on the signal obtained [48], a key consideration of this approach is to design such a system that is capable of inspecting the entire pipe cross-section with the single-line attenuation nature of the source and sensor. Alternative configurations include a scanning densitometer (unsuitable for transient measurements), multi-path configuration, and use of a single broad-beam source [37]. The use of a soft x-ray field source has proven compatible with dilute phase pneumatic conveying due to its much higher radiation attenuation [49].

High-Speed Imaging / Particle Image Velocimetry (PIV)

High speed imaging techniques for measuring particle concentration requires collection of a series of images or frames, which are used to calculate particle position and velocity across known time intervals. This method is best used to observe low-concentration particle flows [11] and detectable particle size is determined by the camera resolution. There is also the drawback of particle masking, where a particle travels in front of another from the perspective of the camera, hiding the latter.

Another approach used to determine the particle concentration is through using a single image captured over a longer exposure time, and thus obtain an image containing particle traces. These traces represent the particle diameter and velocity through the width and length of the trace respectively [50]. A more comprehensive review of PIV techniques can be found in the work of Miyazaki et al. [51].

2.3.2.2 Particle Concentration across the Conveying Pipe Cross Section

In addition to findings mentioned in Section 2.3.1.2, investigations of the cross-sectional particle concentration have found that in steady-state lean-phase conveying, higher concentration levels are found in the lower half of the pipe [52]; such behaviour is also

true of rectangular channels [53]. This has been largely attributed to the influence of gravity on the particle flow, leading to particles favouring a position closer to the bottom of the pipe. Additionally, the immediate straight pipe section following the bend exhibits a cross-sectional solids concentration described as the previously mentioned strand-type flow [25]. This is due to the material being forced to the outer wall of the pipeline in the bend section.

Fokeer et al. [54] summarises the effects of pipe wall roughness, mass loading, and pipe bends on the cross-sectional concentration of solids in lean phase pneumatic conveying. It was reported that as pipe wall roughness increases, the gravitational settling of the solid particles is reduced while increasing the pipeline pressure drop. Increasing mass loading conditions resulted in a reduction of particle velocity fluctuations. Finally, bend orientation and geometry affect the formation of a particle strand in the post bend pipe section. If the conveyed solids have a sufficiently wide particle size distribution, particle size segregation will occur longitudinally in the post bend pipe section; this effect is more prominent at lower conveying velocities and higher mass loading ratios.

Particle pathing has been tracked through a pipeline including a bend and other industrial equipment, using Positron Emission Particle Tracking (PEPT) [55–57]. This method involves labelling a particle with ^{18}F ions, which emit 511 keV annihilation photons. These photons are then detected with a camera, and particle position is triangulated. An example of the results obtained by Chaudhry [56] is shown in Figure 2-4.

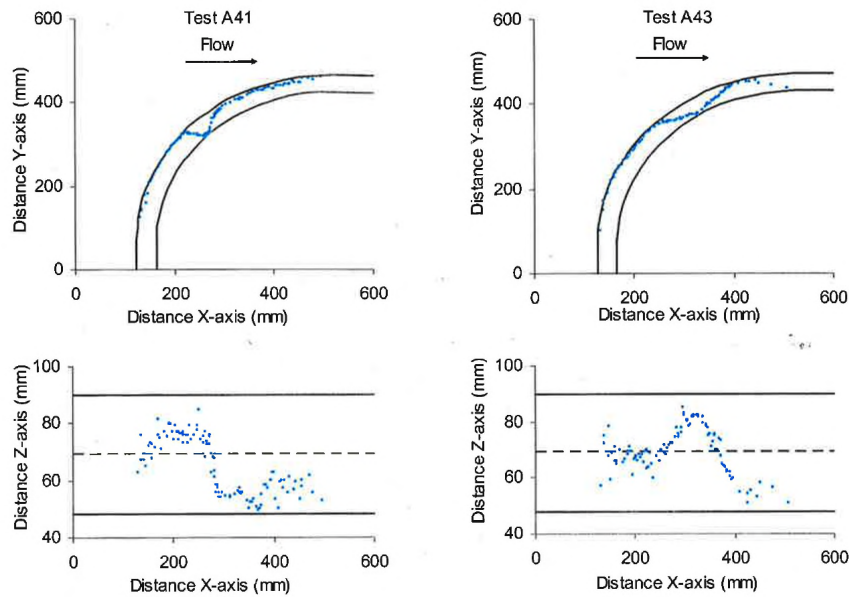


Figure 2-4: PEPT Results obtained by Chaudhry [56]

2.3.2.3 The Influence of Particle Concentration on Particle Attrition

Few studies have looked at the direct relationship between particle concentration and particle attrition in lean phase pneumatic conveying experiments. McKee et al. [58] studied the attrition of sea salt, in a dilute conveying system, 32 m in length. Superficial air velocities in the range of 15-40 m/s and loading factors (kg solid : kg air) in the range of 1:1 to 15:1 were tested. Representative sampling was used throughout the study. The sieve harmonic mean was used to measure changes in particle size (description in Section 2.5.2, Equation (2-10)). It was concluded that particle attrition is inversely related to the solids loading factor. It was also noted however, that at high solids loading and low superficial air velocities, solids deposition occurred on the bottom of the pipe. Such deposition locally reduces the velocity of particles and therefore reduces particle attrition levels. These two phenomena require decoupling before a definitive statement can be made on the relationship between particle concentration and particle attrition in lean phase pneumatic conveying systems.

Particle shielding is a concept that suggests pipeline wear decreases with increasing particle concentration in the pipeline [41, 59]. High-velocity particle-wall impacts are partially mitigated by inter-particle contacts, whereby only a fraction of the conveyed particles come into direct contact with the pipe wall. Little is understood about the

underlying mechanics of this phenomena, however previous studies by Andrews and Horsfield [60], Macchini et al. [41] and Bridle [26], demonstrated the variation that particle concentration had on the operating behaviour of the system. Andrews and Horsfield [60] analysed interparticle collisions from the perspective of wall erosion. While failing to reduce the number of particles striking the wall surface, an increase in interparticle collisions (achieved through increasing particle concentration) resulted in a wider distribution of impact velocities and impact angles. Bridle [26] found that by increasing the particle concentration in a single pneumatic conveying test bend, the percent fines measured was reduced. However the solids to air flow rates (kg of solids per m³ of conveying air) encompassed dilute phase through to dense phase conveying types (more detail in Section 2.5.2), and particle velocity was not measured. Further quantification of the influence of particle concentration on particle attrition is required in order to obtain a greater understanding of how lean phase pneumatic conveying systems operate, and whether the concept of particle shielding can be transferred to particle damage in addition to pipeline erosion.

2.3.3 Concluding Remarks on the Process Factor

It has been widely accepted that the majority of particle attrition occurring in lean phase pneumatic conveying pipelines can be attributed to contacts occurring at the bends. A number of geometrical and operational variables have been the subject of past studies, however the influence of particle concentration remains open for further exploration and understanding as summarised by Table 2-1.

When aiming to control particle attrition, flow obstructions in the pipeline should be avoided, minimising the number of bends and using compression couplings (rather than flanged pipes) to connect pipe sections to minimise the potential for misalignment of the pipe bores. Due to the variation in manufacturing quality and reliance on pipe cross section circularity, further analysis of this geometric factor shall not be undertaken. However, it should be noted that any misalignment of the pipework is expected to lead to increased pressure drop and particle attrition.

The relationship between internal surface finish of the pipework, pipework material, and particle attrition has not been directly elucidated in the literature. However, it logically follows that by varying the surface finish, the frequency and magnitude of friction between the particle and wall will also vary. In this case, particulate attrition is expected to vary based on previous observations of shear load sensitivity. Additionally, the cross-sectional particle concentration within the pipeline have been shown to vary with respect to variation in pipe wall roughness [32, 33]. Therefore, the distribution of particles entering the bend is expected to vary with respect to pipe wall roughness. The influence of pipe material and surface roughness of the internal surface of the pipe remain a gap in the research at present.

Particle concentration is a conveying variable that has been seldom studied within the context of particle attrition. This applied to the averaged longitudinal particle concentration, and the particle cross section at local pipeline cross-sections. One key study addressed this subject [58], however a large (83 mm) diameter conveying pipe was used and particle strands were observed in tomographic images. Furthermore, particle velocity was not measured, and attrition was compared only with superficial air velocity. This calls for a more detailed investigation into the influence of particle concentration on particle attrition, specific to particle velocity and homogeneous lean phase flows. Only then could the presence of a 'shielding effect' be elucidated.

Table 2-1: Summary of the Influence of Conveying and Geometrical Variables on the Attrition of Conveyed Solids

Conveying/Geometrical Variable	Trend	Notes	References
Superficial Air Velocity	Particle attrition increases with increasing superficial air velocity	It is assumed that particle velocity increases with increasing superficial air velocity for all materials	[5, 9, 61]
Particle Concentration	Particle attrition decreases with increasing particle concentration	There are limited studies to reflect this relationship. Further research is required.	[58, 62]
Pipe Bend R/D ratio	Particle attrition decreases with increasing pipe bend r/d ratio		[16, 26, 34]
Number of Pipe Bends	Particle attrition increases with increasing number of conveying pipe bends		[4, 61, 63]

2.4 Influence of Physical Particle Properties on Attrition Behaviour

Particle failure is defined as the separation of a single particle into two or more child particles. The probability of a particle failing and the behaviour by which failure occurs are affected by mechanical and geometrical particle characteristics, dictating breakage behaviour. Further to this, the loading scenario to which the particle is subjected affects the mechanism of attrition observed. Particle physical properties shall be discussed first, followed by responses to specific loading conditions.

2.4.1 Particle Material Characteristics

There is currently a lack in understanding of precisely how the material properties, in conjunction with applied loading conditions, affect attrition behaviour [64]. Key material properties and their influence on particle attrition behaviour are addressed here.

2.4.1.1 *Particle Strength*

Particle strength is the minimum amount of stress that may be applied to a particle to cause macroscopic damage to the particle structure. As shall be demonstrated in Section 2.4.1.3, particle structure plays a fundamental role in the determination of particle strength. This, along with the physical properties of the particle material, as discussed in this section, dictate the response of a particle for a given loading condition.

2.4.1.1.1 Tensile and compressive

Tensile tests can be challenging to execute due to the difficulty in obtaining a suitably sized and shaped specimen appropriate for the test. There is also the case of secondary shear stresses generated in various methods of the tensile test which invoke secondary failure mechanisms in the material [65]. While Griffith's theory proposes that the ratio of

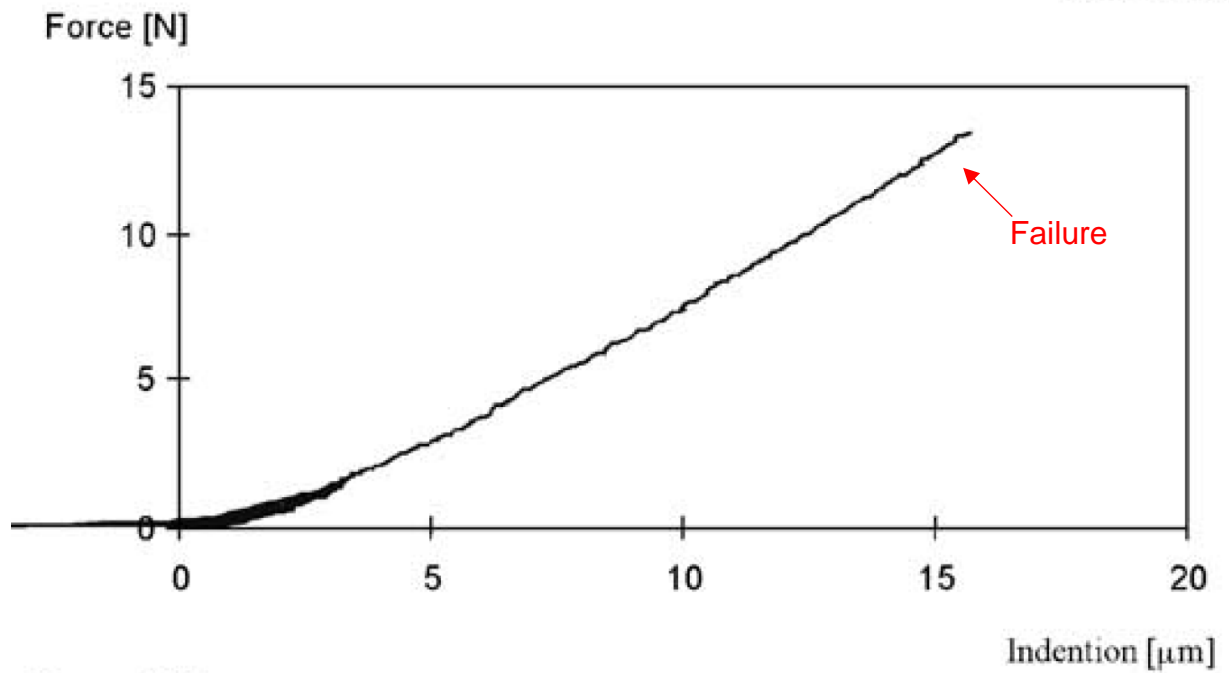
compressive to tensile strength is equivalent to a value of 8 where tensile failure is the dominant failure mechanism [66], further experimentation has not supported such a simple relationship [67]. In addition to this, the strain rate is critically important for agglomerate materials in obtaining representative characteristics of material properties [3].

2.4.1.1.2 Yield Stress and hardness

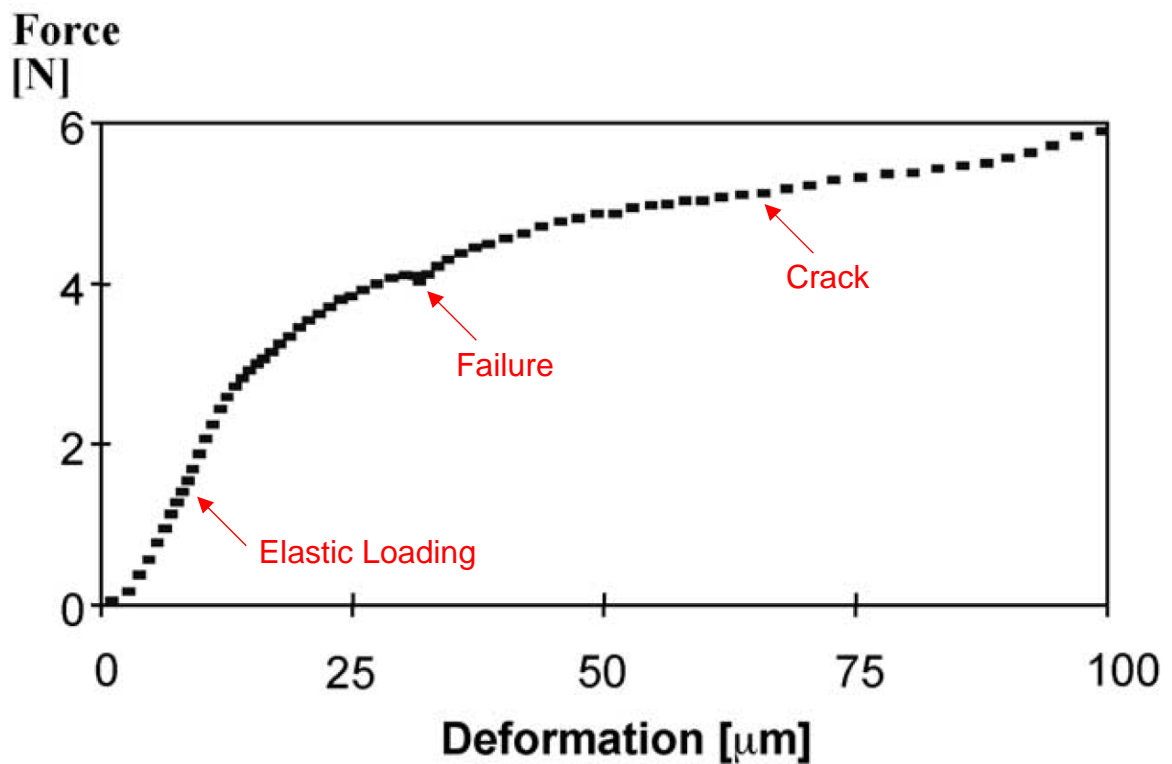
Yield stress can be measured with a number of methods, of which indentation and compression are common.

Indentation uses an indenter of known geometry to penetrate and inflict plastic deformation in the material surface. Such a test proves challenging on particulate materials where little surface area is available, requiring the use of the nanoindentation technique [68]. According to Bika et al., hardness is a function of tensile yield strength, elastic modulus, Poisson's ratio and total strain (depending on material behaviour) [69]. The subsequent conclusion drawn from these observations is that the hardness value is exclusive to the conditions under which the test was performed, and may not be used as a holistically defining material property. This extends to the Young's modulus or fracture toughness which can also be calculated from these measurements.

The compression test places the particle between two flat surfaces which are brought together, loading the particle with a compressive force. This has been used in numerous works to quantify the yield stress of particulate materials. As demonstrated in the work of Beekman et al. [70], if a constant strain rate is maintained throughout the compression test, a force-displacement profile can be generated. The maximum applied force is taken as the particle strength, however as demonstrated in Figure 2-5, the particle strength profile after primary yielding is also captured in the test.



(a)



(b)

Figure 2-5: An example force-displacement curve for a constant strain-rate compression test of a (a) brittle particle and (b) non-brittle particle as presented by Beekman et al. [70] with additional annotation in red text.

2.4.1.1.3 Dynamic Yield Strength

Especially in the case of wet agglomerates, viscous effects play a significant role in determining the particle deformation behaviour. These viscous effects are strain-rate dependant [71], therefore calling for a definition of yield strength that accounts for strain rate. The concept of dynamic yield strength is introduced by Hawkyard [72], to address this behaviour in the form of Equation (2-1) for a cylindrical specimen.

$$\frac{1}{2}\rho U^2 = Y \left[\frac{A_0}{A_1} - 1 + \ln \left(\frac{A_1}{A_0} \right) \right] \quad (2-1)$$

Where A_0 is the initial contact area, Y is the dynamic yield stress, U is the impact velocity, ρ is the particle density, and A_1 is the deformed (post-impact) contact area. Conversion between the results of dynamic measurement methods has been stated to be irreconcilable with the equivalent quasi-static method due to the significant difference in strain rate [3].

2.4.1.2 Fracture toughness

Defined as the critical crack driving force, fracture toughness is a measure of a material's ability to resist crack growth in the presence of an existing crack [73]. This property is typically measured through the flexural bending of notched bars, specified in ASTM E399-90 [74]. Preparation of very specific material geometries to ensure that a valid result is obtained; such geometries are unobtainable for many particulate materials. Furthermore, increased complexity is found in the testing of agglomerate materials in defining fracture area corrections accounting for sample porosity [69]. It has also been argued that the failure mechanism for porous agglomerates may not be due only to the failure of a single primary crack, but rather the simultaneous propagation of multiple fractures (for example, [75]).

Two approaches are well known in fracture mechanics to fundamentally explain crack propagation through a material. Griffith [66] proposed that specific surface energy should

be considered as one of the material properties of primary importance, whereas Irwin [76] proposed that strain energy release rate is of primary importance, especially in ductile materials. More recently, Ouchiyama et al. [77] found that the fracture toughness cannot be exclusively used to fully describe the attrition behaviour of particulate materials.

2.4.1.3 Particle Structure

The microstructure of a particle dictates the distribution of defects or cavities, which along with the atomic structure, influence the location and orientation of fracture planes.

2.4.1.3.1 Agglomerate Particles

Agglomerates present a unique challenge in terms of understanding their fracture modes due to the lack of continuity in their structure. Reynolds et al. [3] define three different types of agglomerate structure; *binderless* describes an agglomerate whereby van der Waals or other similar micro-scale forces hold the constituent particles together, *solid* describes agglomerates where solid connections are in place between the constituent particles, and *wet* describes agglomerates containing liquid in the interstitial spaces between constituent particles.

Through acknowledgement of the complex and diverse structures of agglomerate materials, it may be appreciated that their attrition behaviours embody a number of distinct mechanisms. Such mechanisms have been the focus of a number of studies both experimental [75, 78] and simulated [79–83] in nature, some of which are summarised in Figure 2-6.

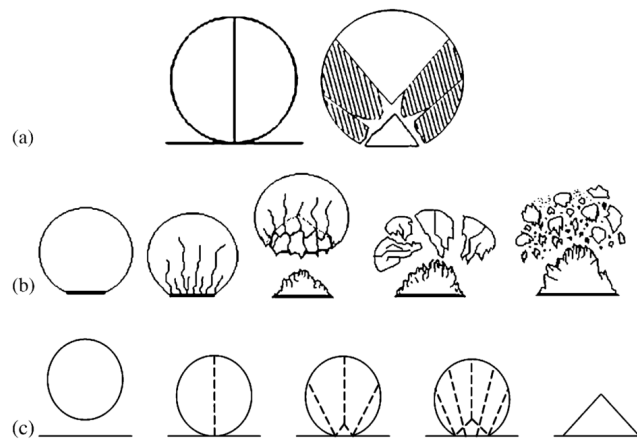


Figure 2-6: Agglomerate failure methods by impact as described by Reynolds et al. [3] and adapted from the work of Salman et al. [84], for (a) solid, (b) wet, and (c) binderless structures. Impact velocity increases from left to right.

2.4.1.3.2 Crystalline Particles

The production process by which crystalline materials are manufactured has been shown to have a significant influence on their attrition propensity [85]. This has been demonstrated not only with respect to the crystal drying mechanism selected, but also for subsequent handling processes within the manufacturing plant attributed to various applied loads on the particles. If a crystalline material is of a semi-brittle nature, it will typically fail via the previously described, chipping mechanism [86]. If the crystal fails via a pure brittle mechanism, rupture along preferred fracture planes is expected. The selection of the failure mechanism by which a crystal fails can be due to the distribution of loading forces across the topography of the particle (i.e. particle orientation with respect to impact plane).

In the case where a particle is composed of two or more crystals, cleavage may occur at the interface. It is worth noting that such a particle failure would yield child particles that are relatively undamaged [85]. This is important when considering the fatigue characteristics of particulate materials, and the formation of child particles in the form of whole crystals as opposed to platelets of significantly smaller mass.

2.4.1.3.3 Pelletised Materials

Pelletised materials demonstrate a wide range of attrition behaviours due to the extensive range of feed materials and manufacturing processes that are used. Thomas et al. [87–89] published a series of articles acknowledging these factors. Particular emphasis was given to the evaluation of pellet hardness and durability, along with the influences of feedstock and manufacturing processes on these qualities. Furthermore, pellets are generally required to give a specified nutritional content (in animal feeds) or calorific value (in combustion processes) adding another layer of physical requirements to the product. Such diversity in material composition and form inevitably leads to an equally diverse range of failure modes.

2.4.1.4 *Coefficient of restitution*

When considering elastic-plastic collisions in dynamic processes, the kinematic/kinetic/energetic and tangential coefficients of restitution should be accounted for. Furthermore, a work-hardening model is required if the material in question displays such behaviour, as this will alter the coefficient of restitution of subsequent impacts and the mode of kinetic energy dissipation [90]. If irregularly shaped particles are being considered, as is the case in the majority of existing processes, resulting rotational effects must be considered in the selection of the coefficient of restitution [91].

A number of studies consider almost fully plastic impacts [71]. Fu et al. [92] investigated the influence of various wet agglomerate material parameters on the coefficient of restitution and contact ratio observed across a range of impact velocities. Primary particle size, binder viscosity, binder ratio, and granulation time were all compared against impact velocity with respect to the measured coefficient of restitution. As these particles demonstrate adhesive elastic or elastoviscoplastic behaviour, it was found that a minimum of 97% of the impact kinetic energy is dissipated in intra-particle viscous flow at low impact velocities, or bulk viscoplastic flow at high impact velocities. This work is further supplemented by Mangwandi et al. [93] who looked at the coefficient of restitution

of wet, melt and binderless agglomerates and proposed a model to account for strain-hardening.

2.4.1.5 Comminution Functions

Many approaches have been adopted in modelling particle failure in comminution processes. Some examples of these will be discussed here, however this list is by no means be exhaustive.

Meier et al. [94] modelled comminution data for nine different particulate materials with data obtained from a gas-blast style particle attrition tester [95] (see Section 2.4.5.1). they proposed that the complete breakage function of a material can be predicted if the impact energy, initial particle size, and the breakage parameters f_{Mat}^* and $x \cdot W_{m,min}^*$ are known. When expressed in terms of the complete (material dependent) dimensionless stressing parameter, $f_{Mat}^* \cdot x \cdot k \cdot W_{m,eff}^*$, all collected data points conformed to a single curve. f_{Mat}^* is the adjusted material parameter (kg/Jm), x is the particle size (m), k is the number of impacts, $W_{m,min}^*$ is the adjusted mass-specific threshold energy for particle breakage (J/kg), and $W_{m,eff}^*$ is the mass-specific effective impact energy (J/kg). The breakage parameters can be determined from comminution experiments, or estimated from the brittleness index of the material [96]. The breakage functions derived were consistent for impact angles of 60° and 90°. Particle shape was not considered in this work, even though a variety of particle shapes were present in the test materials.

Rozenblat et al. [97] used a double compression test (see Section 2.4.4.3) to determine strength distributions for eight different materials, across two different test apparatus units. Virgin particles ranged from 0.71 to 5 mm in diameter. They proposed a function that describes the force required to induce failure in a particle, described by Equation (2-2).

$$F_c = (A_F + B_F \cdot d_{mean}^2) \left(\frac{S_F}{1 - S_F} \right)^{1/D_F} \quad (2-2)$$

Where F_c is the crushing force (N), d_{mean} is the particle mean sieve diameter (mm), and S_F is the breakage probability under specific force (-). A_F , B_F , and D_F are empirically obtained model parameters used to obtain best-fit to experimental data. An identical approach was proposed to describe particle strength distribution in terms of crushing energy. The relationship between crushing energy and crushing force was found to be independent of particle size. Crushing force was concluded to be a more useful parameter as opposed to crushing stress, due to removal of particle shape factors which add significant complexity. It was acknowledged that crushing stress is however, more physically correct.

Soni et al. [98] tested five different ores with a double impact tester (see Section 2.4.5.4.2), and measured the subsequent full particle size distribution. The one-parameter breakage model contained within King [99] (Equation (2-3)) was evaluated, where t_n represents the cumulative mass fraction passing $1/n^{\text{th}}$ of the parent particle size, and α is a material characteristic. As α is held constant for a given material, this model is considered to contain only one parameter.

$$t_n = 1 - (1 - t_{10}) \left(\frac{9}{n-1} \right)^\alpha \quad (2-3)$$

It was concluded that α and t_{10} are the distribution and size moduli respectively, as α alters the particle size distribution and t_{10} changes the degree of breakage.

2.4.2 Particle Geometry

Particle geometry refers to the physical profile of a particle, which influences breakage propensity and resulting child particle size distribution.

2.4.2.1 Particle Morphology

Spherical particles have been the subject of numerous studies across a wide range of loading conditions [78, 79, 82, 92, 100, 101]. This simplifies the attrition model, as this particle geometry demonstrates no variation with orientation. It has been generally found that spherical particles can fail at low impact energies through the propagation of meridional cracks, producing a small number of large fragments. As the impact energy is increased, a greater number of fragments are produced [80], in addition to complete disintegration of the contact zone for agglomerate structures [75]. This relationship with applied force is also observed for double impact testing [102].

Cubic particle failure has been studied in some detail, with simulation work [103], and experimental work with materials such as salt, magnesium oxide and potassium chloride [104]. In terms of impact attrition, it has been shown that the orientation of impact is critical to the mode of attrition observed. If the impact occurs at one of the corners or edge of the particle, semi-brittle failure is observed due to a concentrated stress distribution. Ghadiri et al. [85] studied cubic NaCl particles where a 'full face' impact (a side of the cube impacts parallel to the wall surface) was observed. The particle was observed to unload elastically from the impact, and did not suffer any of the damage due to chipping, as was observed when corners or edges of the particle form the contact surface.

Antonyuk et al. [105] studied the breakage behaviour of L-threonine crystals and Al₂O₃ agglomerates by impact and compression respectively. Both particle geometries were of cylindrical form, however, the aspect ratio of the crystalline material conformed to a needle shape. The compression experiments (applied force perpendicular to longitudinal axis) found that the agglomerates cracked longitudinally along the axis of the cylinder whereas the crystals typically result in two or three transverse cracks.

Other particle shapes such as orthorhombic [86], and generally random-shaped particles [106] have also been investigated on a qualitative basis, however the stress distribution becomes more complicated under these circumstances. Briesen [107] modelled crystal attrition with respect to impeller collisions and found that if a crystal geometry contains sharp corners, it is more likely to break than if it was spherical.

2.4.2.2 Particle Size

It has been repeatedly demonstrated that particle strength decreases with increasing particle size [85, 101, 104]. Additionally, when repeated impacts have been considered, the rate of attrition across subsequent impacts increases with initial particle size [86]. These trends have been attributed to the likelihood of a greater number of imperfections in larger particles, which in turn provide a greater number of cracks which may propagate as a result of an imposed load [78].

Considering mineral ore particles (size ranges in the order of 1-100 mm in diameter), Shi and Kojovic [108] modified the breakage probability model of Vogel and Peukert [109] to describe the t_{10} (%) breakage index (Equation (2-4)), and by incorporating particle size-dependent parameters explicitly (Equation (2-5)).

$$t_{10} = M\{1 - \exp[-f_{mat.} \cdot x \cdot k(E_{cs} - E_{min})]\} \quad (2-4)$$

$$A \times b = 3600 \cdot M \cdot f_{mat.} \cdot x \quad (2-5)$$

Where t_{10} is the percent of child particles passing one tenth of the initial mean particle size, E_{cs} is the specific comminution energy (kW h/t), and A and b are the ore impact breakage parameters. They compared the goodness of fit of their model with the experimental work of Banini [110], with positive results. It was also noted that only one set of parameters required defining for each type of ore, as opposed to requiring individual values for each particle size considered.

This accepted, it has been demonstrated that even for particles of the same material composition, size and shape, a range of particle strengths are observed [111]. The size distribution of the child particles is commonly approximated by a Weibull distribution function [17, 78, 112–117].

In the case of agglomerate primary particle size, it has been shown that a narrowing of the particle size distribution corresponds to a reduction in the agglomerate strength [118]. This is due to the inability of primary particles to layer themselves within agglomeration processes such as a high shear mixer. Generally a smaller primary particle size is

associated with a higher agglomerate strength (in conjunction with other factors such as binder viscosity and agglomerate density) [119].

2.4.3 Particle Fracture

The particle failure mode captures the particle response to an applied load for the case when the particle strength (whether locally or globally within the particle) is exceeded. Particle fracture modes will be defined, followed by discussion of the fracture plane distribution and resulting distribution of particle fragments.

2.4.3.1 *Fracture modes*

Particulate failure modes have been broadly divided into three categories [75]; brittle failure where there is no significant plastic deformation, ductile failure characterised by extensive plastic deformation, and the transitional semi-brittle failure describes the occurrence of fractures initiated by plastic deformation [64].

The failure mode of a particulate material is subject to a wide range of physical factors. In the case of materials such as polymers, temperature of the particle is critical in determining the failure mode [120] with respect to the material-specific glass transition temperature. Agglomerate failure modes are heavily dependent on the binding mechanism, the properties and proportion of the binder, and in the case of wet binders, the interaction between the binder and the primary particles [3, 101].

2.4.3.2 *Fracture Plane Distribution*

The resulting size distribution of child particles can be described by one of two mechanisms: fragmentation and chipping. Both of these mechanisms correlate to different fracture planes within the particle body.

Particle fragmentation is the separation of a particle into two or more child particles of comparable size. This mechanism is the result of the formation and propagation of median, oblique or radial fissures throughout the entire volume of the particle [64]. This is typically associated with high-magnitude loading conditions, whereby the stresses applied to the particle exceed the particle strength and generate free surface area via fracture planes.

Chipping or surface erosion, results in the removal of small fragments from the particle surface through the creation and propagation of sub-surface lateral cracks. These cracks are produced during the unloading phase of a particle impacting on a surface due to the production of residual tensile stresses [121]. The fragments produced as a result of this process are typically much smaller than the parent particle, and tend to originate from the corners or edges of the particle [64]. Ghadiri and Zhang [64, 104] developed and validated a mechanistic model to predict the rate of attrition of semi-brittle materials. MgO, NaCl and KCl cuboid particles were prepared and impacted upon a hard surface. It was determined that the hardness of the target had little influence on the attrition results when the ratio of particle hardness to target hardness was less than, or equal to, unity. It was shown that attrition by impact (addressed in Section 2.4.4.1) did not follow a first-order relationship, attributed primarily to a work-hardening effect where particles become harder with subsequent impacts. This contrasts with previous work performed by Vervoorn and Austin [122], who had originally proposed that this attrition mechanism could be described as a first order process.

2.4.4 Particle Attrition Mechanisms

The loading conditions to which a particle is subjected, define the mode of failure and the size distribution of the resulting fragments. Shear, crush and impact loading, along with the influence of fatigue will be addressed. Focus is attributed to particle attrition due to impact as this research accounts for dilute phase pneumatic conveying, whereby the dominant source of attrition is expected to be caused by particle-wall impacts [9].

2.4.4.1 *Impact*

Particle failure by impact has been identified with processes such as lean phase pneumatic conveying [43], dependant on the type of particulate material under consideration [15]. Various aspects of this mechanism will be discussed in turn, followed by a survey of the current testing methods available.

2.4.4.1.1 Impact Velocity

Impact velocity has been repeatedly shown to have the greatest influence on the degree of particle attrition observed. With increasing impact velocity, the impact energy increases, and hence is more likely to exceed the inherent strength of the particle. The mechanism by which particles fail with respect to impact velocity is fundamentally dependent on the particle material, which is why the probability of particle fracture and the subsequent size distribution of fragments can only be compared between particles of the same mechanical properties. An example of the influence of breakage behaviour of agglomerates was published by Subero and Ghadiri [75]. This behaviour was resolved into a map against the void characteristics of the particle (Figure 2-7). It can be seen that not only the breakage behaviour changes with increasing impact velocity, but also the frequency (and hence probability) of particle fragmentation.

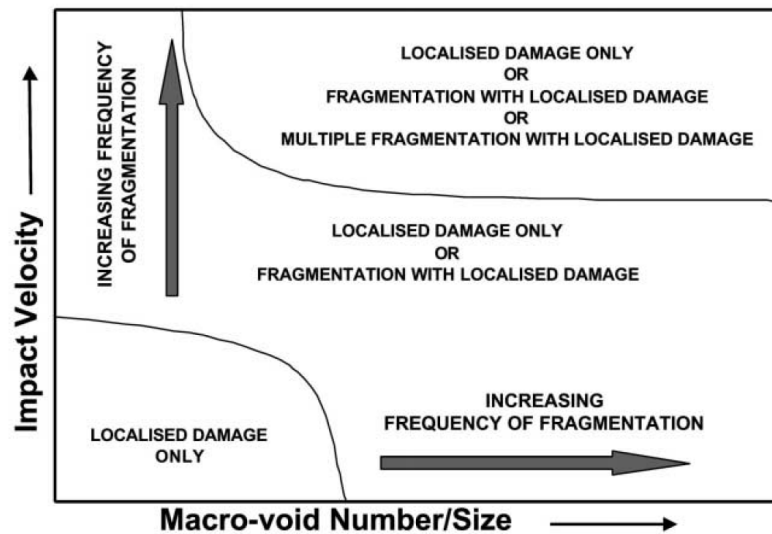


Figure 2-7: Agglomerate Breakage Behaviour Map as presented by Subero and Ghadiri [75]

To further illustrate the variable response of materials Zhang and Ghadiri [104] demonstrated that the attrition propensity of three different crystalline materials could be approximated with a power law relationship – with the indices unique to each respective material. Furthermore, these indices changed with subsequent impacts due to the work-hardening behaviour of the crystals.

Chen et al. [23] studied the attrition of limestone under impact conditions at temperatures ranging from 25 to 580°C and conveying air velocities from 20-100 m/s. The particles were accelerated along a 1 m length of pipe and then impacted onto a steel target. The particle velocity at impact as estimated using the equations of Clift et al. [123] for spherical particles at high Reynolds Number flows. It was concluded that the mean particle diameter decreased proportionally to the square of the impact velocity. Additionally, it was found that attrition levels reduced with increasing conveying temperature. It was proposed that this could be due to a reduction of particle velocity with an increase of conveying air temperature. It is important to note that in this study, the particle velocity was not directly measured.

It is therefore apparent, that while in the vast majority of cases, particle attrition increases with increasing impact velocity, the response of the particle is specific to the physical properties of the particulate material.

2.4.4.1.2 Impact Angle

The impact angle of a particle against a surface is here defined by the angle subtending the particle velocity vector and the plane represented by the material surface.

It has been shown that the severity of particle attrition increased as the impact angle increased towards a normal impact scenario [124]. This is due to the relatively large normal force vector in comparison with the tangential force vector. An idealistic study was conducted by Cheong et al. [125] looking at the attrition behaviour of glass spheres. It was concluded that the mean size of the fragment size distribution reduced with increasing impact velocity. The fragmentation regime and its relationship with respect to the angle of impact are summarised in Figure 2-8. A similar regime is given by Laarhoven et al. [61], shown in Figure 2-9.

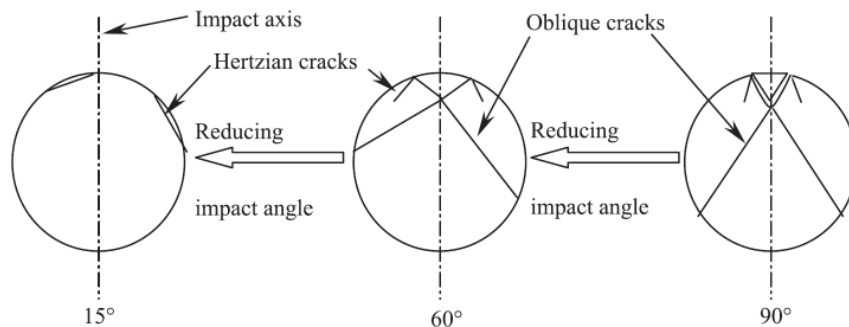


Figure 2-8: The influence of impact angle on the breakage mechanism of glass spheres as reported by Cheong et al. [125]


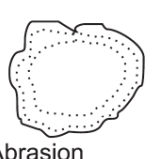
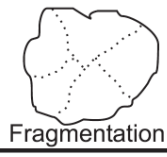

Magnitude	Direction	
	Normal	Tangential
Low force "Wear"	 Attrition	 Abrasion
High force "Fracture"	 Fragmentation	 Chipping

Figure 2-9: Influence of Impact Angle and Impact Force as Reported by Laarhoven et al.[61]

The influence of impact angle on soft agglomerate structures was studied by Samimi et al. [126]. In contrast to the commonly obtained result, it was found that these agglomerates suffered greater damage as the impact angle was reduced. It was concluded that this was due to the ductile nature of the materials, which were more sensitive to attrition by a shearing mechanism.

When studied numerically through the application of Discrete Element Method simulations, Moreno et al. [127] reported that the observed damage ratio increased with respect to both impact angle and impact velocity. The simulation contained particles representative of glass beads (in the form of an isotropic, spherical agglomerate) and a wall surface representative of steel. The damage ratio was defined as the ratio of broken interparticle contacts to the initial number of interparticle contacts within the unbroken particle. When the normal component of the impact velocity was held constant, the damage ratio was approximately constant, regardless of the impact angle. Furthermore, the number of fragments are reduced with reducing impact angle. Overall the magnitude of the normal velocity vector was found to be the most influential, with the tangential velocity vector influencing the size distribution of the child fragments. These findings were later supported experimentally by Samimi et al. [126], who also confirmed the importance of the particle mechanical response in the determination of the breakage characteristics, and sensitivity to tangential impact velocities. Namely, materials failing in a ductile regime, will be more sensitive to the shear loading experienced at shallow impact angles.

2.4.4.1.3 Strain Rate

Impact and quasi-static compression experiments have been used to compare the effects of strain rate on particle failure and crack propagation. Particles are typically well-defined in such studies, taking the form of spherical agglomerates or isotropic solids. Cheong et al. [125] conducted such an investigation into the breakage behaviour of glass spheres. The analysis of the results proceeded by equating critical loads required for initiation of a Hertzian cone crack. It was concluded that the impact velocity required to initiate a Hertzian crack (pictured in Figure 2-8) can be reasonably predicted through slow compression testing. According to Subero-Couroyer et al [128], Couroyer [129] had earlier found that for ceramic particles failing via a brittle mechanism, the breakage characteristic observed through impact could be correlated to quasi-static crushing.

The work of Schönert [120] also found that spheres and discs made of glass and poly(methyl methacrylate) (PMMA) exhibit the same failure scheme under both impact and compression loading. However, the strain rate was concluded to influence the material flow during loading, and therefore influence the stress field within the particle and the resulting crack pattern.

Chau et al. [130] compared compression tests performed under quasi-static and dynamic conditions with respect to the failure of plaster spheres of various concentrations. In the dynamic series of tests, the impact velocity varied between 1.349 to 2.485 m/s. The key finding from this study was that the contact force was larger in the quasi-static case, and the energy required for fracture was larger in the dynamic case.

The variation of material properties with respect to strain rate has been investigated through the application of microindentation testing of salt particles [85]. Absolute values of microhardness are dependent on the strain rate imposed by the indenter. This is due to the presence of material behaviours such as creep caused by a viscoplastic response. In this context, it is recommended to specify a strain rate across which materials can be quantitatively compared. This observation demonstrates that material failure can be sensitive to loading strain rate, and not only the magnitude of maximum load alone. This concept is supported by Reynolds et al. [3] and Iveson et al. [131], who explicitly state that the breakage of agglomerate particles are strain-rate dependant within the granulation context. Furthermore, Gorham et al. [132] concluded that PMMA spheres are

sensitive to the strain rate caused by an applied load, and this therefore dictates the particle failure mechanism.

In summary, the influence and significance of strain rate on the attrition mechanism for a given particle is fundamentally dependant on the particle material and the failure mode that is characteristic of that material.

2.4.4.2 Shear

Shear forces in lean phase pneumatic conveying are primarily attributed to particles sliding along the pipe around bends and the lower surface on straight sections. While this form of particle attrition is not expected to find direct relevance to lean phase pneumatic conveying systems, it is included here for completeness.

Ghadiri et al. [133] performed a number of shear experiments on porous silica catalyst carrier beads (spherical) at low normal stresses (25 and 50 kPa) with respect to attrition evolution within an annular shear cell. The theories of Ouwerkerk [134] and Neil and Bridgwater [135] were evaluated and modified, showing a good fit to high normal stresses, yet less-than-adequate fitting to low normal stress results. A potential reason for this observation was attributed to the presence of particle breakage and subsequent generation of smaller particles through the fragmentation process. With respect to the magnitude of fines generated by surface wear, this was deemed to increase constantly with the strain rate. It is worth noting that experiments using the annular shear cell stress particulate materials at very low strain rates – in the order of 1 RPM or 6.8 mm/s. Such strain rates may struggle to find similarity with the conditions within lean phase pneumatic conveying systems, where particle velocities are of the order of 25 m/s. Furthermore, it was suggested that the presence of fine particles in conjunction with coarse particles may reduce stress localisation within a particle bed, therefore reducing the overall rate of attrition.

Hare et al. [136] considered the attrition of pharmaceutical powders during the crystallisation process within agitated driers. The key findings from this work were the determination of relationships between the bed height and the relative strain rates imposed by an impeller. These results were then compared with experiments performed

in an annular shear cell. The difference in relative velocities may be sufficient to cause a shearing effect in a lean phase pneumatic conveying system. Whether the bed thickness reaches a sufficient depth around the bends in the pipe, remains to be seen.

As alluded to in the preceding section on attrition as a function of impact angle, sensitivity to shear stresses was used to explain the increasing particle attrition with decreasing impact angle. This was typical of materials failing predominantly through a ductile mechanism [126].

2.4.4.3 *Crushing*

Crushing is the application of a compressive load to a particle under quasi-static conditions. Quasi-static compression tests typically take a physical form similar to the Brazil Test, whereby two surfaces are brought together at low speed in order to apply a load to a specimen. This test methodology is the subject of a number of standards, particularly with respect to the analysis of catalytic particles such as in ASTM D6175 [137].

This approach to evaluating the particle strength of a given material is appropriate only to well-defined, regular particle geometries such as spheres or cylinders, as the crushing stress can be resolved [128]. Irregular particle shapes prove challenging for this test methodology as numerical methods are required to resolve the complex stress analysis or analytical considerations as in the case of Aman et al. [106].

Quasi-static compression loading using 12.7 mm diameter acrylic spheres has been conducted by Chaudhri [138], who described the development of stresses within the sphere and subsequent fracture patterns. Similar experiments were performed by Wu et al. [100] with 50, 60, and 75 mm diameter plaster spheres, Gorham et al. [132] with 8 mm diameter PMMA spheres, and Antonyuk et al. [78] using three types of spherical granulate materials (γ -Al₂O₃, Köstrolith, and sodium benzoate). Each material exhibited prominent meridional cracking, however the exact geometry of the fissures and the proportion of smaller fragments produced were specific to both the particle material and loading conditions.

The material used to form the surfaces applying the load to the particle is of equal importance in quasi-static testing. This was investigated by Shipway and Hutchings [139] who tested a range of surface materials broadly categorised into plastically deforming and elastically deforming behaviours. When a plastic surface was used to apply load, particle failure was initiated at the surface of the particle, whereas the use of elastic surfaces results in internal failure initiation of the particles by shear forces.

2.4.4.4 *Fatigue*

Fatigue is a phenomenon whereby particles undergo repetitive loading, and as a result, suffer strength reduction and catastrophic failure.

Goder et al. [140, 141] looked at a bed of narrow size range of particles, subjected to repeated compressions applied by a platen. The materials under scrutiny were classified as; brittle, high strength granulated, and ductile materials. Fatigue curves were generated for each of these materials with respect to the percentage of material passing through a specified sieve. Particle damage was generally found to increase with increased loading magnitude and number of compressive cycles. The ductile material was found to agglomerate under conditions of high compressive stress.

Through modification of Griffith's Theory of crack propagation, Han et al. [142, 143] proposed a model for prediction of particle failure by repeated compressive loading. The ratio of fatigue compressive strength (P_m') of a particle to the compressive strength (P_m) of the original particle was defined as in Equation (2-6); where σ^* and P^* are dimensionless numbers, N is the number of compression cycles, and P_1 , P_2 , and P_3 are dimensionless groups whose definition may be found in Han et al. [142]. The results of this analysis correlated well with NaCl and MgO crystals, and with granulated fertiliser particles. In a later publication, Han et al. [144] extend this theory to impact loading with deviations of up to 25%.

$$\frac{P'_m}{P_m} = \sigma^{*3} = \left\{ 1 + \frac{P_1}{\exp [P_3 - P_2(P^*)^{1/3}]^2} \right\}^{-3/2N} \quad (2-6)$$

This model was later modified by Rozenblat et al. [145] in order to discretise for loading magnitude. In order to achieve this, the calculation method was modified to define particle strength in terms of crushing force instead of stress. Application of this model to experimental results showed good correlation, however only Dead Sea salt crystals were considered.

A broad study looking at the fatigue failure of the same three materials used by Han et al. [142], was reported by Kalman et al. [63] across four different impact tests. Fatigue curves were presented and correlation across each of the impact methods was demonstrated. General trends in the results supported the vast majority of current research in that particle damage increases with increasing impact velocity and increasing the number of impact cycles.

Tavares and King [146] applied damage mechanics concepts to particle fatigue by impact loading. Through the use of the Ultrafast Load Cell (UFLC) impact tester, they developed Equation (2-7), which describes the amount of damage sustained (D_n^*) by the particle in the n th impact; where γ is the damage accumulation constant, $E_{k,n}$ is the kinetic energy of the striker at the n th impact per unit mass of the particle, and E_{n-1} is the energy required to completely disintegrate the particle per unit mass of the particle in the previous event. This method requires the calibration of a single factor, γ , from experimental data and found excellent correlation with experimental results.

$$D_n^* = \left[\frac{2\gamma}{(2\gamma - 5D_n^* + 5)} \frac{E_{k,n}}{E_{n-1}} \right]^{\frac{2\gamma}{5}} \quad (2-7)$$

In a further study Tavares [147] resolves the significance of the only empirical factor in the model, γ , to be independent of particle shape, and weakly dependant on particle size within the range tested. Additionally, the model was successfully applied to results

obtained from gas-blast apparatus testing, and therefore not specific to the particle stressing mode.

2.4.5 Experimental Techniques for Measuring Particle Attrition

All experimental tests with respect to particle attrition may be broadly categorised into one of two groups: single-particle, and multi-particle tests. Single particle tests enable the study of particle behaviour under closely controlled, well-defined conditions in order to investigate the fundamental particle behaviour. The drawback of single-particle testing, is that the test conditions are often difficult to correlate with the conditions present in industrial processes. Multi-particle experimentation is the vice-versa of this situation. While the loading conditions experienced by each particle are not known (discounting numerical simulations), the conditions the material is subjected to can be more easily correlated with industrial processes, and it is more time efficient to obtain statistically relevant results.

The experimental approach specific to impact testing can be broadly grouped into two areas;

Impacting a particle with a rigid surface and include:

1. Gas-Blast Tester: See Section 2.4.5.1 for description.
2. Centrifugal Accelerator: See Section 2.4.5.2 for description.
3. Drop Test: particles are allowed to fall under the influence of gravity to impact on a surface or bed of material. This can be achieved through dropping individual particles, or a flexible bag filled with particles. This method has the drawback that the highest impact velocity achievable is the terminal velocity of the sample. Additionally, sufficient head room is required to accelerate the sample.
4. Rotating Arm Test: A particle stream is dropped under the influence of gravity into the path of an array of targets attached to a rotating disc. Close control of impact velocity and angle is achieved, however the particles must be decelerated without inflicting further attrition on the sample. Additionally, there is the potential for high local air speeds generated by the rotating targets. In order to minimise the

influence of this on the particle trajectory, the air in the impact chamber should be evacuated.

5. **Tumbling Box Test:** A sample of particles are placed in a box, which is then closed and rotated about a single axis. This method is typically used for pelletised materials. The degraded material is then sieved, with the passing material being classified as fines.
6. **Oscillating Box:** Using a sample size of approximately 100-200 particles, the sample is placed in a box and oscillated along the vertical axis for a specified number of repetitions. The impact velocity of the particles is adjusted by changing the amplitude of the oscillation (distance travelled throughout one oscillation), and the frequency is maintained at a pre-set value. Once the test is complete, the sample is sieved using a sieve with aperture size equal to half of the original particle diameter. The advantages of this test device include the ability to perform a large number of impacts with relative ease. However a drawback is that the impact velocity is limited (a value of 4.1 m/s was reported [61]).
7. **Resonate Cantilever Impactor:** A cantilevered beam is mounted on a sieve shaker, and supports a closed vessel at the other end containing 6-8 particles. The sieve shaker enables vertical oscillation of the vessel with amplitudes ranging from 0.5 to 8 mm and frequencies of approximately 0-1000 Hz. As with Method 6, a large number of impacts can be tested efficiently, however only a small number of particles can be tested at a time.

Crushing a particle between a hammer and anvil made from a rigid material and include:

8. **Swing Pendulum Tester:** See Section 2.4.5.4.1 for description.
9. **Double Impact Tester:** See Section 2.4.5.4.2 for description.

As the particle-wall impact mechanism is expected to dominate in lean phase pneumatic conveying systems, test methods without secondary applied loads (such as those applied by other particles) shall be further examined. The gas blast tester, centrifugal accelerator and static particle tests have been used across several studies and shall be examined in further detail.

2.4.5.1 Gas Blast Tester

The Gas Blast Tester consists of a compressed air flow to which particles are introduced and accelerated along a straight channel. Upon exit of this channel, the particle impacts a hard surface placed in the air stream. This test method is the subject of ASTM G76 – 13 [148] and was that of DIN 50 332 (Withdrawn) [149] which offer guidance on the methodology of the test. As illustrated by Figure 2-10, many arrangements can be utilised in terms of mixing the particulate and gas flows, and extracting impact data.

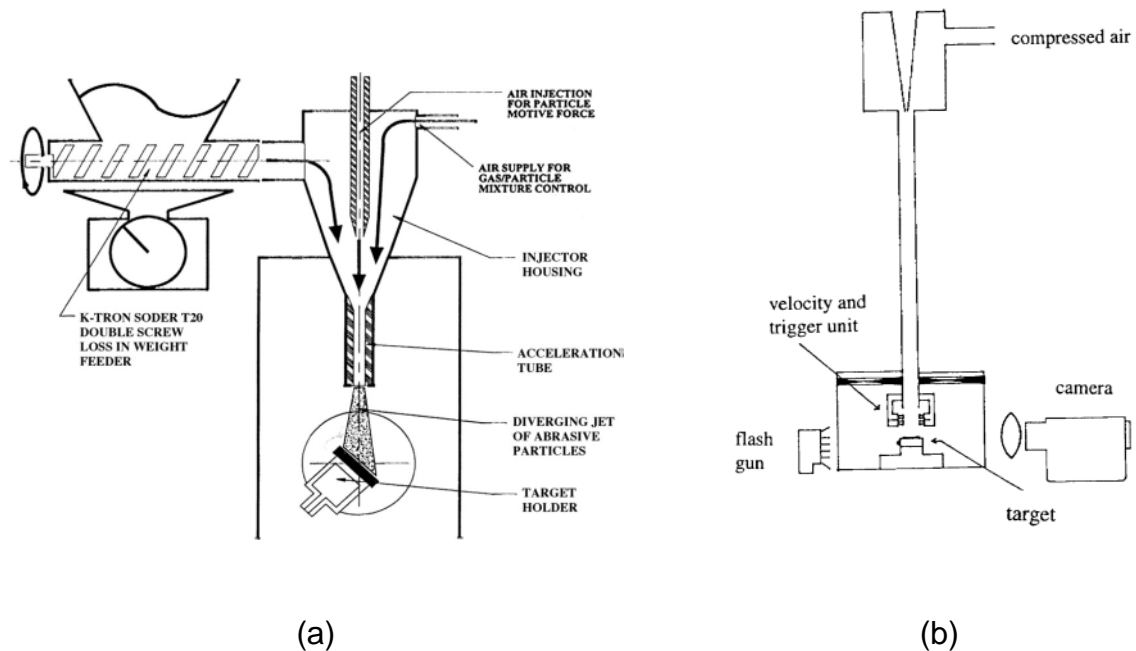


Figure 2-10: Gas Blast Tester as Investigated by: (a) Deng et al. [150]; (b) Zhang and Ghadiri [104]

Shipway and Hutchings [151] investigated the influence of the roughness of the air-particle outlet nozzle on the impact conditions within a gas-blast erosion tester. They found that the roughness of the nozzle bore had a significant influence on the velocity and trajectory of the ejected particles. The characteristics of this analysis are also dependant on the nature of the ejected particles. Generally, the rougher the nozzle bore, the lower the ejected particle velocity and wider the resultant particle stream, for a given air flow rate. Another study by the same authors looked at the influence of the target

material [139]. Ductile and elastic target materials were found to yield different crack initiation locations within lead glass spheres of $(700 \pm 50) \mu\text{m}$.

2.4.5.2 Centrifugal Accelerator

The centrifugal accelerator apparatus has been widely used for erosion studies and was the subject of the former Soviet Union Standard, GOST 23.201-78 [152]. This apparatus has more recently been used for the evaluation of particle attrition by impact [153] and comprised a rotating disc that contained a number of radial tubes. The disc was surrounded by an array of targets. The particulate samples were fed into the centre of the rotating disc and radially accelerated via the tubes and impacted against the target array. Figure 2-11 shows a schematic of such an apparatus.

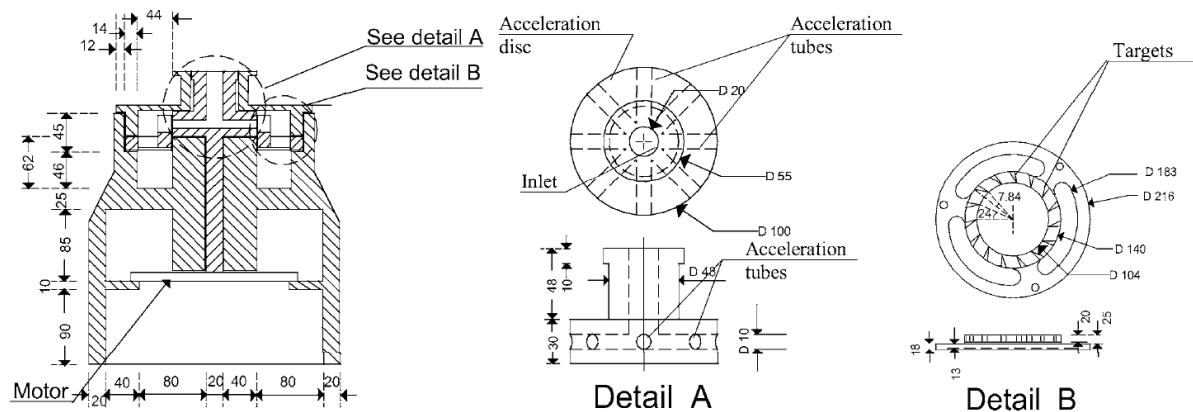


Figure 2-11: Centrifugal Impact Tester as Investigated by Chapelle et al. [154]

Burnett et al. [155] analysed the results obtained from a centrifugal accelerator test apparatus and the subsequent variations within are discussed in depth within the context of erosion. Here, the effect of particle spin was addressed, imparted by the method of acceleration within the test device. Angling the targets about the horizontal axis was suggested as a method in which to reduce the effects of particle spin on the impact (and hence particle loading) mechanics. Deng et al. [35], modelled the particle velocity vector at the outlet of the disc tube. The particle shape was found to influence the particle's tendency to spin on ejection from the disc tube, and below a specified shape angle, pure

sliding was expected along the tube wall. The effects due to aerodynamic drag were deemed negligible.

2.4.5.3 Comparison of Impact Testers

A comparison of the gas blast tester and the centrifugal accelerator tester was conducted by Burnett et al. [156] and Deng et al. [150]. Particulate materials included two ceramics, one metallic, one elastomeric and one polymeric material, representing a wide range of material categories and behaviours with respect to erosion of the target material. With regard to the operational capacity of each apparatus (the operational parameters relevant for use in particle attrition studies), the conclusions of this study are summarised.

With regard to the gas blast tester:

- The identification of steady-state operation and particle impact velocity are difficult to define
- The range of particle concentrations that can be achieved are limited
- Greater particle stream divergence is observed in comparison to the centrifugal tester

With regard to the centrifugal tester:

- Determination of particle impact velocity is straightforward
- Particle-gas interactions are lower than those of the gas-blast tester
- Steady state conditions are more readily defined
- The spread of particle velocities for a given particle size range is smaller

2.4.5.4 Static Particle Tests

The kinetic tests (Methods 7 and 8) where a hammer impacts a static particle at a specified velocity, have been widely studied (see Table 2-2, Section 2.4.5.5). The quasi-static form of the test is addressed in Section 2.4.4.3. Figure 2-12a and b show examples of the Swing Pendulum Test and the Double Impact Test respectively.

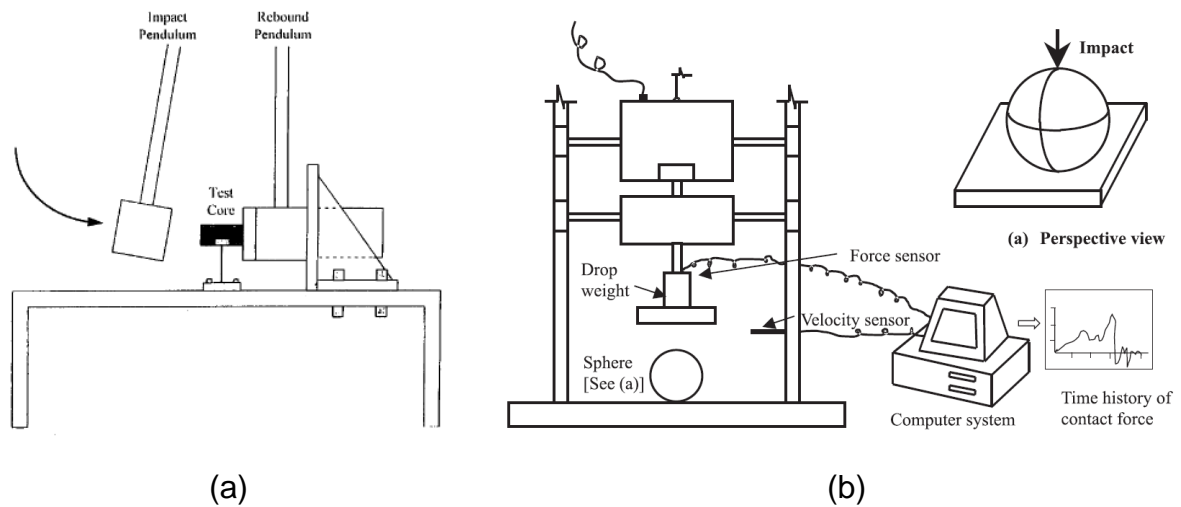


Figure 2-12: Examples of the Swing Pendulum Tester [157] and the Double Impact Tester [130]

2.4.5.4.1 Swing Pendulum Tester

Weedon and Wilson [158], and Sahoo et al. [159] utilised a twin pendulum apparatus to evaluate the degradation of iron ore and coal respectively. In both cases a spherical hammer was used to degrade particles, and the former of these two studies proposes a semi-empirical model to predict fines generation as a result of dropping material from heights during handling processes. A further publication from Sahoo et al [160] modifies this model for application to the prior study on coal. Upon inspection of the approach undertaken by these studies, it is evident that a significant number of particles must be studied in order to define the material-specific model best suited to the material. Furthermore, the methodology demands particles of sufficient size with respect to the measurement resolution in order for the test to be successful. The pendulum test is, however, capable of measuring the energy associated with particle breakage [161].

2.4.5.4.2 Double Impact Test

Krogh [162] investigated the influence of the impact velocity of the hammer dropped onto the particle sample within a double-impact tester. The analysis progressed by defined by three attrition functions:

- Crushing probability function
- Energy function
- Breakage function

These three functions account of the strength distribution of the particle sample, the strength of the particles with respect to their size, and the subsequent size distribution of the resulting fragments respectively. It was found that the velocity of the hammer did not noticeably influence the attrition behaviour of the particle; rather the impact energy (modified by changing the mass of the hammer) was determined to be the defining variable.

Tavares and King have published a number of works in which the data collected from a modified double impact test was used [146, 163–165]. The Ultrafast Load Cell (UFLC) (see Figure 2-13), was a hybrid design between a double impact tester and a split Hopkinson Bar, capable of measuring the applied force to a resolution of 0.2 N, with a time step of 100 ns. Evaluation of particle fracture energy and the influence of material structure was achieved. From a fundamental fracture mechanics perspective, this apparatus is potentially the best equipped for particle failure analysis. However, the requirement of testing particles individually limits the size range of interest and may not conform to user time constraints.

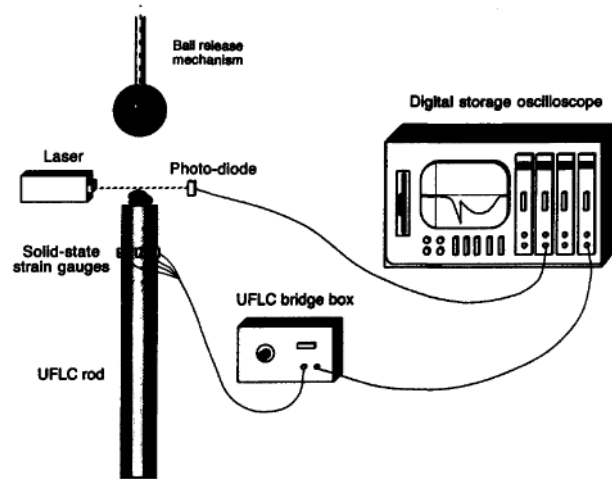


Figure 2-13 :The Ultrafast Load Cell [164]

2.4.5.5 Summary of Particle Attrition Testers

Table 2-2 presents a summary of each of the particle attrition testers considered in this review. While each of the testers referenced from other works were not necessarily considered within the context of lean phase pneumatic conveying systems, the entire range is included for completeness and quick comparison for the reader.

Table 2-2: Summary of Particle Attrition Testers

Tester	Operating Variables					Notes	Studies Used
	Impact Velocity/Strain Rate Control	Impact Angle Control	Level of Inter-Particle Interaction	Secondary Impact Velocity	Feed Rate Control		
Gas Blast Tester	**	***	Low	Medium	***	Variations in velocity profile are difficult to closely control. Particle stream divergence greater than centrifugal accelerator.	[9, 101, 117, 126, 166]
Centrifugal Accelerator	***	***	Low	Medium	***	Close control over impact velocity and impact angle. Secondary impacts require mitigation.	[154, 167–169]

Drop Test	*	***	Variable	Low	***	Impact velocity limited to particle terminal velocity. Considerable head-room requirement.	[170]
Rotating Arm Test	**	***	Low	High	***	Particles are accelerated by impact with the target requiring careful consideration of how to mitigate secondary impacts.	[171]
Tumbling Box Test	*	-	High	-	-	Low impact velocities coupled with limited control of impact conditions.	[87, 172]
Oscillating Box Test	*	-	High	-	-	Low impact velocities coupled with limited control of impact conditions, however has the potential to inflict more impacts normal to the wall than the tumbling box test.	[61, 173]
Resonate Cantilever Impactor	***	-	High	-	-	Limited control of impact conditions. Offers the ability to apply a large number of particle loading events in a relatively short amount of time.	[174]
Swing Pendulum Tester	***	-	None	-	-	Single particle test that requires a significant number of experiments in order to characterise a material. Close control of loading condition.	[157]

Double Impact Tester	***	-	None	-	-	Single particle test that requires a significant number of experiments in order to characterise a material. Close control of loading condition.	[100, 147, 162]
Annular Shear Cell	***	-	High	-	-	Applicable only for the characterisation of particle failure under shear loading conditions.	[133–136]
Quasi Static Crushing	***	-	None	-	-	Single particle test that requires a significant number of experiments in order to characterise a material. Close control of loading condition.	[78, 100, 106, 128, 132, 138, 139]

*** High Level of Control

** Medium Level of Control

* Low Level of Control

- Not Applicable

2.4.6 Concluding Remarks on the Material Factor

Some conflicts exist in the research. One such conflict is with respect to the influence of strain rate on particle attrition behaviour. This may, in part, be attributed to the conditions specific to each study. For isotropic materials failing in a brittle manner, it may be stated with reasonable confidence that the results between quasi-static compression testing and impact testing at low velocity are comparable. Once the impact velocity exceeds that of the elastic wave speed of the material, then this statement loses its applicability [139]. It is therefore important that within the context of lean phase pneumatic conveying, that this relationship is fully explored.

As has been demonstrated throughout the literature, the combination of particulate material, particulate structure and subjected loading conditions dictate the form of particle failure exhibited. These failure mechanisms are diverse in nature, and result in a variety of particle size distributions specific to each mechanism. When considering particle attrition in lean phase pneumatic conveying systems, it is important to consider the full spectrum of particle properties and loading scenarios. As has been demonstrated, different materials are more sensitive to specific loading scenarios, and any approach adopted in quantifying this behaviour requires sufficient flexibility to account for these. It is therefore imperative that experimental attrition testing be completed for each material whose behaviour is to be described.

When selecting a test method by which to characterise particle attrition behaviour, it is vital that the method be representative of the scenario for which the attrition behaviour is to be explain. For example, within lean phase pneumatic conveying systems, particles should be tested within a high-velocity impact regime, with the potential to supplement this information with other testing approaches. It should be noted that many methods of particle characterisation have been presented in the literature, however little standardisation has been adopted with respect to tester geometry or the associated attrition indices [140].

2.5 Modelling of Particle Attrition in Lean Phase Pneumatic Conveying

Studies conducted specifically into particle attrition within pneumatic conveying systems will be reviewed in this section. Works are arranged primarily by the nature of the work (whether derived from first principles, or through empirical modelling), and then chronologically by research group.

2.5.1 Numerical Modelling Approaches

Modelling approaches which draw on fundamental physical mechanics in order to describe the particulate flow and subsequent occurrence of particle attrition will be reviewed here. While numerical modelling methods are not within the core scope of the current research, the results from the studies acknowledged in this section provide valuable insight into particle attrition mechanisms. Attention shall be given primarily to the particle breakage model used.

Han et al. [62]

Han et al. [62] applied a two-dimensional Discrete Element Method (DEM) coupled with Computational Fluid Dynamics (CFD) model to simulate the results published by Bell et al. [175] and Jacobs [176]. The Navier-Stokes equations were used in conjunction with the models presented by Papadopoulos et al. [177], to describe the air flow and particle attrition behaviour respectively. A number of simplifying assumptions were also made: idealisation of particle shape to spherical geometry, particles smaller than 0.1 mm are disregarded, and two-dimensional flow. Dilute phase pneumatic conveying was confirmed with a void fraction of 0.8 or higher. The simulations were conducted within a 2D channel: three straight sections (12, 4.8, and 9.6 m respectively) connected by 0.35 m radius bends with a height of 8 cm. Solids loading ratios of 1 and 4.5 were used. The reduction ratio describes the ratio of the surface area of the particles before and after the test and was the attrition criteria used. The simulated results were comparable to the experimental data of Bell et al., however,

under-prediction of particle attrition was observed with increasing numbers of passes through the system. This was attributed to the lack of a fatigue function within the breakage calculations, limitations of assuming a two-dimensional flow (as opposed to a three-dimensional flow), and use of different initial particle size distributions. Increasing the solids loading ratio was found to reduce particle attrition on a qualitative basis.

Hanley [178] and Hanley et al. [6, 113, 179]

The doctoral work presented by Hanley [178] produced two models to describe particle attrition: the first was a discrete element model of a single particle, and the second described the breakage of a particulate population using statistical methods. The investigation utilised quasi-static compression testing of individual particles, and trials in a pneumatic conveying rig (Figure 2-14). Superficial air velocities up to 20 m/s were considered along with a range of conveying pipeline geometries. Particle fatigue and inter-particle collisions were not accounted for as sources of particle damage.

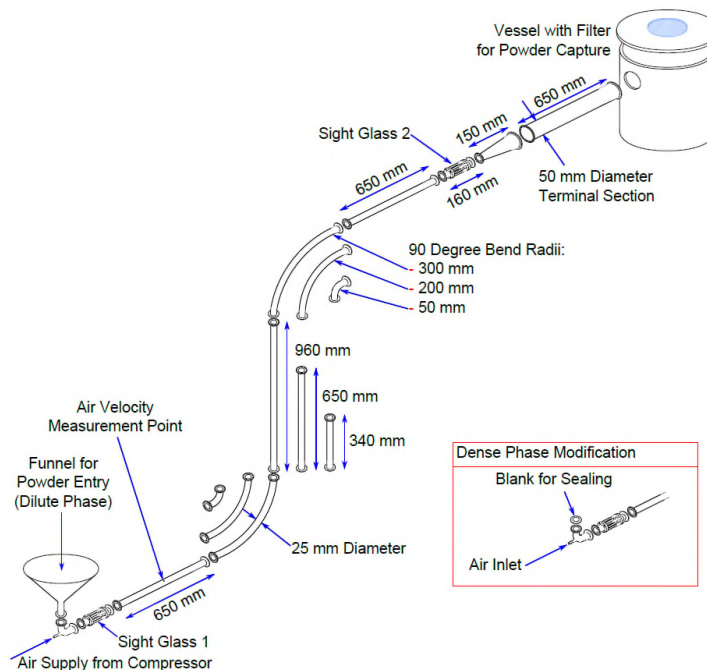


Figure 2-14: Pneumatic Conveying Rig used by Hanley [178]

In another investigation, the variation in bulk density of infant formula through pneumatic conveying was presented by Hanley et al. [6]. This variation of bulk density was attributed to the breakage of particles through such processes. The Taguchi Method of experimental design [180] and ANOVA analysis [181] of the experimental results were utilised, in addition to the generation of polymeric models and subsequent analysis. It was concluded that the mode of conveying (dense/lean phase), air velocity and number of passes (particle fatigue), were all statistically significant factors with respect to variation of the bulk density of the material. It should be noted however, that particle concentration was tested over a narrow range for dilute phase pneumatic conveying (mass flow rates 1-3 g/s) and therefore may not have captured the full spectrum of attrition behaviours.

Particle impact at pipeline bends within lean phase pneumatic conveying systems was described stochastically by Hanley et al. [113]. Through the use of a Weibull distribution to describe the initial particle strength distribution, a uniform particle distribution at the pipe inlet, and assuming a single impact within a pneumatic conveying bend, the breakage probability of agglomerate particles was reported. The fluid flow was described by a model presented in a companion paper [179]. These results were compared with Monte Carlo Simulations, and the mean of the impact angle compared well, although a discrepancy of 20 % was reported for the standard deviations.

Brosh et al. [182–184]

Brosh et al. [182] addressed the challenges relating to spawning child particles in the scenario where a mother particle is fractured. These challenges were specified as the allocation of initial conditions for each of the new child particles, and the subsequent interaction of these particles. The model developed in this paper was able to accept the use of any breakage function, and unlimited specification of resulting fragment size fractions. The model was applied to a jet milling process with reasonable correlation.

The above model was then applied [183] in the context of pneumatic conveying. The overall method of predicting particle breakage used in this simulation was composed of four sub-functions (comminution probability functions) as suggested by Kalman et

al. [185]: initial strength distribution, equivalence/selection, fatigue, and breakage functions. Combined with a 3D CFD-DEM model, particle attrition was predicted for potash within a pneumatic conveying line containing four blind-T bends. The results were compared to experimental data, and it was found that the model over-predicted the degree of attrition occurring in the pipeline. Subsequently, methods for accelerating such simulations are presented [184], and include approaches such as the construction of a DEM grid, in which the empty cells were disregarded. Additionally, a sub-DEM grid was constructed for comminution calculations and with the same approach, the calculation could be further accelerated. Stiffness reduction of the smallest particles (or total removal of the smallest particles from the simulation) was also found to improve calculation speed, as the time step could be increased.

Uzi et al. [38]

Uzi et al. [38] presented a model of particle attrition within pneumatic conveying systems that adopted the two-phase flow model of Levy et al. [186] and the probability comminution functions of Kalman et al. [185], and subsequently applied a new one-dimensional breakage algorithm to describe the breakage behaviour. Particle collision data was obtained through CFD-DEM analysis to inform the model. A known particle size distribution at the inlet of the pipeline was used, and by selecting a 'tracking mass', progressively calculated the changes in the size distribution along the pipe length. The pipeline was divided into elements, and a collision detection algorithm was used in each element. Impact conditions were compared with the strength of the particle (obtained from empirical analysis). If the particle strength was insufficient to withstand the collision, child particles were generated, however, if the particle was able to withstand the collision, a fatigue algorithm was employed for particle strength reduction. A block diagram describing the model is shown in Figure 2-15. Validation of the model was performed through comparison with the results obtained by Kalman et al. [63] and an absolute deviation was found to be 5.8 % on average. Furthermore, particle-particle interactions were found to have significant influence on the results, especially in the bends of the pipeline.

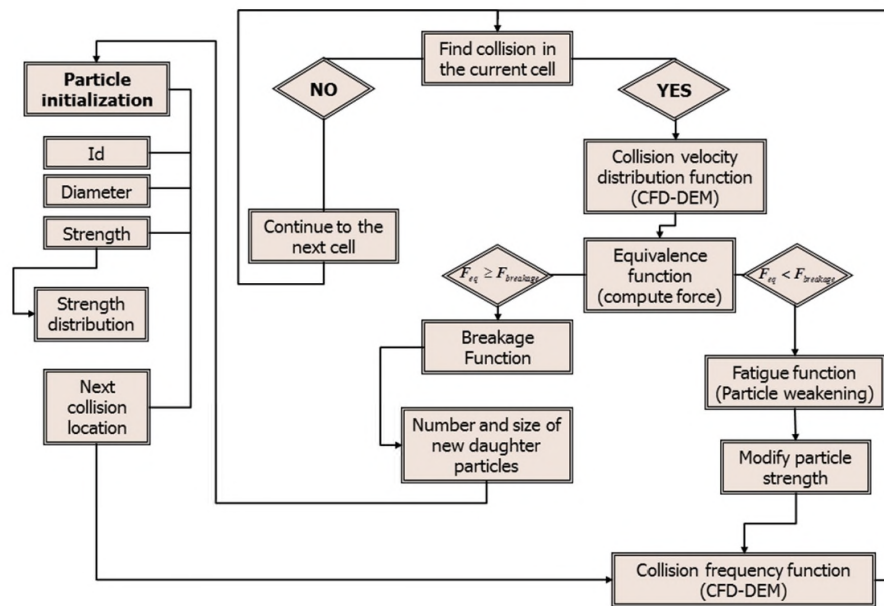


Figure 2-15: Block Diagram of the One-Dimensional Breakage Algorithm as described by Uzi et al. [38]

2.5.2 Empirical Modelling Approaches

Empirical approaches to modelling particle attrition within lean phase pneumatic conveying systems are considered to be those which employ a data-fitting model. Presented here are a selection of key studies, organised by research group and year.

Salman [9]

Salman et al. [9] proposed a model for predicting the particle breakage characteristics during lean-phase pneumatic conveying, combining a particle trajectory model [187] with empirically-derived breakage relationships. This study focused on single-particle impacts across a range of particle sizes, impact angle, mean transportation velocities, and fatigue behaviour. Two testers were used to obtain the experimental results; the first tester was similar to that of a gas blast tester, and the second consisted of a pneumatic conveying line with a single bend. Breakage data was collected in the 'gas blast' tester through manual examination of the tested particles under known conditions, and each of the data points was represented by the average of 100 test particles. Particles were classed as 'broken' or 'unbroken'. A two-parameter Weibull distribution was fitted to the test data as shown in Equation (2-8), where N_o is the

number of unbroken particles, C_p is the particle impact velocity, and c and m are curve fit parameters.

$$N_o = 100e^{-\left(\frac{C_p}{c}\right)^m} \quad (2-8)$$

It was found that there exists an impact velocity below which no particle attrition occurs. The conclusions are based on particles of a near-spherical geometry. The necessary acceleration length as reported by other researchers varies from 4-5 m to 6.5 – 9.3 [24, 56], and the longest acceleration length in this research is 4.5 m. This implies that there is scope for further validation with industrial pneumatic conveying systems.

Aked et al. [188], Kalman and Goder [10], and Kalman [4, 5]

Aked et al. [188] looked at the conveying behaviours of five different pneumatic conveying bend types with respect to pressure drop, particle attrition, and material build-up on the pipe walls. The study concluded that the observed particle attrition increased with increasing superficial air velocity, and decreased with increasing solids mass flow rate. These findings support the concept that particle shielding occurs at higher particle concentrations.

Kalman and Goder [10] applied the failure design theory for machine parts, to particle attrition behaviour. Single and multi-particle tests were considered across impact, compression and fatigue loading conditions. Experimentation was conducted through a 0.7 inch, 6 m pneumatic conveying line that contained 6 bends. General findings were that particle attrition increased with increased number of loading cycles and increased superficial air velocity. A long radius flexible bend was found to inflict the lowest attrition rates on the potassium sulphate used in this work.

Kalman [4] considers the attrition mechanism within the context of controlling attrition levels through pneumatic conveying systems. It was concluded that by applying vibrations to a pneumatic conveying line with turbulence drums for directional

changes, the measured degree of particle attrition could be reduced. Kalman [5] subsequently considers four different pneumatic conveying arrangements with various pipeline and bend geometries. It was demonstrated that the screw feeder used in two of the four testers generated more attrition than the pneumatic conveying line for particles larger than 3000 μm in diameter. For particles smaller than 1000 μm in diameter, it was found that less than 5% of the total attrition caused by the pneumatic conveying system could be attributed to the screw feeder. Such results indicate that particle size is of key importance when determining the level of article breakage attributed to a screw feeder, and subsequently, pneumatic conveying systems incorporating these feeders. Such observations could be attributed to the grinding that takes place between the flights of the screw and the screw conveyor casing. When the particle diameter is of the same order of magnitude as the clearance between the screw flights and casing, the relative motion of the surfaces could apply significant loads on the particle, leading to attrition.

Attrition caused by a cyclone separator was found to be up to 20% of the total attrition occurring within the system. Particle attrition was found to decrease with increased solids loading ratio. Whilst only qualitative observation is presented, results are in support of previous works, and the diverse range of materials tested demonstrate the variable nature of particle attrition within such systems.

Bridle [26]

Bridle [26] presents a study specific to particle attrition in lean phase pneumatic conveying. A bespoke single bend pneumatic conveying test line was designed and constructed (Figure 2-16), and the modification of an existing full-scale pneumatic conveying line was carried out. Three particulate materials were tested: sugar, malted barley, and basmati rice. The conveying conditions investigated in the single bend apparatus, along with their values are summarised in Table 2-3.

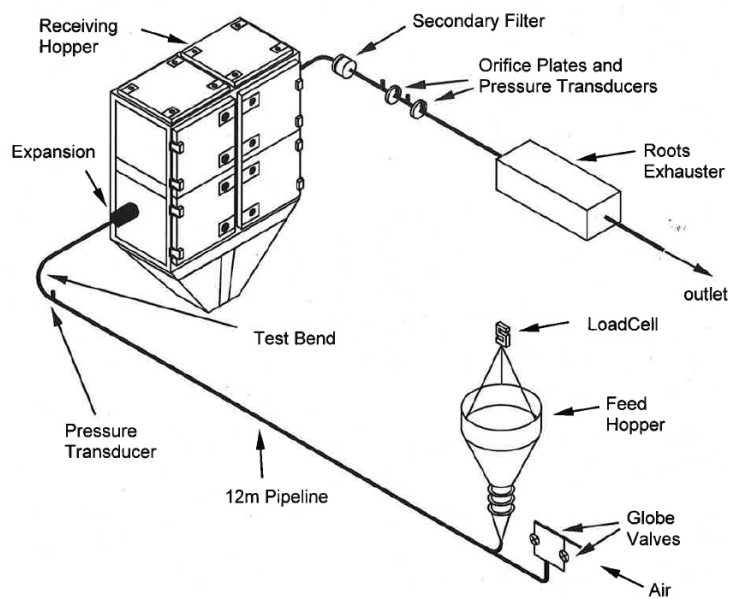


Figure 2-16: The Single Bend Test Apparatus as used by Bridle [26]

Table 2-3: Variables and associated values tested by Bridle [26] in the Single Bend Pneumatic Conveyor

Conveying Variable	Values Tested
Bend geometry (R/d)	0 (Blind T), 3.6, 13
Superficial air velocity (m/s)	9, 16, 22, 26, 30, 34, and 38
Suspension density (kg/m ³)	5, 12, 23, 35, and 60

In order to simulate the conveying conditions in the full scale pneumatic conveying pipeline, the single bend test apparatus was used to replicate these conditions using only the short radius ($R/d = 3.6$) bends. The amount of degradation observed in the single bend test facility was approximately double that measured in the full scale conveying system. The measurement criteria used for the comparison was the percentage fines generated below $300 \mu\text{m}$ for sugar, percentage fines generated below $1200 \mu\text{m}$ for barley and percentage of broken grains for the rice. A methodology is presented where a linear relationship between the magnitude of degradation observed in the single bend apparatus and the magnitude of degradation in the full scale conveying line is empirically calibrated. This method was demonstrated to give differences of up to 40%, with data variances of up to 20%. This work also forms the foundation of Bridle et al. [189].

Frye and Peukert [15, 190–192]

This work was the subject of four publications, and focused on the study of the attrition behaviour of various polymers within lean phase pneumatic conveying systems. Two functions were used throughout the course of the research in order to define the attributes responsible for particle attrition: a process function, and a material function. The process function describes the loading conditions to which the particles are subjected, and the material function describes the reactive behaviour of the particles to these loading conditions.

Frye and Peukert [190, 191] use an Euler-Lagrange approach to predict the loading conditions that the particles are expected to be subjected to. The material function was then evaluated through conducting tests with a centrifugal impact tester and a modified pin-on-disc tribometer, resolving the material response to impact and sliding friction respectively. For the polymers under inspection, sliding friction was deemed to play a more significant role in the attrition of these particles than what has been previously reported in literature.

Subsequently, Frye and Peukert [192] numerically derived stress conditions and used them in conjunction with data from both of the previously mentioned test apparatuses. The results were compared with results obtained from a single test bend pneumatic conveying line apparatus. A significant variety of polymeric materials were tested in this work. Dynamic mechanical analysis (DMA), a technique whereby a pre-prepared sample of the material is cantilevered with a clamp and sinusoidally oscillated, was applied to each test material. It was concluded that the glass transition temperature of the material was of critical importance.

The final piece of research [15] that forms this series of work, follows on from the previous publications, and finds that the attrition of different polymeric materials is more closely resembled by different attrition mechanisms.

Abou-Chakra et al. [193] and Chapelle et al. [43, 154, 194]

Abou-Chakra et al. [193] applied the particle dynamics theory presented by Deng et al. [35] to a bench scale centrifugal attrition tester. Two crystalline materials were tested; using 10 g samples with two repetitions at each test condition. Experimental errors were reported to be below 3%. As the impact velocity and impact angle were increased, the level of attrition was also observed to increase. To validate these results, the apparatus of Bridle [26] was used to determine the level of attrition caused by a single bend in a pneumatic conveying line. Good correlation was found at high impact velocities/conveying speeds.

This centrifugal attrition tester then formed the basis of another piece of work by Chapelle et al. [154], which presents a degradation model for particles subjected to lean-phase pneumatic conveying. This model utilises a breakage matrix approach drawing from population balance theory and is given in Equation (2-9). Where $[B]$ is the empirically-obtained breakage matrix, $\{i\}$ is the input particle size distribution going into the bend, and $\{o\}$ is the output particle size distribution going out of the bend. The latter two of these terms are defined by column matrices. A polynomial interpolation procedure is also presented for intermediate test conditions. Only impact angles of 90° to the surface of the target were considered. The breakage matrix is an upper or lower triangle matrix, whereby the main diagonal describes the amount of material removed from each size fraction. The remainder of the elements describe the amount of material entering each size fraction from each fraction larger than itself.

$$[B] \cdot \{i\} = \{o\} \quad (2-9)$$

Validation was presented in [194], where the degradation model was coupled with a two-phase flow model. The flow model specifies two regimes: strand flow, and fully-suspended flow. The model used for the strand flow was based on that presented by Bradley et al. [25], and the calculation progresses numerically along the pipeline which was divided into 'elements'. The concept of a 'harmonic mean size' of a particle size distribution was presented, as defined by Equation (2-10); where X_h is the harmonic mean particle size, w_i is the fraction of material retained on a given sieve size, and d_i

is the mean size of the size fraction correlating to w_i . The results of this model were compared against experimental results from both a single-bend pneumatic conveying laboratory test rig, and an industrial lean-phase pneumatic conveying pipeline. Good agreement was obtained between predicted and experimental results. Two different particle concentrations and air inlet velocities were considered.

$$\frac{1}{X_h} = \sum \frac{w_i}{d_i} \quad (2-10)$$

The final paper publication from Chapelle et al. [43] applies this degradation and flow model to two more industrial case studies. Both find good agreement with the experimental results.

Pitchumani et al. [173] and Laarhoven et al. [61]

A new particle attrition tester was developed by Pitchumani et al. [173] (operation principle identical to that presented in Figure 2-17, and used to study the attrition of sodium benzoate. They mapped the specific rate of breakage against oscillation frequency and amplitude. Specific rate of breakage was found to increase with increasing oscillation frequency and amplitude; however this increase was only linear at high values of these operating variables. It was also concluded that the number of particles in the test chamber significantly influenced the results due to the dispersion of particle kinetic energy through inter-particle collisions.

Through continued development of a new particle attrition tester (Figure 2-17) and subsequent validation with a lean phase pneumatic conveying system, Laarhoven et al. [61] were able to correlate breakage patterns between the two loading methods for two types of fertiliser granule. A significant discrepancy between the two loading methods was that of impact velocity, which was accounted for by increasing the number of loading events. The mass specific kinetic energy was comparable across both systems for sodium benzoate granules where surface attrition dominated, up to a threshold of approximately 7 kJ/kg. Above this value, the results diverged. For

scenarios where attrition occurred by particle fragmentation, no such correlation could be achieved.

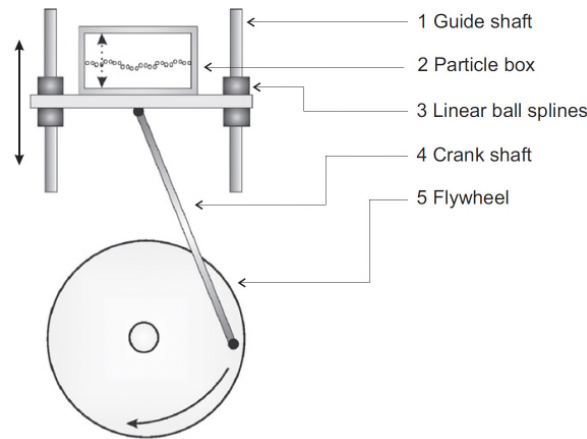


Figure 2-17: Particle Attrition Tester as used by Laarhoven et al.[61]

Macchini et al. [41]

Macchini et al. [41] considered the effect of particle size, density and concentration on the erosive wear caused to pipe bends in lean phase pneumatic conveying systems. While the particle attrition characteristics were not specifically investigated, as previously mentioned, pipe erosion and particle attrition are considered to be closely related as they are both results of the same impact event. The series of experiments used a full scale pneumatic conveying line with an insert in the test bend of interest (Figure 2-18), which could be removed for analysis. The key findings from this study were that increasing particle density was found to increase the magnitude of particle attrition mitigation to a greater degree, than increasing the particle size. In essence, the amount of 'shielding' observed is more sensitive to changes in particle density, than changes in particle size. When compared to the results from a centrifugal erosion tester, the erosion observed in the pneumatic conveying line was found to be smaller. Therefore, a greater shielding effect was concluded to exist in the conveying line.

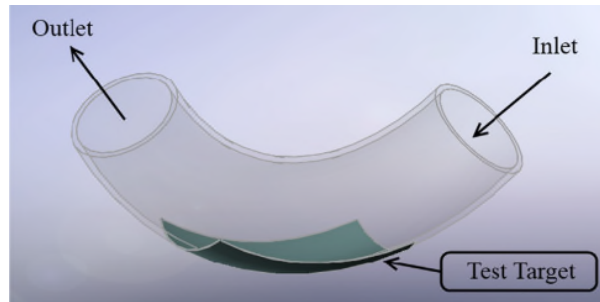


Figure 2-18: Test Bend used by Macchini et al. [41]

2.5.3 Concluding Remarks on Modelling Approaches

Through review of previous studies into particle attrition within lean phase pneumatic conveying systems, based on both empirical and theoretical approaches, it remains evident that considerable work is still required to understand the fundamental mechanisms involved. The findings are summarised in Table 2-4. This observation is even more applicable when looking at the influence of particle concentration within the pipeline on particle attrition behaviour. Whilst in most studies the solids feed rate is specified, further research into how this interacts with the particulate material type and variation in pipeline geometry is required. It is evident from the review of these studies that factors such as superficial air velocity are well understood, however there is significant scope for further investigation with respect to particle concentration. Furthermore, particle velocity is not always measured. Considering the conclusions from Section 2.4.4.1.1, particle velocity is the most important factor in characterising particle attrition from the system perspective (as the impact angle is specified by system geometry) and requires direct measurement.

Table 2-4: Summary of Key Point from Numerical and Empirical Studies of Particle Attrition in Pneumatic Conveying Systems

Author	Particulate Material	Numerical (N) / Empirical (E)	Variables Investigated with respect to Attrition						Fatigue	Key Points	Reference
			Impact Velocity / Superficial Air Velocity	Impact Angle	Particle Conc.	Bend r/D	Particle Density	Particle Size			
Han et al.	Salt	N ¹	X		X				X	Superficial air velocity is more influential than solids loading ratio on particle attrition. 3D flow, and fatigue function required for more accurate simulation.	[62]
Hanley	Infant Formulae	N & E	X		X	X			X	Air velocity was found to be a more significant factor than the other operating variables investigated by a large margin.	[178]
Hanley et al.	Infant Formulae	N & E	X	X	X	X			X	Mode of conveying (dilute/dense phase) was the only significant factor affecting change in particle volume mean diameter, however a wider range of variable values require exploration. Comparison to Monte Carlo Simulation showed disparities of up to 20% for impact conditions.	[6, 113, 179]

Brosh et al.	Potash	N ²	X						X	<p>New initial particle strength distribution [195] and selection [196] functions implemented in 3D CFD-DEM Simulation. Some over-prediction of particle breakage by the comminution function, and under-prediction of particle weakening by fatigue function.</p> <p>CFD-DEM simulation times were shortened by implementation of a DEM grid, where empty cells were skipped in the calculation step. Further improvements were obtained by eliminating the finest particles.</p>	[183, 184]
Uzi et al.	Potash	N ²	X						X	<p>Novel One Dimensional Breakage Algorithm presented. Inter-particle collisions were found to be very important in determining particle breakage.</p> <p>Flow parameters are very sensitive to particle size.</p>	[38, 197]

Salman	General-purpose Fertiliser (30% N, 20% P ₂ O ₅ , 20% K ₂ O)	N & E	X	X				X	X	Impact angle and impact velocity are highlighted as key variables in determining the level of particle attrition. No fragmentation was measured in a straight conveying line. A threshold velocity was found, below which no particle attrition was measured. A two-parameter cumulative Weibull distribution could be used to describe variation of particle breakage with change in impact angle and velocity.	[9, 187]
Aked et al.	Unspecified	E	X		X	X			X	Five different bend types were studied. Particle attrition was found to increase with increasing superficial air velocity and decreasing particle concentration.	[188]
Kalman and Goder	Potassium Sulfate Potash Coal	E	X			X			X	A flexible long-radius bend was found to inflict less attrition than a rigid long-radius bend or blind tee.	[10]
Kalman	Unspecified	E	X		X	X		X	X	As particle size decreases, particle strength increases for the same material.	[4, 5]

										Through applying vibrations to the conveying section (containing turbulence drums for changes in direction), the amount of dust measured at the end of the line was reduced.	
Bridle	Barley Rice Sugar	E	X		X	X				Particle attrition was found to increase with increasing superficial air velocity, reducing particle concentration, and in using blind tee connections. Attrition in the pilot plant was approximately twice that observed in an industrial system.	[26]
Frye and Peukert	Polypropylene Polyethylene Polystyrene Polymethylmethacrylate	N & E	X	X		X			X	Process function determined by CFD simulation. Material function determined empirically. Particle-wall friction plays a greater role in particle attrition than what is generally assumed. For polymeric materials, the glass transition temperature is fundamental in the	[15, 190–192]

										determination of the particle failure regime.	
Abou-Chakra et al.	Unspecified	E	X	X						Centrifugal accelerator particle degradation tester presented. 90° impact angle compared to single bend pneumatic conveying line with reasonable correlation in particle attrition. No account of slip velocity.	[193]
Chapelle et al.	Granulated Sugar	E ³	X		X			X		Particle attrition tester presented by Abou-Chakra et al. [193] used to predict degradation in industrial conveying systems. Using the breakage matrix approach, an average error of 15% was achieved. A polynomial interpolation for particle size and impact velocity was implemented with acceptable results.	[43, 154, 194]
Pitchumani et al. and Laarhoven et al.	Sodium Benzoate Ammonium Nitrate	E	X						X	A new Repeated Impact Tester was introduced and attrition levels compared to a pneumatic conveying system. Attrition during the round-off phase (surface chipping) was found to be comparable. High	[61, 173]

										transportation velocities show no correlation due to the presence of the fracture mechanism.	
Macchini et al. ⁴	Wood Dust Silica Flour Olivine Sand	E			X		X	X		The 'shielding effect' was investigated. It was found that particle density has a greater influence in wear reduction compared to the particle size. It was concluded that the effect of shielding is far smaller when compared to the material effect within the context of pipeline erosion.	[41]

¹ With comparison to empirical data from Bell et al. [175] and Jacobs [176]

² With comparison to empirical data from Kalman et al. [63]

³ With the use of the analytical strand flow model of Bradley et al. [25]

⁴ Variables investigated with respect to pipeline wear

2.6 Experimental Method Considerations

This section will address experimental methodology specific to the sample preparation and size analysis of particulate materials.

2.6.1 Sampling of Particulate Materials

Sampling theory is of fundamental importance in the mass reduction and analysis of bulk materials, not least of all due to the fact that sampling errors typically far outweighing analytical errors [198–200]. A quantitative approach was detailed by Gy [201–203], whereby extraction of correct samples was specified.

From a bulk solids perspective, there are a number of different mechanical subdividing machines available. Petersen et al. [204] conducted a critical survey of these devices. It was concluded that the best overall methods of mass reduction for particulate materials were the calibrated Boener divider, Rationel Kornservice A/S splitters containing 34 chutes, Rotating 32-divider, and a Vario Divider with a splitting ratio of 1:4 + 1:5. These methods have been contrasted with the commonly used “grab sampling”, which was concluded to be the worst for of mass reduction in terms of statistical representativeness.

One aspect of the Theory of Sampling to be aware of in attrition studies, is that particle size is inherent to the fundamental process under scrutiny. Therefore, Sampling Unit Operation (SUO) 5 as detailed by Petersen et al. [199], ‘Comminution whenever necessary’, cannot be applied to particle attrition research. Subsequently, alternative SUOs require application where feasible.

2.6.2 Particle Size Measurement

In many works, the method by which particle size is measured, is described in little or no detail. Such a key element in particle attrition studies requires considerable attention.

Kulkarni [205] presents an extensive review of particle size measurement by various sieving methods. There was insufficient or complete lack of literature published on the influence of sieve diameter or amplitude of applied vibrations on the results obtained. Criticality was attributed to the sieving duration and sieving load. It was recommended to use a mass based system in data representation, without the use of size distribution modelling curves to smooth a measured size distribution. Presentation of the data in the form of histograms (showing the mass retained on each sieve) was deemed to provide more detailed size information, however the cumulative size distribution curve was deemed to better quantify the information holistically.

Standards describing the method by which solid particle size is to be measured with sieves are BS 410 (1986) (withdrawn), ISO 330-1 and ISO 3310-2. BS 410 was considered to be a pertinent standard [206], however BS 410-2:2000 remains in circulation, and outlines the technical requirements of testing and sieve geometry.

When considering other size measurement techniques such as Image Analysis, and Laser Diffraction, care must be taken to ensure that the technique is optimised for the particulate material under consideration. Li et al. [207] found that particle shape can significantly influence the measured particle size distribution output, depending on the method used. While spherical particle returned comparable results across three of the four measurement methods, non-spherical particle size distribution outputs could not be correlated (without the use of correlation factors obtained through image analysis). However, even for the case of spherical glass beads, differences between image analysis and laser diffraction have been reported by Bowen [208] as shown in Figure 2-19.

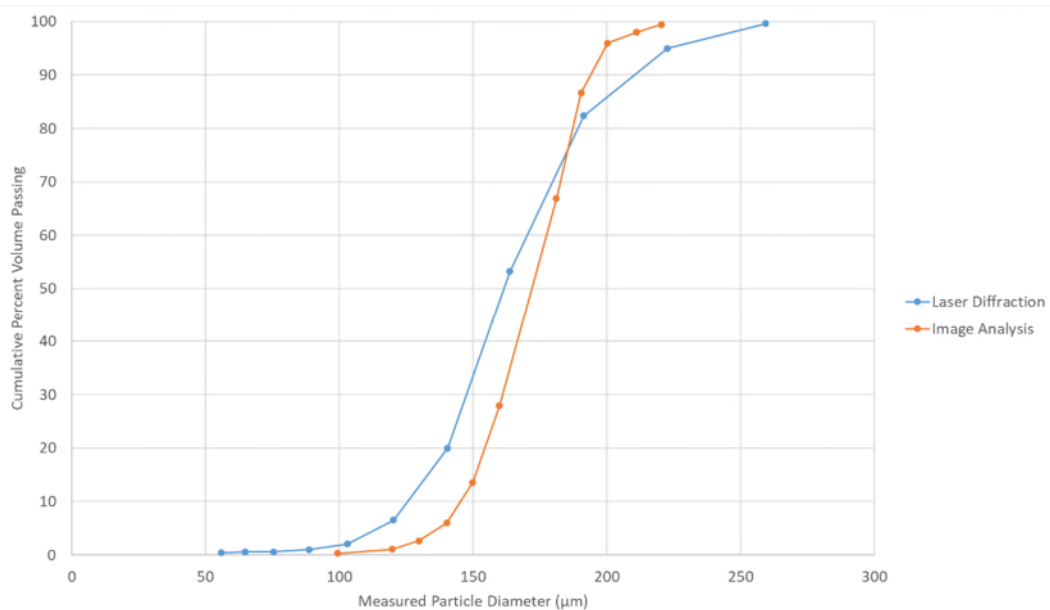


Figure 2-19: Comparison of laser diffraction and image analysis cumulative particle size distributions for sieved glass beads adapted from Bowen [208]

Not only the method by which particle size is measured is important, but also how that information is selected for presentation and how it is used. Some studies have used the cumulative particle size distribution curve previously mentioned, whilst other studies have adopted the use of the damage ratio (for example [209]). This was defined as the fraction of particle that are broken after being subjected to a defined loading condition, or number of loading conditions. Used predominantly in the modelling of comminution mechanisms, this was a simple measurement which must be defined for each particle type (size, shape, etc.). Such a function has been used to determine the probability of a given particle to break under a specified set of conditions, however, this does not produce the particle size distribution of the child particles. Further functions are required in this sense to describe the subsequent particle size distribution, similar to the breakage matrices presented by Chapelle et al. [43].

2.7 Conclusions of the Review

The phenomenon of particle attrition within lean phase pneumatic conveying was broken down categorically and has been systematically addressed. The primary categories addressed were the contributions of the material and process factors, and selected studies conducted from empirical and fundamentally derived approaches. Experimental considerations were also highlighted as an important factor in obtaining accurate and representative data. Throughout the course of this review, some key findings became evident:

1. Wear of wall surfaces and particle attrition are intimately connected. Both mechanisms result from the same contact event.
2. Particulate materials are diverse in nature, and fail by drastically different mechanisms dependant on their composition. Even particles residing within the same sample have been demonstrated to show a strength distribution. Furthermore, the failure mechanism was specific to the nature and magnitude of the loading event. This suggests that particle characterisation testing will always have a role in informing particle attrition models. The materials selected for the present research failed under a non-ductile regime and had a maximum particle size of no more than 2 mm. This enabled a wide range of testing to be completed on these materials, and is described in Chapter 4.
3. There remain a significant number of gaps in the research to be explored, especially with respect to linking the method of characterisation to the process under consideration. These include:
 - a. Determining the influence of particle concentration at the impact surface under the attrition by particle impact failure regime.
 - b. Determination of the change in particle velocity distribution and acceleration within pneumatic conveying systems with respect to change in particle concentration.
 - c. Benchmarking of particle attrition behaviour characterisation testers across the full range of conditions expected to be manifested in lean phase pneumatic conveying systems.
 - d. Definitive measurement of the magnitude of particle attrition associated with a single bend in a lean phase pneumatic conveying system.

- e. Determination of the influence of particle slip velocity, and potential implications for the prediction of particle attrition behaviour as measured with a characterisation apparatus.
4. Multiple impacts are expected in pneumatic conveying systems, and hence the literature highlights the importance of a fatigue function in the method used to predict particle attrition levels.
5. The diversity of test equipment was highlighted, and concern was attributed to the lack of correlation between different equipment types. There is no widely accepted testing method or predictive model to predict attrition levels in lean phase pneumatic conveying. However, it was evident from the reviewed studies, that the centrifugal accelerator was the most appropriate due to close control of impact velocity, impact angle and ability to perform multi-particle tests.
6. The particle velocity is not measured in a number of pneumatic conveying research works when considering particle attrition. The velocity of the conveying air, while much easier to measure, should not be used to approximate particle velocity without understanding the slip velocity characteristics specific to the system and material. As particle velocity is repeatedly reported to be the most influential factor in particle attrition, it should be measured directly.
7. There exists a distinct lack of evidence correlating increased particle concentration in homogeneous lean phase pneumatic conveying lines and reduced particle attrition on any scale.
8. A successful particle attrition modelling approach will need to capture both the material and process functions of the phenomenon in order to achieve meaningful results.
9. Sampling methods were seldom defined in the literature. Sample preparation was highlighted to be one of the most significant sources of measurement error with respect to particle attrition studies (as analysis of the full batch size is inefficient and laborious). Industrial-scale testing should employ full-stream cross-cut sampling techniques, in addition to further statistical subdivision to obtain sample sizes appropriate to particle size measurement techniques.

CHAPTER 3: Research Approach and Scope

It was evident from the literature review conducted in Chapter 2, that the influence of particle concentration on the magnitude of particle attrition measured in lean phase pneumatic conveying systems is not definitively understood at present. In addition to this, it was clear that no consensus exists with respect to a particle attrition model that can be applied to lean phase pneumatic conveying systems.

To investigate the influence of particle concentration on the magnitude of particle attrition measured in lean phase pneumatic conveying systems, the subject was first broken down into key concept areas, where the variables significant to the research could be identified. Then, to ensure the viability of the research, the scope was defined to narrow and guide the approach to the problem and the subsequent identification of key research objectives to be addressed by the experimental work. This in turn, informed the generation of a particle attrition model.

3.1 Aims of the Present Research

- 1) To ascertain the influence of particle concentration on the magnitude of particle attrition inflicted by a homogenous lean phase pneumatic conveying system.
 - a. To develop an experimental apparatus capable of quantifying the influence of particle concentration on the magnitude of particle attrition inflicted by a homogenous lean phase pneumatic conveying system
 - b. To determine the relationship between particle concentration and the magnitude of particle attrition inflicted by a homogenous lean phase pneumatic conveying system, should such a relationship exist.
- 2) To develop an improved particle attrition characterisation method.
 - a. To quantitatively evaluate two pre-existing centrifugal accelerator particle attrition testers
 - b. To evaluate the appropriateness of the testers in Aim 2a
 - c. To develop an improved tester if the testers in Aim 2a are deemed inadequate

- 3) To develop an empirically-informed model enabling the quantitative prediction of the magnitude of particle attrition inflicted by a homogenous lean phase pneumatic conveying system.
 - a. To incorporate the results addressing Aim 1b if applicable, and the results from Aim 2

3.2 Breakdown of the Subject Area

Based on the review of the literature, the general concept of particle attrition in pneumatic conveying systems was conceptualised into two primary categories of contributory factors: the influence of physical material characteristics; and the influence of pneumatic conveying system geometry and operating conditions. Generally, in reverse order, these categories describe the load applied to the conveyed particles, and the material response to these loads. To visualise these categories, Figure 3-1 shows the breakdown of the influence of the physical particle material characteristics, and Figure 3-2 shows the breakdown of the influence of the system geometry and conveying conditions.

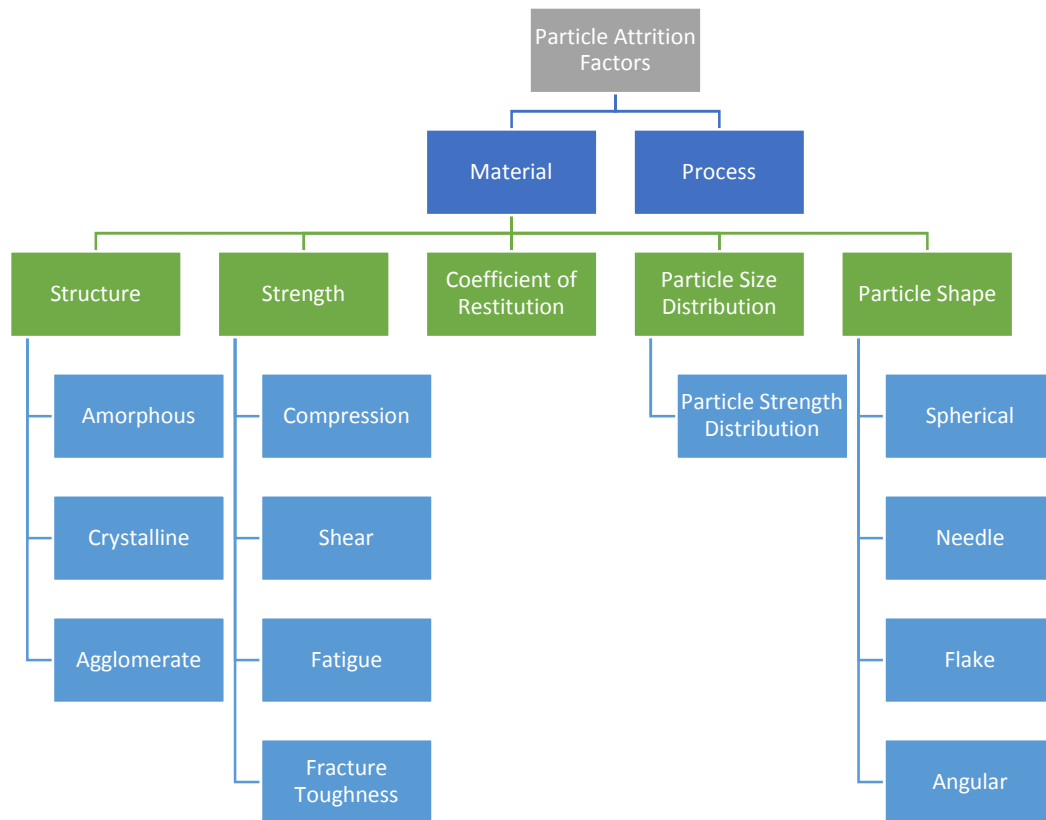


Figure 3-1: Variable map of the influence of the particle material physical characteristics

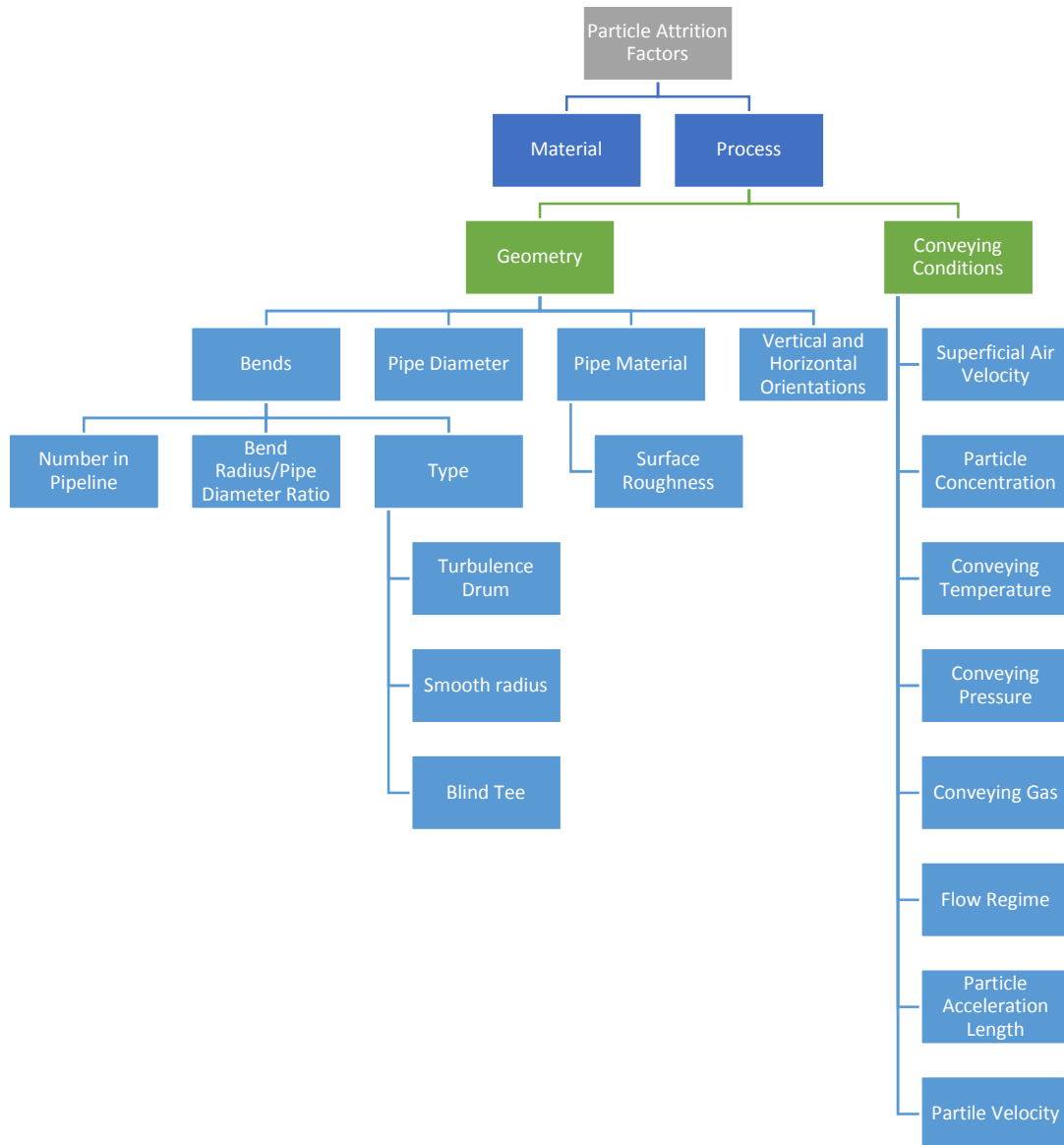


Figure 3-2: Variable map of the influence of the system geometry and conveying conditions on particle attrition

It should be recognised that these figures do not present an exhaustive list of variables, however, they do enable the reader to appreciate the vast number of variables involved in such processes. To add further complexity to the mechanism, many of these variables interact with each other; such relationships also required investigation and elucidation.

3.3 Scope of the Present Work

As was evident in the variable maps presented in the previous Section, the vast range of variables could not be addressed sufficiently within a single research programme. It was therefore decided that the following variables would form the core focus of the present research.

Characterisation of the Physical Material Characteristics

- Particle structure
- Particle strength (as measured by resistance to fragmentation under applied impact forces)
- Particle size
- Particle strength distribution (as measured by resistance to fragmentation under applied impact forces of varying impact velocity and impact angle)
- Particle shape (limited by a small selection of materials)

Characterisation of the System Geometry and Conveying Characteristics

- Bend radius (smooth radius bends only)
- Superficial air velocity
- Particle Concentration

As was addressed in Chapter 2, some other key variables require quantification to holistically characterise particle attrition in lean phase pneumatic conveying systems. The present research programme focuses on the prediction of particle failure in the first bend of a pneumatic conveying line. This prediction did not take into account the attrition caused by various feeding systems or by various receiving systems.

It was recognised that a typical industrial pneumatic conveying system normally contains multiple bends in the pipeline. These bends will typically cause different degrees of particle attrition, as described by the fatigue failure mechanisms exhibited by the specific

material. Multiple bends in a pneumatic conveying system (and hence the particle material fatigue behaviour) were not addressed within the present research. Such testing is intensive and time consuming to obtain, and was deemed unfeasible in light of the wide range of variables already under consideration.

Figure 3-1 shows a selection of the wide array of material characteristics that can be used to describe the attrition behaviour of a particulate material. The approach adopted in the present research was not to measure each of these characteristics and develop a mechanistic model, but rather to characterise particle attrition through direct observation of particle attrition events and develop an empirically informed model (further detail on this approach is given in Section 3.4 next section). Therefore, particle properties such as fracture toughness, hardness and porosity were not directly measured.

As shall be detailed in Chapter 4, the morphology for a selection of test materials was quantitatively measured. The remainder were described on a qualitative basis. It was recognised that particle morphology is a key determiner in defining particle attrition behaviour (see Section 2.4.2.1), however as testing this variable is exceedingly time and labour intensive, it was not a variable that was isolated and evaluated as a part of the present research. Similarly, it was not possible to isolate and evaluate the influence of the pipe diameter, vertical conveying orientation, conveying gas temperature and pressure, and various conveying gas types.

The materials selected for the research had to conform to a brittle or semi-brittle form of particle failure (see Section 2.4.3.1). This restricted particle failure modes to those including the chipping and fragmentation regimes, as measurement of plastic deformation in the absence of crack propagation (and ultimate fracture of the 'parent' particle into 'child' particles) could not be facilitated. The model produced as a result of this research would be specific to particulate material types conforming to these failure regimes.

3.4 Approach to the Problem

The research question was firstly divided into the two primary areas as described in Figure 3-1 and Figure 3-2; the Material Factor and the Process Factor (also called the System Factor). These two areas were then used to inform the modelling process. This approach is visualised in Figure 3-3.

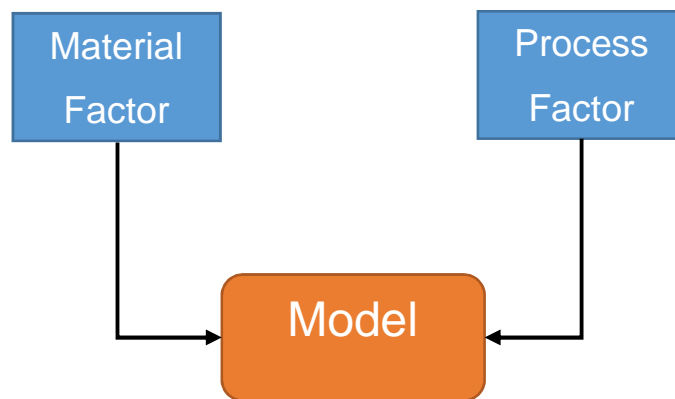


Figure 3-3: Structure of the Research Approach

3.4.1 Material Factor

The material factor describes the response of a particulate material to a given loading condition. In the context of the present research, this refers to a particle-wall impact scenario (See Section 2.4.4.1 for justification). The following parameters were identified as key variables defining the particle loading condition:

- Impact velocity
- Impact Angle
- Particle concentration at the impact surface

For a given particle material type, the particle size was the only material property that could be altered from an operator perspective (within the scope of the research), and was therefore also considered.

This required improvement of an apparatus that could isolate each of the variables detailed above, with which the operator could distinguish the influence of each on the magnitude of particle attrition observed. Once each of the variables had been characterised for a given material, the material factor for that product had been defined.

A bench-scale centrifugal accelerator particle attrition tester was developed to characterise the material factor, and is described in Section 4.3.2. The results obtained from this tester are detailed throughout Chapter 5.

3.4.2 Process Factor

The process factor describes the loading conditions applied to a particulate material; and in the context of the present research, the loading conditions that cause particle failure. The pneumatic conveying parameters that were identified as key variables in defining the particle loading condition were:

- Bend radius / pipe diameter ratio
- Superficial air velocity (and hence particle velocity) immediately prior to a pipe bend
- Particle concentration immediately prior to a pipe bend
- Particle size distribution of the conveyed particulate material

The material used for the impact surface (the pipe bend material), was recognised as a key factor in determination of the particle attrition behaviour for a given impact scenario. However, within the scope of the present research only steel pipe was used throughout the experimental programme. The rationale for this decision was that the vast majority of pneumatic conveying systems implemented in industry use steel pipework.

In order to isolate each of these parameters, a simplification of an industrial pneumatic conveying system was required in the form of a single bend pneumatic conveying line (see Section 4.4.2 for description). This enabled the quantification of the magnitude of particle attrition that could be attributed to a single bend in a pneumatic conveying system. This also minimised the influence of the material-specific fatigue behaviour.

Through a full-factorial exploration of the range of each operating variable, the process factor was defined.

3.4.3 Modelling

The data sets obtained from the Material Factor study and the Process Factor study were reconciled in order to develop a model to describe the interaction between the two attrition test types. This model enabled the testing of a relatively small sample size across a minimal selection of test conditions in order to characterise the material factor.

3.5 Research Objectives

A number of objectives were identified as core milestones required to achieve the aims of the research programme. These have been summarised in Table 3-1.

Table 3-1: Objectives of the research by topic

Objective Subject	Description
Material Factor	
Impact Velocity	To determine the relationship (if any) between the probability of a particle breaking under given impact conditions, and how this changes with changing impact velocity.
Impact Angle	To determine the relationship (if any) between the probability of a particle breaking under given impact conditions, and how this changes with changing impact angle.
Particle Size	To determine the relationship (if any) between the probability of a particle breaking under given impact conditions, and how this changes with changing particle size.
Particulate Material	To test a modest number of different particulate material types, and to determine qualitatively how propensity for particle attrition changes with changing particle structure and morphology.

Characterisation Method	To determine the feasibility of a centrifugal accelerator particle attrition tester (see Section 2.4.5.2), and improve upon the design if required.
Process Factor	
Particle Concentration	To determine the relationship between changing particle concentration at the entry point to a bend in a pneumatic conveying line, and the magnitude of particle attrition measured.
Slip Velocity	To determine how slip velocity (see Section 2.3.1.1) changes in a pneumatic conveying line with respect to superficial air velocity. Furthermore, how this relationship changes with changing size of the conveyed particle, and change in particle concentration. All of which under homogeneous lean phase flow conditions.
Modelling	
Particle Size	To develop a model that accounts for the virgin particle size when determining probability of attrition under given impact conditions.
Reconciliation of Data Sets	To reconcile the conditions in the material characterisation tests, and the process characterisation tests, and determined whether the impact conditions are equivalent in the magnitude of particle attrition measured.
Material Characterisation Approach	Validate the particle material factor characterisation method and comment on its appropriateness for the requirements of the model developed.

CHAPTER 4: Description of Test Equipment, Method and Materials

The vast majority of experimentation was conducted in the powder testing laboratory of the Wolfson Centre for Bulk Solids Handling Technology. The use of external facilities shall be identified where relevant.

In order to address the shortcomings of existing equipment and to acquire novel measurements, two bespoke pieces of test apparatus were constructed. The first, a Bench Scale Particle Attrition Tester (BSPAT) was constructed to address the shortcomings of the QPM Degradation Tester (see Section 4.3.1). The second, a Single Bend Test Apparatus (SBAT) was constructed with the objective of determining the particle breakage occurring at a single bend of a pneumatic conveyor. The conveying conditions at this bend had to be measured to a higher degree of accuracy than what other pieces of existing equipment were capable of. In addition to this, other sources of particle breakage inherent in many pneumatic conveying systems had to be either well defined, or removed from the system so that the breakage due to a single bend could be isolated.

The statistical sampling method used shall be described first (Section 4.1), followed by particle size distribution measurement methods (Section 4.2). Following these, particle characterisation devices and their methods shall be described, consisting of centrifugal accelerator testers (Section 4.3). Large scale apparatuses are then described and the associated methods elucidated (Sections 4.4). Finally, the consideration and selection of particulate materials for test work is discussed, and justification provided for the decisions made in Section 4.5.

4.1 Sample Preparation

Statistical subdivision is paramount in ensuring that all tests are performed using statistically representative samples of the master batch. This ensures that the virgin size distribution measured for the master batch was relevant to each of the tests performed

using sub-samples. Depending on batch size, this has been achieved through a combination of methods.

For samples up to approximately one litre in volume, riffle boxes (Figure 4-1a) were used to obtain two sub-samples. The dividing unit was positioned above two boxes and contains a series of slots which empty alternatively into the two receptacles. If further subdivision of the sample was required, the process was repeated until the desired sample size was obtained.

For samples up to approximately 40 litres in volume, the spinning riffler (Figure 4-1b) was used. This apparatus consists of a plane flow hopper that uses a vibratory feeder to feed onto a rotating carousel of collection vessels. The amplitude of vibration of the feeder can be altered to control the flow rate of material into the carousel. Once the subdivision was complete, eight statistically representative samples are obtained. If a smaller sample was required, the sample can be subdivided further through the use of either the spinning riffler or the riffle boxes as required.



(a)



(b)

Figure 4-1: Riffing Apparatuses

4.2 Measurement of Particle Size Distribution

Particle size measurement was conducted using two fundamental approaches: dry mechanical sieving, and laser diffraction size analysis.

All dry mechanical sieving was performed with a square root of two progression in aperture size was achieved using two devices:

1. **Manual.** A stack of woven wire mesh sieves conforming to ISO 3310, and agitated on an Endecotts Octagon 200 mechanical sieve shaker for 10 minutes at a moderate amplitude. The material retained on each sieve was then manually collected and weighed on a set of electronic scales accurate to 0.01 g.
2. **Automatic.** A Rotex Gradex 2000 automated mechanical sieving machine. The sample was introduced to the top of the sieve stack, and was mechanically agitated for 10 minutes. The results were automatically generated by the unit accurate to 0.1 g.

The laser diffraction size analysis was performed on a Malvern Mastersizer 3000 with an Aero S dry powder feeder system.

The particle size measurement method shall be specified throughout the present work where relevant data sets are presented.

4.3 Particle Characterisation Devices

Particle characterisation devices within the context of the present research refer to bench-scale attrition testers. The review of the literature revealed that particle attrition by impact was the mechanism most-representative of the attrition phenomena that manifests in a lean phase pneumatic conveying system. The centrifugal accelerator-style of particle impact tester was adopted for the reasons addressed in Section 2.4.5. More specifically, the control of impact velocity was considered paramount in tester selection. The centrifugal accelerator-style tester was concluded to address this requirement best, in addition to its relatively small laboratory footprint and small sample size (approximately 0.1 kg of material). A pre-existing tester was available in the laboratory (QPM Degradation

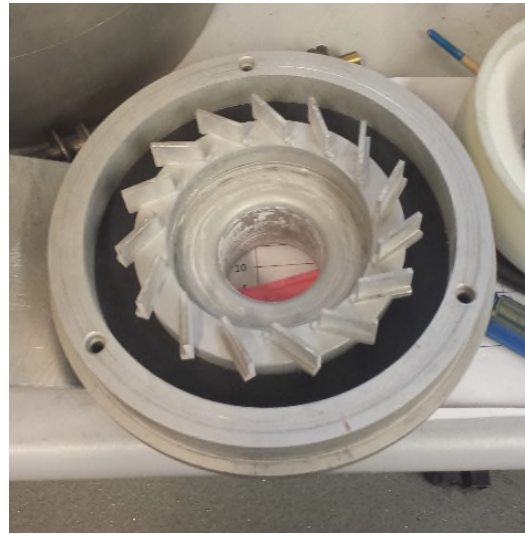
Tester), and shall be discussed first. A new centrifugal degradation tester was designed, constructed and commissioned to address the flaws in the existing apparatus and is subsequently described and discussed.

4.3.1 QPM Degradation Tester (QPM)

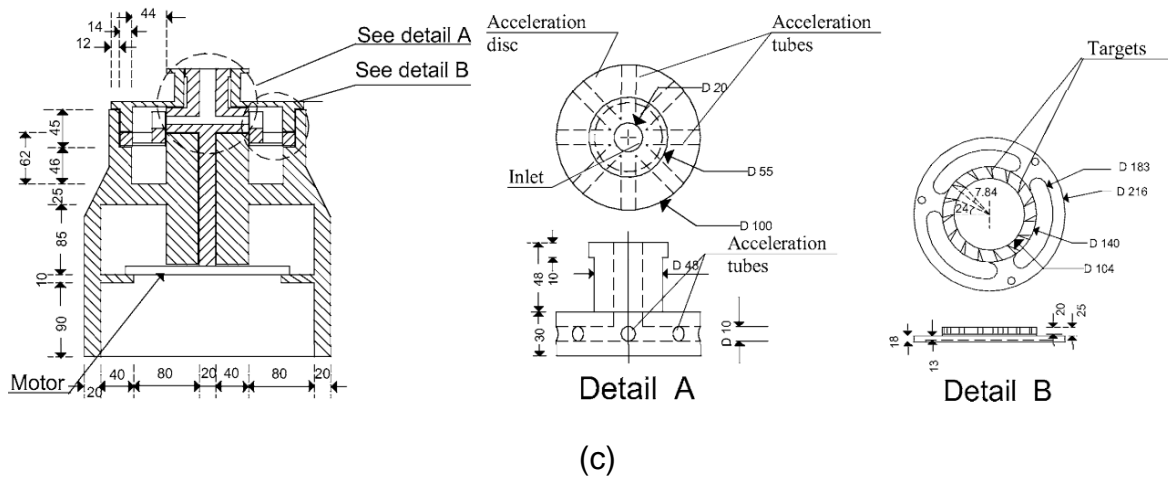
The QPM Degradation Tester (Figure 4-2a) consists of a solid, anodised aluminium chassis, which houses a spinning disc and a target array. The particle sample is fed into the top of this disc. The particles are then accelerated by centrifugal forces out of one of the eight radial tubes in the spinning disc. Positioned radially outwards from the spinning disc, the target array consists of a series of flat, stainless steel surfaces angled with respect to the horizontal plane (Figure 4-2b). This angle determines the impact angle of particles with respect to the target surface.



(a)



(b)



(c)

Figure 4-2: QPM Degradation Tester (a) overview, (b) target array, and (c) schematic presented by Chapelle et al. [154]

The feed rate of material introduced into the top of the spinning disc is controlled through the use of a screw feeder mounted on an aluminium frame above the tester. A mass flow hopper provides material to a screw with increasing volumetric capacity along the length of the shaft. This screw design is aimed at minimising segregation in the hopper and to produce a material mass flow rate that is consistent as possible during the testing.

Table 4-1 provides geometrical specifications for the QPM Degradation Tester.

Table 4-1: Geometrical Characteristics of the QPM Degradation Tester

Characteristic	Value
Spinning Disc Diameter (m)	0.1
Acceleration Tube Diameter (m)	0.01
Number of Acceleration Tubes	8
Diameter of Target Array (m) (Centreline)	0.122
Sample Size per Test (L) (approx.)	0.1
Maximum Testable Impact Velocity (m/s) [†]	50
Testable Impact Angles (deg)	30, 45, 90

[†]As estimated from Equation (4-1) on page 94.

At the outset of the research programme, some shortcomings of the design of the QPM tester were identified:

1. The screw feeder to the apparatus provided intermittent operation with frequent (but regular) stoppages in the screw rotation, exacerbating the influence of feed rate transience in the results.
2. Rotational velocity of the spinning disc did not remain constant at a constant operation setting. The value read on the screen changed with respect to time and the rate of material fed into the device. Additionally, a conversion chart was required to obtain the rate of rotation as the readout does not give this information directly.
3. The size of the impact chamber was relatively small and has led to degradation behaviour whereby secondary and tertiary impacts were suspected to have a major influence. This was undesirable if the tester was to be considered for use in studying the effects of a single impact.
4. The recollection method of the sample post-test made it difficult (due to the design of the impact chamber) to retrieve very fine particles; these fine particles were vital to the current research.

5. Beyond the scope of the present work, the testing of hazardous materials requires a high level of hygiene. This would be challenging with the current design, as efficient cleaning of all cavities was not possible at the time.

In order to address the shortfalls of the QPM Degradation Tester, a new Bench Scale Particle Attrition Tester was designed, constructed, and commissioned. Further detail is available in Section 4.3.2.

4.3.1.1 Test Method

Representative samples for testing were prepared as described in Section 4.1 from a master batch of material. Preparation of master batches will be described alongside the relevant experimental results.

Virgin particle size distributions were determined as per the manual dry mechanical sieving method described in Section 4.2. Samples were then tested across the impact velocity and impact angle conditions as specified by the experimental programme in the following manner:

1. Configure the target array to the desired angle
2. Place the lid, closing the impact chamber
3. Insert the sample into the hopper of the screw feeder
4. Initiate the accelerating disc motor and wait until steady state is achieved
5. Initiate the screw feeder motor
6. Wait until the whole sample has been fed into the accelerating disc, then deactivate the screw feeder motor
7. Deactivate the accelerating disc motor
8. Disconnect power from the tester
9. Wait 10 minutes for any dust to settle within the impact chamber
10. Remove the lid from the impact chamber, and using a brush, dislodge any particles from the underside of the lid into the impact chamber
11. Brush the inside of the impact chamber so that all material is deposited into the collection vessel

12. Remove the collection vessel from the impact chamber and deposit the tested sample into the top of the sieve stack
13. Vacuum clean all surfaces of the centrifugal accelerator to minimise cross-sample contamination
14. Analyse the sieve stack as described in Section 4.2 for manual dry mechanical sieving
15. Vacuum clean sieve testing equipment as required

In order to estimate the particle impact velocity on the target array, the particle stream was estimated to exit the spinning disc at an exit angle of 40 degrees. This was approximated from the work of Deng et al. [35] for soda beads. The tangential component of the spinning disc velocity was reconciled with that of the accelerated particles, which was subsequently used in the trigonometric calculation of the impact velocity. Equation (4-1) was developed to calculate the impact velocity, V_i in m/s, for a given rotational velocity, ω_d in RPM, of the spinning disc; where D_d is the diameter of the spinning disc in m, and θ_e is the particle stream exit angle in degrees.

$$V_i = \frac{\pi D_d \omega_d}{60 \cos \theta_e} \quad (4-1)$$

4.3.2 Bench Scale Particle Attrition Tester (BSPAT)

To address the shortcomings of the QPM degradation tester, a new design based on the same operating principles was devised. This section will summarise the key differences in apparatus design that were implemented, and the effects that these are expected to exact on experimental results.

4.3.2.1 Apparatus Design

The design process for this apparatus was driven by a number of key requirements relating to ease of operation as follows:

1. Small sample size required. This was to ensure that when plant design for a new material is considered, only a small amount of sample may be available. This objective did not restrict the potential use of large sample sizes, however it did drive the need for high data resolution through factors such as efficiency in material retrieval from the apparatus.
2. Small laboratory footprint. To address ease of use, transportation, and practicality of operation.
3. Hygiene. The apparatus must be able to test potentially toxic materials, and therefore, must be able to be cleaned to a very high standard at the conclusion of a test programme.

Accuracy of the test results, as follows:

4. Close control over impact velocity. As defined at the outset of the research programme, the impact velocity has the highest influence on particle attrition, and therefore needs to be closely controlled. Without high resolution control over this variable, the influence of other operating variables may be masked in the noise of the data.
5. Option to test impact angles down to 20 degrees. Impacts in pipe conveying pipe bends are typically of the order of 20-30 degrees. The option to test shallow impact angles will make the results more representative of the systems they are trying to replicate.

6. Ease of material retrieval. In order to analyse the proportions of fine particles generated for a given impact test, the design must strive to minimise the loss of material through the testing and recollection phases of the experimentation. This is made particularly difficult through the propensity of fine particles to be carried away by air draughts into crevices of the device.
7. Control of feed rate. In order to control the particle mass flux at the impact surface of the targets in the apparatus, a close control over the feed rate of material into the accelerating disc must be achieved.

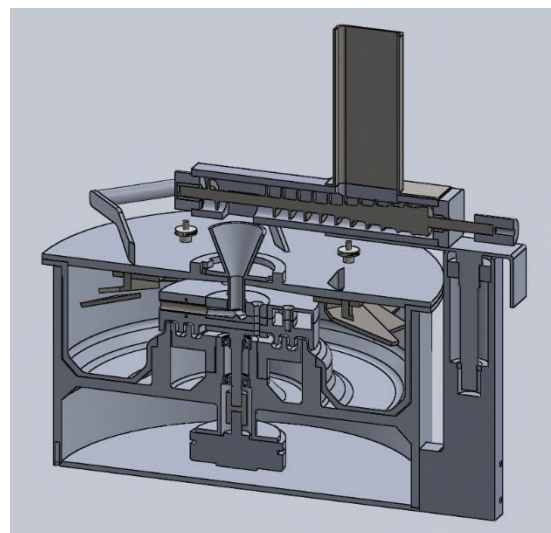
And finally, practical limitations on the materials that can be tested, as follows:

8. Free-flowing bulk materials only, in order to avoid build-up and blocking within the device.
9. Maximum sample particle size no greater than 4 mm in diameter, as industrial granulates form the core focus of this study.

These primary design objectives were individually addressed, and the following resolutions were implemented in the final design. Some geometrical considerations are given in Table 4-2.



(a)



(b)

Figure 4-3: The BSPAT (a) overview, and (b) CAD model of the design

Table 4-2: Geometrical Characteristics of the BSPAT Degradation Tester

Characteristic	Value
Spinning Disc Diameter (m)	0.15
Acceleration Tube Diameter (m)	0.01
Number of Acceleration Tubes	3
Diameter of Target Array (m) (Centreline)	0.235
Sample Size per Test (L) (approx.)	0.1
Maximum Testable Impact Velocity (m/s) [†]	35
Testable Impact Angles (deg)	20, 30, 45, 90

[†]As estimated from Equation (4-1), on page 94.

In order to address the requirement for a high resolution control of impact velocity, the motor selected to drive the accelerating disc required a closed loop control system with a high feedback rate. This would enable the motor to respond to changes in motor loading while minimising the associated deviation in rotational velocity. To this end, the motor selected was the Maxon EC 90 Flat motor, coupled with an encoder capable of 16 000 counts per revolution (rate of feedback to the controller). The result of this is a drive system that is capable of maintaining a constant rotational velocity to within 1 RPM. It was decided that this level of accuracy was sufficient for this programme of research.

The feed rate of material into the centre of the spindle was addressed through the use of a screw feeder. The hopper was designed with a volume of 234 mL, and vertical walls in order to prevent possible core flow from occurring. The receiving vessel was designed in conjunction with the feed hopper; this ensured that the operator could not fill the impact chamber with enough material to interfere with the particles coming out of the accelerating disc (assuming a maximum loose-poured angle of repose of 60 degrees of the test material).

The inner edges of the hopper were given a 5mm radius to prevent material hang-up in these regions. The screw itself was designed with a variation in shaft diameter so that an increasing volumetric capacity is achieved across the outlet face of the hopper. The shaft is then constant in the transport section of the screw. The screw has a constant pitch

across its entire length due to manufacturing complications with a varying pitch design. The final flight of the screw is set back approximately 10 mm from the exit point of the material in order to minimise the pulsation of material feed into the spindle.

Sample material recovery was considered a high priority throughout the course of the design process. A wide number of concepts were considered for the method by which material is recollected after a test, with particular consideration of fine particles. The final concept chosen for implementation was a removable vessel that was housed within the apparatus and formed the inside of the impact chamber. So by removing the vessel, the bulk of the surface area of the impact chamber is removed. This method yielded minimal ledges on which fine particles or dust could reside. All edges of the impact chamber were given a radius in order to maximise the ease with which particles could be removed. This vessel was constructed from a single piece of aluminium and turned with a lathe to ensure concentricity and absence of seams. Finally, it was hard anodised to improve the surface durability of the component.

In the knowledge that this apparatus may be used to test potentially toxic materials in future work beyond the conclusion of this research, a number of components were specifically designed for ease of cleaning or replacement. These features are summarised as follows:

- Removable acceleration tubes. These are constructed of stainless steel and can be cleaned with an ultrasonic bath. The secondary reason for this approach is that the replacement of the acceleration tubes (in the event of excess wear or contamination) requires fabrication of the acceleration tubes only, and not of the entire spining disc assembly.
- Removable labyrinth. The labyrinth reduces the ease of access of fine particles to the bearings supporting the spinning disc. This labyrinth is removable and can be cleaned through the use of an ultrasonic bath.
- In conjunction with making it easier to retrieve the sample from the apparatus, the collection vessel forms the majority of the surface area of the impact chamber. As this component is also removable, it may be cleaned to a high standard at the conclusion of each test if required.
- The spinning disc can be dismantled and maintained to a high degree of cleanliness.

- The screw feeder assembly incorporates a number of features, aiming to facilitate cleaning of the device:
 - The hopper and screw have radii at the intersection of surfaces in order to minimise material retention in these regions
 - Removal of the screw is achieved through unscrewing the end cap of the screw housing and loosening of the coupling to the motor. This almost-tool-less design enables efficient disassembly.
 - All components of the feeder assembly can be cleaned through the use of an ultrasonic bath or other methods depending on the toxicity of the sample material.
 - Stainless steel fasteners and an aluminium coupling have been selected due to their relatively good corrosion resistance.
- All surfaces that come into contact with the sample are primarily anodised aluminium or stainless steel. These materials are relatively inert and hence a high level of hygiene can be maintained. Only a small degree of surface contact with nylon (bushings for screw feeder) is present and can be addressed on a case-by case basis with each sample material.
- The tolerance between component edges within the impact chamber was closely designed with a smooth running fit. While it cannot be guaranteed that particle ingress into these small cavities is not possible, best effort has been made to minimise the potential for this ingress to occur.

The calculation of particle exit angle from the accelerating tubes and the particle impact velocity are identical to that used for the QPM analysis. A full set of engineering drawings for the BSPAT design has been included in Appendix B.

4.3.2.2 Test Method

The method used to test samples was identical to that used for the QPM tester (see Section 4.3.1.1).

4.4 Large Scale Particle Attrition Testing

The test equipment detailed in this section encompasses that which was used to test larger sample sizes (3-500kg) across a range of impact conditions. The first such tester presented is the Large Scale Particle Attrition Tester; a larger version of the QPM and BSPAT addressed in the previous section. The Single Bend Attrition Tester is then described as a simple pneumatic conveying system for the detailed research of key parameters causing particle attrition. Finally, two large scale pneumatic conveying systems are described that contain multiple bends.

4.4.1 Large Scale Particle Attrition Tester (LSPAT)

The Large Scale Centrifugal Attrition Tester (Figure 4-4a) was a pre-existing piece of experimental apparatus in the Wolfson Centre testing Laboratory. Operating under the same principles as the QPM and the BSPAT, this apparatus is capable of testing impact attrition of particle diameters up to 20-25 mm.

A table feeder (Figure 4-4b) was used to meter the particle sample into the centre of the accelerating disc. The accelerating disc itself as constructed from two circular pieces of sheet metal, welded together with channel section. A series of mild steel targets were screwed to a wooden ring to form the target array (Figure 4-4c). The impact chamber is formed from welded mild steel sheet, with a sloping floor emptying out into a collection container below. A vibration unit was attached to the outside of the impact chamber to assist with sample retrieval post-test.



(a)



(b)



(c)

Figure 4-4: Large Scale Centrifugal Attrition Tester (a) overview, (b) table feeder, and (c) impact chamber

The inside of the impact chamber was lined with a polymer foam sheet in order to mitigate the influence of secondary impacts. The lid of the impact chamber was lined with the same foam sheet; however this lid was replaced with a sheet of Perspex in order to visualise the particle-target impacts. The uppermost surface of the impact chamber was therefore rigid.

The control unit for the motor attached to the accelerating disc enabled the user to specify the controller frequency. In order to determine the relationship between this and the

angular velocity of the accelerating disc, a tachometer was used and conversion chart generated.

The geometrical specifications of the LSPAT are summarised in Table 4-3.

Table 4-3: Physical characteristics of the LSPAT

Characteristic	Value
Spinning Disc Diameter (m)	0.450
Acceleration Channel Height (m)	0.035
Number of Acceleration Channels	8
Diameter of Target Array (m) (Centreline)	0.610
Sample Size per Test (L) (approx.)	0.1
Maximum Testable Impact Velocity (m/s) [†]	30
Testable Impact Angles (deg)	45, 90

[†]As estimated from Equation (4-1), on page 94.

Some drawbacks in the design of this apparatus are as follows:

- The feeding arrangement is not volumetric in nature. Average values of mass flow rate of solids can be calculated, however instantaneous mass flow rates were dependant on the flow condition within the hopper, and presence of particles on the rotating table. It is recommended that for future studies, that the feeding arrangement is modified to a screw, or choked-flow vibratory feeder to address the aforementioned concerns.
- The design of the accelerating disc lends itself to promoting high air velocity regions within the impact chamber. It was thought that this could be due to the fan-like construction whereby the channel sections act as fan blades. It is recommended that the acceleration disc is redesigned to minimise the free surface areas between the channel sections.

In general terms, it was not recommended to use the LSPAT to test the attrition behaviour of fine particle sizes (particle diameter <400 μm approx.). This was due to the significant

influence of air currents in the apparatus, coupled with the larger particle flight distance to the target surface.

4.4.2 Single Bend Attrition Tester (SBAT)

The single bend attrition tester Figure 4-5 took inspiration from the design of Bridle [26] in terms of the general configuration of the pipeline and experimental objectives. It essentially consists of a 12 m pneumatic conveying line, followed by a 90 degree bend, and then a 3 m straight into the receiving vessel. As shall be discussed, a number of key design differences were incorporated that enable further elucidation of the conveying characteristics, and the ability to associate these with measured particle attrition levels.

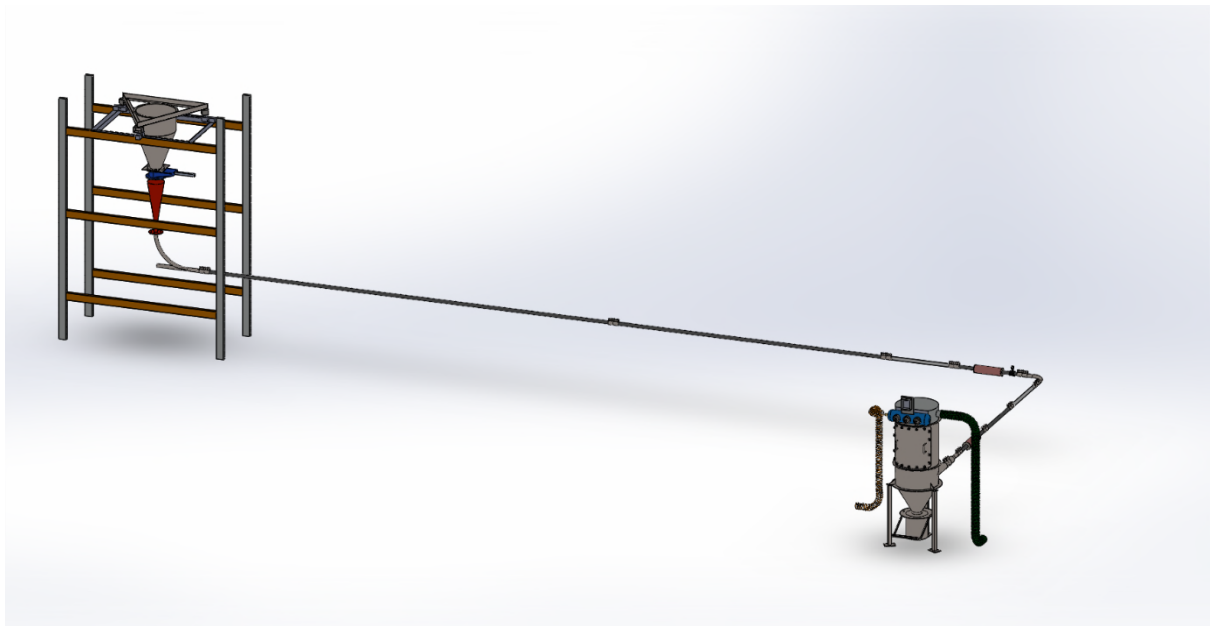


Figure 4-5: Simplified Schematic of the Single Bend Test Apparatus

4.4.2.1 Apparatus Design

The objectives and design response of this testing facility were specified as follows.

It was recognised that ambient humidity could affect the breakage behaviour of the sample particles (as acknowledged in Section 4.5). Pre-treatment of the conveying air

was not performed however, as the samples were all exposed to atmospheric conditions regardless of which test in the experimental programme they were subjected to.

The feeding arrangement should inflict minimal damage on the sample. This was achieved by specifying a vacuum conveying line, preventing the need for a mechanical feeder (such as a rotary valve [210]) which could damage the sample prior to conveying. Instead, an orifice plate coupled with a pneumatically operated slide valve was adopted; and through lack of mechanical handling, expected to inflict negligible attrition on the sample. This emptied into a conical receiver, attached to a swept tee (made of stainless steel) into the vacuum line to ensure that the introduction of the solids to the air stream applied minimal stress to the particles.

High resolution of the mass flow rate out of the hopper (and hence into the conveying line) was required. This was achieved by mounting the hopper on three Tedeo-Huntleigh Model 1260 load cells. Data was acquired with a National Instruments NI9237 card and logged on a custom Labview program.

Two pipe bend types were tested. Both were constructed of stainless steel, and had bend radius to pipe diameter (r/D) ratios of 3 and 12. These were chosen to replicate the material and bend r/D extremes seen in industrial systems (H. Wolf, Personal Communication, July 20, 2015). The straight pipe section was made of PVC, and 1.5" schedule 40 NPS (OD = 48.3 mm; ID = 40.94 mm) throughout the system unless otherwise stated. Pipe sections were connected with Morris Couplings (also known as compression couplings), in order to reduce the likelihood of pipe misalignment and hence an unacknowledged source of particle attrition. Glasswork piping was also used to record footage of the particulate flow behaviour (attrition was not measured), with 1 m straight sections and a short radius ($r/D = 3$) bend implemented. Care was taken to match the internal pipe diameter across piping composed of different materials. The system is capable of accommodating up to 3" schedule 40 NPS (OD = 88.9 mm; ID = 77.92) pipe; even though 1.5" pipe was exclusively used in the present work, it is envisaged that 3" pipe will be used for future experimentation (as recommended in Section 11.2). The 1.5" pipe was selected for the present research as it enabled the testing of the solids feed rate corresponding to a 40 mm diameter orifice plate at the feeding end of the pipeline, for an operational time of approximately 25 seconds. A larger conveying pipe diameter would have restricted the range of particle concentrations that could have been achieved for an

operational time of 25 seconds in the pipeline within the scope of the present research, due to the sample size limitations of the receiver.

Particle velocity is measured through the use of two electrostatic charge measurement units: one placed 0.5 m before the bend, and the other placed 0.5 m before the receiver. The electrostatic signature of particles within the flow is recorded by two ring sensors within each unit. By correlating the two signatures, a time offset is determined and used in conjunction with the known distance between the sensors to determine particle velocity. The sensors used in this research (Figure 4-6) used rings made from copper foil 85 mm (approx.) in width, separated 117 mm by their midpoints. The two sensors within each unit were separated by a 10 mm ring placed at the midpoint between the two sensors and connected to electrical earth. The unit was encased in a copper enclosure, and connected to electrical earth to minimise noise picked up on the sensor rings. A bespoke LabView program was used to process and log the data obtained from these sensors. The operating principles behind this sensing approach are described in detail within the work of Hussain et al. [211].



(a)



(b)

Figure 4-6: The electrostatic sensing arrangement (a) overview in-situ with signal amplifiers, and (b) section view of a 3D model revealing the sensors with respect to the shielding.

The receiving unit inlet size was 3" schedule 40 NPS, in order to accommodate the design specification going up to this pipe size for the entire conveying line. However, for the purposes of the present programme, an expanding section was used to connect the 1.5" conveying line to the 3" receiver inlet. This approach doubles in function to provide an

expanding section of the pipeline, where the superficial air velocity (and hence particle velocity) is reduced prior to entry into the receiving vessel. This, in theory, should have reduced the particle impact velocity in the receiver, and hence overall particle breakage not associated with the pipe bend.

The receiving unit (Figure 4-7a) body was cylindrical with a conical hopper. The pipeline entry was positioned tangential to the cylindrical body of the receiver, and a sheet made of natural rubber was placed over the impact zone to reduce the severity of particle-wall impacts in this region (Figure Figure 4-7b). A vessel to facilitate sample recollection was detachable from the base via a lever-driven compression coupling mechanism. Six pleated filter cartridges (filter material: Mahle Ti 07; >99.99% filtration efficiency at 0.3 μm particle size) were used to separate the gas phase from the solid phase. Filtration was achieved primarily through surface capture instead of in-depth capture, as the latter would result in loss of test sample. After a conveying run, three reverse pulses of compressed air were used to clean the filter material. A large access door was specified on the side of the receiver to assist thorough cleaning. For the same purpose, all internal welds were ground smooth, and no internal ledges were permitted in the design.



(a)



(b)

Figure 4-7: Single Bend Attrition Tester Receiver (a) overview prior to installation, (b) tangential pipeline entry with impact pad

The air mover used was an Adams Ricardo SR113 roots-type blower. This was connected to the receiver via pipework incorporating an 8 m straight length of 3" schedule 40 NPS PVC pipe. A Sierra 640i-VTP insertion thermal mass flow meter was used to measure the mass flow rate of air moving through the conveying system, and logged with a bespoke LabView program. In order to ensure correct air flow conditions for the air mass flow measurement, the meter was placed on the straight pipeline connecting the receiver to the air mover. The thermal air mass flow meter was calibrated against a choked flow nozzle bank which was itself calibrated to BS 1042 (now superseded, withdrawn) [27].

The overall design objective was the creation of an experimental apparatus that was flexible in its capabilities and that could be used to study each conveying variable in relative isolation. The utilisation of compression couplings and placing the apparatus at ground level, enabled the interchange of most components with relative ease. Table 4-4 describes the operating limitations of the apparatus as they were at the conclusion of the present experimentation, however not all configurations were considered in the present work. Other capabilities not considered in the present work include variation of straight length sections, vertical conveying, and the testing of multiple bends in the conveying line.

Table 4-4: Operating Characteristics of the Single Bend Tester

Operating Characteristic	Range of Testable Values
Hopper outlet orifice diameter (mm)	10-90 (in 10 mm increments)
Pipe diameter (-)	Up to 3" schedule 40 NPS
Volumetric air flow rate at receiver (m ³ /hr)	1209
Maximum measurable particle velocity (m/s)	60
Maximum loose poured sample volume (L)	22.6

4.4.2.2 Test method

Representative samples for testing were prepared as described in Section 4.1 from a master batch of material. Preparation of master batches will be described alongside the relevant experimental results.

Virgin particle size distributions were determined as per the manual dry mechanical sieving method described in Section 4.2. Samples were then tested across the pipeline geometry and conveying conditions as per the following method:

1. The pipeline geometry was adapted to the desired arrangement, considering:
 - a. Bend radius
 - b. Orifice diameter of hopper outlet
 - c. Length of straight sections before and after bend
 - d. Positioning of electrostatic sensors
 - e. Positioning of glass sections of pipe
2. Load sample of known weight into feed hopper.
3. Roots blower initialised to required air flow
4. Data logging programs initialised
 - a. Electrostatic particle velocity sensors
 - b. Hopper load cells
 - c. Air mass flow sensor
 - d. Pre-bend pressure transducer
5. Open hopper slide valve (material enters the pipeline).
6. When particulate flow ceases, close slide valve, deactivate roots-blower and data logging systems.
7. Activate reverse-jet pulsing routine of filters in the receiving vessel.
8. Collect material retained in the hopper and record weight.
9. Remove cartridge filters from receiver and record weight of each.
10. Brush down all internal surfaces of receiver so that fugitive material falls into the collecting bucket.
11. Remove the collecting bucket and obtain representative sample of the tested material using the method specified in Section 4.1.

12. Obtained the particle size distribution of the tested sample according to the method detailed in Section 4.2.
13. Vacuum clean the collecting bucket and all internal surfaces of the receiving vessel
14. Vacuum clean each of the filter cartridges and record weight. Return filters to the receiver.
15. Close and seal receiver.

An example calculation from the data obtained from the SBAT is found in Appendix D.

4.4.3 Pilot Plant Test Facility

An industrial-scale pneumatic conveying system (Figure 4-8 and Figure 4-9) was pre-existing in the Wolfson Centre Bulk Solids Testing Laboratory. This system conveyed in the positive pressure regime, with a single blow tank arrangement. This system was of the same scale used in industrial pneumatic conveying systems.



Figure 4-8: Overview of the Pilot Scale Pneumatic Conveying System

The air movers used in the system consisted of two Kaeser CSD 102 oil-flooded screw compressors. Each compressor was capable of providing 0.175 kg/s of air at 10 bar, however cut out was set to 7 bar and cut-in was set to 6.6 bar (all gauge pressures).

The controllers consist of two choked-flow nozzle banks that are used to control the blow tank air and the supplementary air. These banks each contain eight machined orifices, each coupled with a ball valve actuated by a solenoid. The choked-flow air mass flow

rates across each nozzle bank followed a geometric power of 2 progression. This meant that the highest achievable air mass flow rate (0.33 kg/s) was twice that of the largest nozzle, and that the resolution of the system was that of the smallest nozzle (0.013 kg/s) as designed within Bradley et al. [27].

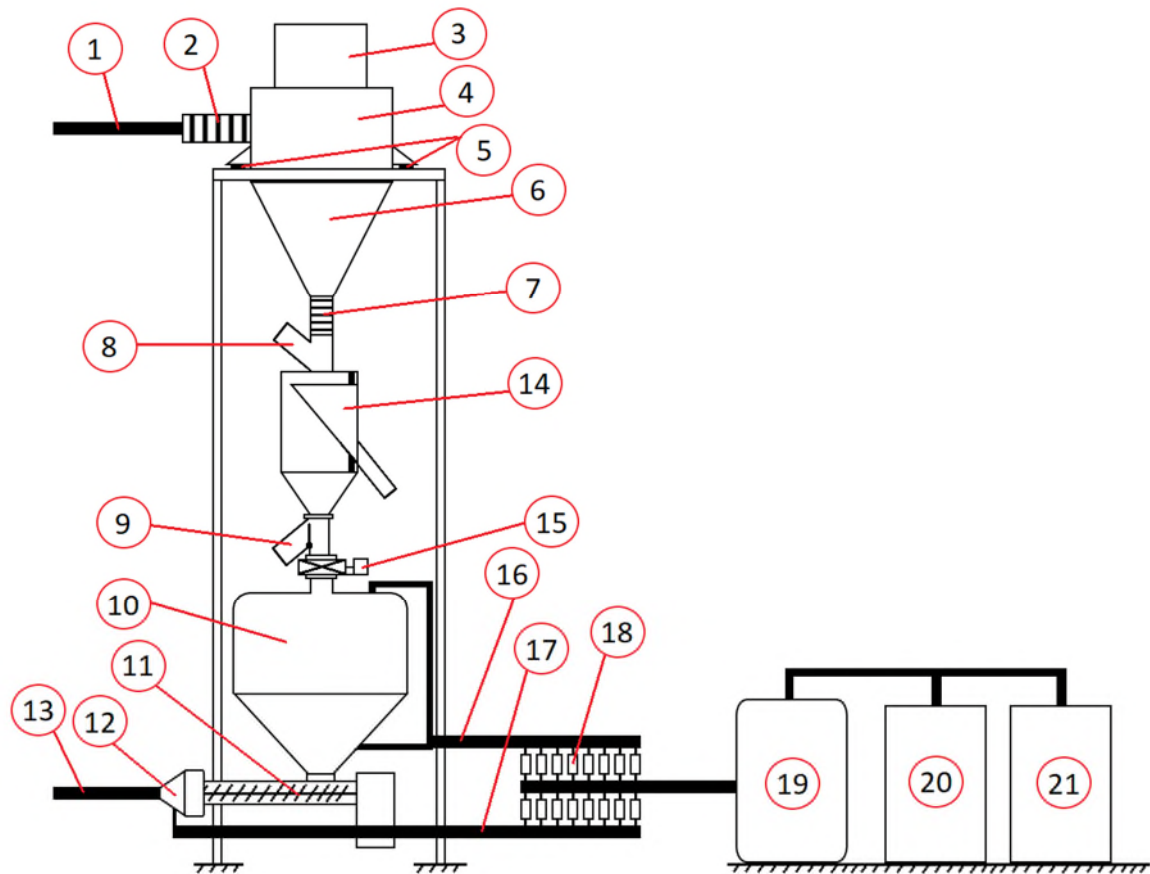
The receiving vessel was mounted on load cells, which were used to determine the average mass flow rate of sample conveyed. Positioned underneath the receiving vessel was an FCE Hogan Bin Discharger square profile of side length 1 m. This consisted of a series of louvres that could be rotated and vibrated to control the flow of material from the receiver.

Located between the Hogan Discharger and the blow tank was an InterSystems GRA gravity chute statistical sampler. This unit sampled across the full particle stream cross section as it was discharged from the receiver. The frequency of sampling cuts could be specified to determine the sample size required from the batch.

Extracting from the bottom of the blow tank was a bespoke screw-feeder mechanism that is described in further detail by Hyder [212]. Depending on the conveying behaviour of the sample, the screw can be used to control the mass flow rate of solids. For all tests conducted within the present research programme, the screw feeder was deactivated and the sample was conveyed past the stationary screw flights.

The pipe diameter throughout this system was 100NB schedule 40, with long radius bends of r/D ratio of 10. The conveying line loop schematic is shown in Figure 4-9b. Pressure transducers were located along the straights of the main conveying line at approximately 2 m spacings, and commencing 1.5 m from the intersection of straight line pipe centres of the previous bend. In using the data obtained from these pressure transducers, the straight-line pressure drop could be calculated. A sight window was located approximately midway along the last long straight section of the conveying system, through which video footage could be obtained. Morris couplings were used throughout the pipeline to connect pipe section to minimise the possibility of pipe misalignment.

The air-solids separation was achieved with bag filters equipped with a shaking mechanism for detachment of fine particles after a conveying test.



1	Return from conveying loop	12	Supplementary air inlet
2	Flexible connection	13	Delivery to conveying loop
3	Vibrating bag filters	14	Statistical sampler
4	Storage / receiving hopper	15	Butterfly valve
5	Load cells	16	Blow tank compressed air supply
6	Hogan discharger	17	Supplementary compressed air supply
7	Flexible connection	18	Nozzle banks
8	Infeed spout	19	Compressed air reservoir
9	Unloading spout	20	Air compressor 1
10	Blow tank	21	Air compressor 2
11	Screw feeder		

(a)

Figure 4-9: Pilot plant (a) schematic of the feeding and receiving arrangement, and (b) conveying line geometry adapted from Macchini et al. [41]

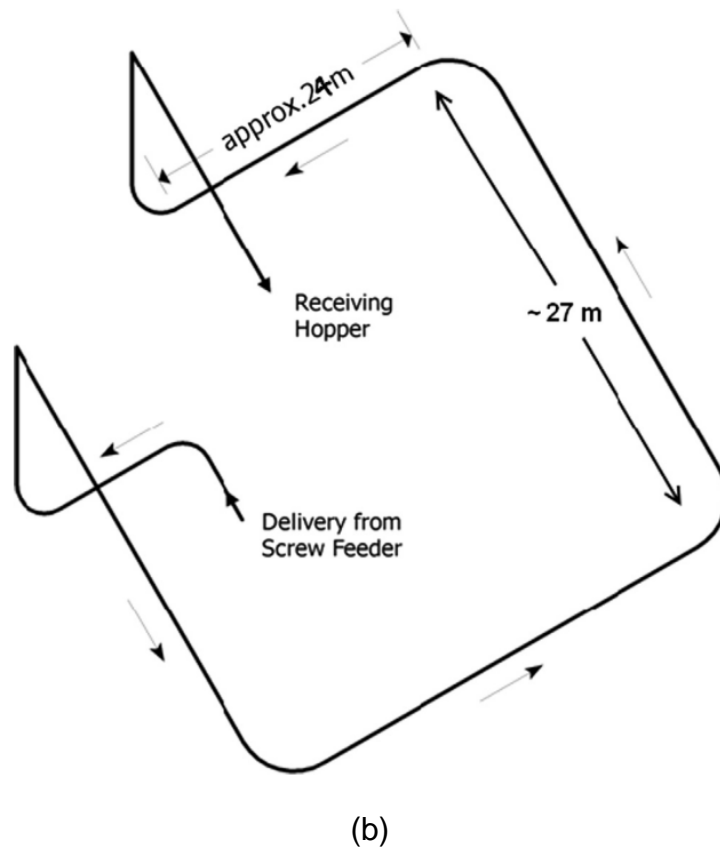


Figure 4 9: Pilot plant (a) schematic of the feeding and receiving arrangement, and (b) conveying line geometry adapted from Macchini et al. [41]

4.4.3.1 Considerations in the Context of Particle Attrition Testing

When this pilot plant was selected for use in the current programme of particle attrition testing, a number of difficulties were acknowledged:

1. The bag filters were not optimised for hygiene or fines detachment. This could have meant that fine particles of the test sample were lost in the filter material and could not be collected
2. The Hogan Discharger, Sampler and diverter valves all had internal surfaces where particles can be retained. This again, presented issues with hygiene and sample recollection.
3. The screw feeder had the possibility of inflicting particle attrition that was unquantifiable. As this was at the start of the conveying line, it was deemed that

the particles had not accelerated sufficiently to cause attrition levels that would excessively distort the data.

4. Even though the facility of a statistical subdivider was available for the experimentation on the pilot plant, it is recognised that there existed significant scope for error in reducing the sample size several orders of magnitude.
5. The entry of the sample into the receiving hopper meant that a significant 90 degree impact occurred. It was possible that this caused significant particle degradation, and was accounted for in the analysis.

4.4.3.2 Test Method

Due to the size of the samples used for this test work, the subdivision of samples described in Section 4.1 was used only to prepare samples for size analysis after first obtaining a sample from the full stream cross-cut sampler in the pilot plant. The method for conducting tests on the pilot plant proceeded as follows;

1. The desired mass of sample was loaded into a large vessel (from 25 kg sacks), which was then lifted onto the pilot plant loading platform with a crane.
2. A vibratory feeder was used to deposit the sample into the blow tank via the sampler, which was operating at the time (to obtain a virgin sample).
3. The blow tank was sealed and pressurised.
4. The conveying air was initiated, followed by material flow.
5. Data was logged from the pressure transducers along the straights of the pipeline and the hopper load cells throughout the conveying run.
6. Supplementary air was used as required to maintain blow tank pressure.
7. High speed video footage was captured through the sight glass on the final straight of the conveying line.
8. Once all material had been conveyed, the conveying air and supplementary air were shut off.
9. The filter bag shaker was activated for 20 seconds.
10. Sample was discharged through the Hogan Discharger into the blow tank, via the Sampler. A sample was collected and analysed.
11. Steps 3-10 were repeated as necessary.

4.4.4 External Pilot Plant Test Facility

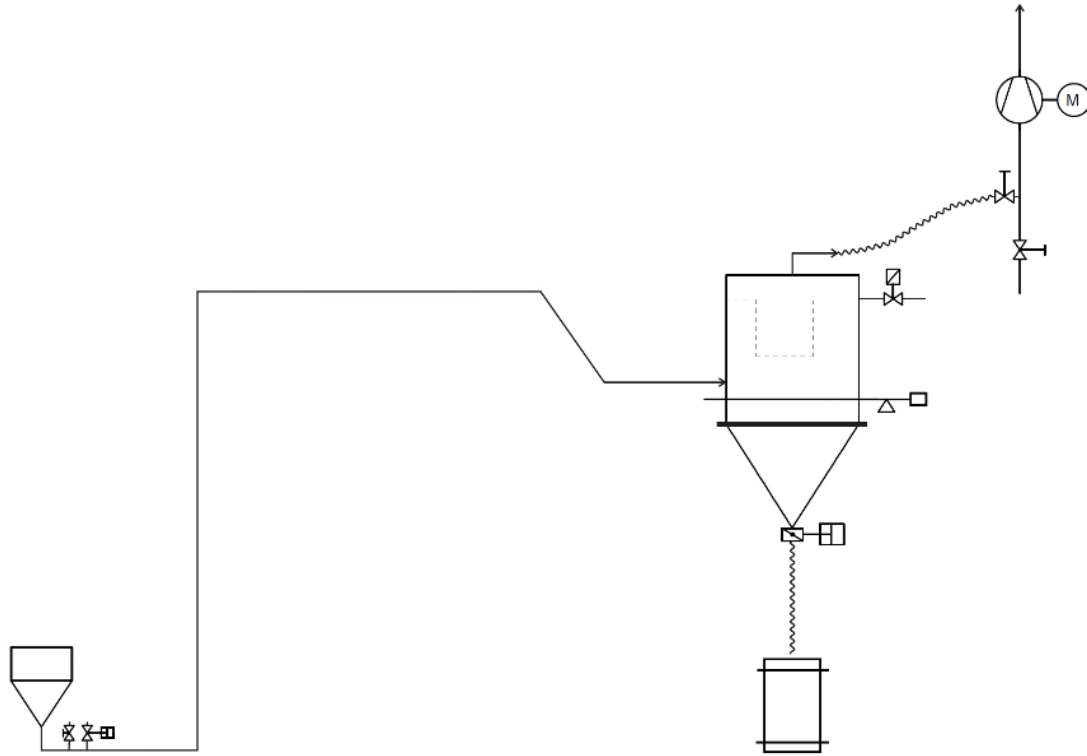
Some pneumatic conveying tests were performed on a pneumatic conveying system outside of the Wolfson Centre Laboratory. These were conducted at the AZO GmbH facility in Germany, on the system described by Figure 4-10.

This was a vacuum pneumatic conveying system with an inside pipe diameter of 47 mm driven by a Busch 1322 AV vacuum pump. The conveying line was 51.6 m long, and contained 7 bends. The dimensions of the pneumatic conveying line are detailed in Table 8-4 on page 252. Compression couplings were used to connect individual pipe section. The material feed rate from the feed hopper (Figure 4-10b) was controlled through the regulation of a manual bypass valve, and initiated through the closing of a second, electronically controlled bypass valve (Figure 4-10c).

The receiving vessel was 500 mm in diameter with a volume of 0.1 m³. It had a filter area of 1.5 m² and was cleaned with reverse pulse jets of compressed air. The conveying pipe inlet to the receiver was positioned coincident with the central axis of the receiver (Figure 4-10d). As a result, the particulate sample underwent a significant near-normal impact with the opposite wall of the receiver body. The air pressure of the line was measured on the pipeline connecting the receiver and the air mover.

The conical hopper of the receiver was connected to a collection vessel positioned below, via a butterfly valve (conforming to DN 300) and a length of sheet plastic tubing (Figure 4-10e).

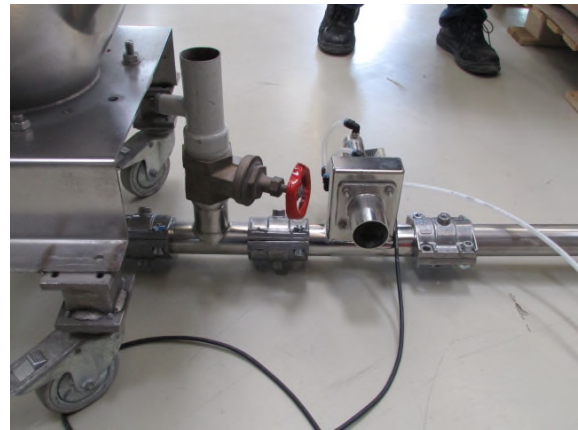
The particle size distribution of the conveyed sample was determined using an Allgaier TSM 600 dry mechanical sieving machine.



(a)



(b)



(c)

Figure 4-10: External pilot Plant facility (a) Schematic (not to scale), (b) Feeding Arrangement, (c) Bypass Valve, (d) Receiver, and (e) Sample Collection



(d)



(e)

Figure 4 10: External pilot Plant facility (a) Schematic (not to scale), (b) Feeding Arrangement, (c) Bypass Valve, (d) Receiver, and (e) Sample Collection

4.4.4.1 Test Method

Tests were conducted according to the following method:

1. A single 25 kg bag of material was loaded into the feed hopper
2. The bypass vent was adjusted to control the solids loading ratio of the conveying run
3. The data logging software and the air flow were initialised
4. The solids flow was initialised by closing the bypass valve.
5. At the conclusion of the conveying run the secondary bypass valve was opened and reverse pulse-jet cleaning of the filters was conducted.
6. The butterfly valve was opened and the sample was taken from the collection vessel.
7. The sample was sieved using a Allgaier TSM 600 dry mechanical sieving machine. The oversize sample from this analysis was taken and further sieved in a Retsch Vibrotronic VE1 dry mechanical sieve vibrator.

4.5 Particulate Materials

A wide range of materials were considered in the test programme, however only few could be studied in depth. This section will detail each of the materials considered throughout the programme of experimentation.

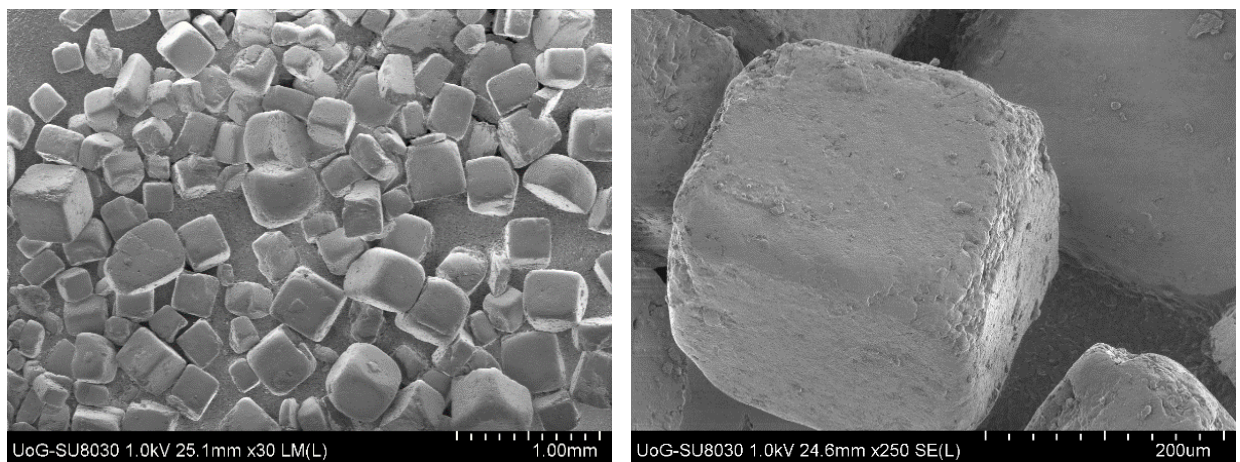
In selecting test materials, the following criteria were considered:

- Health hazards (See Appendix C for details)
- Inert. The material could not react or degrade under the storage and testing conditions applied within the timeframe of the experimental programme. This includes caking and softening of particles due to interaction with atmospheric moisture.
- Failure mechanism. The scope of the research dictated that the material must fail according to a non-ductile regime. Therefore, materials prone to large amounts of plastic deformation prior to fracture were not considered in the selection process.
- Morphology. High particle aspect ratios or 'extreme shaped particles' are not easily measured in the dry mechanical sieving process. Therefore, the particles with high sphericity were favoured, and 'needle' or 'flake' shaped particles were rejected.
- Particle size distribution. As the research scope required the study of particle size with respect to particle attrition, the material had to be available in particle sizes varying from approximately 200-1000 μm . Whether available in pre-cut sieve fractions, or in a single particle size distribution that could be later cut through dry mechanical sieving.
- Availability. The product needed to be readily available in quantities ranging from 25 kg, up to approximately 5 t, to cater for each of the test apparatuses forming part of the programme. It was also of interest to the sponsoring party to test specific materials; these will be identified where relevant.
- Particle structure. It was deemed desirable to account for a range of different particle structures (amorphous, agglomerate, crystalline, etc) in the experimental programme.

Taking into account each of these considerations, the materials tested throughout the experimental programme shall be detailed below. The D10, D50, and D90 for all materials is summarised in Table 4-7, on page 131.

4.5.1 Sodium Chloride (Salt)

Sodium chloride is a crystalline material conforming to a face centre cubic particle morphology. As shown in the scanning electron microscope image (Figure 4-11), the corners of the crystals are rounded in their 'as received' state. It was thought that this could be due to damage attained during the handling stages subsequent to the crystallisation process.



(a)

(b)

Figure 4-11: Scanning electron microscope images of sodium chloride crystals

The virgin particle size distribution is given in Figure 4-12, and could be seen that overall, the product had a relatively narrow distribution. There was a small amount of very fine particles (sub 50 μm) on a mass basis; however, when the material was poured, some fine dust could be seen to be entrained in the air.

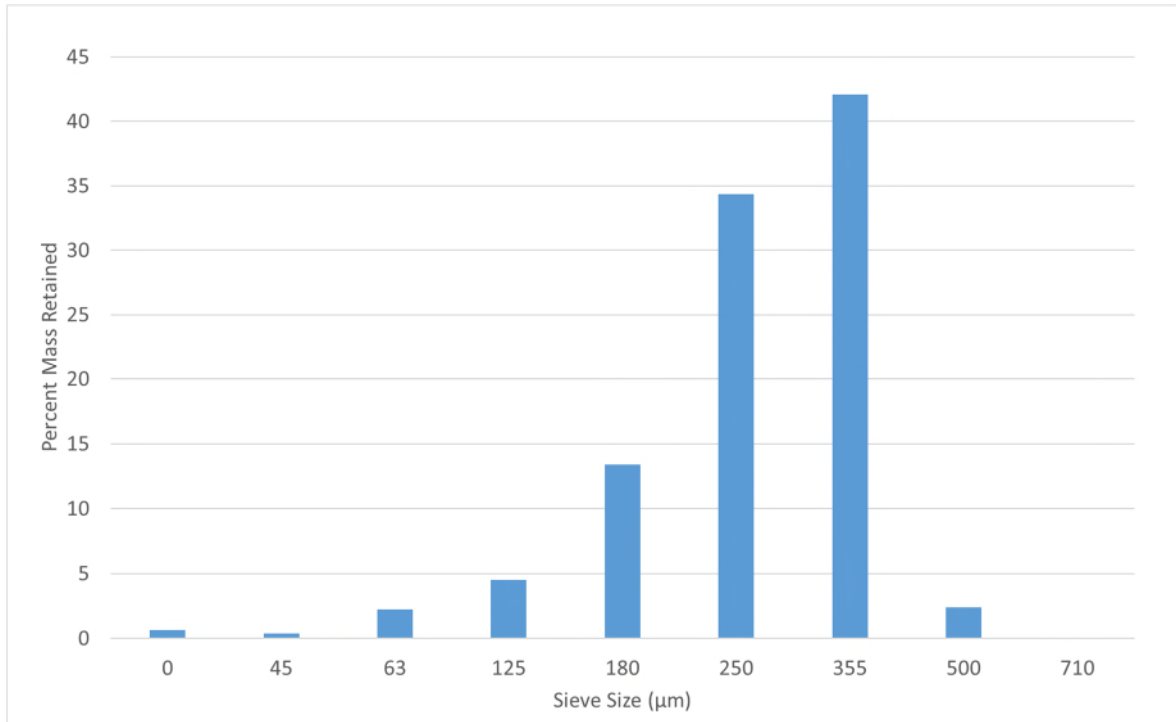


Figure 4-12: Virgin Particle Size Distribution of Sodium Chloride

As was determined in the literature review (Chapter 2), sodium chloride has been previously investigated by other researchers and found to fail according to the semi-brittle regime [64]. Both chipping and fragmentation behaviours have been observed with this material in previous works by other researchers.

The primary difficulty in using this material for the full spectrum of test work was that sample was only available in 3 kg bags. Therefore, for logistical reasons, this material was appropriate only for the apparatuses requiring a small sample size.

4.5.2 Golden Breadcrumbs

Golden breadcrumbs (Figure 4-13) are a commercially available cooking product that have an amorphous particle structure. Particles visually pertain to an angular morphology, with wide variability from particle to particle. This presented some difficulties in the dry mechanical sieving analysis as discussed in Section 4.2. The particle size distribution of the virgin material is given in Figure 4-14. It is noted that golden breadcrumbs have a

relatively wide particle size distribution when compared to that of sodium chloride in the previous section.



Figure 4-13: Golden Breadcrumbs

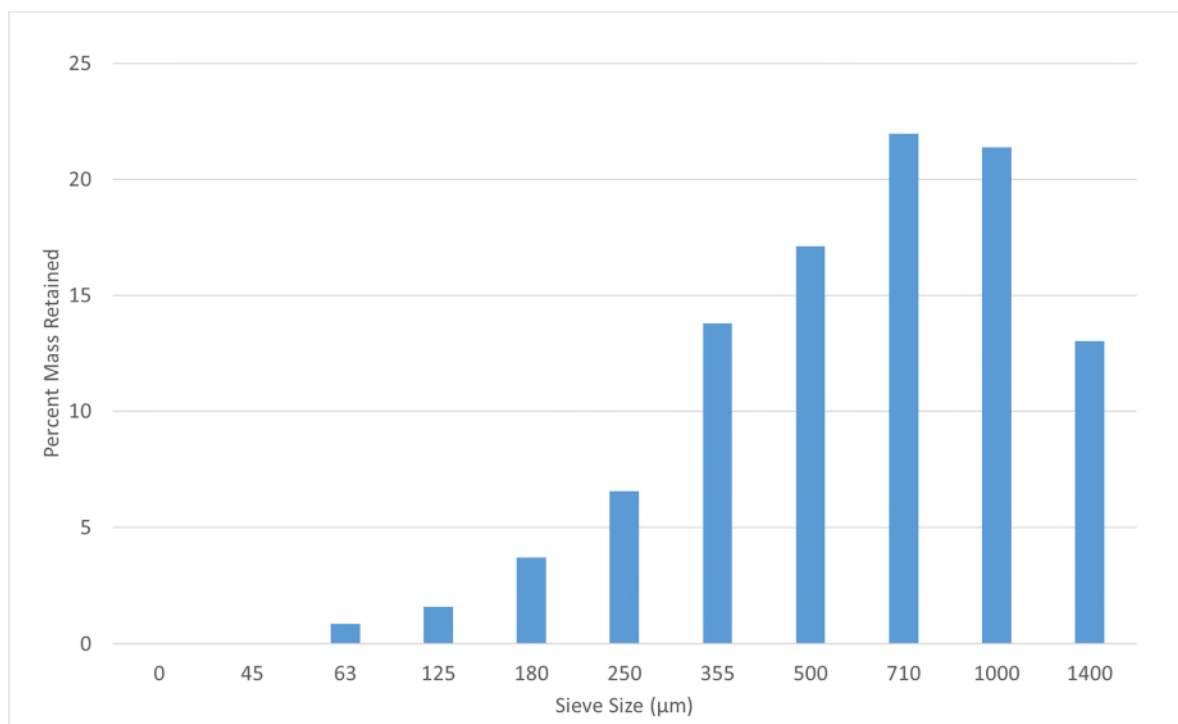


Figure 4-14: Virgin Particle Size Distribution of Golden Breadcrumbs

As was the case with the sodium chloride, this product was only available for purchase in 3 kg bags, making it logistically difficult to use in testing at the large scale.

4.5.3 Sucrose (Granulated Sugar)

Sucrose (Figure 4-15) is a solid conforming to a monoclinic crystal structure. It was commercially available in 25 kg bags. The particle size distribution for this product is presented in Figure 4-16, and it can be seen that it had a relatively wide particle size distribution.



Figure 4-15: Granulated Sugar

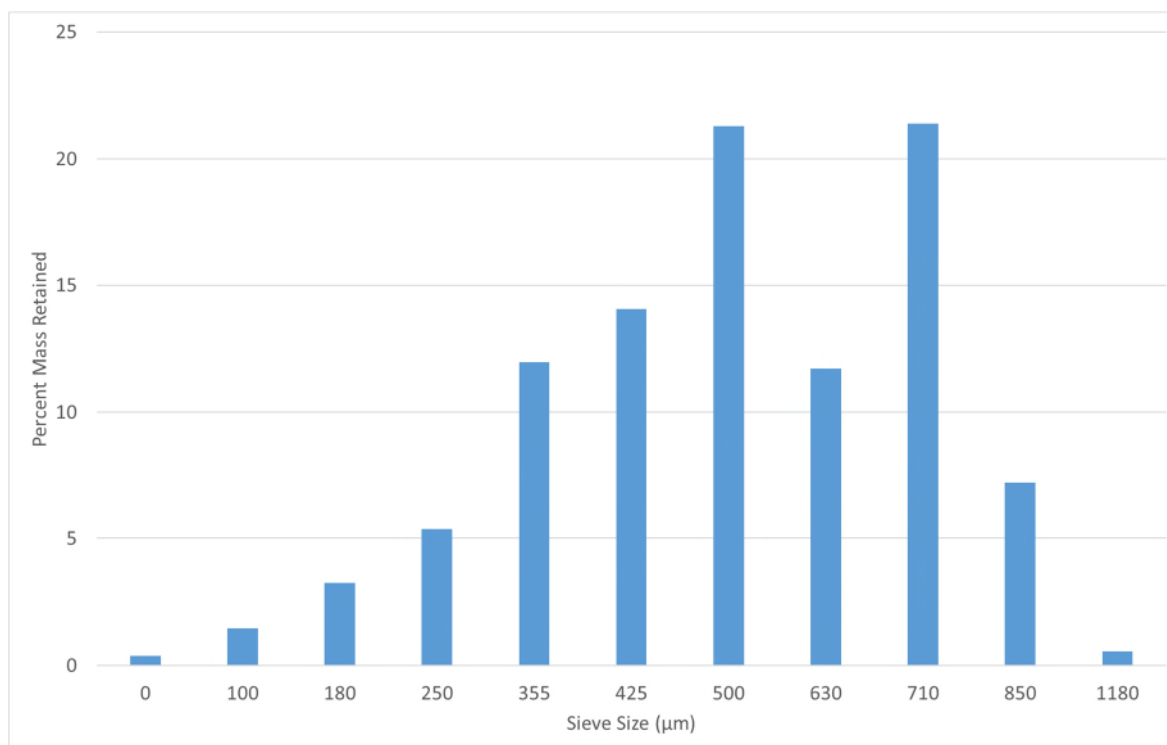


Figure 4-16: Virgin Particle Size Distribution of Granulated Sugar

If exposed to cyclic variations of high and low humidity as temperature varies between night and day, crusting occurs on the exposed surface. Potential for agglomeration makes it difficult to determine the particle size distribution of the primary particles. While an anti-caking agent is generally included with commercial products to alleviate this, the phenomenon cannot be mitigated in its entirety. Caking was particularly concerning within attrition testing as the increased surface area to volume ratio of the smaller particles increases the propensity for caking. Further to this, fine particles are concentrated in the smaller sieve sizes (below 100 μm) when dry mechanical sieving analysis is conducted. Again, this presents challenges in obtaining an accurate particle size distribution measurement.

4.5.4 Biomass Pellets

The pelletisation of biomass materials is common in both the animal feed and the power generation industries. In the present study, wood pellets of varying methods of manufacture (standard white pellet, thermally treated pellet) were considered (Figure 4-17), in addition to one pellet type manufactured from straw feedstock.



(a)

(b)

Figure 4-17: Biomass Pellets

The method of manufacture of these pelletised materials enables them to be largely classified as a type of agglomerated material. The rationale for this stems from the fact that these particles are inhomogeneous, and contain an array of constituent particles bonded together. The child particles resulting from breakage events of pellets should be considered within this context; it is possible that the constituent particles have a greater strength than the agglomerated whole.

Pelletised biomass was available in industrial quantities; however, pellet lengths were generally greater than what can be tested on the particle attrition characterisation testers (namely the QPM and BSPAT).

4.5.5 Carbolux SK

Carbolux SK (Figure 4-18) is a form of granulated carbon material (99.6% carbon, 0.01% sulphur) used as a recarburiser and derived from acetylene synthesis. This product is produced by calcination at 1400 °C, and then sieved into size cuts, which could then be obtained individually. It was of interest to the Sponsoring Party to test this material for its breakage behaviour, and hence was supplied by them for the present research.

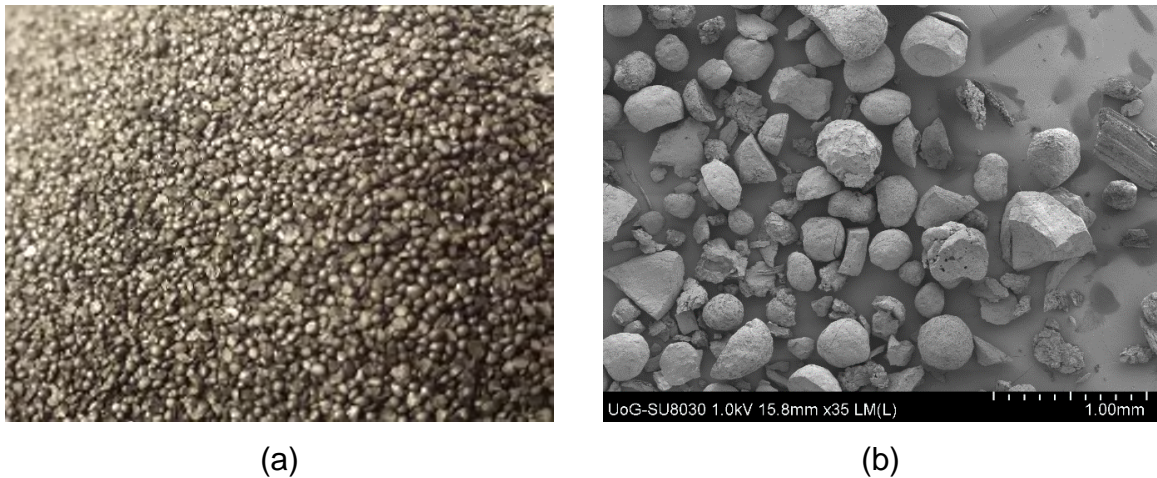


Figure 4-18: Carbolux (a) Photograph, and (b) SEM Image (post-breakage)

As shown in Figure 4-18b, the carbolux failed by chipping and fragmentation, as opposed to failure by prominent plastic yielding. Therefore, this material was suitable for the present experimental programme in terms of the particle failure mechanism manifested under impact loading conditions.

The particle shape was analysed with a Malvern Morphologi G3, and particle densities as measured by a Micromeritics Accupyc II 1340, are summarised in Table 4-5. These values were averaged across the entire particle size distribution for each particle. Therefore, as there were more individual particles in the smaller size fractions, the values of circularity were skewed towards the characteristics of the smaller particle size fractions. Noting that smaller particles were more likely to have been generated from the fracture of larger particles (as this material was pre-sieved), the values in Table 4-5 indicated a circularity lower than what was visually present in the size fractions of interest.

Carbolux was acquired in three primary size fractions (classified as A, B, and C within the scope of the present work). The virgin particle size distribution for each of these acquired size ranges is shown in Figure 4-19.

Table 4-5: Particle Shape Analysis and particle Density Measurement for Carbolux SK

Feature	Value
Aspect Ratio (-)	0.688 (0.160)
Circularity (-)	0.787 (0.153)
Density - Carbolux SK B (g/cm ³)	1.8231 (0.0001)
Density - Carbolux SK C (g/cm ³)	1.7788 (0.0004)

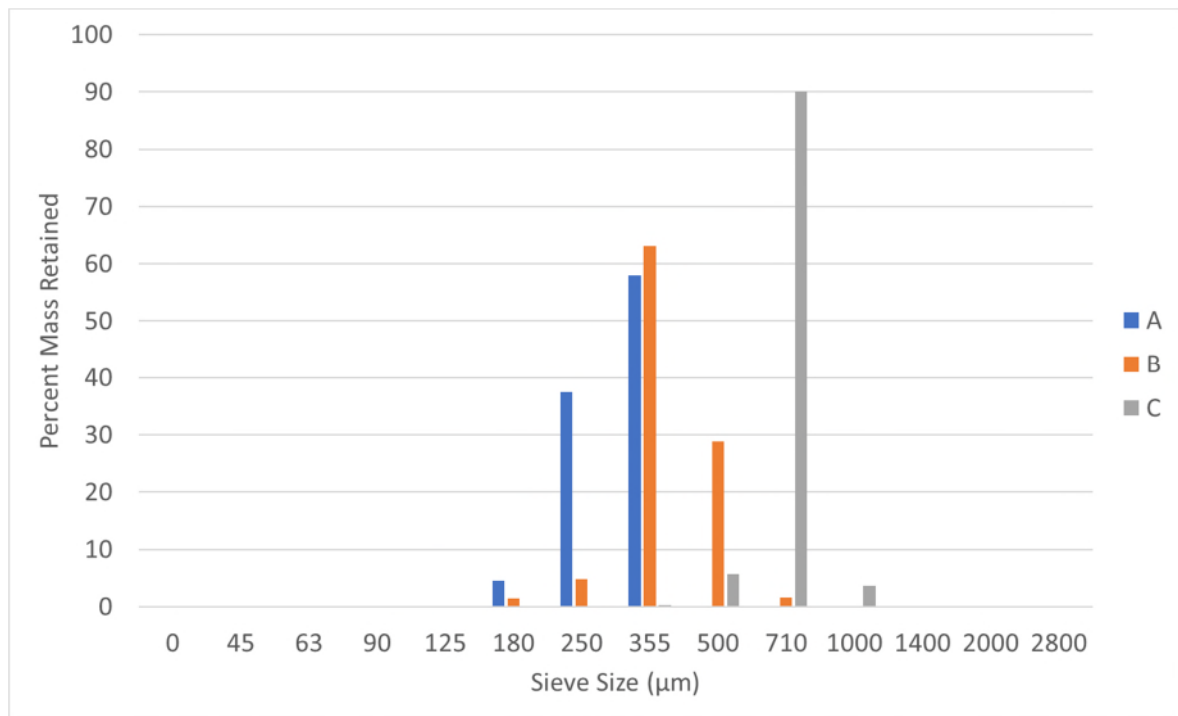


Figure 4-19: Virgin Particle Size Distribution of the three size classes of Carbolux SK

4.5.6 Adipic Acid

Adipic acid is a white powder with a monoclinic crystal structure. Used in the production of plastics, detergents and cleaning agents, this material was found to cake when allowed to rest for extended periods of time as shown in Figure 4-20. These material cakes were weak in nature, and were easily broken as soon as a small amount of force was applied. It was deemed that this material was appropriate for testing in the large scale pneumatic conveyors (as any cakes would be easily broken at the first bend), however smaller test equipment was incompatible due to the smaller material flow cross-sections required (such as the QPM, BSPAT and SBAT). It was of interest to the Sponsoring Party to test this material for its breakage behaviour, and hence was supplied by them for the present research.



Figure 4-20: Adipic acid sample demonstrating the caking behaviour of the material

The virgin particle size distribution of adipic acid is given in Figure 4-21. The presence of fine particles made dry mechanical sieving difficult, but was still possible if care was taken to clean the sieves well.

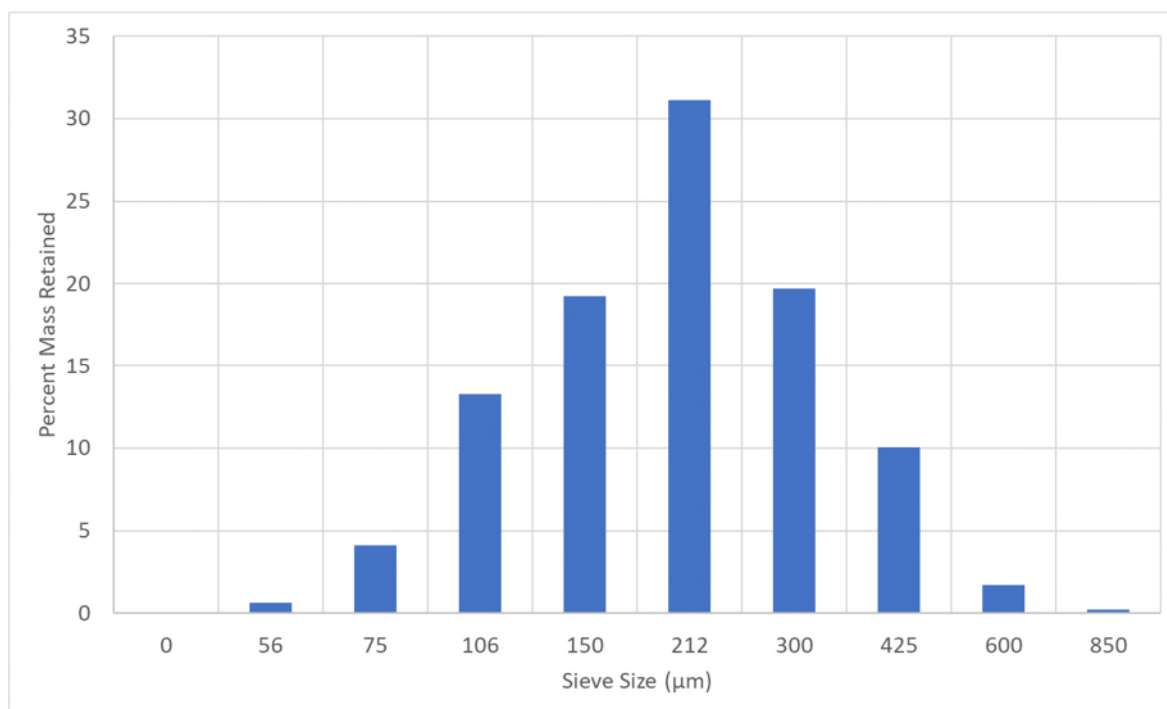


Figure 4-21: Virgin Particle Size Distribution of Adipic Acid

The availability of this product was in a single particle size distribution in 25 kg bags. This product could be obtained in large quantities appropriate to the experimental programme.

4.5.7 Spent FCC Catalyst

A fine off-white powder, spent FCC catalyst contained 40-75 % amorphous silica, 25-60 % aluminium oxide, and 0-0.15 % Nickel. Table 4-6 shows average values of the particle morphology as measured by a Malvern Morphologi G3, Figure 4-22 shows a scanning electron microscope image of the material, and Figure 4-23 shows the particle size distribution of the virgin particles as measured by laser diffraction size analysis. It can be seen that this product was significantly smaller in mean particle diameter when compared to the other particulate materials considered in this research. This material also has a very high value of particle circularity.

This particulate material was available as a once-off acquisition of 30 kg. This meant that spent FCC catalyst could be tested only on the smaller characterisation equipment (i.e.

the QPM and BSPAT), and limited test runs on the single bend attrition tester. Two types of Spent FCC Catalyst were tested; denoted by Type T and Type C.

Table 4-6: Particle shape analysis results for Spent FCC Catalyst particles (values of standard deviation in parentheses)

Number of Particles	CE Diameter Mean (μm)	HS Circularity Mean	Convexity Mean
2122	55.58 (27.12)	0.913 (0.160)	0.844 (0.062)

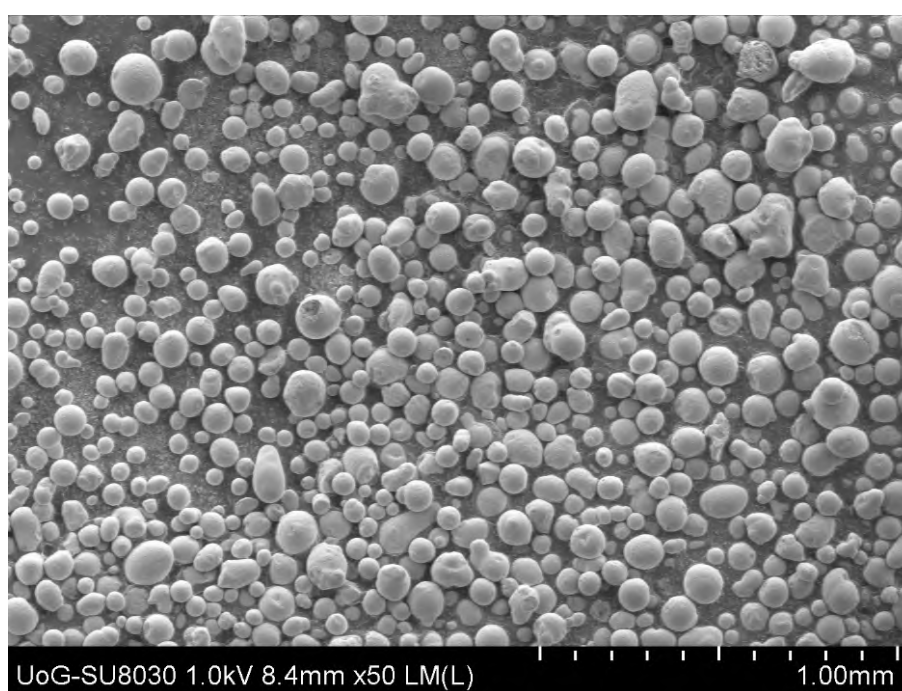


Figure 4-22: Scanning Electron Microscope image of Spent FCC Catalyst particles

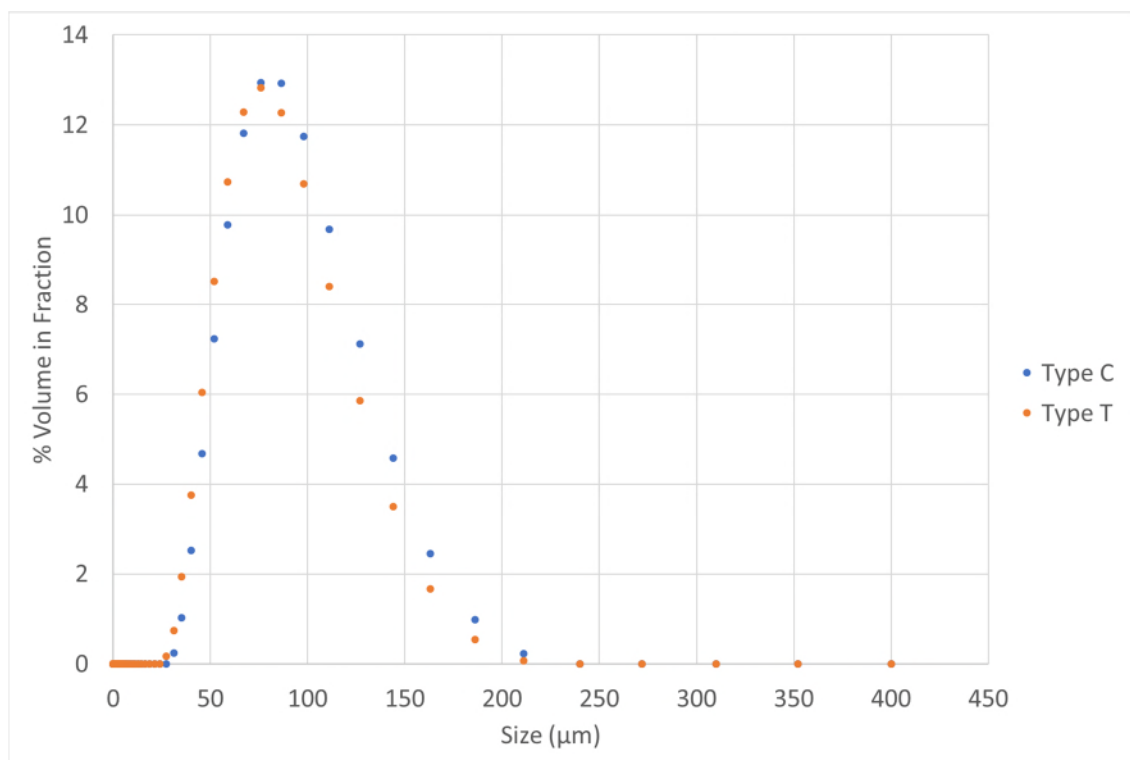


Figure 4-23: Virgin particle size distribution of Spent FCC Catalyst Type C and Type T

4.5.8 Summary

A variety of materials were selected for various courses of experimentation. Table 4-7 summarises the d_{10} , d_{50} , and d_{90} particle size distribution characteristics for each material, and Table 4-8 summarises the apparatuses used to test each material.

Table 4-7: Particle size characteristics for each of the materials tested in the experimental programme

Material	D10 (µm)	D50 (µm)	D90 (µm)
Sodium Chloride	134.1	238.5	336.1
Golden Breadcrumbs	223.7	569.0	1109.2
Sucrose	244.5	477.4	708.2
Biomass Pellets*	N/A	N/A	N/A
Carbolux SK – Type A	190.1	264.4	336.9
Carbolux SK – Type B	255.8	322.3	457.4
Carbolux SK – Type C	509.1	602.4	695.6
Adipic Acid	123.5	248.1	458.9
Spent FCC Catalyst – Type C	53.2	86.1	139.6
Spent FCC Catalyst – Type T	49.1	80.5	131.3

Table 4-8: Combinations of particulate material and experimental apparatus tested throughout the experimental programme

Material	QPM	BSPAT	LSPAT	SBAT	Wolfson PP*	External PP*
Sodium Chloride	X					
Golden Breadcrumbs	X	X				
Sucrose	X		X			
Biomass Pellets			X			
Carbolux SK	X	X		X	X	X
Adipic Acid					X	
Spent FCC Catalyst		X		X		

*Pilot Plant

CHAPTER 5: Results and Observations: Particulate Material Attrition Behaviour Characterisation

This chapter shall present the key results and observations obtained from the particle attrition characterisation experiments, namely those obtained from centrifugal particle attrition testers. The influence of each of the operating parameters shall be addressed in turn, as investigated with the BSPAT apparatus. Following this, comparative studies shall be presented using the results obtained from the QPM and LSPAT apparatuses. Finally, conclusions shall be drawn in terms of the effects of operating conditions, and in terms of the tester geometry on the levels of particle attrition measured.

5.1 BSPAT Testing

The Bench-Scale Particle Attrition Tester, BSPAT, as described in Chapter 4, was used to obtain all results presented in this Section. Section 5.1.1 to 5.1.3 shall elucidate the influences of each operating parameter with respect to the attrition of Carbolux SK. Finally, the comparison of the attrition behaviour of Carbolux SK, Sodium Chloride and Spent FCC Catalyst shall be given in Section 5.1.4.2, along with the influence of particle size. At the conclusion of this section, all possible user-controlled variables will have been systematically isolated for a given apparatus geometry, barring the particle feed rate (addressed in Section 5.2.2). Results shall be presented in the form of 'Magnitude of Deviation'. This describes the magnitude of change in the percentage mass retained on a given sieve, and is defined by Equation (5-1) and Equation (5-2). This descriptor indicates the change in the percent mass retained on a given sieve (and hence retained within a given size fraction within the particle size distribution). For example, take the following scenario: 45% of the sample mass is retained within the 710-1000 μm size fraction prior to the test, and 35% of the sample mass is retained within the 710-1000 μm size fraction after the test. The magnitude of deviation is the simple difference between the two values (initial state subtracted from the final state) and is equal to -10%, where the sign indicates material has left the size fraction.

$$\Delta\% = P_2 - P_1 \quad (5-1)$$

$$P = \frac{M_{sieve}}{M_{sample}} \quad (5-2)$$

Where:

$\Delta\%$ Magnitude of deviation (dimensionless)

P_1 Percentage mass retained on the sieve in question for virgin sample (%)

P_2 Percentage mass retained on the sieve in question for post-test sample (%)

M_{sieve} Mass retained on sieve (kg)

M_{sample} Mass of total test sample (kg)

All percentages presented in this work shall be given in decimal form unless otherwise specified.

5.1.1 Influence of Impact Velocity

Within the regime of particle attrition by impact, impact velocity has been repeatedly demonstrated to have the greatest influence on the level of particle breakage observed (as stated in Chapter 2). As the superficial air velocity of lean phase pneumatic conveying systems is generally operated in the region of 10 – 40 m/s, the range of particle velocities selected for this work was 10 – 35 m/s in 5 m/s increments. The particle size distribution of the Carbolux SK used in this testing is shown in Figure 5-1. This pre-sieved size fraction was selected due to the very narrow cut achieved, whereby approximately 96.5 % of the virgin sample was retained on a single sieve size.

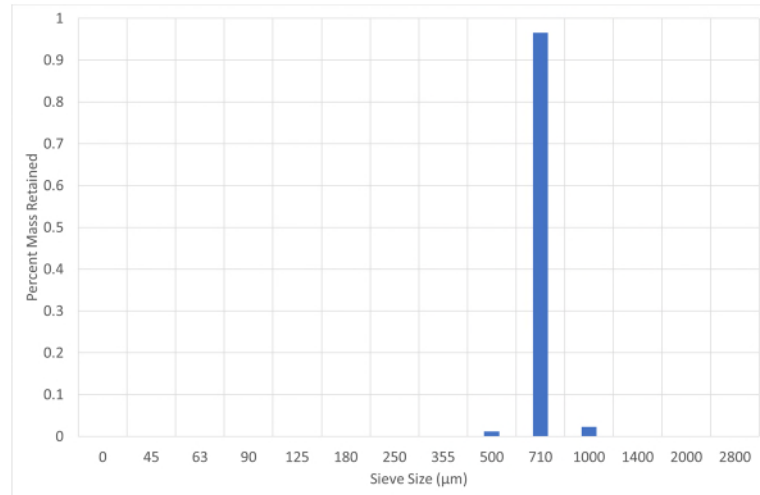


Figure 5-1: Particle size distribution of pre-sieved sample used for BSPAT impact testing

As the impact forces normal and tangential to the target face change with changing impact angle, Figure 5-2 shows the results obtained at each of the tested impact angles: 20, 30, 45, and 90 degrees. The magnitude of deviation shows how much sample mass is lost or gained from a size fraction, based on the difference of the percent mass retained in that size fraction, before and after the test. Therefore, as the vast majority of material resides in the 710-1000 µm size fraction for the virgin particle size distribution, it would be expected that the magnitude of deviation for this size fraction in the post-test state would be negative; indicating a loss of percent mass retained. Similarly, it would be expected that the size fractions smaller than the 710-1000 µm size fraction would accumulate the child particles of breakage events, and therefore show a positive magnitude of deviation.



(a)

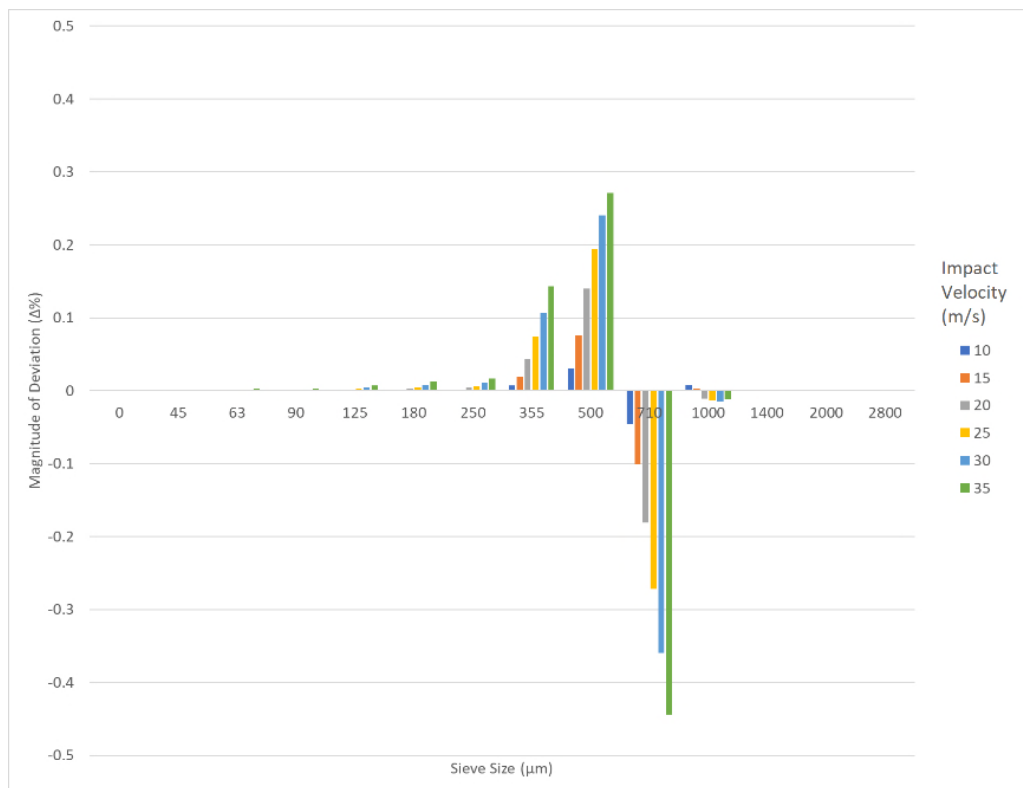


(b)

Figure 5-2: Magnitude of deviation results for Carbolux SK tests at impact angles of (a) 20, (b) 30, (c) 45, and (d) 90 degrees



(c)



(d)

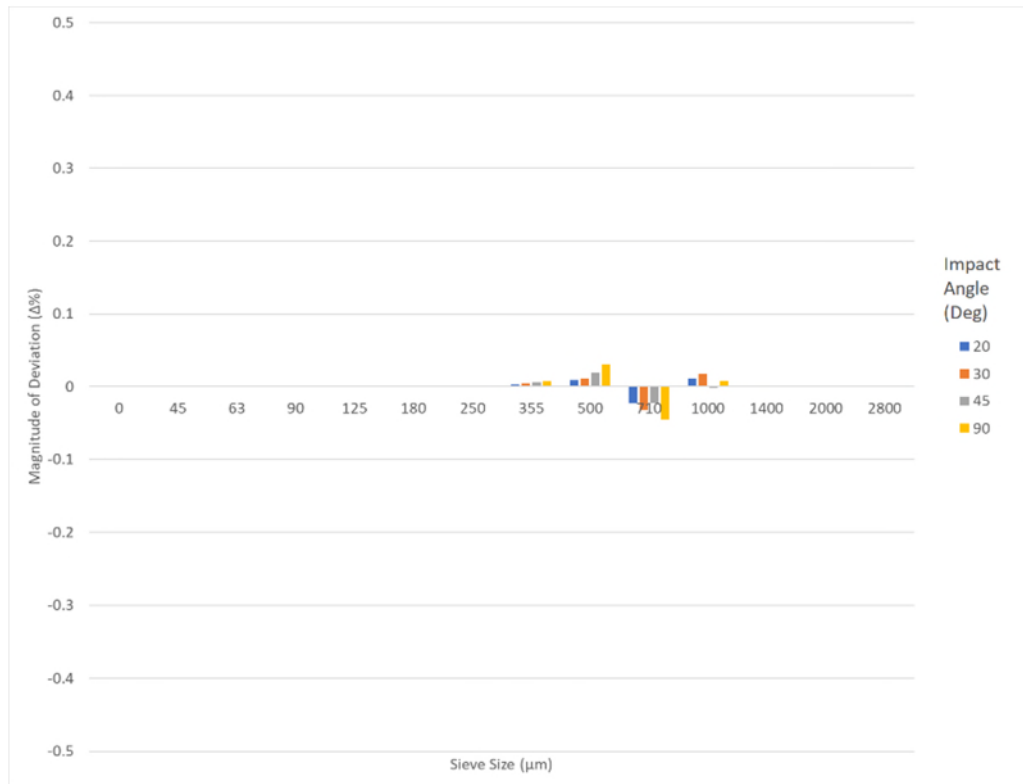
Figure 5 2: Magnitude of deviation results for Carbolux SK tests at impact angles of (a) 20, (b) 30, (c) 45, and (d) 90 degrees

It can be clearly observed that across all impact angles, particle breakage increases with increasing impact velocity. Furthermore, it can be stated that as the impact angle is increased (approaches a normal impact scenario), the influence of impact velocity further increases. For example, relatively similar amounts of material departed the 710-1000 μm size fraction at 10 m/s impact velocity across all impact angles. However, when considering 35 m/s impact velocities, there was considerable difference in particle attrition levels between the 20 and 90 degree impacts.

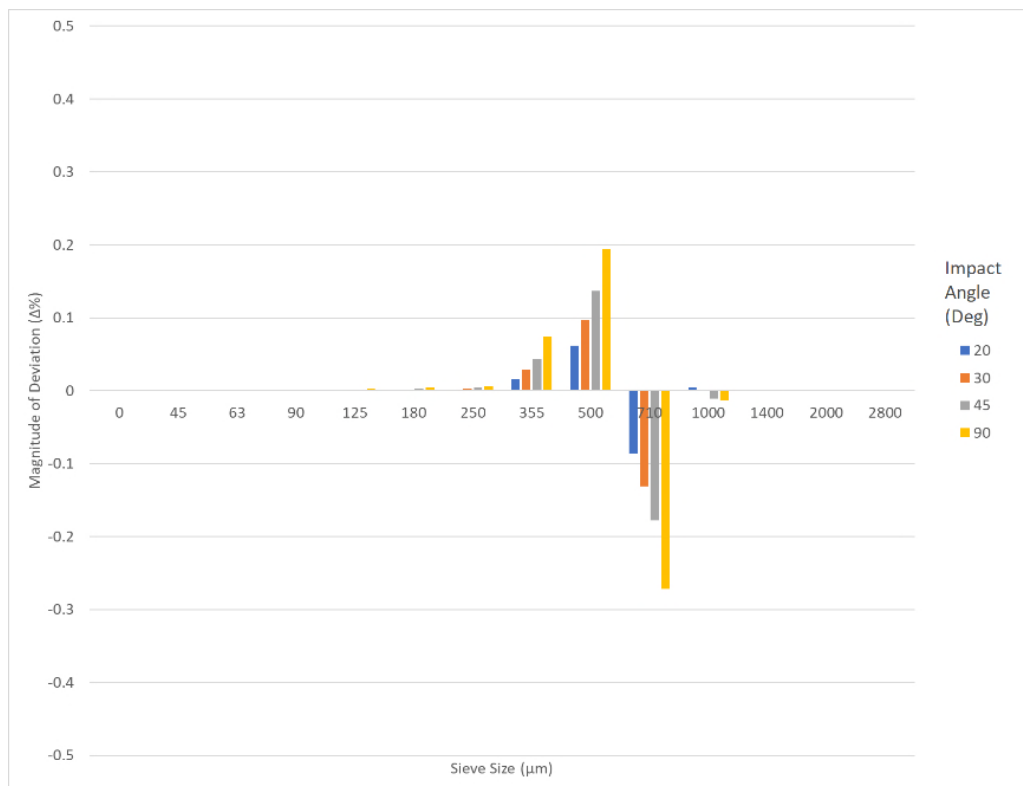
The general trends observed for the influence of impact velocity suggest that the normal velocity component contributes significantly more to particle failure than the tangential velocity component.

5.1.2 Influence of Impact Angle

Impact angle is defined within the present work as the angle subtending the particle velocity vector and the plane coincident with the impact target face. Modification of this variable adjusted the normal and tangential impact velocities with respect to the target surface. This in turn altered the ratio of applied shear force and normal force to the particle. The impact angles considered in this Section are 20, 30, 45, and 90 degrees, and are equivalent to the available test impact angles of the BSPAT. Figure 5-3 gives the results for the sample material identical to that considered in Section 5.1.1, across impact velocities of 10, 25, and 35 m/s.

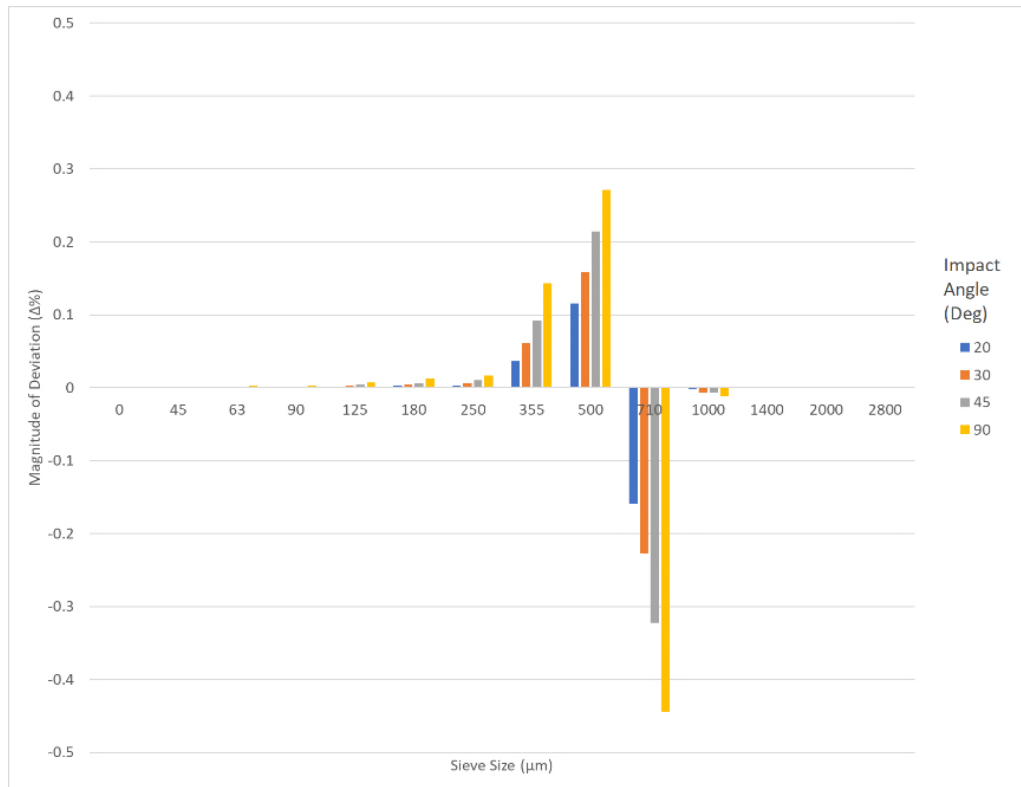


(a)



(b)

Figure 5-3: Magnitude of deviation results for carbolux tests at impact velocities of (a) 10, (b) 25, and (c) 35 m/s



(c)

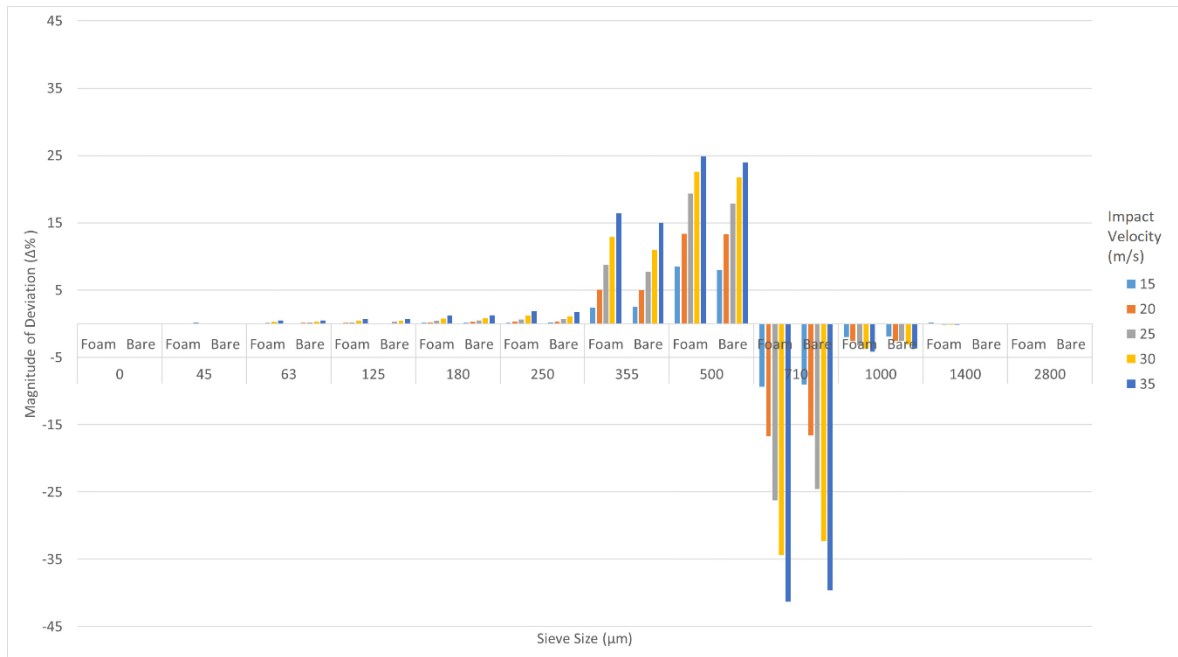
Figure 5.3: Magnitude of deviation results for carbolux tests at impact velocities of (a) 10, (b) 25, and (c) 35 m/s

Clear trends in the above data are present in support of the comments made in Section 5.1.1 regarding the influence of the normal component of the impact velocity. An increase in the level of particle attrition with respect to increasing impact angle was clearly observed for the 25 and 35 m/s impact scenarios; however, this was less-clear in the 10 m/s impact scenario. An explanation for this observation would be that the impact energies were insufficient across all cases to break any but the weakest of particles in the particle strength distribution.

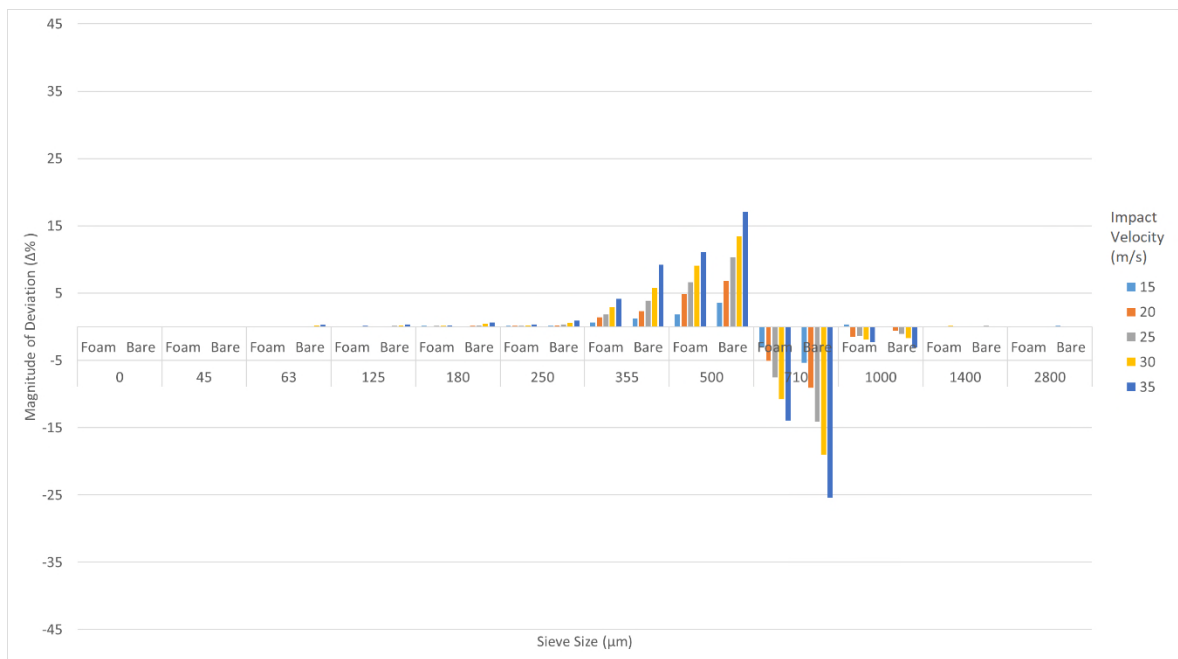
5.1.3 Influence of Secondary Impacts

Prior to the commencement of the experimental programme, it was determined that the influence of secondary impacts within the BSPAT on the particle attrition results required quantification. To achieve this, a closed-cell foam lining was applied to the outer wall of the impact chamber. Carbolux (virgin particle size distribution given in Chapter 4) was

tested across a range of impact conditions both with and without the lining. Samples were tested across impact velocities of 15 – 35 m/s, and impacts angles of 20 and 90 degrees. At a 90-degree impact angle, it is not expected that particles would impact the outer wall of the impact chamber, and was therefore used as a control test throughout the investigations. Conversely, as a 20-degree impact is only a glancing contact across the target face, it was expected that the particle would continue to undergo a significant secondary impact at the outer wall of the impact chamber. Figure 5-4 presents the results of this experimental programme. For ease of comparison, the results for each size fraction are presented for the case of the applied foam lining (denoted by 'Foam') and without (denoted by 'Bare').



(a)



(b)

Figure 5-4: BSPAT post-test particle size distribution results for (a) 90 degree impacts, and (b) 20 degree impacts

With respect to the 90 degree impact scenario, it can be observed that there was little difference in the level of particle attrition measured across all impact velocities and secondary impact mitigation scenarios. However, when the 20 degree impact angle was considered, large differences in the magnitude of particle attrition was measured.

Approximately 11% of the sample mass was removed from the 710-1000 μm size fraction in the bare wall condition, in addition to that removed by the foam wall condition at 35 m/s.

When the material removed from the 710-1000 μm size fraction is considered in isolation, a second power polynomial relationship can be used to describe the particle attrition behaviour to a high level of accuracy (Figure 5-5). Furthermore, it was found that the 'Bare' outer impact chamber wall condition inflicts 79.5% more damage across all impact velocities with a standard deviation of 0.053.

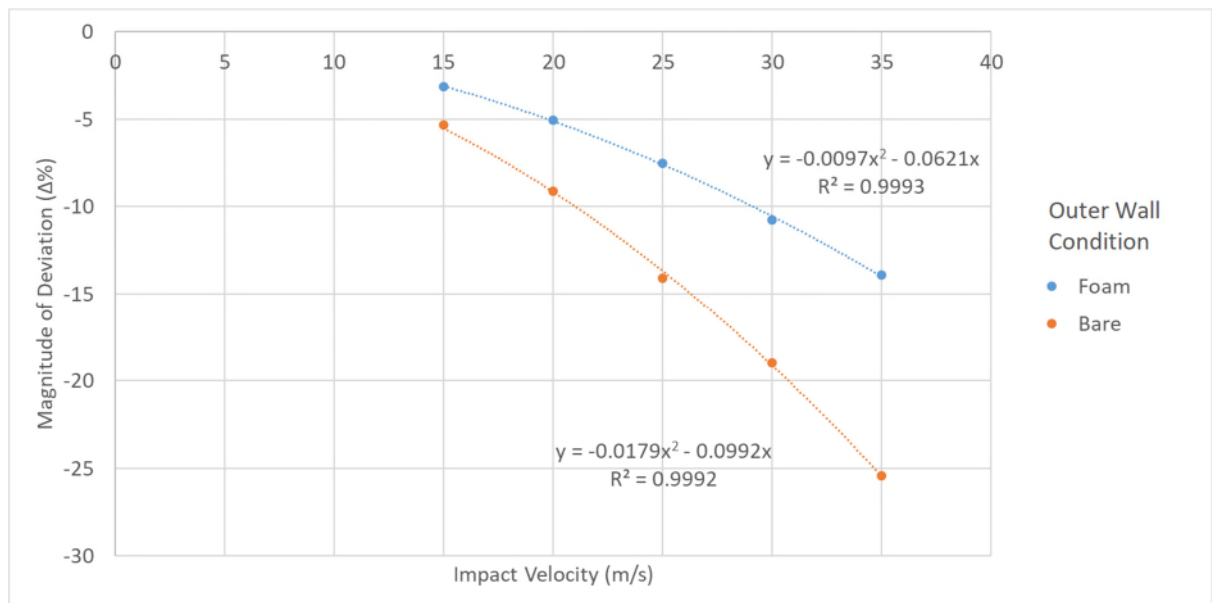


Figure 5-5: Magnitude of Deviation vs. Impact Velocity for 'Foam' and 'Bare' outer impact chamber wall test conditions

This conclusion has important repercussions for apparatus design (as alluded to in Chapter 4), and in the application of such data to predict particle attrition levels in real-world systems. These results confirm and quantify the influence of secondary impacts in centrifugal accelerator particle attrition testers at shallow impact angles. This form of analysis is addressed in more detail in Chapter 9.

5.1.4 Influence of Sample Material

Within the context of the present work, two material characteristics were considered with respect to the influence of the sample material on the particle attrition behaviour observed: particle size, and material composition.

5.1.4.1 Particle Size

Particle size was investigated by pre-sieving Carbolux SK into four distinct size fractions via the dry mechanical sieving process. Each of the different Carbolux batches (See Chapter 4) were sieved, and the material retain on the 250, 355, 500 and 710 μm sieves were stored separately (hereafter denoted as the primary batch size fraction). The resulting particle size distributions of each fraction are given in Figure 5-6.

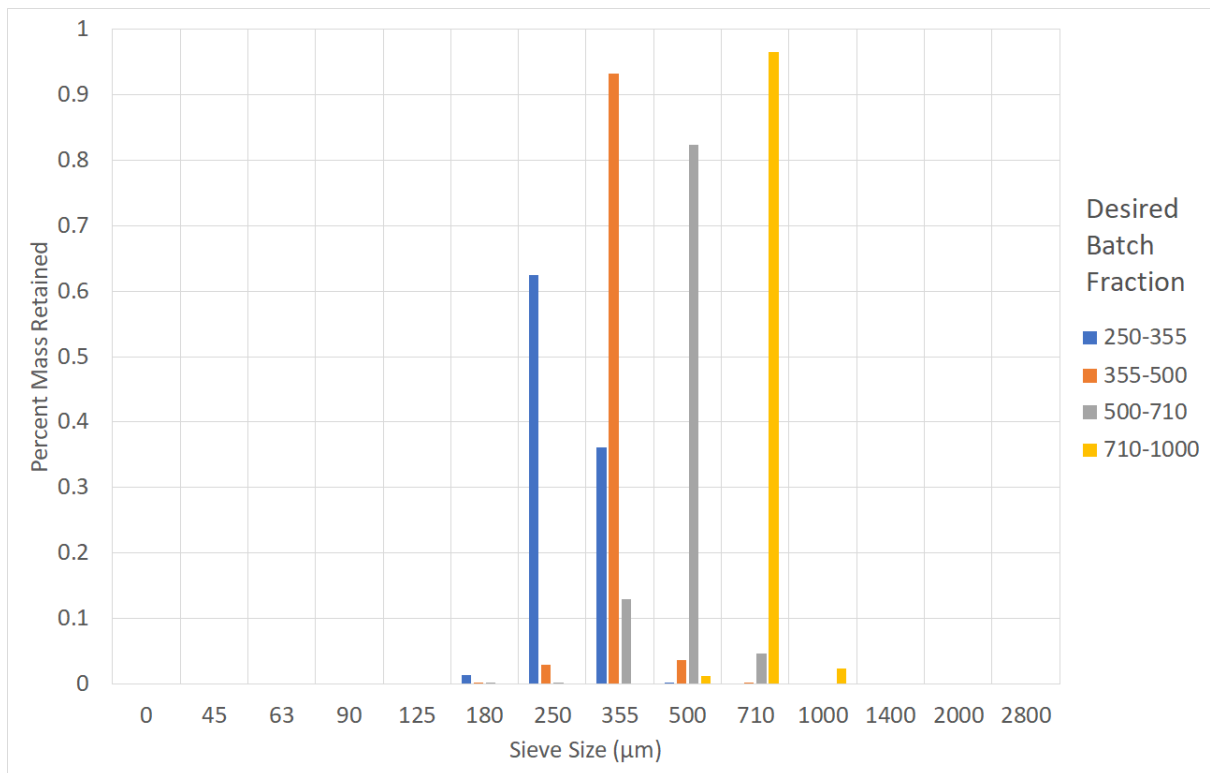


Figure 5-6: Particle Size Distributions of Pre-Sieved Carbolux SK Size Fractions

It can be seen that the pre-sieving procedure was imperfect, with some of the sample falling outside the desired batch fraction size upon secondary sieving analysis. This may have been due to irregularities in particle shape, whereby particle orientation with respect to the sieve mesh could have played an important role in determining whether that particle would pass through or not. Additionally, localised sieve blinding could have been responsible for some undersize particles being retained in sizes with aperture sizes larger than that of the particle.

A significant source of error in preparation of the batch fractions was due to the use of two different sieve stacks used to prepare the batches. As shown in Figure 5-7, each sieve stack returned a different particle size distribution for samples from the same batch fraction (samples statistically subdivided from 355-500 μm batch). This difference was deemed too large to be attributed purely to unrepresentativeness of samples. It was therefore decided to use the same sieve stack for all measurements across the entire experimental programme.

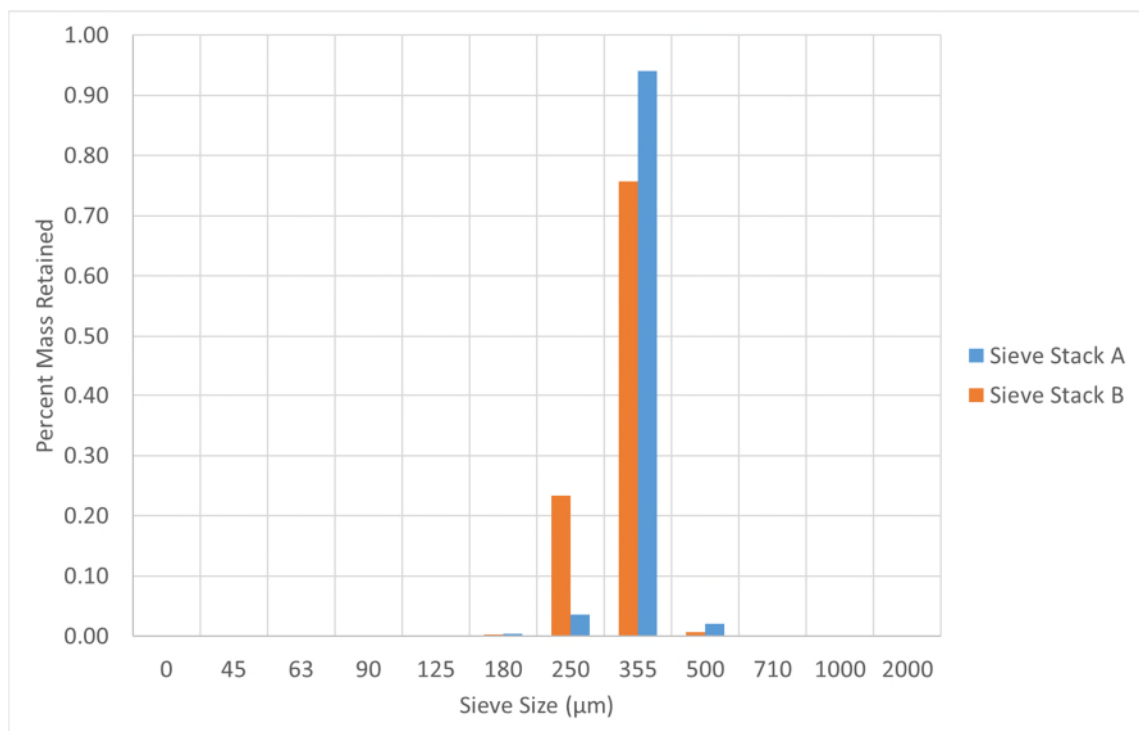
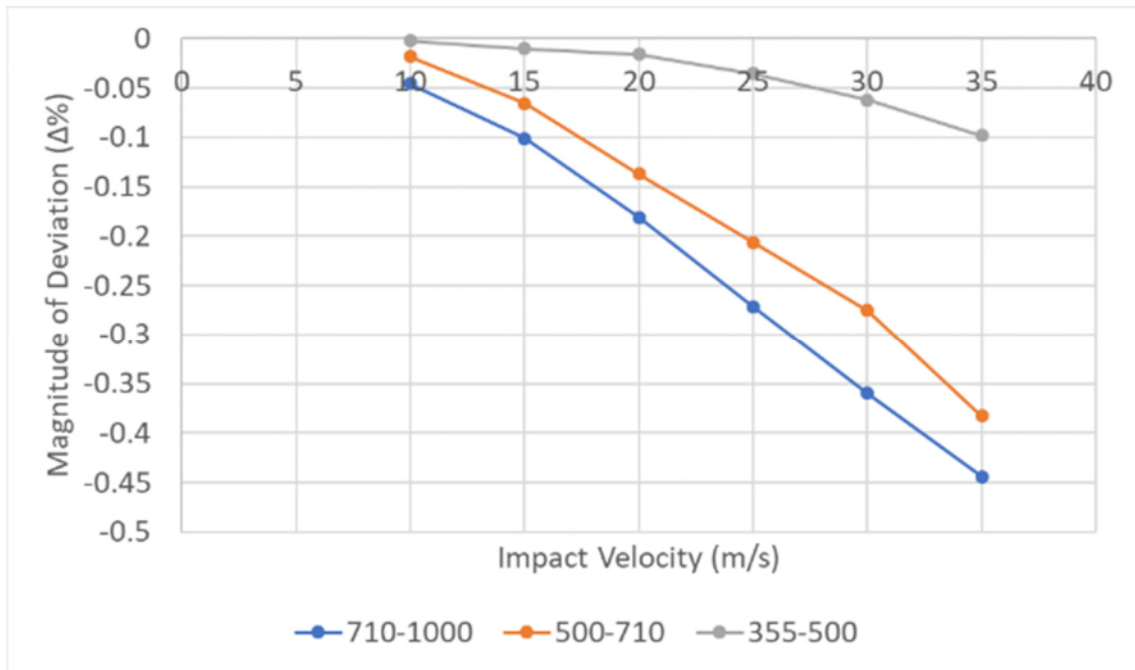


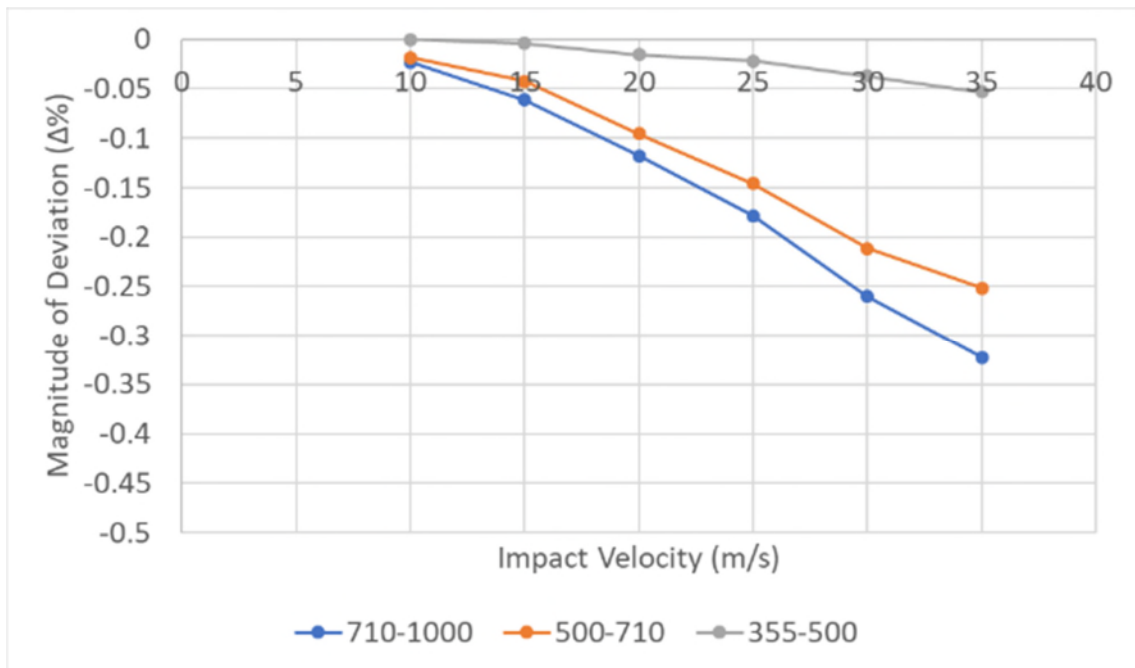
Figure 5-7: Comparison of particle size distribution results obtained from two different sieve stacks

It was determined that all pre-sieved fractions were acceptable, apart from the 250-355 μm batch, as more than 35% of the sample was out of specification.

Figure 5-8 compares the particle attrition behaviour of each of the three batch fractions, for all four impact angles. It was clear that the smaller the particles were able to statistically survive higher impact velocities than the larger particles. However, the progression of strength is not linear; the mean particle diameter of the smallest fraction is half that of the largest fraction. No cases were observed where the attrition of the largest fraction was twice that of the smallest fraction. It appeared that the smaller particles were significantly stronger in comparison to the larger particles in all cases.

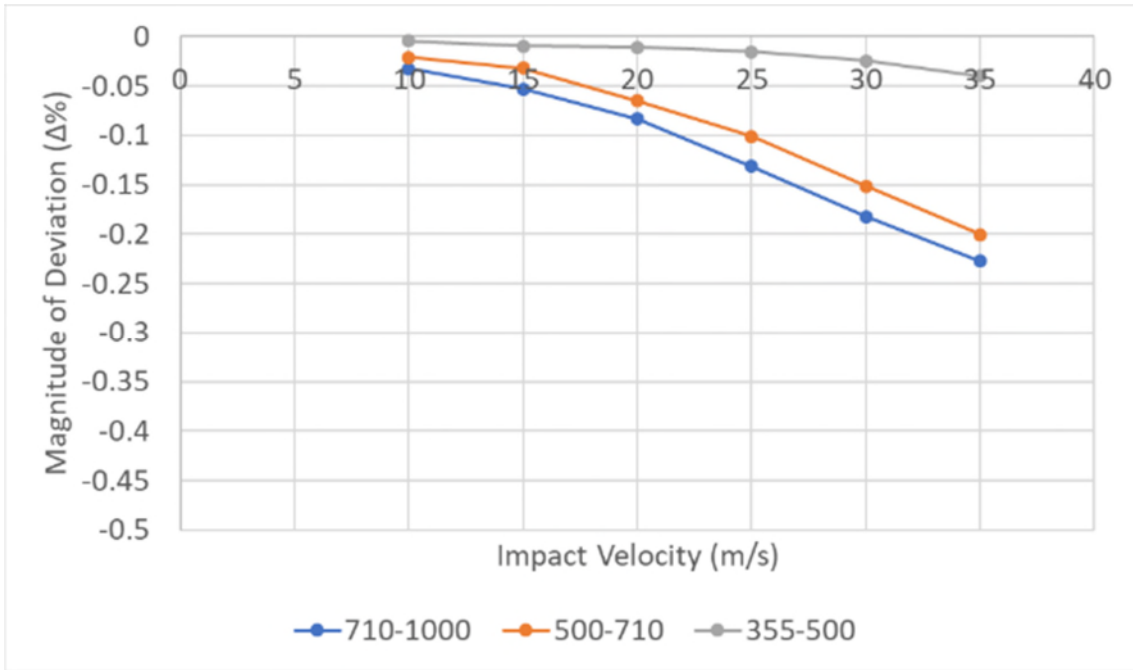


(a)

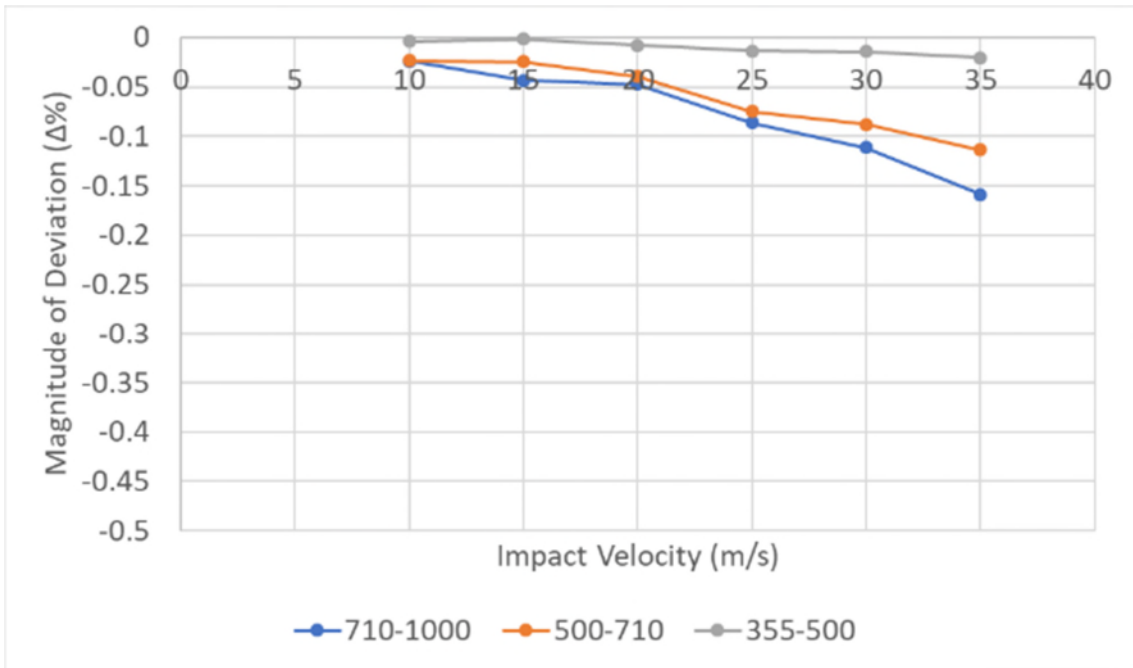


(b)

Figure 5-8: Influence of particle size on the level of attrition measured for the primary size fraction of each batch for impact angles (a) 90, (b) 45, (c) 30, and (d) 20 degrees. The legend describes the primary batch size fraction in μm .



(c)



(d)

Figure 5.8: Influence of particle size on the level of attrition measured for the primary size fraction of each batch for impact angles (a) 90, (b) 45, (c) 30, and (d) 20 degrees. The legend describes the primary batch size fraction in μm .

It was evident that a 'strength threshold' exists with respect to the carbolux particle size. This describes the clear behavioural difference between the 710-1000 μm and 500-710 μm fractions, and the 355-500 μm fraction. In order to better visualise this, Figure 5-9 shows the mean particle diameter on the x-axis, and it can be observed how the particle strength decreases with particle size, with the strength threshold in the region of 400-600 μm mean particle diameter.

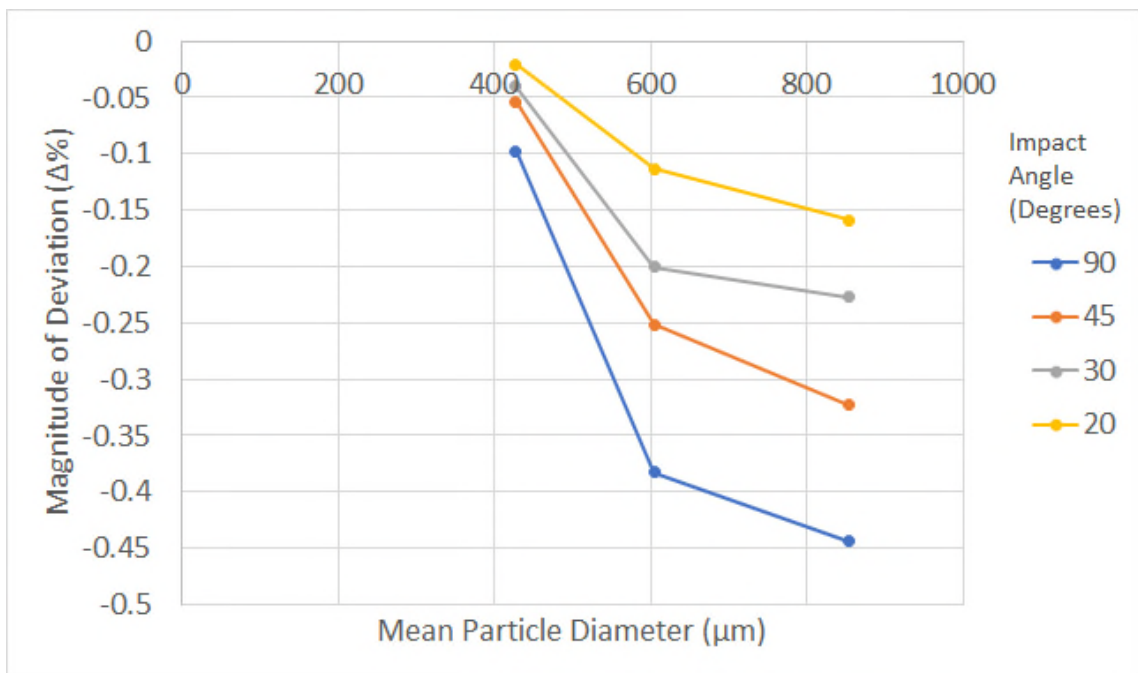
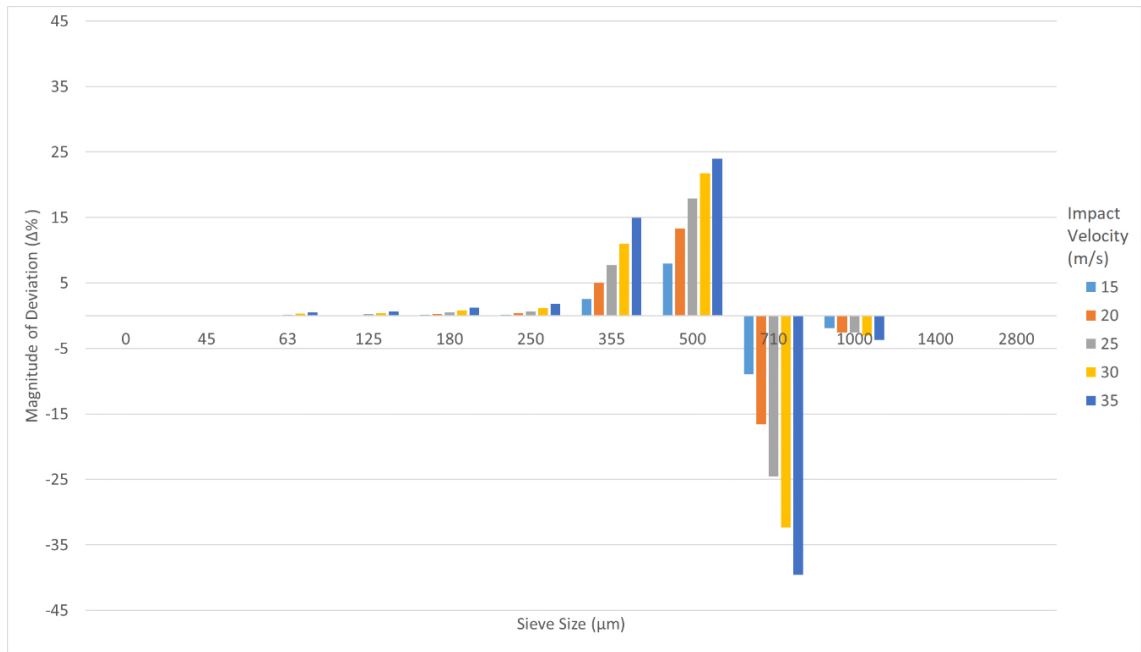


Figure 5-9: Influence of particle size on attrition behaviour for an impact angle of 35 m/s

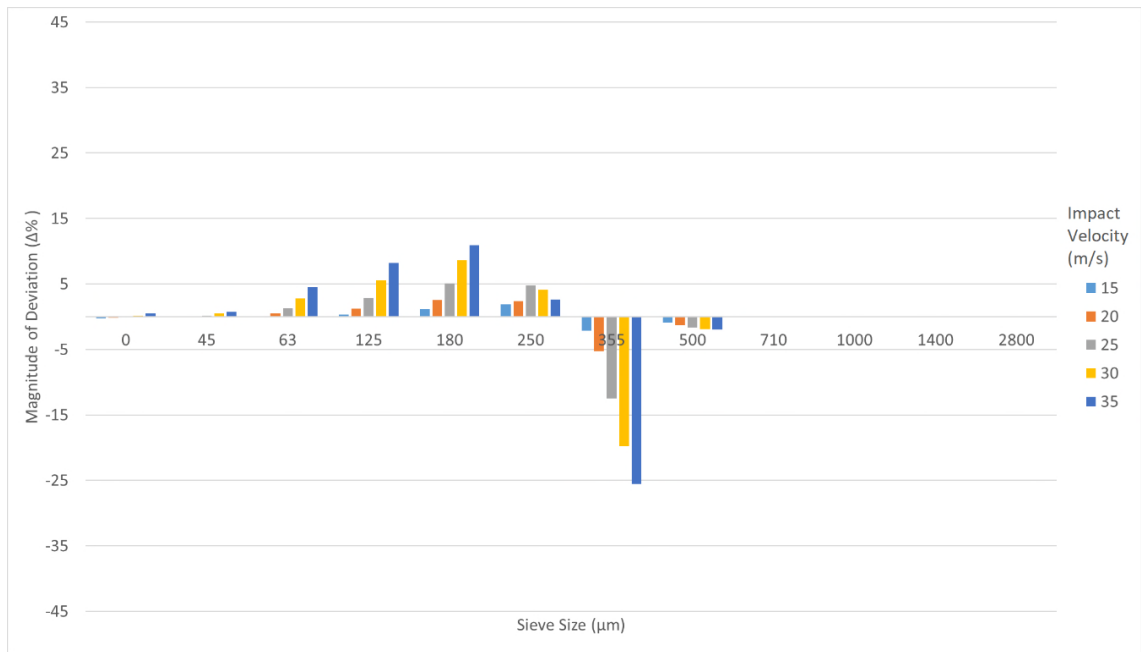
5.1.4.2 *Material Composition*

As was elucidated in Chapter 2 the material composition has a significant influence on the strength of the particle. While there are numerous different particle materials and morphologies that exist, the present work shall consider the comparison of sodium chloride and Carbolux SK. The results obtained for this study were acquired prior to the application of the foam lining of the BSPAT apparatus, and therefore will be analysed in this context. The particle attrition behaviour of Spent FCC Catalyst (Type T and Type C) within the BSPAT will also be addressed.

The testing conditions selected for the comparative study were impact velocities from 15 to 35 m/s in 5m/s increments. Impact angles included 90 degrees and 45 degrees. Figure 5-10 shows the magnitude of deviation across all tests. The virgin particle size distributions are given in Chapter 4 for Sodium Chloride and Figure 5-1 for Carbolux SK. All results in this Section shall be given in terms of non-decimal percentages.

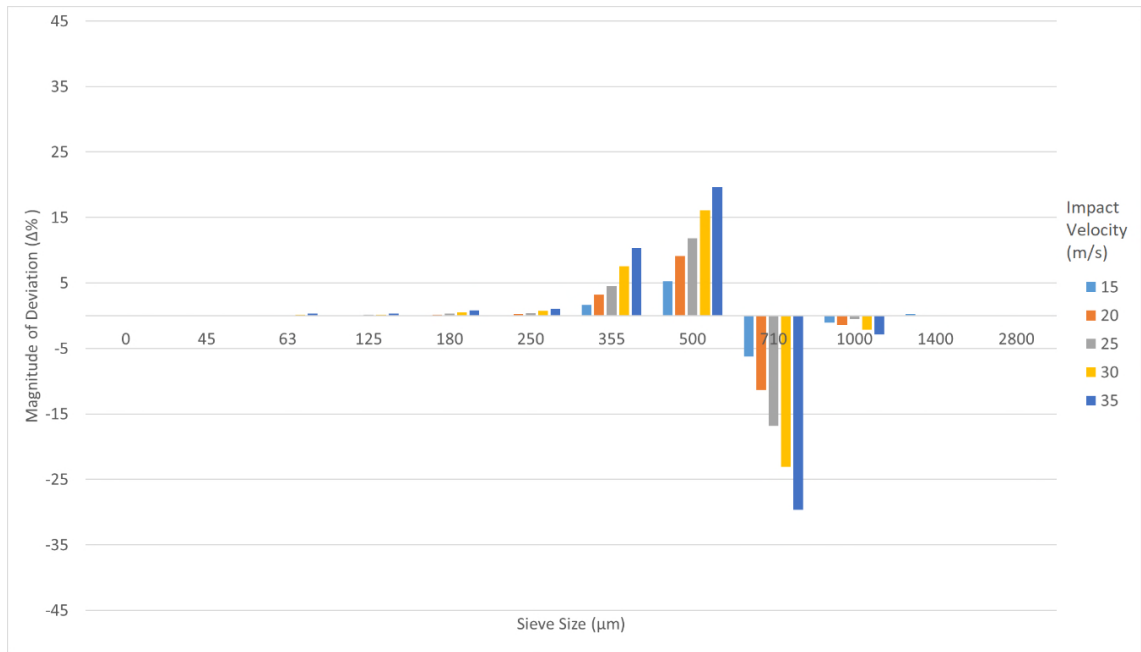


(a)

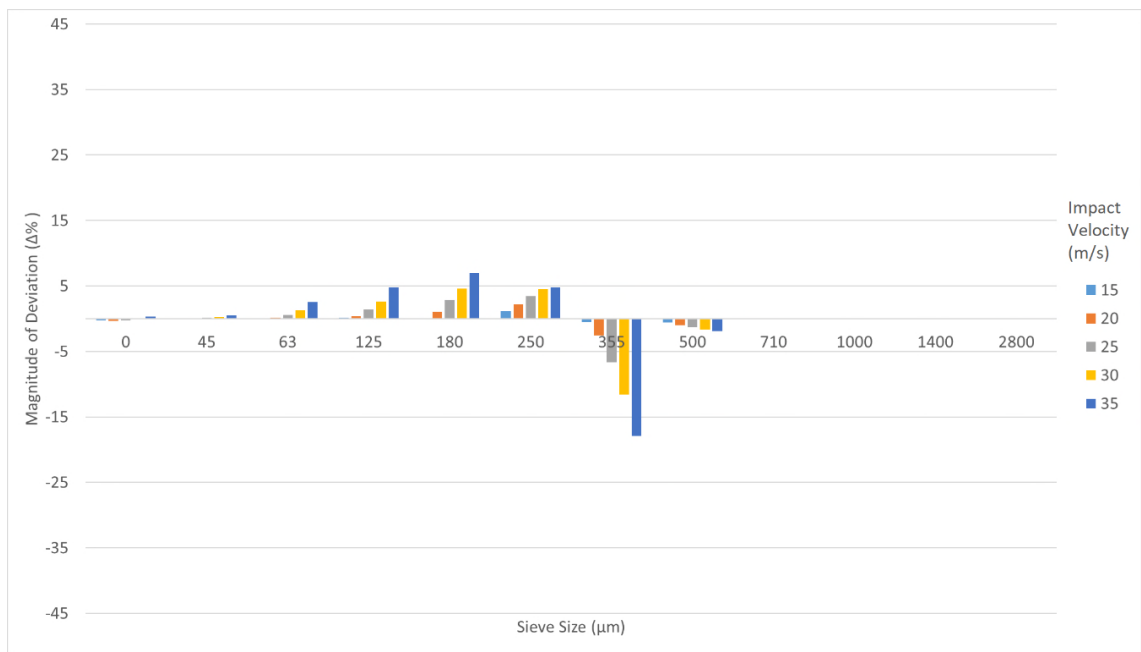


(b)

Figure 5-10: Magnitude of deviation results for 90 degree impact angles (a) carbolux SK, and (b) sodium chloride; and 45 degree impact angles (c) carbolux and (d) sodium chloride



(c)



(d)

Figure 5 10: Magnitude of deviation results for 90 degree impact angles (a) carbolux SK, and (b) sodium chloride; and 45 degree impact angles (c) carbolux and (d) sodium chloride

By inspection, it is evident that Carbolux SK has a lower particle strength than the sodium chloride, prior to consideration of particle size effects. All results supported previous findings whereby particle attrition increases with increasing impact velocity and increasing impact angle. Considering only the 710-1000 μm size fraction for Carbolux SK and the 355-500 μm size fraction for sodium chloride (the fractions where most breakage is evident and subject to little material addition from larger size fraction), Figure 5-11 compares the materials across all impact velocities. Second power polynomial functions have been fitted to the data, and are defined in Table 5-1.

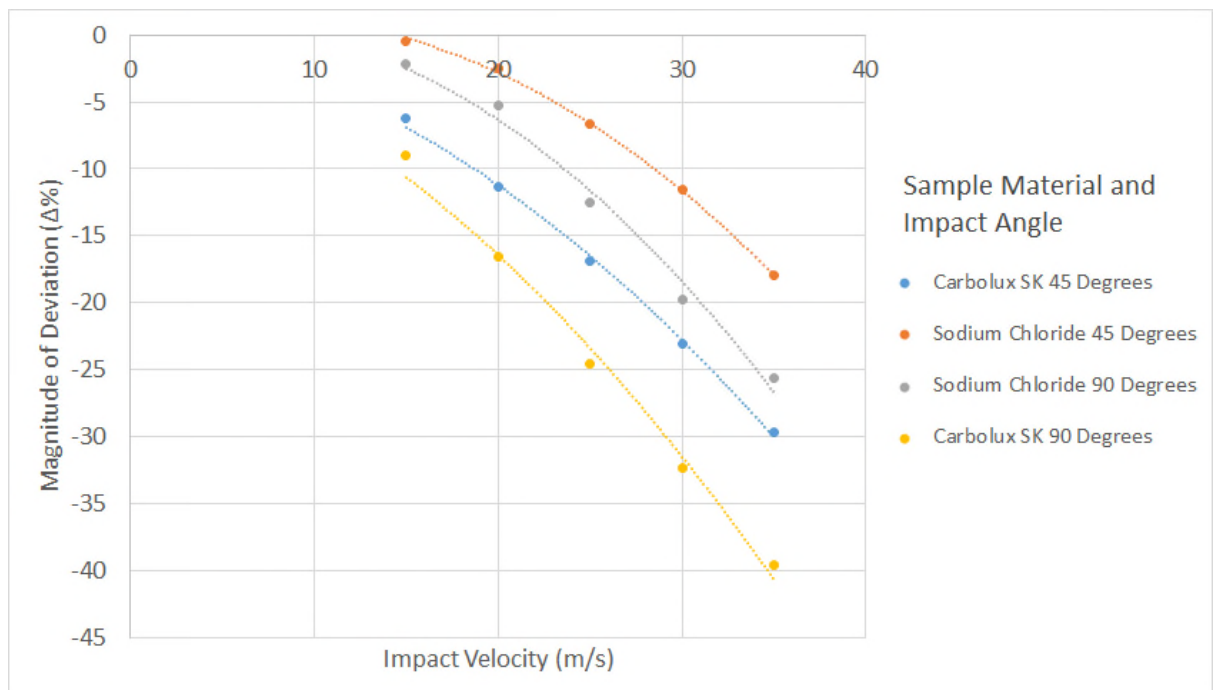


Figure 5-11: Comparison of magnitude of deviation of primary fraction sizes across 90 and 45 degree impacts

Table 5-1: Details of fitted curves as shown in Figure 5-11

Material	Impact Angle (Degrees)	Size Fraction (μm)	Equation	R ²
Carbolux	90	710-1000	$y = -0.0226x^2 - 0.3685x$	0.9898
Carbolux	45	710-1000	$y = -0.0199x^2 - 0.1627x$	0.9976
Sodium Chloride	90	355-500	$y = -0.0297x^2 + 0.2779x$	0.9866
Sodium Chloride	45	355-500	$y = -0.0247x^2 + 0.3538x$	0.9993

It was evident that sodium chloride demonstrated a high particle strength for any combination of impact angle and impact velocity. However, in order to account for the discrepancy in particle size, Figure 5-12 compares the magnitude of deviation for 355-500 μm sodium chloride and carbolux particles at a 90 degree impact angle (the condition at which secondary impacts have been shown to be negligible in Section 5.1.3).

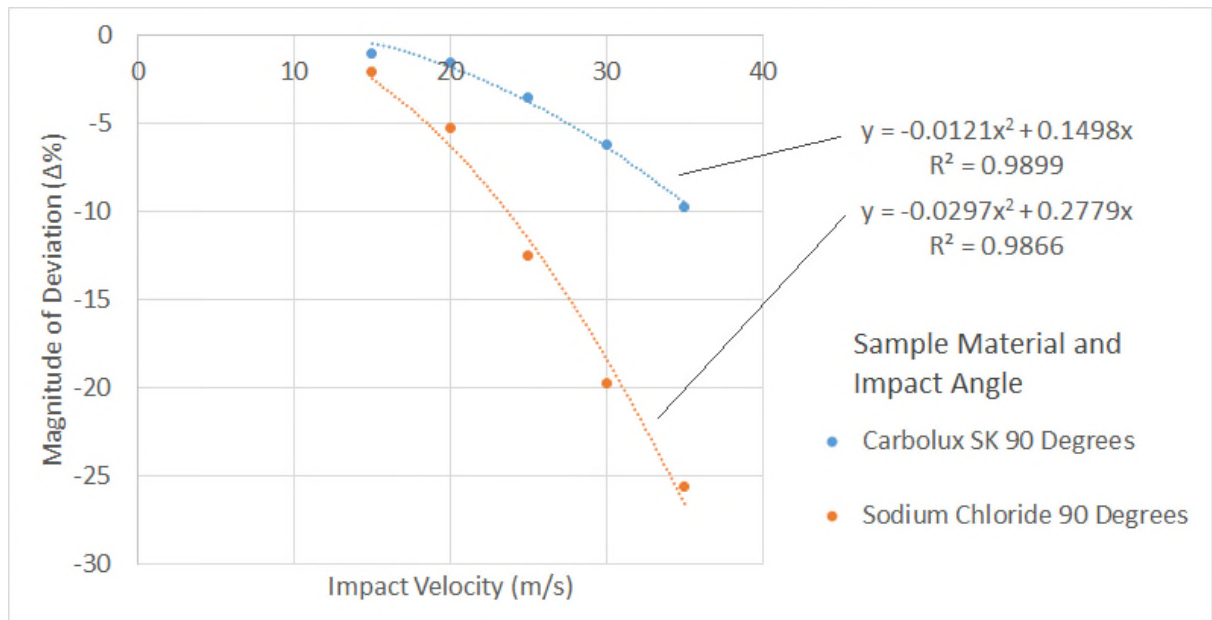
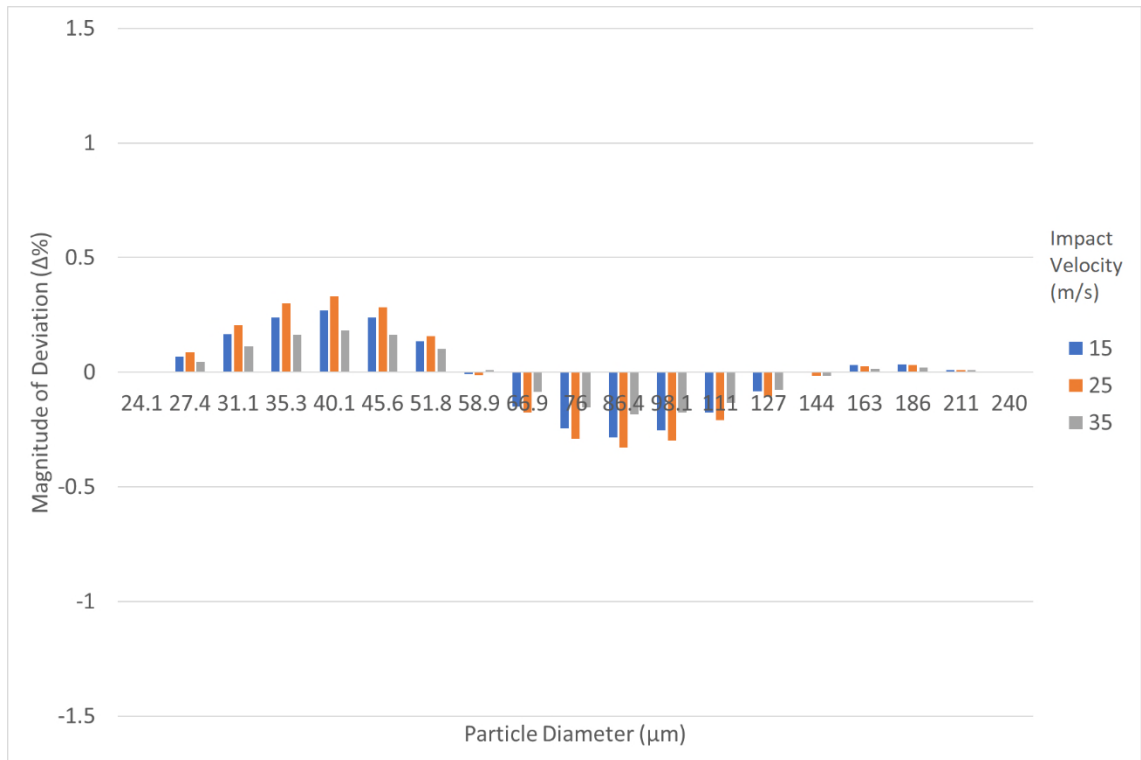


Figure 5-12: Comparison of magnitude of deviation for sodium chloride and Carbolux SK for 355-500 μm size particles

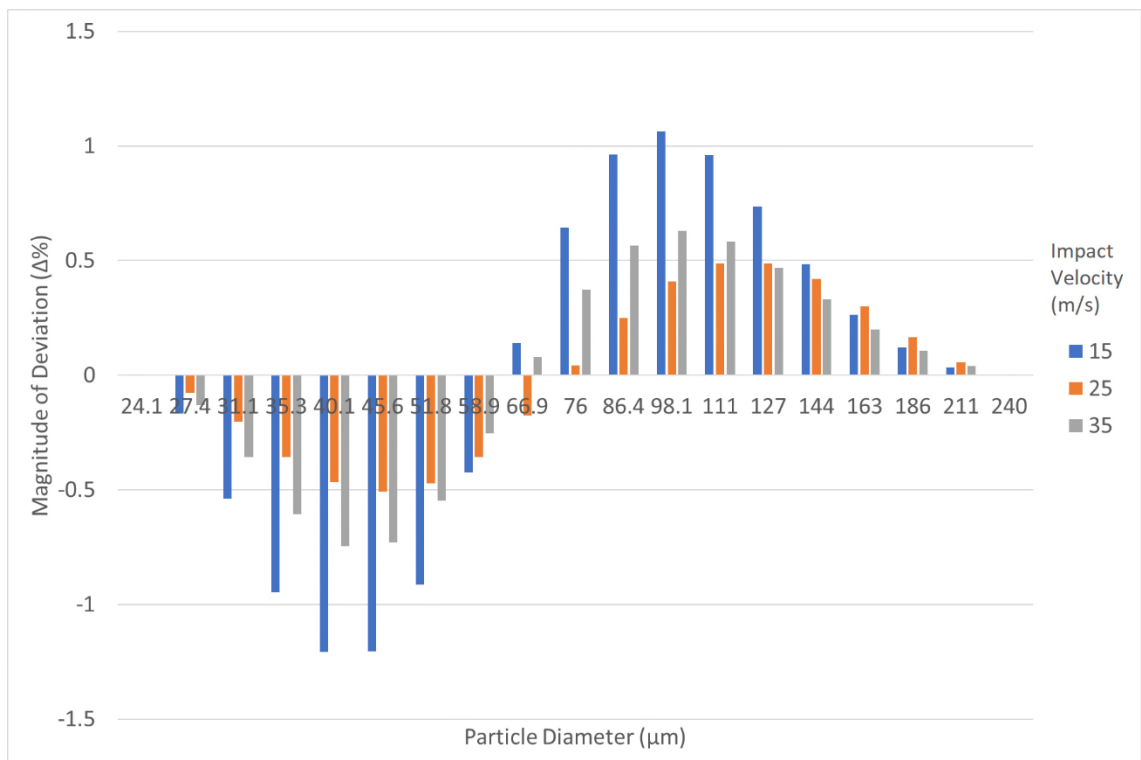
It was evident that when particle size was accounted for, the sodium chloride particles demonstrated a lower particle strength in comparison to the Carbolux SK.

This study demonstrated the requirement to characterise the particle strength distribution across the entire range of particle sizes. Furthermore, different particulate materials can only be directly compared when the impact conditions and virgin particle diameter are equivalent.

To further develop understanding of the influence of particle size within centrifugal accelerator-style particle attrition testers, two types of Spent FCC Catalyst were tested across the full spectrum of impact conditions. These were all combinations of impact velocities (15, 25, and 35 m/s) and impact angles (20, 30, 45, and 90 degrees). The results from this study are presented in Figure 5-13 for Type T and Figure 5-14 for Type C, considering impact angles of 20 and 90 degrees. The magnitude of deviation is presented in non-decimal format.

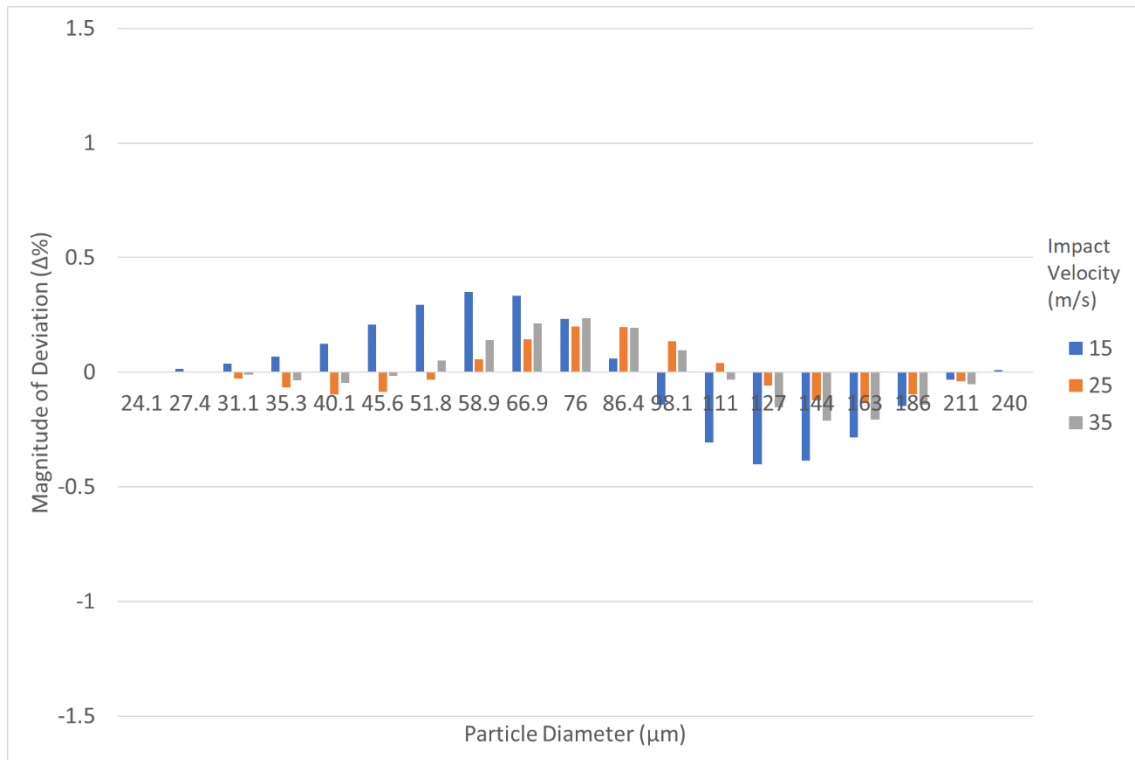


(a)

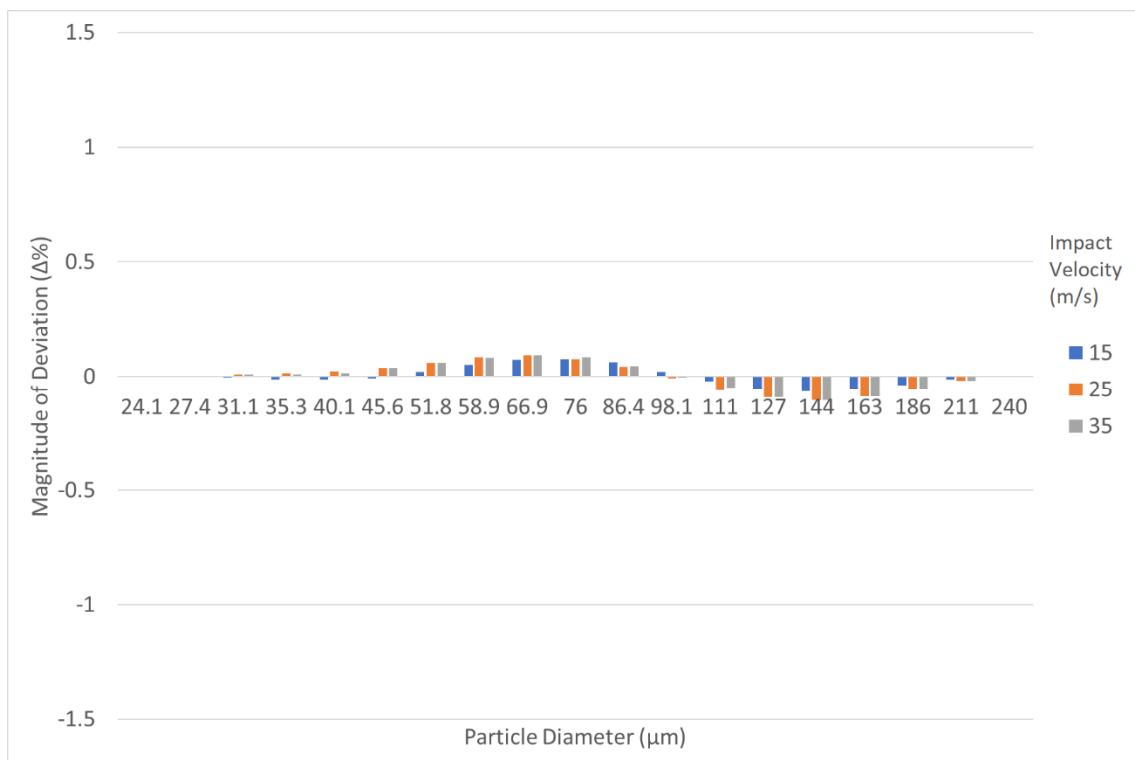


(b)

Figure 5-13: Results for Type T attrition tests at impact angles of (a) 20 degrees, and (b) 90 degrees



(a)



(b)

Figure 5-14: Results for Type C attrition tests at impact angles of (a) 20 degrees, and (b) 90 degrees

It was evident from this study that only minimal damage occurred across all test conditions. Furthermore, there was no clear trend between variations of impact angle and impact velocity with respect to the magnitude of particle attrition measured. In one case, Figure 5-13b, particles appeared to increase in diameter. Even as great care was taken to ensure the accuracy of the results obtained, it was apparent that the centrifugal accelerator-style particle attrition tester was not appropriate for testing this material type.

Potential explanations for these observations include that the degree of particle attrition inflicted by the BSPAT testing was not greater than the magnitude of the error. Additionally, when measuring the particle size distribution of samples containing such small particle diameters, the measurement of particle diameter becomes sensitive to contamination. Even though best effort was made to clean the BSPAT before the Spent FCC Catalyst testing, it was possible that a small number of foreign particles could have contaminated samples, and, considering the negligible attrition measured, given the impression that particles had increased in diameter.

5.2 Supplementary Studies

This section consists of investigations conducted with the objective of supplementing the information collected in the previously described studies to enhance understanding of particle attrition behaviours. Firstly, the attrition behaviour of various types of biomass pellet are addressed. Afterwards, the influence of mass feed rate, and the action of the screw feeder on observed levels of particle attrition in the centrifugal accelerator particle attrition testers is addressed. Finally, the QPM and the BSPAT apparatuses are directly compared in a full factorial experimental program to elucidate the influence of tester geometry on particle attrition results.

5.2.1 Attrition of Biomass Pellets

Two brief studies were conducted on pellet attrition in order to better understand the diversity of particle attrition behaviours. Biomass pellets can contain a wide variety of substructures that become apparent upon attrition. Depending on the feed material used and the manufacturing process of the pellet, these substructures could take the form of flakes, fibres or fine powders. For this reason, the method of particle size analysis used, took one of two forms:

1. A binary condition, whereby attrition was measured as percent of sample mass passing a 3.15 mm round-holed perforated sieve (classified as fines by ISO 18846:2016).
2. Measurement of the length of each individual pellet with a digital Vernier calliper.

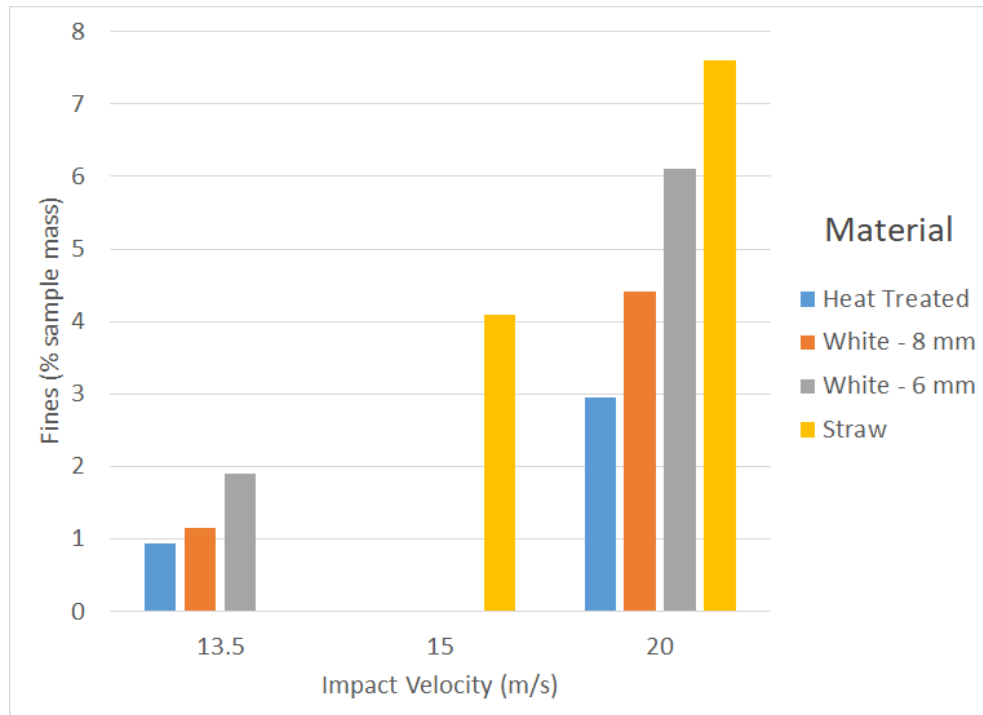
Method 1 was time-efficient, and provided useful information in terms of fines generation, however no detail on the full particle size distribution was achieved. Conversely, Method 2 was labour-intensive, but gave a very clear insight into the size reduction of pellets undergoing impact.

5.2.1.1 Influence of Pellet Material and Diameter

The first study compared the fines generated from tests conducted on the LSPAT apparatus at an impact angle of 45 degrees. Four different pellet types were considered: white (diameter 6 mm and 8 mm), heat treated, and straw. All virgin samples were screened beforehand with a 3.15 mm round-holed perforated sieve to remove any pre-existing fines present. The sample mass feed rates into the LSPAT used for each pellet type are specified in Table 5-2. The mass feed rate was maintained as low as possible to minimise the particle mass flux at the target surface; reducing likelihood of any possible inter-particle collisions affecting the attrition results. A sample size of approximately 2 kg was used for all material types except the straw pellets, for which approximately 2.5 kg sample sizes were used. Figure 5-15 shows the fines measured as a percentage (non-decimal) of the sample mass.

Table 5-2: Mass Feed Rates of Pelletised Materials into the LSPAT

Pellet Material	Mass Feed Rate (g/s)
White – 6 mm diameter	6.6
White – 8 mm diameter	8.3
Heat Treated	7.9
Straw	8.6

*Figure 5-15: Sub-3.15 mm fines as a percent of sample mass for pellet tests on the LSPAT*

In observing the results, it is evident that the straw pellets were the weakest of the materials considered, while the heat-treated pellets were the strongest. A qualitative observation made during the experimentation was the difference in the size and shape of the fragments produced. These observations are summarised as follows:

- Heat treated pellets: a mixture of very fine dust and thin flakes with diameters of the same order of magnitude as the parent pellet diameter.
- White pellets (both diameters): Angular chips and flakes mixed with fine dust.
- Straw pellets: A mixture of fine dust and fibres.

With respect to the influence of the two diameters of white pellet considered, the 8 mm pellet was consistently stronger than the 6 mm pellet. This trend could be attributed to differences in the production process. If both processes were found to be equivalent, then the difference in pellet strength could be explained by the 8 mm pellet's increased yield moment capacity (due to the increased second moment of area of the pellet cross-section). The second moment of area and yield moment calculations are described by Equations (5-3) and (5-4) respectively.

$$I_c = \frac{\pi}{4} r^4 \quad (5-3)$$

$$M_y = \frac{\sigma_y I}{c} = \sigma_y S \quad (5-4)$$

Where:

I_c Second moment of area of a circle (m⁴)

r Circle radius (pellet radius) (m)

M_y Yield moment (Nm)

σ_y Yield stress (N/m²)

I Second moment of area (m⁴)

c Distance to point farthest from neutral axis (m)

S Corresponding section modulus (m³)

If the ratio of second moment of area and yield moment for each pellet type is determined for an arbitrary material, the results given in Table 5-3 are obtained. These calculations assume a 20 mm pellet length for each material. It can be seen that the yield moment of the 8 mm diameter pellet was significantly higher, and this could have contributed to the trends seen in the results.

Table 5-3: Second moment of area and moment capacity calculations for 8mm and 6mm Pellets 20mm in length

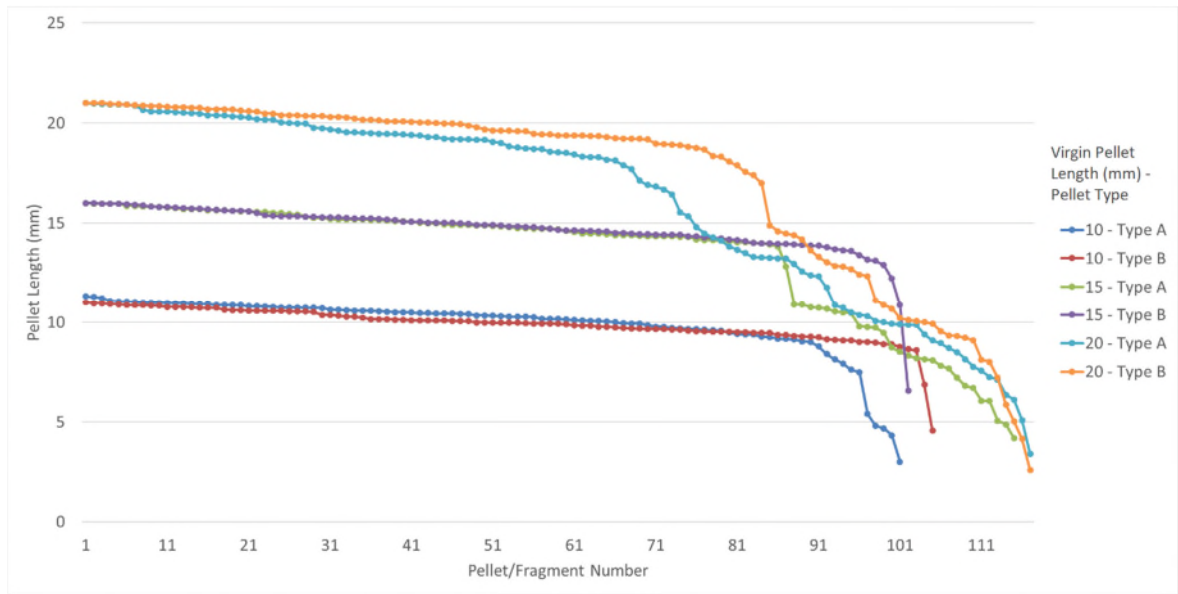
Characteristic	8 mm Pellet	6 mm Pellet
Second Moment of Area (mm ⁴)	3217.0	1017.9
Ratio I_c (-) [8mm/6mm]	3.16	
Ratio M_y (-) [8mm/6mm]	2.37	

The above analysis applies only to the propagation of major transverse cracks across the pellet. This alone does not describe the trends observed with respect to fines generation. However, it is reasonable to argue that fines are generated from the free ends of the pellet. Therefore, the greater the free-end surface area contained within the sample, the greater the proportion of fines will be generated.

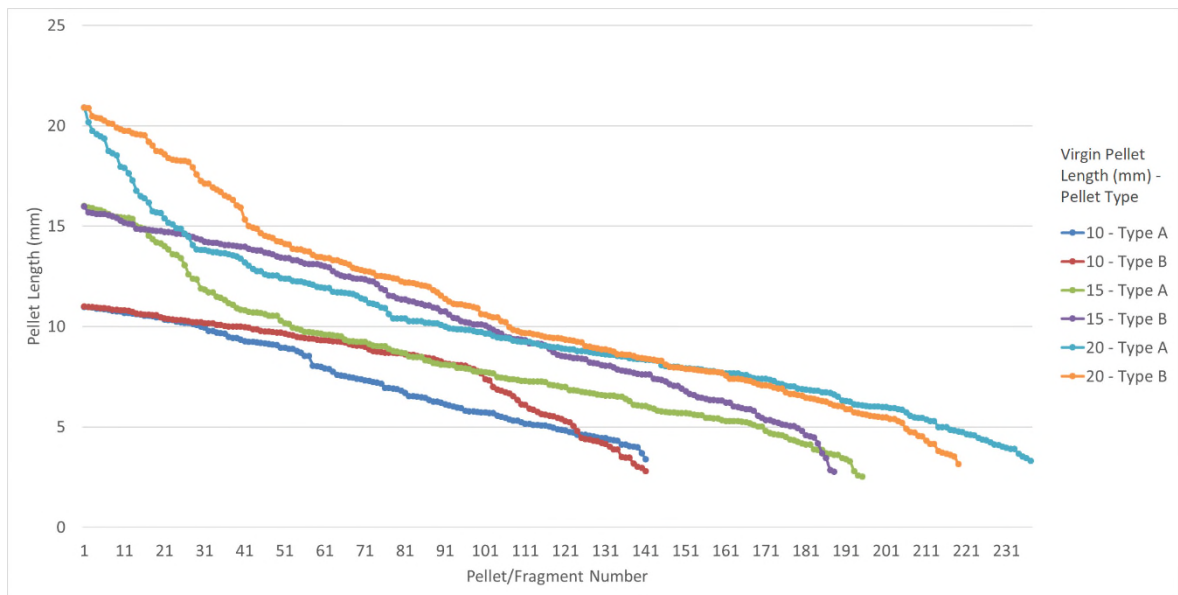
5.2.1.2 Influence of Pellet Length

The control over particle morphology is generally limited to length and diameter, for a cylindrical pellet. While pellet diameter is determined by the diameter of the die from which it was made, the pellet length can vary considerably throughout a sample. It was therefore desirable to determine the influence of pellet length on the amount of pellet breakage observed. This was achieved by measuring pellet length (according to Method 2, Section 5.2.1) before and after impact testing on the LSPAT (measurement of Feret's diameter). Test samples were pre-prepared, containing pellets of length 10, 15, and 20 mm with an accuracy of ± 1 mm. Each sample contained 100 pellets, and these were individually fed into the LSPAT by hand, one pellet at a time. For this reason, there is no specification of feed rate associated with this study. The impact angle across all experiments was 45 degrees, and impact velocities considered were 10, 20, and 30 m/s. Within this study, Type A refers to a 6 mm diameter white pellet, and Type B refers to a heat-treated pellet.

The post-test analysis consisted of the aforementioned measurement of pellet length (for all pellet fragments down to approximately 2-3 mm as practical) to an accuracy of ± 0.01 mm, followed by measurement of the fines content (material passing a 3.15 mm round-holed perforated sieve). The raw measurement data obtained for all tests is given in Figure 5-16. The x-axis details the fragment number associated with each measurement of fragment length (i.e. the greater the span of the data set along the x-axis, the greater the number of fragments produced by the test).

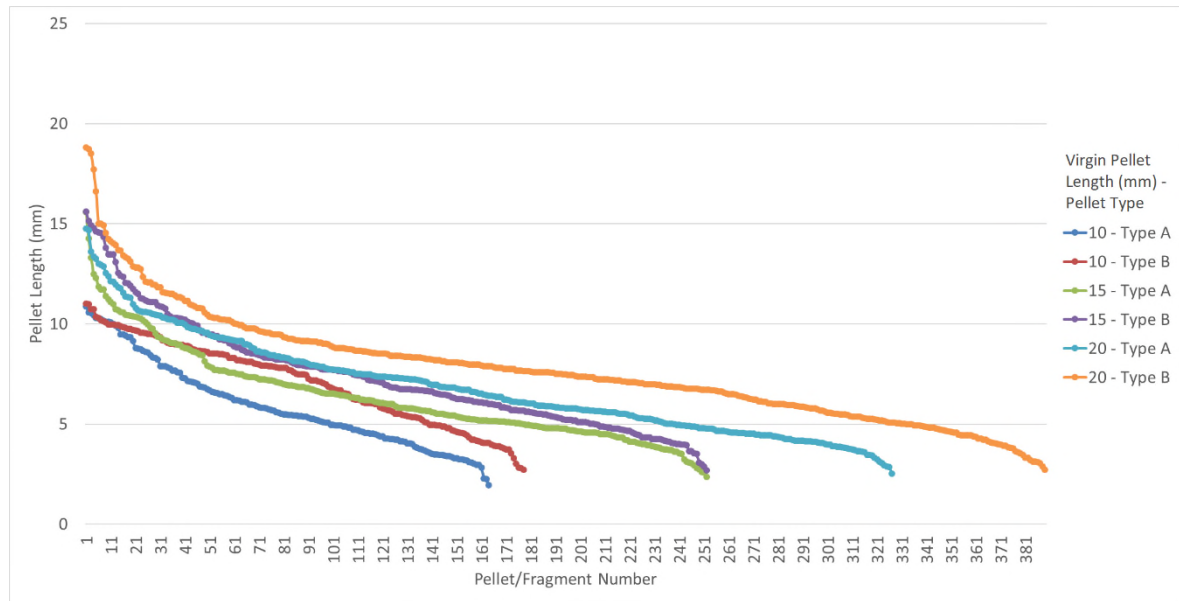


(a)



(b)

Figure 5-16: Pellet length results for pellets of varying pre-measured virgin lengths for impact velocities of (a) 10, (b) 20, and (c) 30 m/s

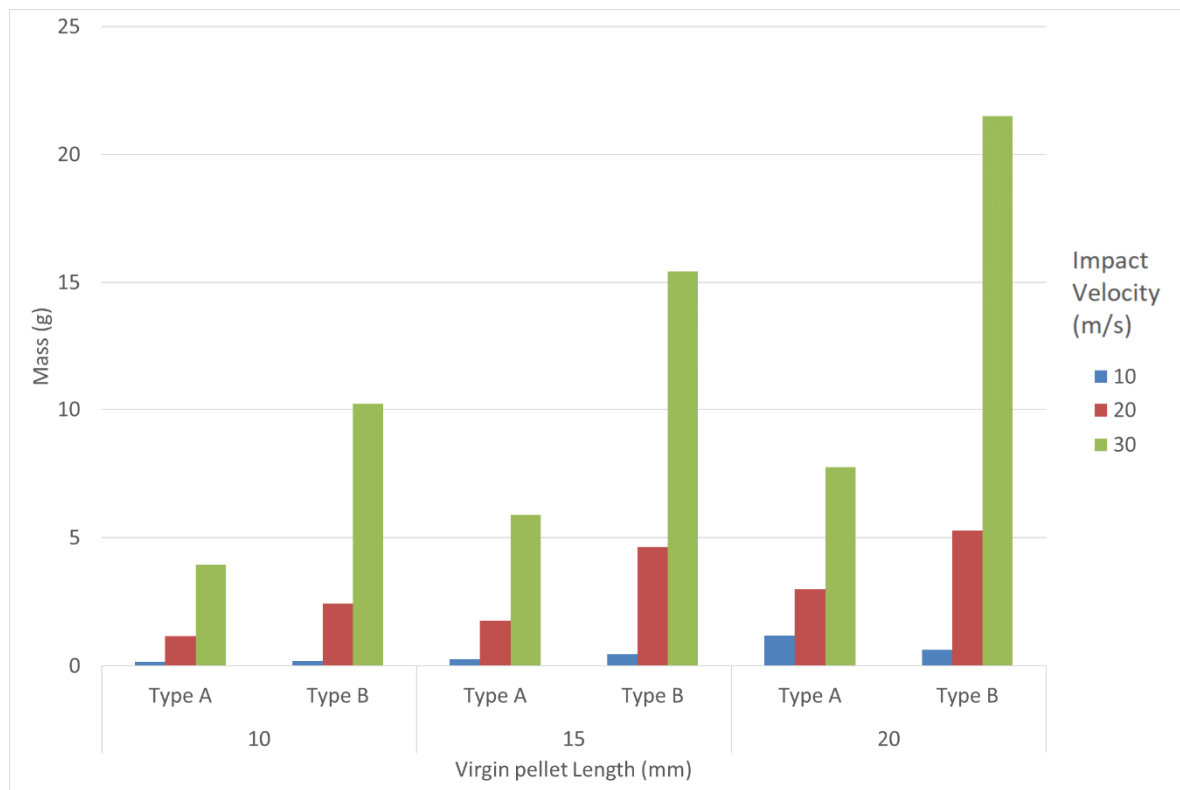


(c)

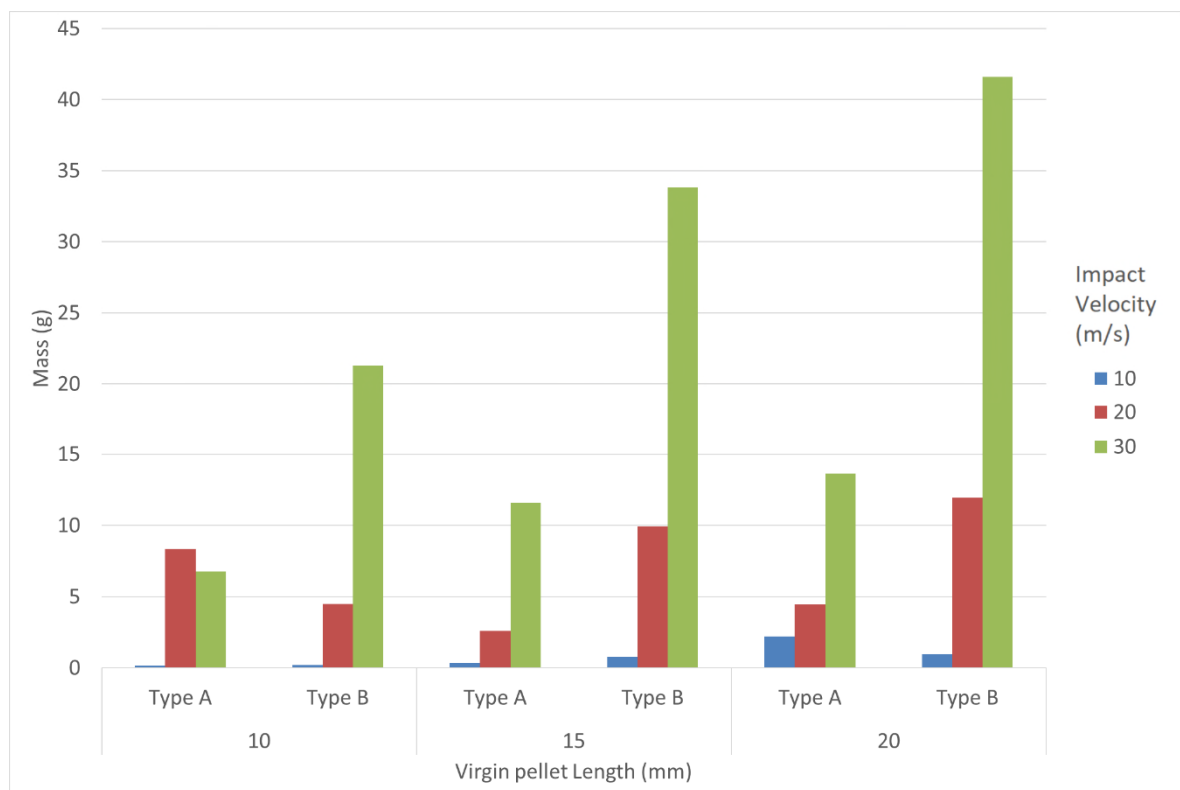
Figure 5-16: Pellet length results for pellets of varying pre-measured virgin lengths for impact velocities of (a) 10, (b) 20, and (c) 30 m/s

It was evident that particle fragmentation increased with increasing impact velocity. When comparing the results on the basis of virgin pellet length, it was observed that the fragmentation increased with increasing pellet length. An example of this is found in Figure 5-16c where pellets with virgin lengths of 20 and 15 mm retain 0 and 2 possibly unbroken pellets, whereas the virgin 10 mm sample retained a possible 20 unbroken pellets. This could be explained with the increased bending force applied to longer pellets (due to increased end to midpoint length and pellet mass). Another explanation could be the increased likelihood of weak points between the fused pellet material in longer pellets (longer pellets have larger fused volumes of constituent particles). These results support the argument to reduce the virgin pellet length at the production stage to reduce the propensity of pellet fragmentation. The heat-treated pellets suffered less fragmentation than the 6 mm diameter white pellets across all experimental conditions, which was in agreement with the results presented in Section 5.2.1.1.

To now consider the production of fines measured in this study, Figure 5-17a shows the magnitude of sub 3.15 mm material (denoted 'Fines') and Figure 5-17b shows the mass of fragments too small to measure pellet length (denoted 'Fragments'; >3.15 mm).



(a)



(b)

Figure 5-17: Mass collected of (a) Fines and (b) Fragments, for all pellet test conditions

In contrast to the fragmentation analysis, the heat-treated pellets were found to produce a greater quantity of fines and fragments per pellet. This may have been partly due to a difference in density of constituent particles. Future studies should adopt a mass-percentage basis to account for this possibility.

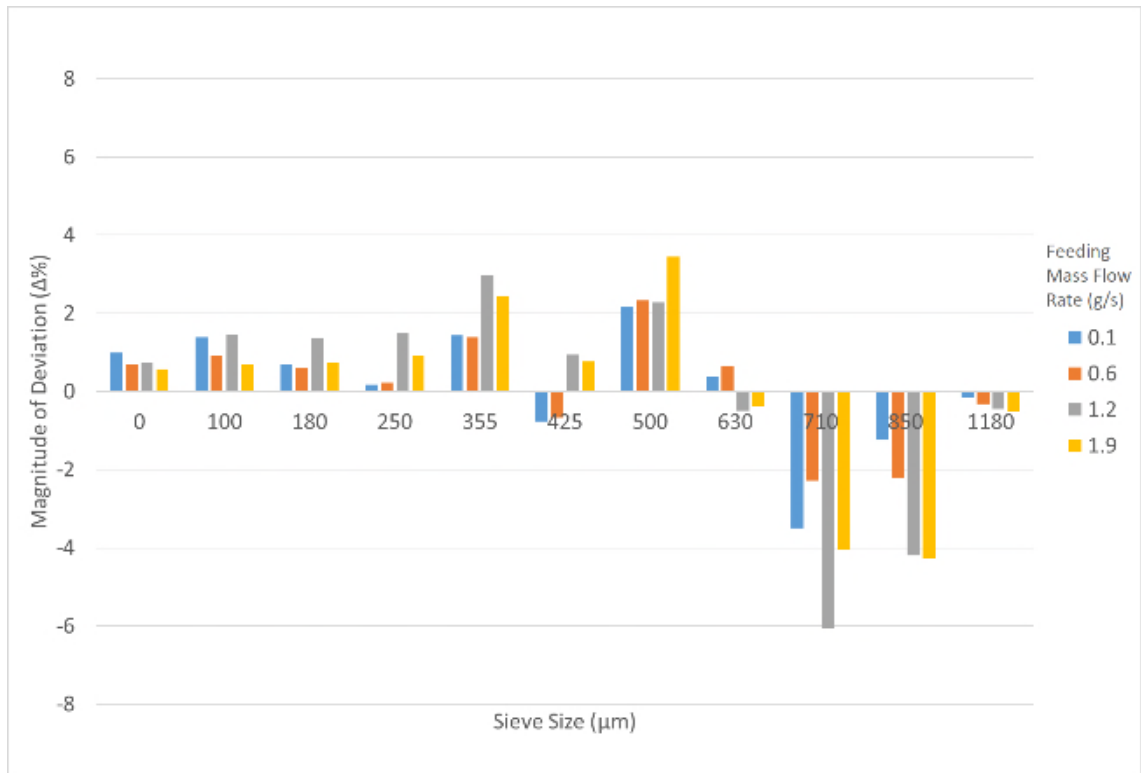
It is envisaged by adopting the described test approach and analytical method, biomass pellets can be compared quantitatively based on fragmentation propensity, and the quantity of fragments and fines produced as a result of impact events.

5.2.2 Influence of Mass Feed Rate on the QPM and BSPAT Testers

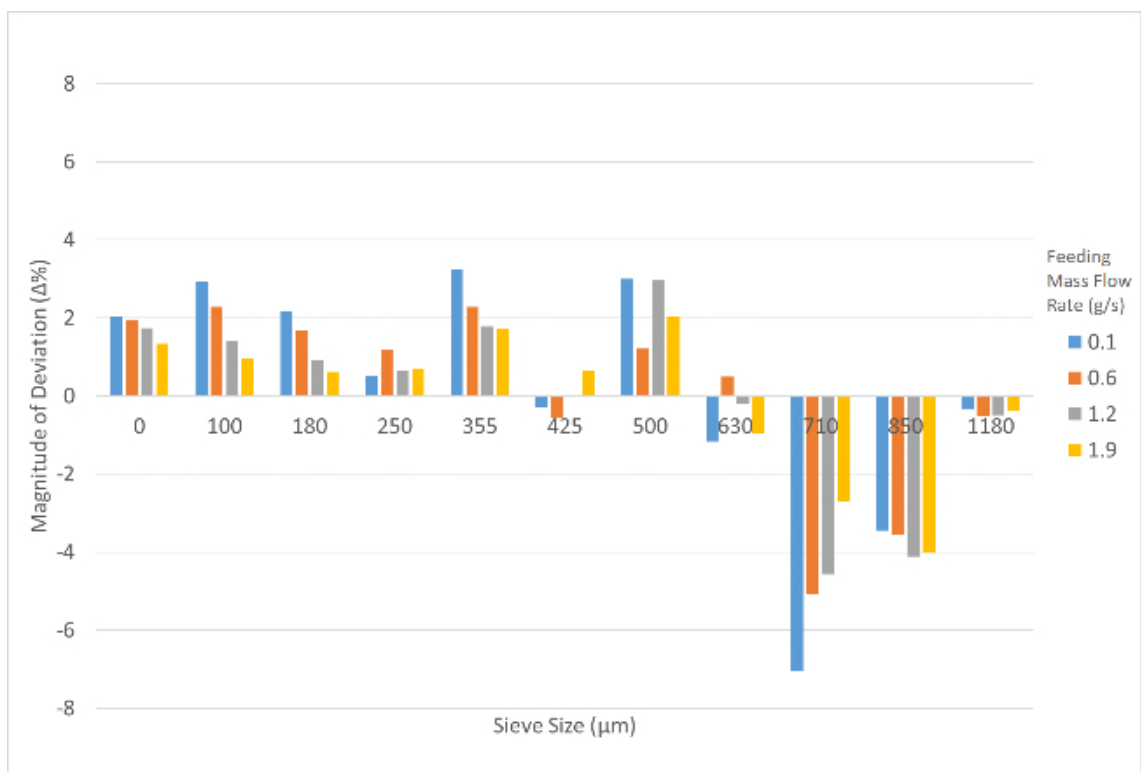
In order to determine the appropriate feed rate to use on bench scale centrifugal accelerator particle attrition testers, Golden Breadcrumbs was tested on the BSPAT and Sucrose was tested on the QPM at a range of mass feed rates. The variables considered in this study are summarised in Table 5-4. An impact angle of 45 degrees was specified, as this angle was available on both apparatuses, and causes maximum deflection of the particle trajectory (that is not a normal impact). A 90 degree impact was not selected as this scenario is not representative of a pneumatic conveying system containing radiused bends. Impact velocities of 30 m/s and 15 m/s were considered. Figure 5-18 summarises the results obtained in this study. The particle mass flux was calculated according to Equation 8.1, located in Chapter 8.

Table 5-4: Test conditions used to study the influence of mass feed rate into the QPM and BSPAT apparatuses

Apparatus	Sample Material	Impact Angle (deg)	Impact Velocity (m/s)	Feed Rate (g/s)	Mass Flux at target Surface (kg/m²/s)
QPM	Sucrose	45	15	0.1	0.023
QPM	Sucrose	45	15	0.6	0.136
QPM	Sucrose	45	15	1.2	0.271
QPM	Sucrose	45	15	1.9	0.430
QPM	Sucrose	45	30	0.1	0.023
QPM	Sucrose	45	30	0.6	0.136
QPM	Sucrose	45	30	1.2	0.271
QPM	Sucrose	45	30	1.9	0.430
BSPAT	Golden Breadcrumbs	45	15	2.2	0.094
BSPAT	Golden Breadcrumbs	45	15	4.4	0.188
BSPAT	Golden Breadcrumbs	45	15	14.4	0.615
BSPAT	Golden Breadcrumbs	45	30	2.2	0.094
BSPAT	Golden Breadcrumbs	45	30	4.4	0.188
BSPAT	Golden Breadcrumbs	45	30	14.4	0.615

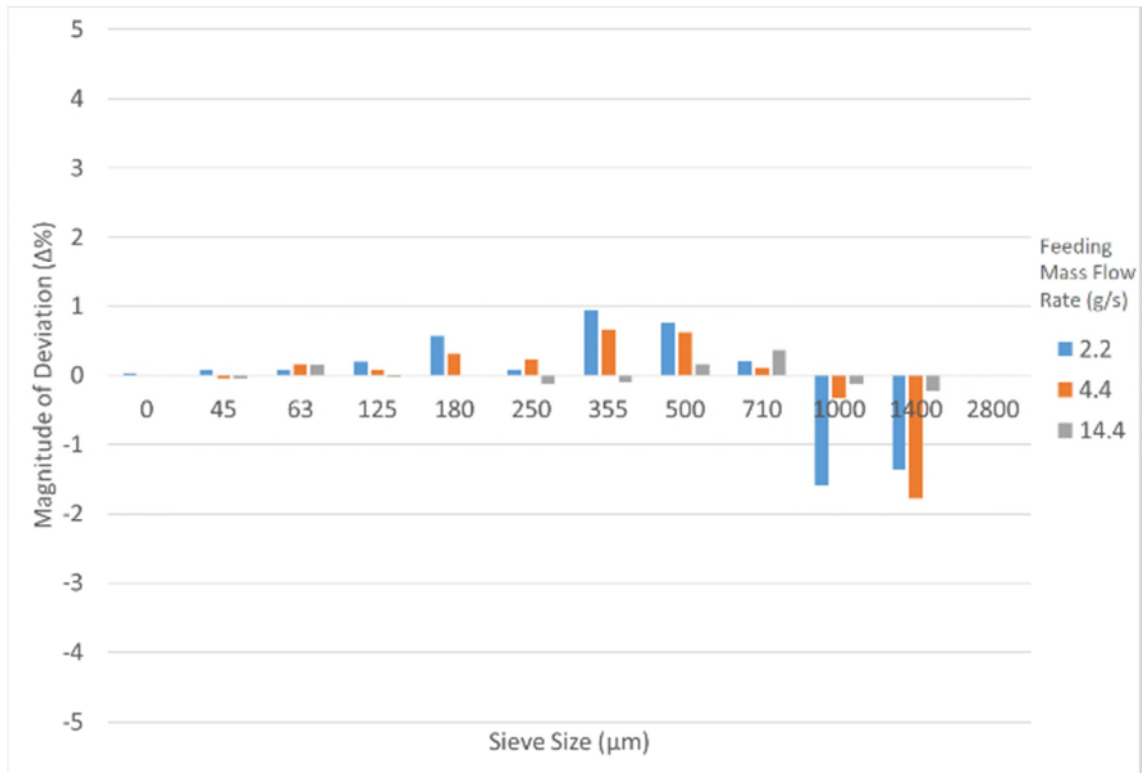


(a)

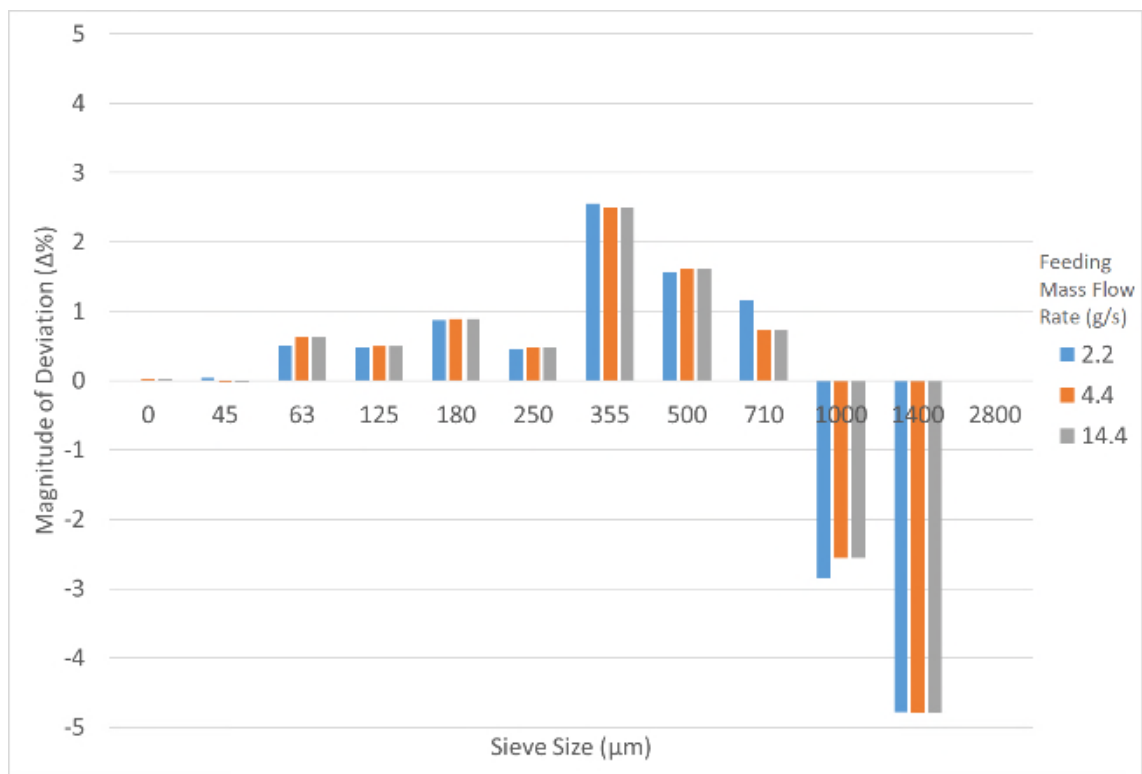


(b)

Figure 5-18: Influence of solids feed rate on the measured level of particle attrition as measured for sucrose on the QPM tester for impact velocities of (a) 15 m/s, and (b) 30 m/s; and as measured for Golden Breadcrumbs on the BSPAT for impact velocities of (c) 15 m/s, and (d) 30 m/s



(c)



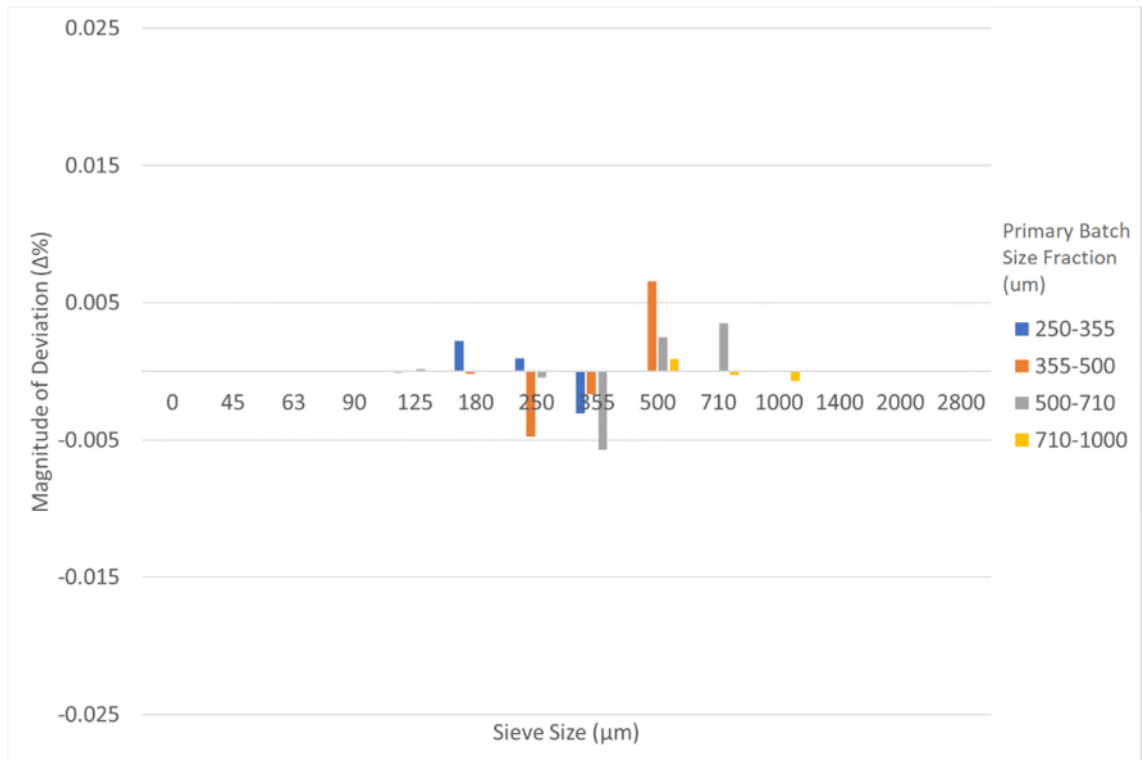
(d)

Figure 5 18: Influence of solids feed rate on the measured level of particle attrition as measured for sucrose on the QPM tester for impact velocities of (a) 15 m/s, and (b) 30 m/s; and as measured for Golden Breadcrumbs on the BSPAT for impact velocities of (c) 15 m/s, and (d) 30 m/s

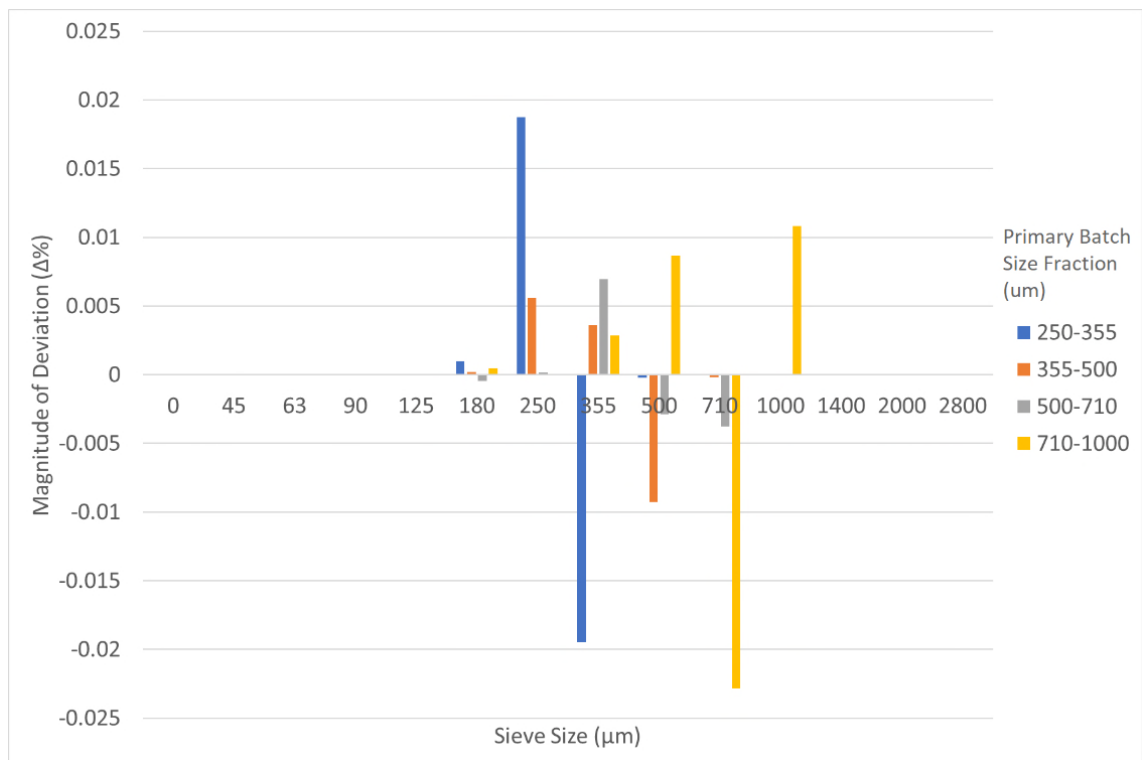
It was evident that no clear relationship exists across all test conditions, however the results obtained on the QPM at 30 m/s impact velocity indicate that particle attrition decreased with increasing mass feed rate of sample. Contrary to this, the 30 m/s impact velocity results on the BSPAT were remarkably consistent, indicating negligible influence of mass feed rate of sample. Considering the very low mass flux at the target surface for all test conditions, it was not expected for the mass feed rate of sample to have a large (if any) influence. While the BSPAT was found to show little influence of mass feed rate of sample on the particle attrition observed, it was determined that all future test work should be performed at the minimum feasible mass feed rate to minimise any possibility of inter-particle collisions within the impact chamber.

5.2.3 Particle Attrition caused by Screw Feeding

Aside from the primary and secondary impacts within the impact chamber, another source of possible particle attrition within the centrifugal accelerator particle attrition tester design is the screw feeder itself. It was envisaged that particles having a diameter of the same order of magnitude as the clearance between the screw flights and the outer casing (1 mm for the BSPAT and 2 mm for the QPM) could be subjected to forces sufficient for fragmentation or chipping. To address this, the particle attrition was measured for all four pre-sieved batch size fractions of Carbolux SK (see Figure 5-6) across the QPM and BSPAT screw feeder arrangements. The results obtained from this study are given in Figure 5-19.



(a)



(b)

Figure 5-19: results for the study of particle attrition attributed to the screw feeding mechanism in the (a) QPM, and (b) BSPAT

By comparing the results obtained in this study, it was evident that the screw feeding mechanism generates negligible attrition within the context of the attrition expected in the entire experimental procedure. The results of the 250-355 μm and the 710-1000 μm batch fractions on the BSPAT apparatus did present a small level of concern, however these values could be attributed to sampling error (as denoted by the increase in the 1000-1400 μm size fraction in the virgin 710-1000 μm dataset). The 'attrition' observed in the 250-355 μm dataset was also unforeseen as these particles are sufficiently small in diameter to pass through the screw-casing clearance with ease.

A single iteration of the experiments was completed in this study due to resource constraints. However, due to the very low levels of particle attrition observed, a sufficient conclusion could be drawn on the approximate magnitude of attrition attributed to the screw feeder.

5.2.4 Comparison of Centrifugal Accelerator Attrition Testers

In the characterisation of particulate material attrition behaviours, it was deemed necessary to quantitatively compare the geometries of the LSPAT, QPM and BSPAT. In this way, recommendations could be made with respect to the optimisation of apparatus geometry to accurately represent the impact conditions at the bend of a lean-phase pneumatic conveying system.

5.2.4.1 Comparison of LSPAT and QPM

The two existing centrifugal accelerator particle attrition testers at the Wolfson Centre Lab pertain to very different physical scales as described in Chapter 4. In order to elucidate the influences of apparatus scale, sucrose was chosen as a sample material and tested according to the conditions summarised in Table 5-5. Some variables could not be matched between the apparatuses due to scaling reasons and availability of impact target material. Scaling reasons included the flight distance between where a particle exits the spinning disc, and impacts the target array. Impact targets made of mild steel were

available on the LSPAT, while impact targets made of stainless steel were available on the QPM. In future studies, it would be more representative to match the material of the impact target array to that of the pipe material in the pneumatic conveying system of interest. This could be achieved through construction of new target arrays, or application of target samples to the impact face of the existing target array.

Possible influences of these discrepancies on the experimental results shall be discussed. Figure 5-20 shows the results obtained from the LSPAT apparatus, and Figure 5-21 shows the results from the QPM apparatus (percentages given in non-decimal form). The full data set obtained from the LSPAT is found in Appendix L

Table 5-5: Variable test matrix for LSPAT and QPM comparative study

Variable	LSPAT	QPM	Units
Sample Size	3000 - 3200	150	g
Mass feed rate	27	0.6	g/s
Impact angle	45	45	Degrees
Impact Velocity	15, 25, 30	15, 25, 30	m/s
Impact Target Material	Mild Steel	Stainless Steel	N/A

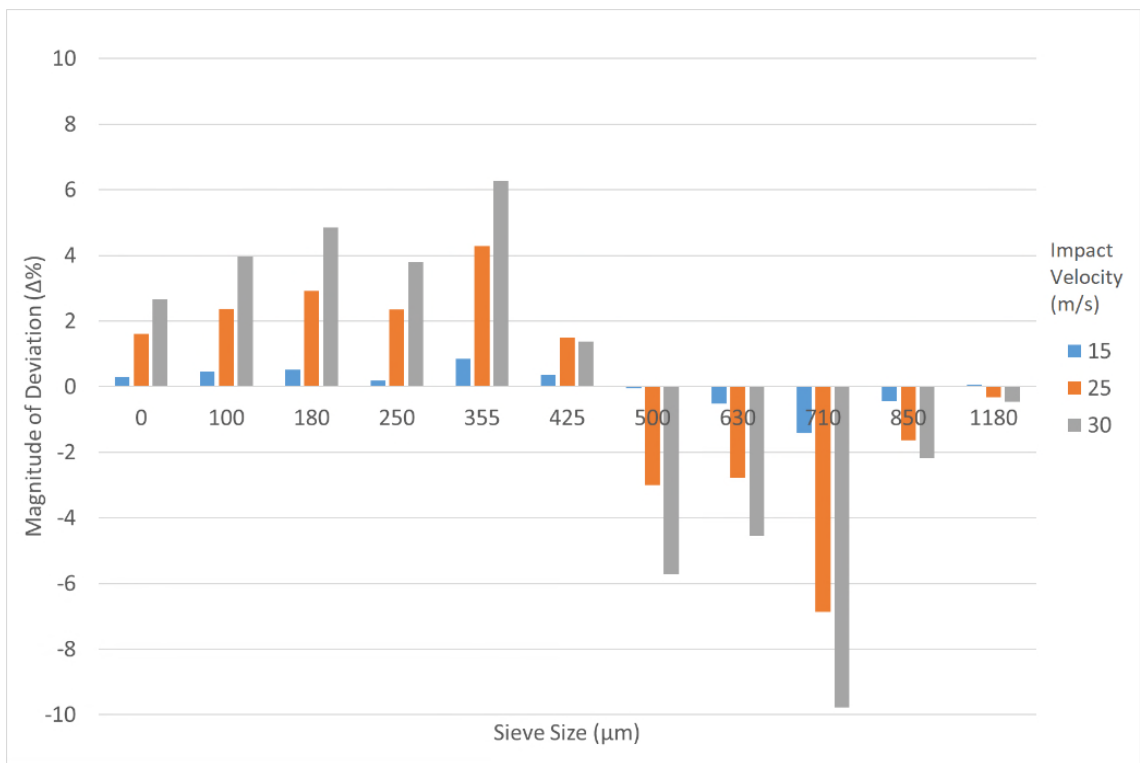


Figure 5-20: Results of attrition tests on the LSPAT at a 45 degree impact angle

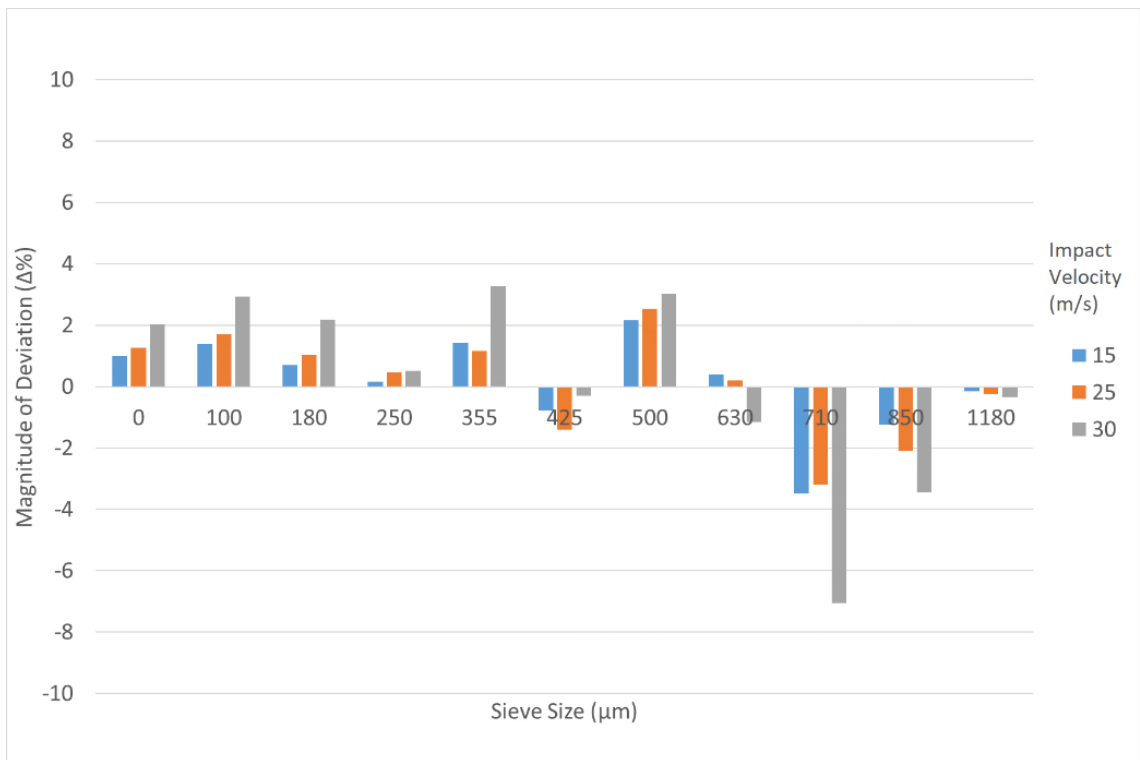


Figure 5-21: Results of attrition tests on the QPM at a 45 degree impact angle

Upon inspection of the results, it was evident that the LSPAT produced a binary form of breakage. This is due to the clear transition from fractions losing material (500-1180 μm) into the fractions that have a net increase in percent material retained (0-425 μm). The transitional size fraction in this case is the 425-500 μm fraction which returns an attrition condition intermediate to the neighbouring size fractions. In contrast to this, the attrition results from the QPM apparatus showed no clear binary trend, implying that mass migrated more equally across the size fractions. An explanation for this behaviour could be due to the large difference in sample size used across the apparatuses. As the sample size used for the LSPAT was approximately 20-21 times larger than that used for the QPM, it would be expected that the results obtained from the LSPAT would be more statistically representative of the material. A single experiment on the LSPAT is equivalent to approximately 20 to 21 experiments conducted on the QPM, in terms of the number of particles tested.

The influence of particle impact velocity was clear within the LSPAT. All size fractions clearly (excluding the 425-500 μm size fraction) indicated that particle attrition increased with increasing particle impact velocity. Again, such a relationship was not observed in the results obtained from the QPM apparatus.

Overall, it was seen that the LSPAT inflicted higher levels of particle attrition than the QPM for equivalent test conditions in all size fractions bar the 850-1180 μm fraction. This was an unexpected results, as it was believed that due to the much smaller flight distance and impact chamber geometry, that the QPM would inflict greater particle attrition for a given test condition. Further work would be required to elucidate the exact mechanism behind this observation, including the use of high speed photography to capture sample particle trajectories and velocities.

5.2.4.2 Comparison of QPM and BSPAT

In order to validate the statements previously made regarding the flaws in the design of the QPM degradation tester, a full factorial comparative study was carried out to look at the differences in attrition data obtained from this device and the BSPAT. The two testers were compared on the influence of impact angle, virgin particle size, and impact velocity.

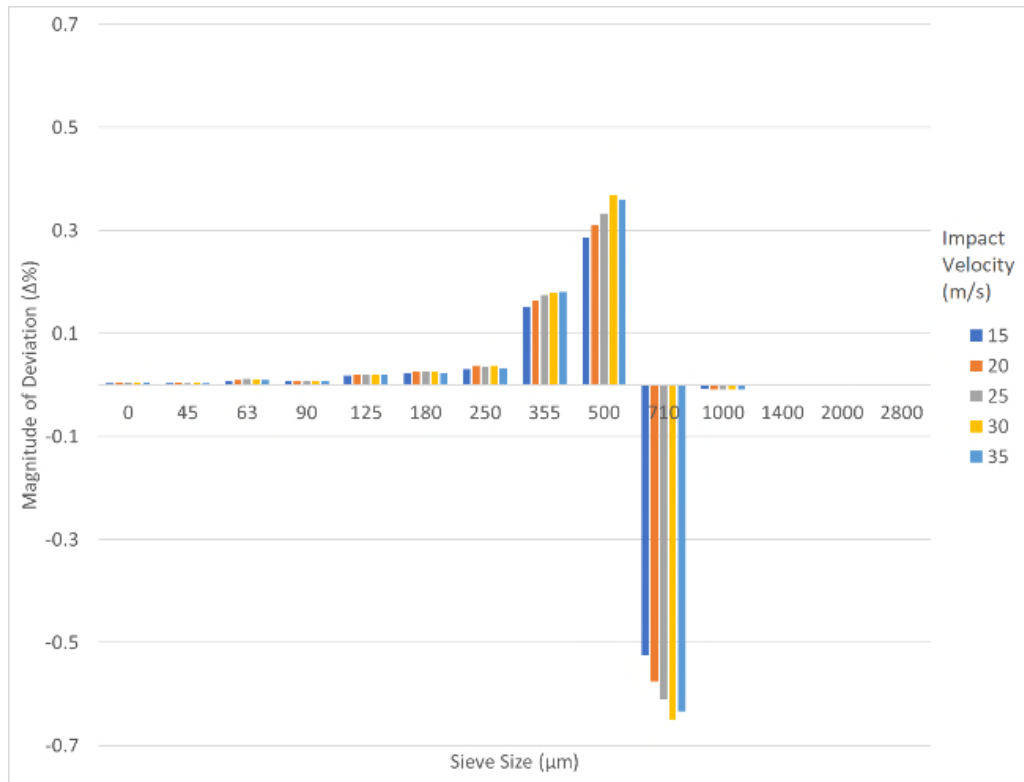
Table 5-6 lists the matrix of test variables undertaken. The specified extent of experimentation was deemed necessary due to the similarity of tester size and arrangement of components. The full data sets for the QPM and the BSPAT are found in Appendix K and Appendix M respectively.

Table 5-6: Variable test matrix for QPM and BSPAT comparative study

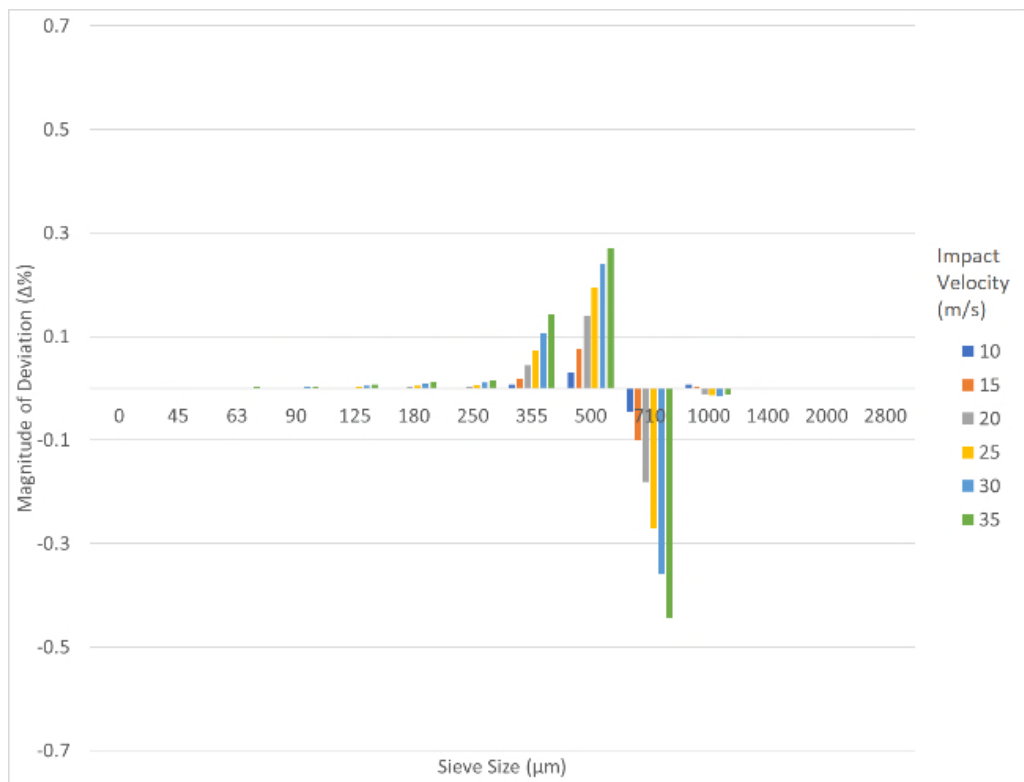
Variable	Values
Material	Carbolux SK
Impact Velocity (m/s)	10*, 15, 20, 25, 30, 35
Impact Angle (degrees)	90, 45, 30, 20*
Material Size Fractions (μm)	710 – 1000 500 – 710 355 – 500 250 – 355

*Tested on BSPAT only

Selected data is given in Figure 5-22 to Figure 5-24, to highlight and contrast the general trends present in the data sets. Figure 5-22 compares the influence of particle impact velocity, Figure 5-23 compares the influence of impact angle, and Figure 5-24 compares the influence of particle size.

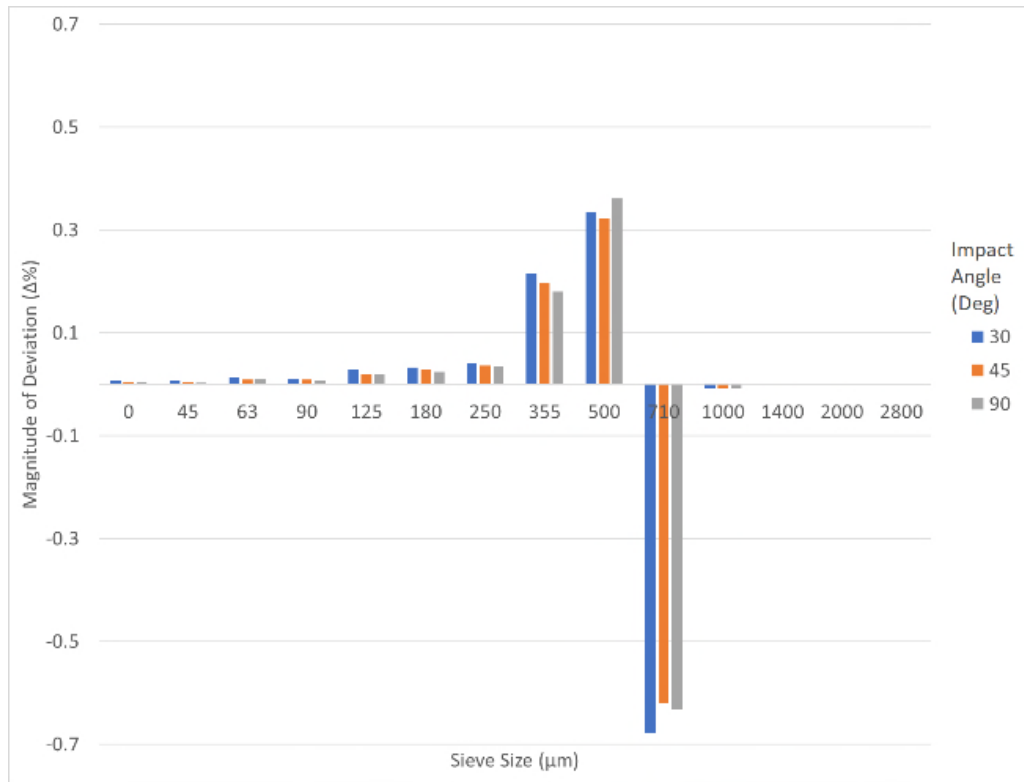


(a)

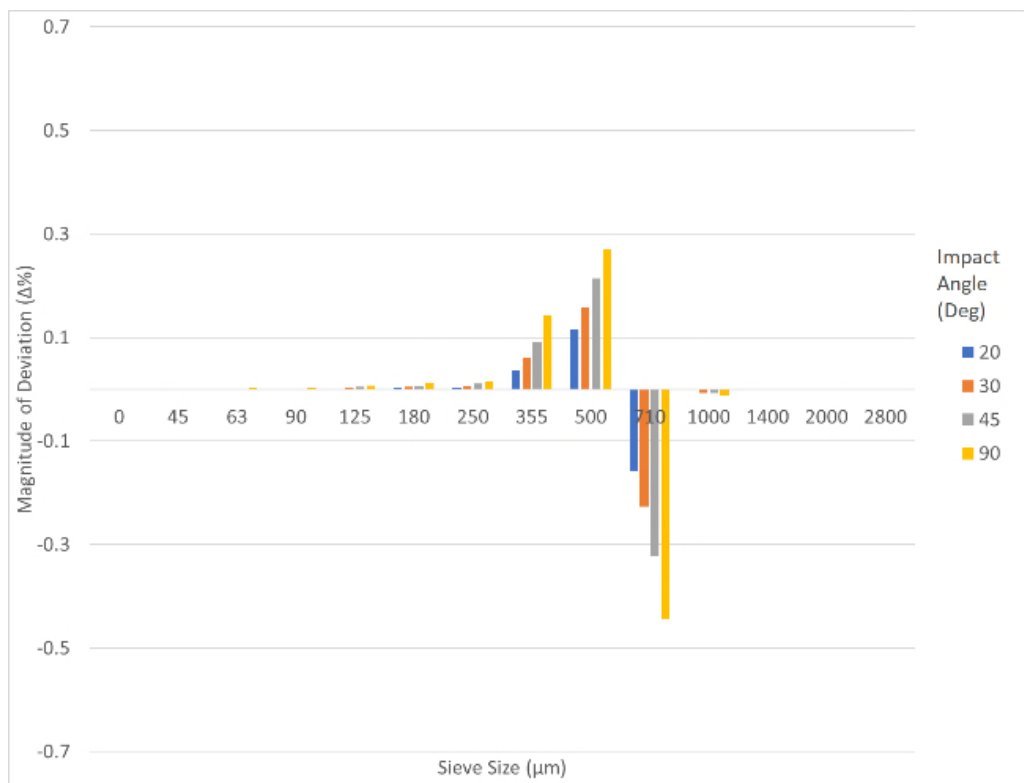


(b)

Figure 5-22: Results of attrition tests of 710-1000 μm virgin batch size Carbolux SK at 90 degree impact angle for (a) QPM and (b) BSPAT

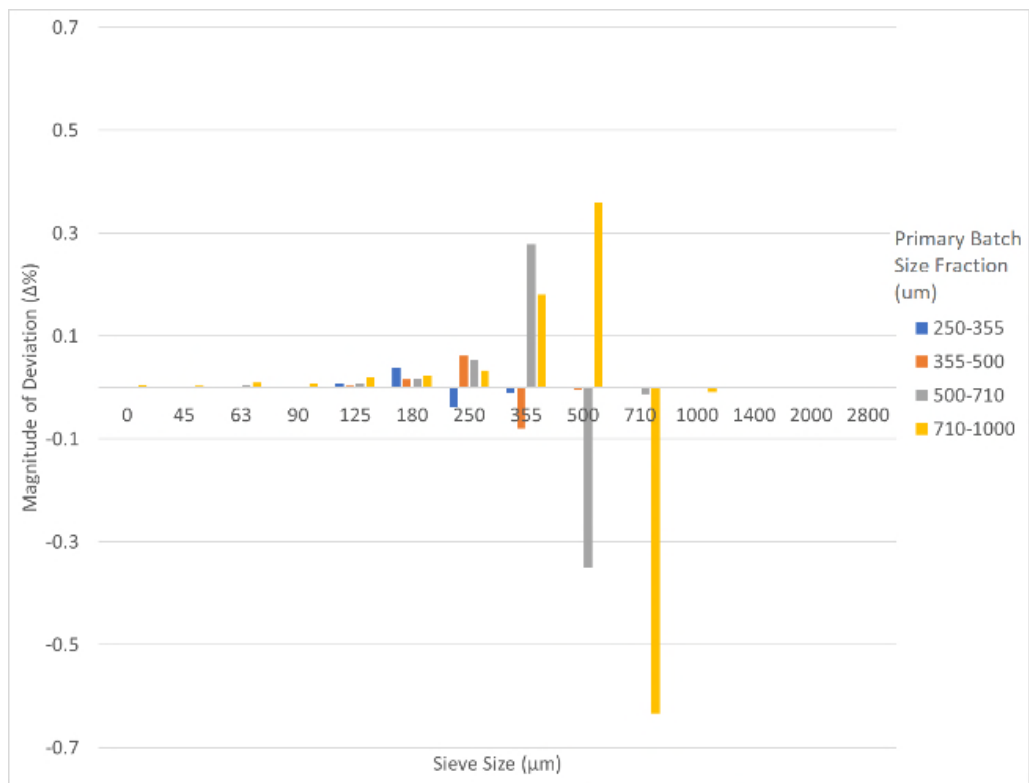


(a)

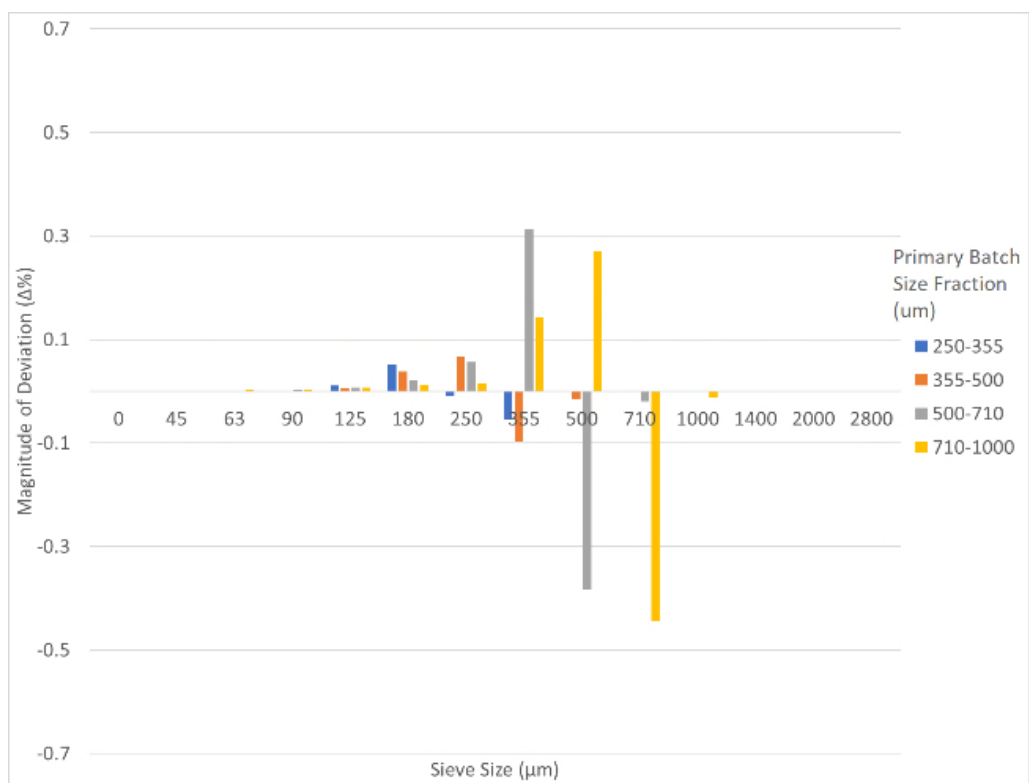


(b)

Figure 5-23: Results of attrition tests of 710-1000 μm virgin batch size carbolux at 35 m/s impact velocity for (a) QPM and (b) BSPAT



(a)



(b)

Figure 5-24: Results of attrition tests for carbolux at 35 m/s impact velocity and 90 degree impact angle for (a) QPM and (b) BSPAT

The comparative data presented clearly shows that the QPM apparatus inflicted significantly more secondary and tertiary impacts on the particles across all impact conditions. This is exemplified most visibly in the comparison of impact angles (Figure 5-23). It can be seen that in the BSPAT apparatus, a gradual progression from low attrition to high attrition correlates with a progression from low impact angle to high impact angle. The results from the QPM apparatus however indicate that maximum particle attrition is achieved at an impact angle of 30 degrees – contrary to the results obtained from all other apparatuses and the previously presented mechanical analysis (whereby attrition increases with increasing normal force due to the impact). This suggests that within the QPM apparatus, the particles underwent at least two significant impacts (primary on the target surface, and secondary on the wall of the impact chamber), as opposed to the single significant impact for which the apparatus was designed.

A second key point of difference is found within the results obtained for the comparison of impact velocities (Figure 5-22). The overall magnitude of attrition measured for each impact velocity was greater in the QPM in comparison to the BSPAT. In addition to the previously described rationale regarding secondary impacts, at an impact angle of 90 degrees there was the possibility that particles could rebound back into the accelerating disc. This would mean that particles would undergo an impact force far greater in magnitude than that specified in the test design. The observations could also be attributed to the design of the accelerating disc. The BSPAT was designed so that the sample particle would be accelerated over a longer period of time (owing to the longer acceleration tube), and therefore the associated force would be reduced.

Finally, the results of the comparison of the influence of particle size between the two apparatuses (Figure 5-24), reflect most of the results previously discussed. A single discrepancy is seen in the comparison of the attrition of 500-710 μm material. More material is lost from the 500-710 μm size fraction in the BSPAT than what was measured in the QPM apparatus. The difference in the magnitude of attrition observed is not large, however, it contradicts the trends observed across all other studies. It is possible that this experiment contained a greater virgin sampling error, which would be attributed to the operator. To remedy this, future studies should perform at least two repetitions (three experiments in total) and average the results.

5.3 Conclusions

The impact conditions and tester geometry have been systematically isolated and studied to describe the influences of each variable. A brief study was also conducted on how different material types respond to varying impact conditions. The following conclusions were found to be generally applicable across the full range of data collected:

1. Particle attrition increases with increasing impact velocity.
2. Particle attrition increases with increasing impact angle (approaching the normal of the target surface).
3. Particle feed rate (particle mass flux at the target surface) has negligible influence on the level of particle attrition measured (across the range of mass fluxes tested), however, it appears to be specific to the tester.
4. Secondary impacts can have significant influence on the measured levels of particle attrition (especially for low impact angles) if they are not sufficiently mitigated.
5. The particle attrition attributed to a screw feeder is negligible for the materials and conditions tested.
6. Vast differences are evident in the attrition behaviour of different particulate materials.
7. Data obtained on the attrition behaviour for one particulate material composition cannot be used to predict the magnitude of particle attrition for another particulate material composition.
8. Particle size has a strong influence on the level of particle attrition measured for a given set of test conditions, and for the materials tested.
9. Significant differences were observed in the particle attrition behaviours manifested across the three centrifugal accelerator particle attrition testers. The attrition behaviour observed is specific to the tester geometry from which it was obtained.

This chapter has presented all studies undertaken to elucidate the mechanisms behind the characterisation of particle attrition behaviours. All test variables have been addressed and investigated. The relationships presented in this chapter shall be drawn on in subsequent chapters to apply, and further analyse how particle attrition behaviours

in centrifugal accelerator attrition testers can be linked to the behaviours existing in lean phase pneumatic conveying systems.

CHAPTER 6: Results and Observations: Characterisation of Pipeline Geometry and Conveying Conditions with respect to Particle Attrition

This chapter shall present the results and observations obtained to characterise the influence of the process factor on the magnitude of particle attrition measured. To adequately isolate each of the variables associated with the process factor, the Single Bend Attrition Tester (see Section 4.4.2 for description) was used. The characterisation of the apparatus shall be presented first, followed by the influence of particle velocity, and particle concentration on the level of particle attrition measured. Following this, the influence of the bend radius and the particle size distribution of the sample on the magnitude of measured attrition shall be given. Finally, a brief study on the influence of particulate material type shall be summarised.

Carbolux SK was the particulate material used for all of the experimentation presented in this chapter, unless otherwise specified. The magnitude of particle attrition is presented in the manner described in Section 5.1.

The matrix of variables considered in this study are summarised in Table 6-1. A full factorial approach was adopted in determining the process factor. The test conditions describing particle velocity and concentration are shown in Figure 6-1 and Figure 6-2, with the detailed records of each test condition found in Appendix E, and the full set of results found in Appendix N.

Particle concentration can be measured in various ways as summarised by Table 6-2.

Table 6-1: Variables tested on the Single Bend Attrition Tester

Variable	Values Tested
Particle Material	Carbolux SK Type C Carbolux SK Type B
Feed Hopper Orifice Diameter (mm)	10 [0.013] {0.017} 20 [0.096] {0.112}
Approximate feed rate in (kg/s) of: [Type C] {Type B}	30 [0.273] {0.302} 40 [0.602] {0.654}
Length of Straight Pipe Prior to Test Bend (m)	12
Length of Straight Pipe After Test Bend (m)	3
Internal Pipe Diameter (mm)	40.94
Bend Radius / Pipe Diameter Ratio	3, 12

Table 6-2: Methods of quantifying Particle Concentration in Pneumatic Conveying Lines

Method	Equation
1) Mass basis (Solids Loading ratio)	$SLR = \dot{m}_s / \dot{m}_g$
2) Volumetric basis (Volumetric Loading Ratio)	$VLR = \dot{V}_s / \dot{V}_g$
3) Mass – Volume Basis (Mass Volume Ratio)	$MVR = \dot{m}_s / \dot{V}_g$
4) Spatial Volumetric Basis (Spatial Volumetric Ratio)	$SVR = \dot{m}_s / (v_s \rho_s A_p)$

Where:

A	Area (m ²)
\dot{m}	Mass flow rate (kg/s)
v	Velocity (m/s)
\dot{V}	Volumetric flow rate (m ³ /s)
ρ	Density (kg/m ³)

Subscripts

g	Gas Phase
p	Pipe
s	Solid Phase

Due to the ease of measurement, Methods 1 to 3 are often used to characterise the solids concentration of a pneumatic conveying system [5, 38, 41, 42]. However, as there was a difference between the particle velocity and the air velocity (slip velocity), Methods 1 to 3 did not give an absolute indication of the solids concentration in the pipeline at the point of interest. Method 4 was therefore selected as an approximation of solids concentration prior to the test bend as particle concentration is calculated using the pipe geometry as a frame of reference. Variation of solids concentration across the pipe cross-section was not considered, and a uniform solids distribution was assumed.

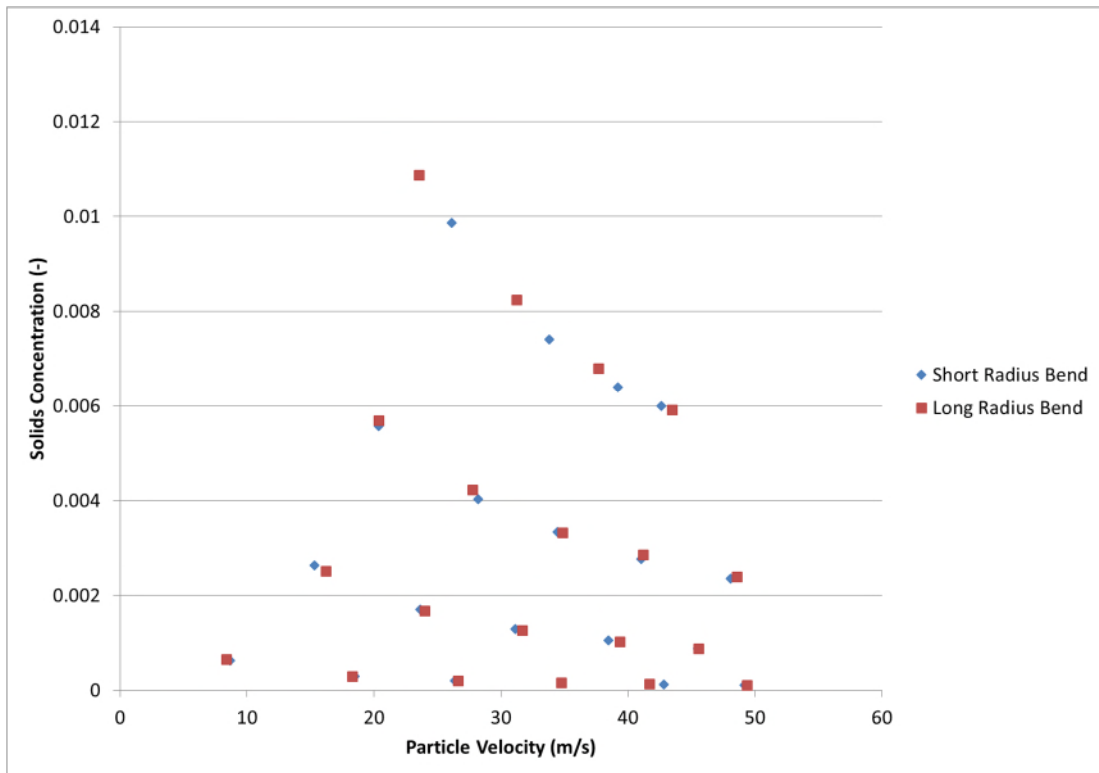


Figure 6-1: Test conditions for carbolux SK Type C

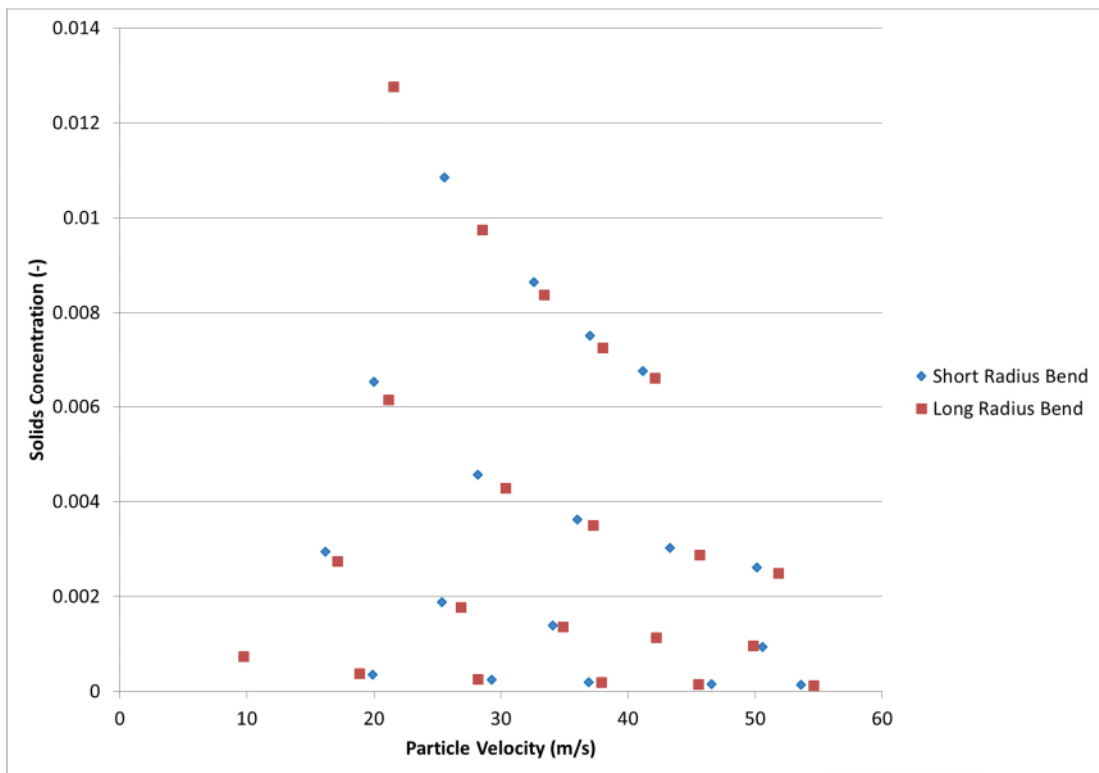


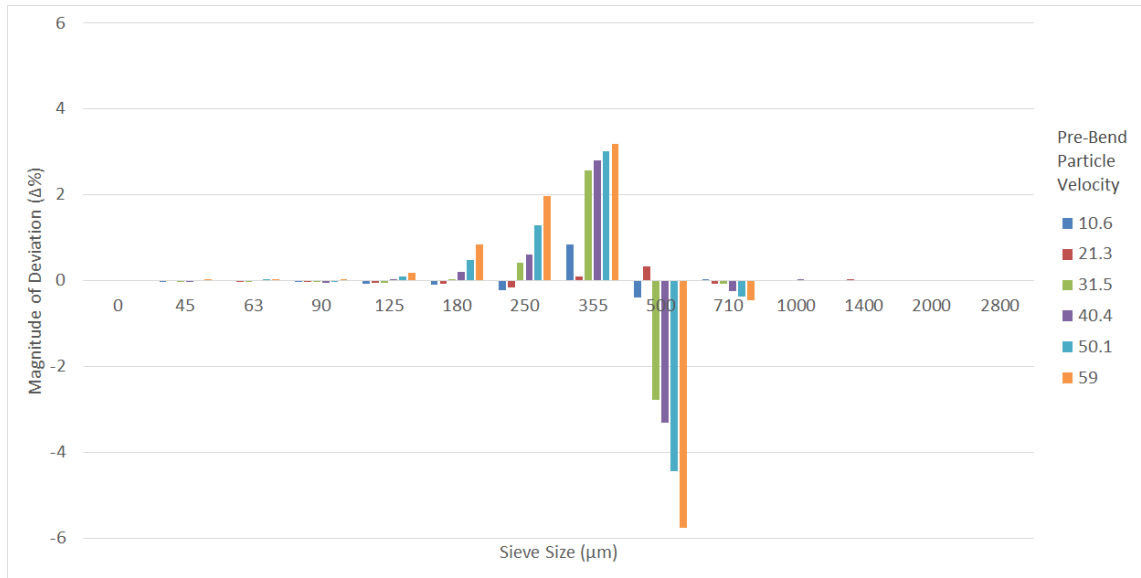
Figure 6-2: Test conditions for Carbolux SK Type B

6.1 Characterisation of the Apparatus

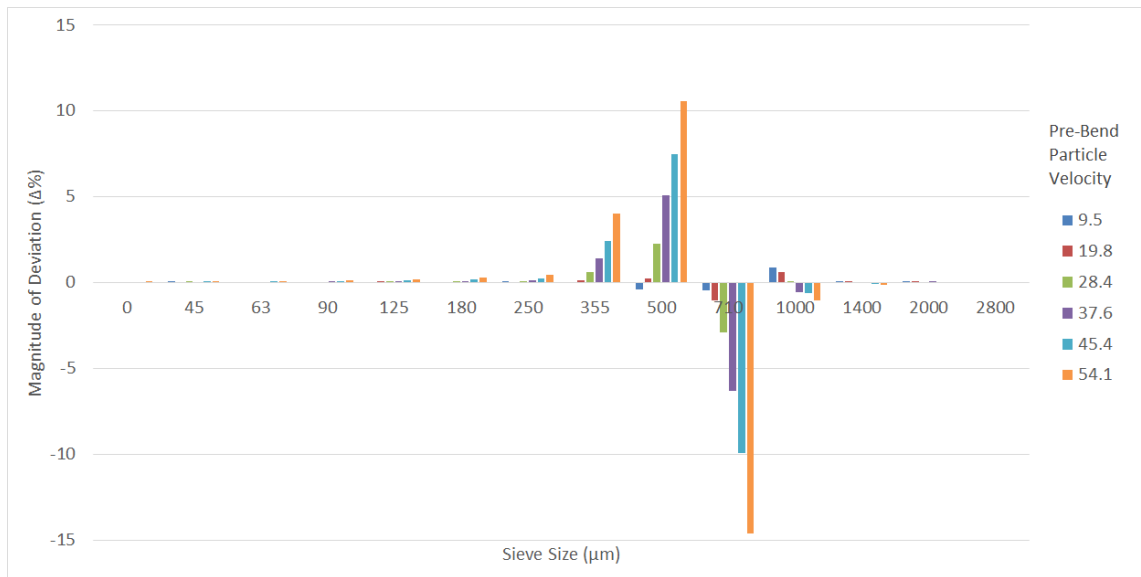
As was demonstrated throughout Chapter 5, the geometry and operating conditions of the apparatus used to test particle attrition can have significant influence on the results obtained. It was therefore prudent to conduct a series of tests to characterise the apparatus so that the results could be considered within the context of the relevant flow conditions and secondary sources of particle breakage other than the test bend. This test work consisted of the magnitude of particle attrition that could be attributed to the receiving arrangement at the end of the pipeline, visual characterisation of the flow regime, and finally, the determination of the mass flow rate of material through the series of orifice plates used to control the flow out of the feed hopper.

6.1.1 Attrition Attributed to the Receiver

In Chapter 2, it was found that many of the studies published by other researchers did not acknowledge or measure the magnitude of particle attrition caused by the feeding or receiving arrangement of a pneumatic conveying system. In the present research, the feeding arrangement was expected to inflict minimal particle damage (due to the orifice plate arrangement) and was therefore exempted from characterisation. However, significant effort was made to minimise the magnitude of particle attrition attributed to the receiving vessel, but characterisation was required nonetheless. Therefore, the test bend from the Single Bend Attrition Tester was removed, so that the pneumatic conveying line consisted of a straight, 12 m length, of pipeline feeding tangentially into the receiver. In this way, the magnitude of attrition attributed to the test bend was removed, and any particle attrition observed could be associated with the receiving vessel. Figure 6-3 presents the results obtained from this study for both grades of Carbolux SK (described in Section 4.5.5 as Type B and Type C).



(a)



(b)

Figure 6-3: Attrition results for straight-line conveying directly into the receiver for (a) Type B and (b) Type C, Carbolux SK

It was clear that the smaller particle sizes of the Carbolux SK material degraded significantly less than the larger particle sizes. This was further emphasised by the differences in particle velocity; the smaller particles degraded less at higher conveying velocities.

6.1.2 Flow Characterisation

As stated in Chapter 2, a variety of different flow regimes are capable of manifesting themselves within a pneumatic conveying system. It was deemed necessary to visualise the flow during an experiment to identify the flow regime and confirm that homogeneous, lean phase flow was present. To achieve this, a 1 m long section of pipe was fabricated from soda lime glass and positioned immediately before the test bend in the system. Figure 6-4 shows an example of a side elevation view of the pipe during conveying, and Figure 6-5 shows a plan view of the temporary glass bend used to visualise flow. It was clear by inspection that all particles were suspended in the air flow and there was no bed of material forming on the floor of the pipe. One can observe a dark section towards the floor of the pipe in Figure 6-4, however due to the optical arrangement of the image capture, this dark section is in fact a reflection of the darker surface below the pipe. It could be observed in Figure 6-5 that the particle stream detached from the wall by the time it passed the downstream edge of the post-bend compression coupling. This observation indicated that the full effect of the bend was applied to the particles throughout the experimental programme by the steel bend.

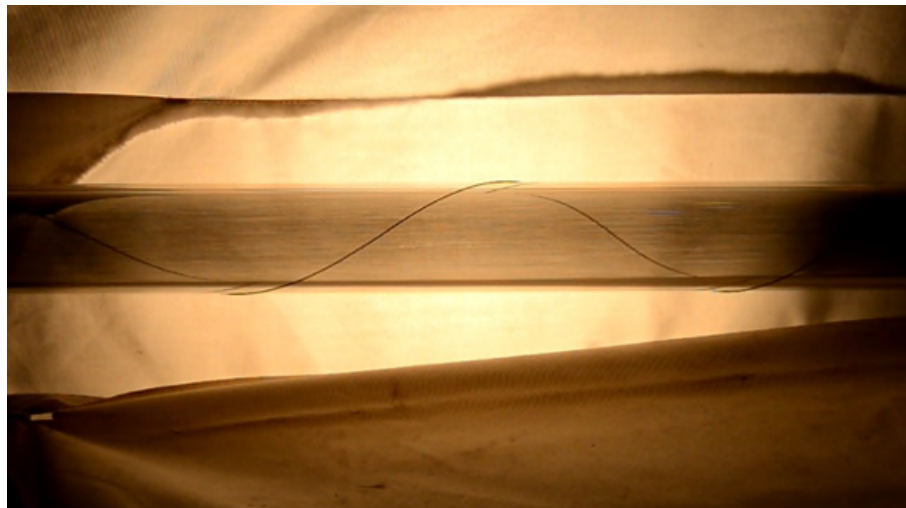


Figure 6-4: Elevation view of the pipeline sight glass demonstrating homogeneous lean phase flow

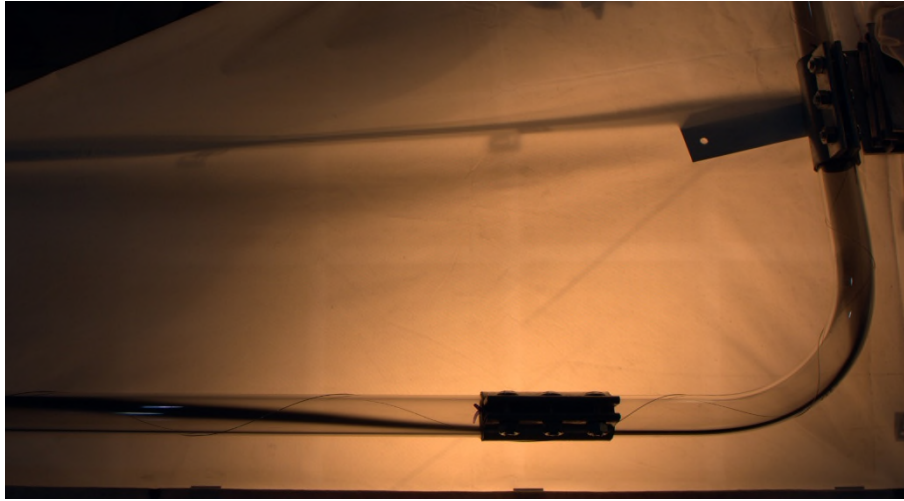


Figure 6-5: Plan view of the glass bend to observe two-phase flow characteristics

6.1.3 Mass Flow Rate through the Orifice Plates

As the secondary aim of the present research was to determine the influence of solids concentration on the level of particle attrition measured in a lean phase pneumatic conveying system, measurement and control of the solids feed rate out of the feed hopper was fundamentally important. To ensure that the mass flow rate out of the hopper was consistent with the experimental design, a simple orifice mass flow rate tester was fabricated to determine the relationship between orifice diameter and mass flow rate. The tester consisted of a Perspex tube, 150 mm in diameter and 450 mm in height. A series of end caps were machined to fit into the end of the tube, and orifices of 15, 30, 50, 80 and 100 mm were cut. A mass of particulate material was timed with a stopwatch as it flowed out of the tube. The mass of material that passed through the orifice was measured on a set of digital laboratory scales to an accuracy of ± 0.01 g. Figure 6-6 shows the results of this series of experiments, and compares them with the mass flow rates obtained in the main experimental programme from the feed hopper load cells for Type C of Carbolux SK.

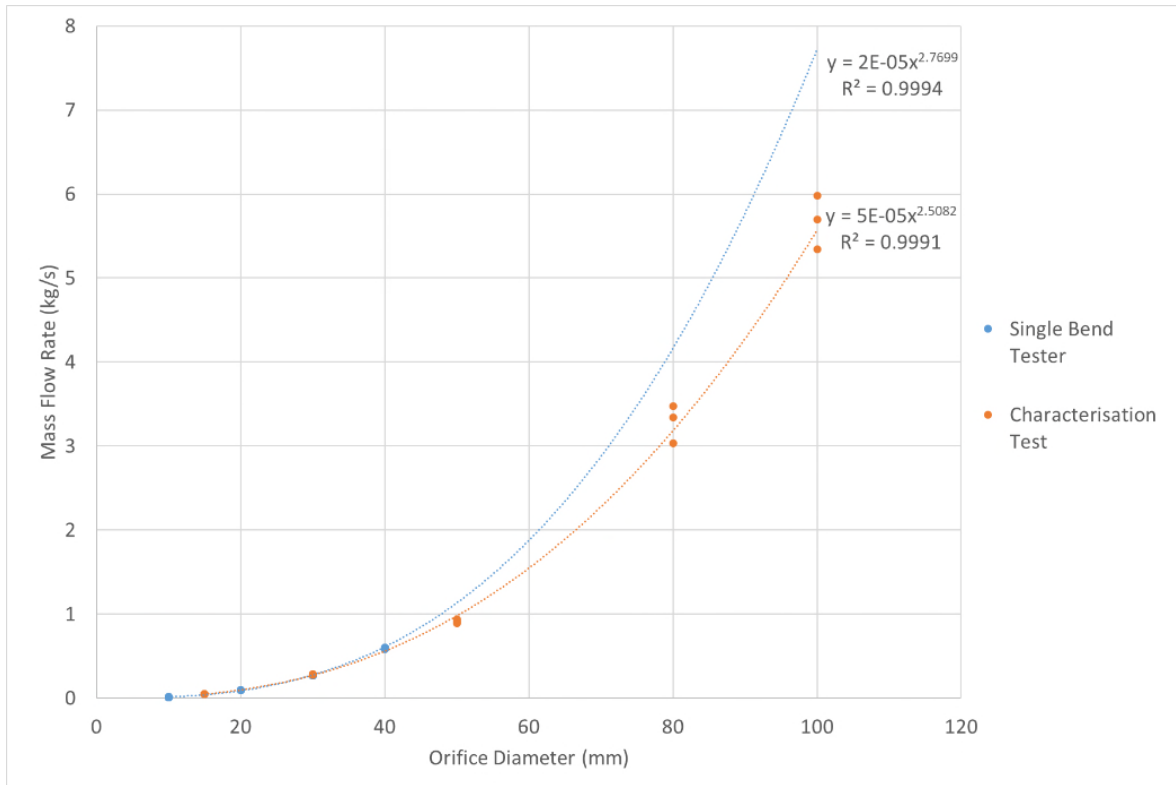
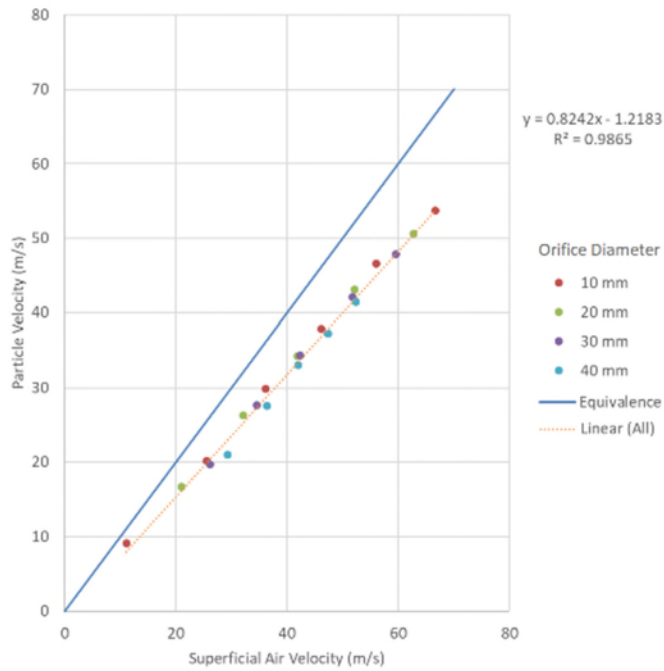


Figure 6-6: Comparison of mass flow rates through orifices of specified diameter

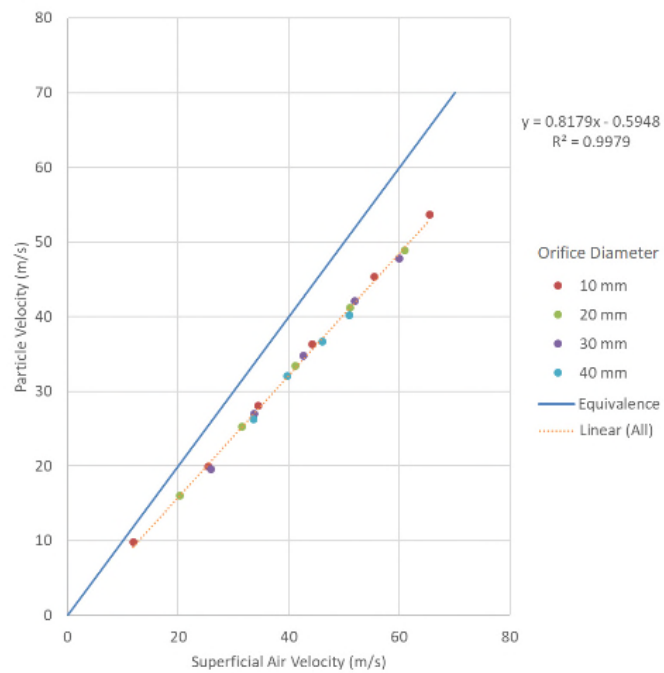
Exponential functions were fit to the data and it was found that the data obtained from the characterisation test and the feed hopper load cells agree well within the range of orifice diameters considered in the single bend attrition tester. However, when orifice diameters greater than those experimentally tested (namely; 50, 80 & 100mm) were considered, the fitted functions diverged. This could have been attributed to the increased human errors introduced into the characterisation test (where the operator reaction time formed a larger percentage of the duration of the characterisation test). If the test work was to be repeated, a larger volume of tube would be used to increase the sample size and therefore increase the duration of the characterisation test. Overall, this method of mass flow rate through an orifice characterisation proved adequate for the purposes of predicting mass flow rate of sample material out of the feed hopper and into the conveying line of the single bend attrition tester.

6.1.4 Slip Velocity Characterisation

In order to reconcile the data obtained in Chapter 5 with the data obtained in the Single Bend Attrition Tester, it was necessary to measure the particle velocity. However, measurement of the particle velocity is often not possible with the resources available within industry. Therefore, to inform the model developed in Chapter 9, it was necessary to characterise the particle slip velocity over the full range of conveying conditions under consideration defined in Figure 6-1 and Figure 6-2. The results from this study are presented in Figure 6-7.

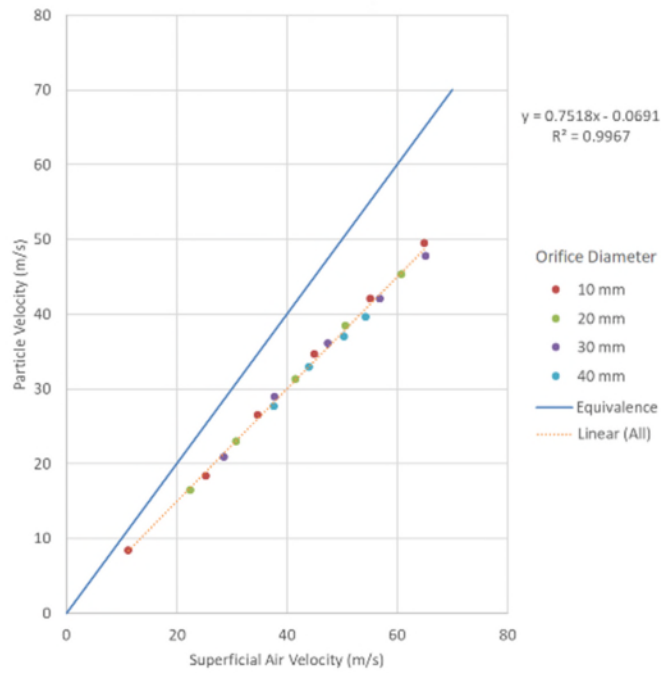


(a)

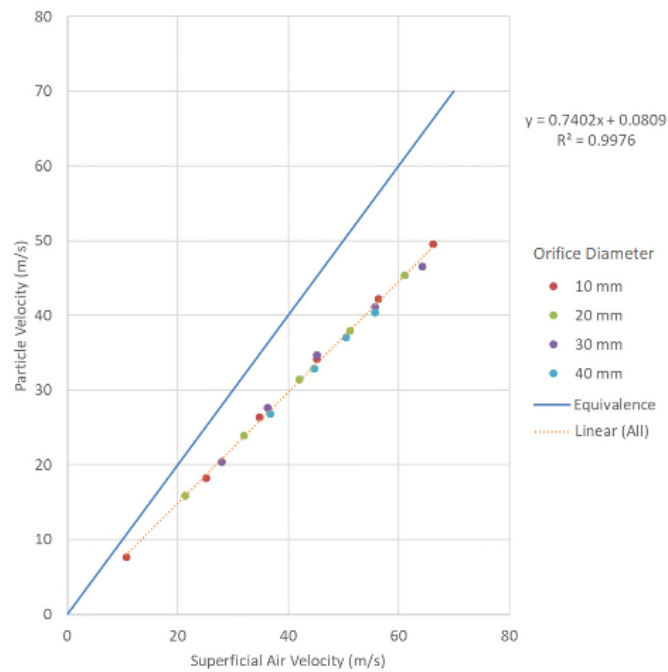


(b)

Figure 6-7: Particle Velocity vs. Superficial Air Velocity across each of the four Orifice Plate Diameters considered for (a) Carbolux SK Type B long radius bend, (b) Carbolux SK Type B short radius bend, (c) Carbolux SK Type C long radius bend, and Carbolux SK Type C short radius bend



(c)



(d)

Figure 6.7: Particle Velocity vs. Superficial Air Velocity across each of the four Orifice Plate Diameters considered for (a) Carbolux SK Type B long radius bend, (b) Carbolux SK Type B short radius bend, (c) Carbolux SK Type C long radius bend, and Carbolux SK Type C short radius bend

It was evident that the influence of particle concentration on the magnitude of slip velocity observed was negligible. All data points conformed to a linear relationship, and as demonstrated in Figure 6-7, the fitted linear relationships all had coefficient of determination values close to unity.

When comparing the results obtained for the same material type across both bend radii, the linear relationship changed little. This was expected, as the bend radius positioned after the acceleration section of the conveying line should have no influence over the observed slip velocity relationships; this served as a checking method to ensure that the experimental approach was sound.

The particle size distribution of the conveyed material had a significant influence on the slip velocity relationship displayed. This is most clearly communicated through observation of the 'x' coefficient of each of the fitted relationships in Figure 6-7. For a given material type, the magnitude of change in this coefficient is small; less than 0.012. However, the magnitude of difference between the two material types is in the region of 0.06. The value of this coefficient essentially translates to the magnitude of the particle velocity as a percentage of the superficial air velocity. It is therefore possible to state that the slip velocity profile of Type C material is 6% less than that of Type B material, where the percentage is that of the superficial air velocity.

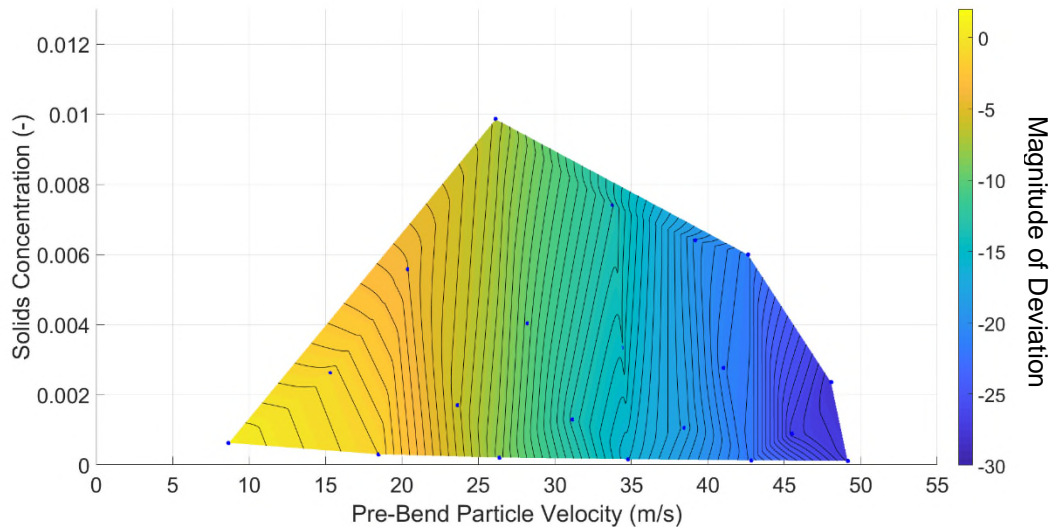
6.2 Single Bend Attrition Tester Results

This section shall systematically address the attrition results obtained from the Single Bend Attrition Tester in terms of each operating variable. Firstly, the results will be given in the form of breakage maps (Figure 6-8 to Figure 6-11). These maps take the data points presented in Figure 6-1 and Figure 6-2, and plot the magnitude of deviation for a specified size fraction. The contour lines have been generated through triangular interpolation and signify regions of equal particle attrition. The MATLAB code used to generate the breakage maps is given in Appendix F. Figure 6-8 shows the amount of breakage observed for the primary size fraction of each type of Carbolux. Figure 6-9 shows the amount of material addition to the 180 μm size fraction, and Figure 6-10 shows

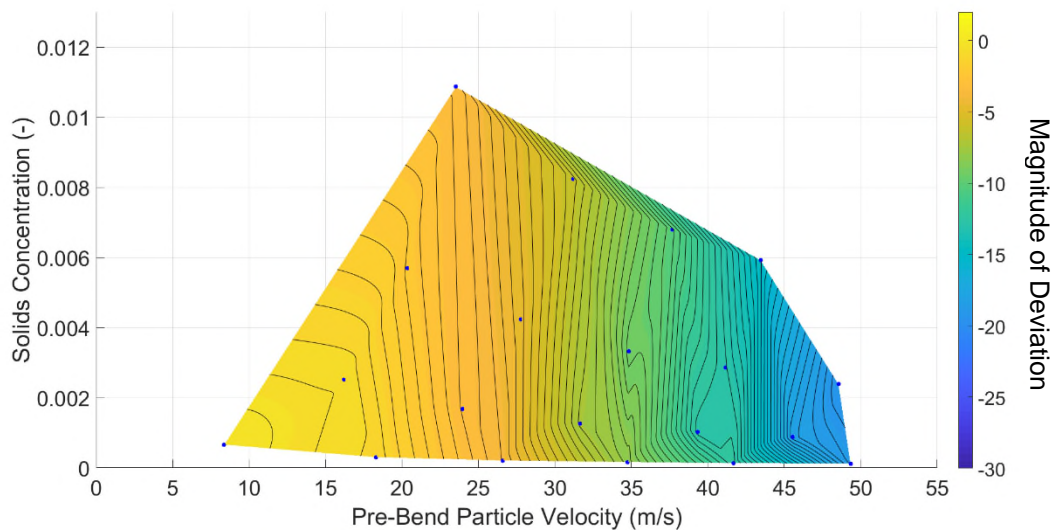
the amount of material addition to the 250 μm size fraction. Finally, the figures contained within Figure 6-8 were re-plotted with respect to superficial air velocity (not pre-bend particle velocity) in Figure 6-11.

The influences of pre-bend particle velocity, pre-bend particle concentration, bend radius and particle size distribution will then be addressed. Finally, a brief analysis of the influence of a different material type shall be given.

The breakage maps are coloured according to the amount of particle attrition measured. For the breakage maps measuring mass loss from a particular size fraction (Figure 6-8 and Figure 6-11), the yellow signifies negligible breakage in the sample, and purple indicates maximum breakage in the sample. For the breakage maps measuring mass addition to a particular size fraction (Figure 6-9 and Figure 6-10), purple indicates negligible particle breakage in the sample and yellow indicates maximum particle breakage in the sample. If contour lines take the form of a line with a positive gradient, this indicates that particle attrition to high concentration, high velocity conditions, is equivalent to low velocity, low concentration conditions. This indicates the presence of a 'shielding' effect where particle attrition is partially mitigated with increased particle concentration. However, vertical contour lines indicate that the magnitude of particle breakage is reliant solely on the particle velocity (for the pipeline geometry tested).

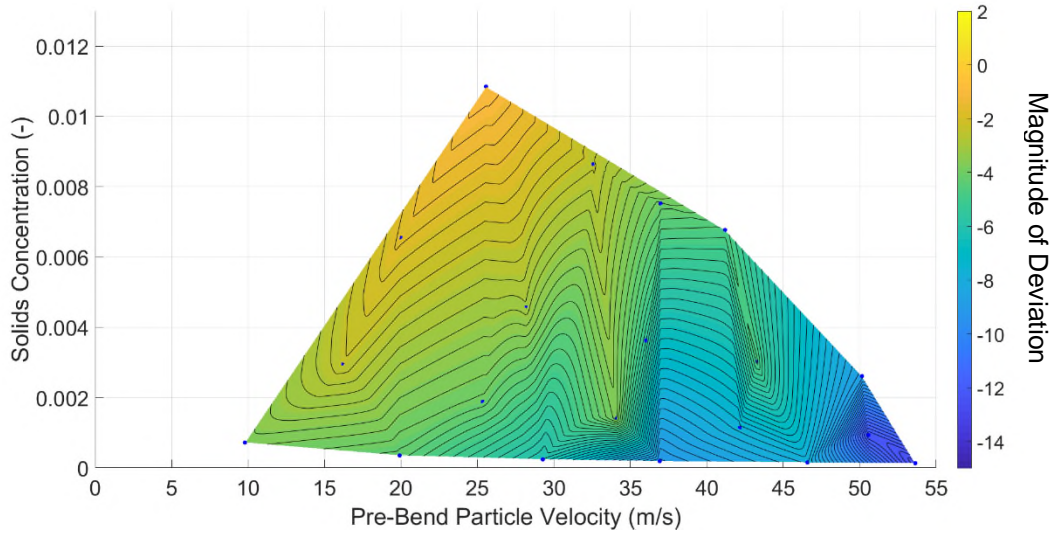


(a)

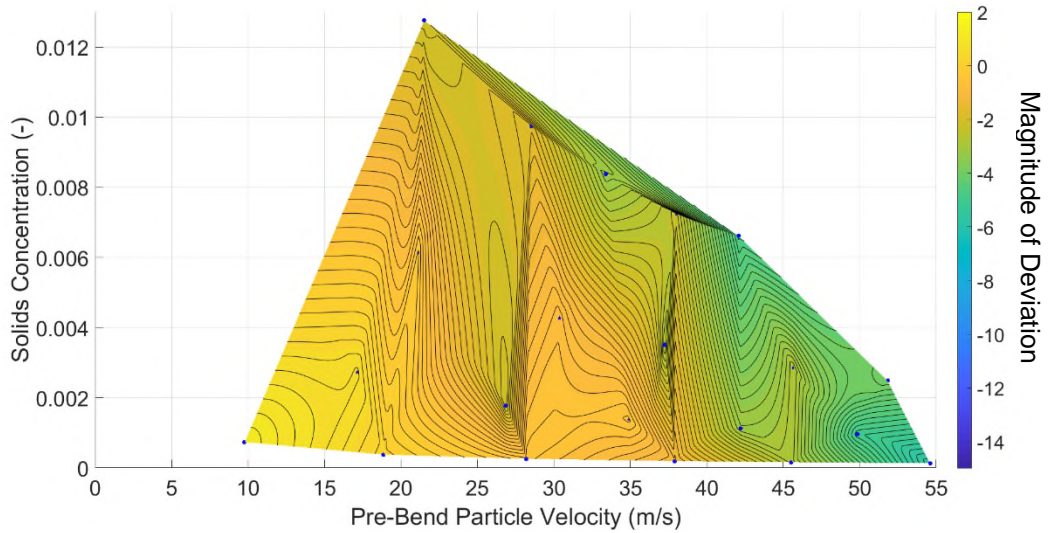


(b)

Figure 6-8: Particle attrition as measured by the magnitude of deviation in the 710 μm sieve for Carbolux SK type C for a (a) short radius bend and (b) a long radius bend; and magnitude of deviation in the 500 μm sieve for Carbolux SK Type B for a (c) short radius bend and (d) long radius bend

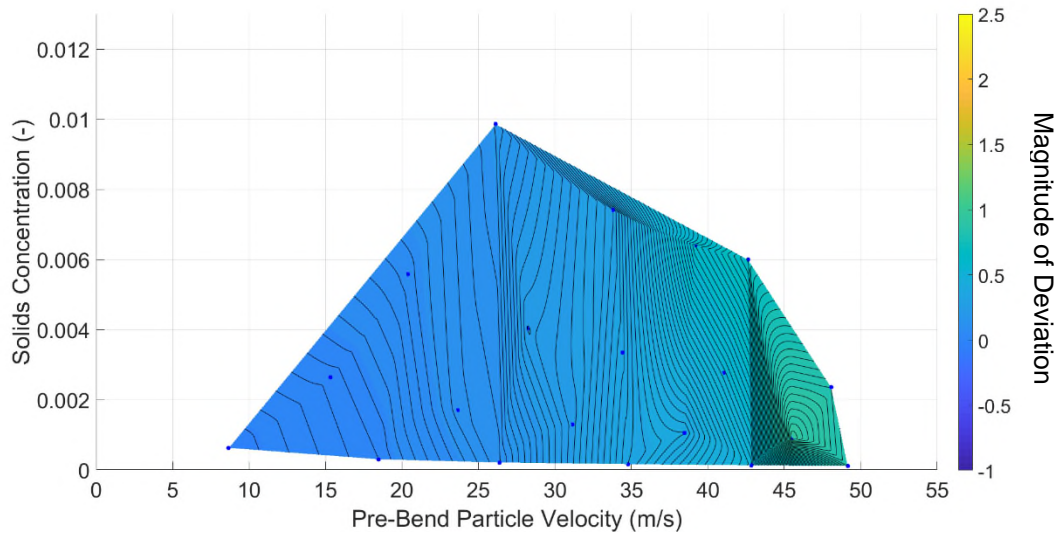


(c)

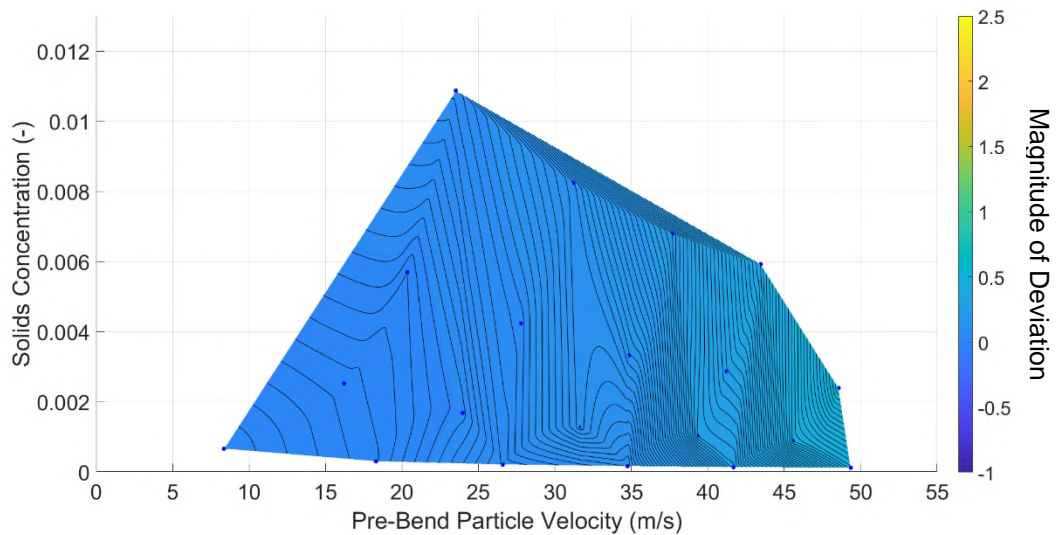


(d)

Figure 6 8: Particle attrition as measured by the magnitude of deviation in the 710 μm sieve for Carbolux SK type C for a (a) short radius bend and (b) a long radius bend; and magnitude of deviation in the 500 μm sieve for Carbolux SK Type B for a (c) short radius bend and (d) long radius bend

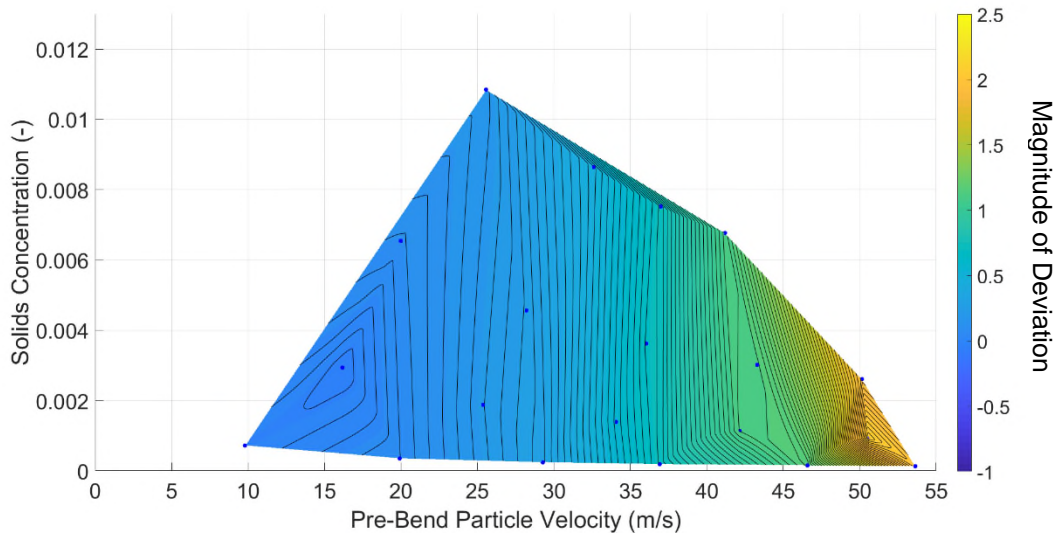


(a)

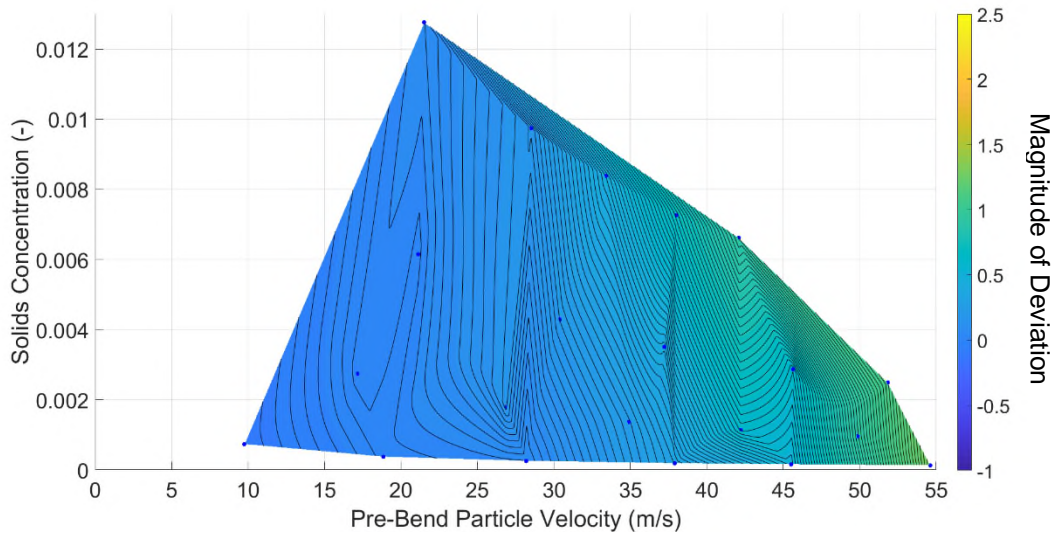


(b)

Figure 6-9: Particle attrition as measured by the magnitude of deviation in the 180 μm sieve for Carbolux SK type C for a (a) short radius bend and (b) a long radius bend; and for Carbolux SK Type B for a (c) short radius bend and (d) long radius bend

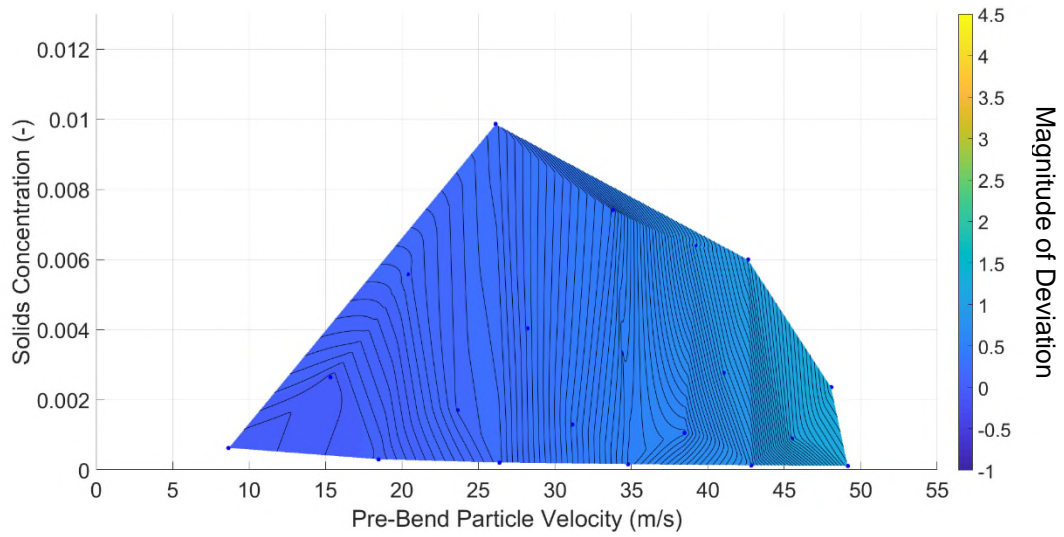


(c)

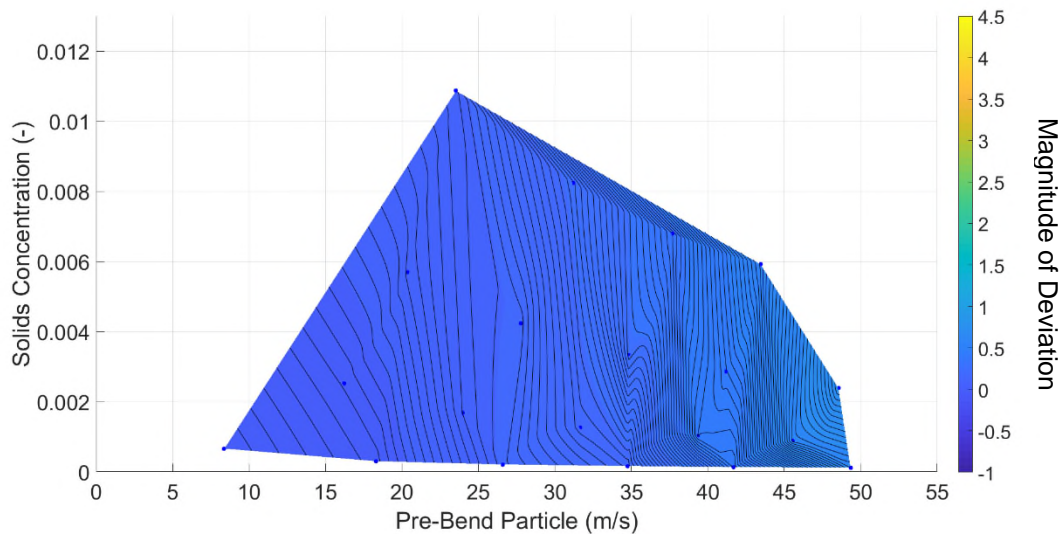


(d)

Figure 6 9: Particle attrition as measured by the magnitude of deviation in the 180 μm sieve for Carbolux SK type C for a (a) short radius bend and (b) a long radius bend; and for Carbolux SK Type B for a (c) short radius bend and (d) long radius bend

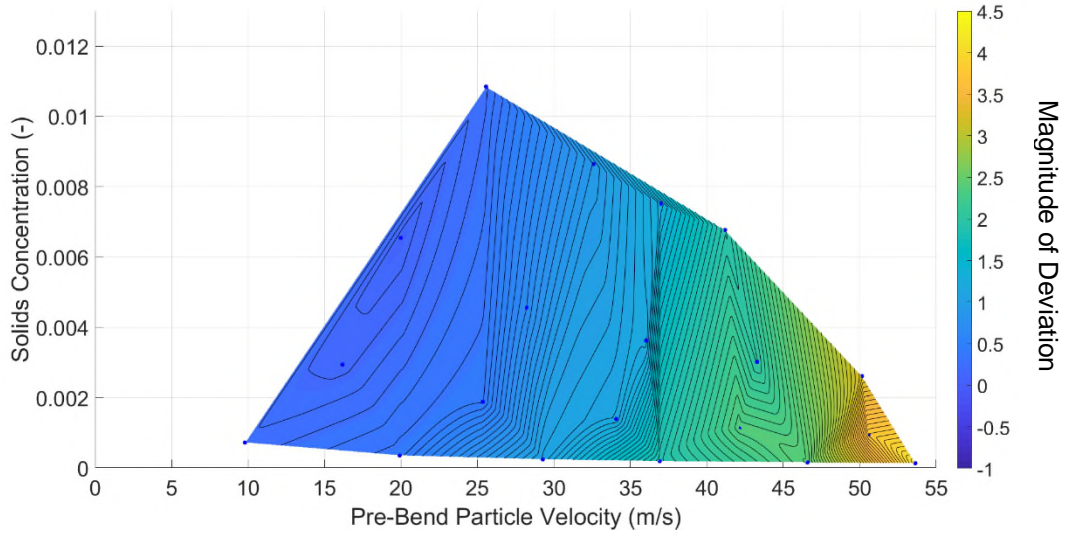


(a)

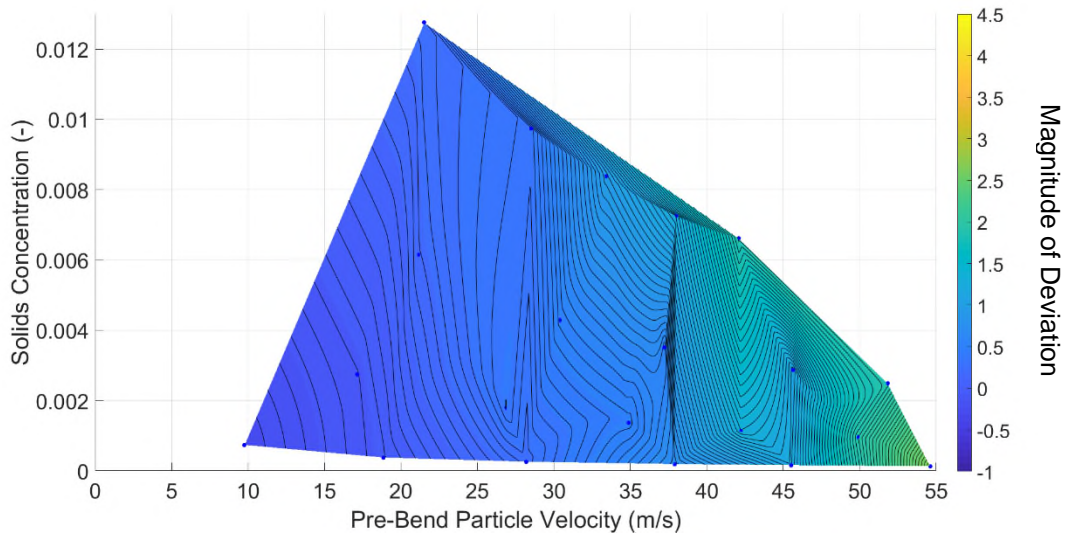


(b)

Figure 6-10: Particle attrition as measured by the magnitude of deviation in the 250 μm sieve for Carbolux SK type C for a (a) short radius bend and (b) a long radius bend; and for Carbolux SK Type B for a (c) short radius bend and (d) long radius bend

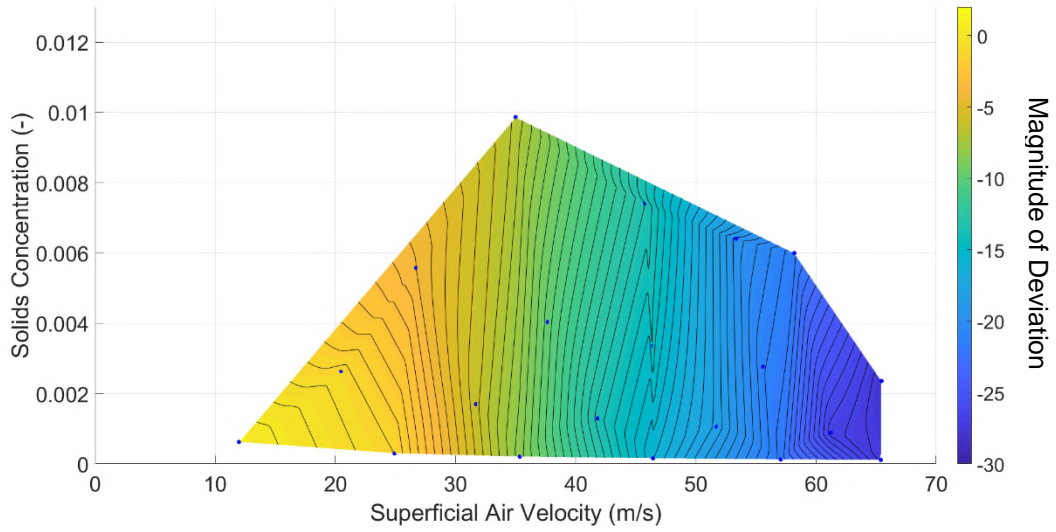


(c)

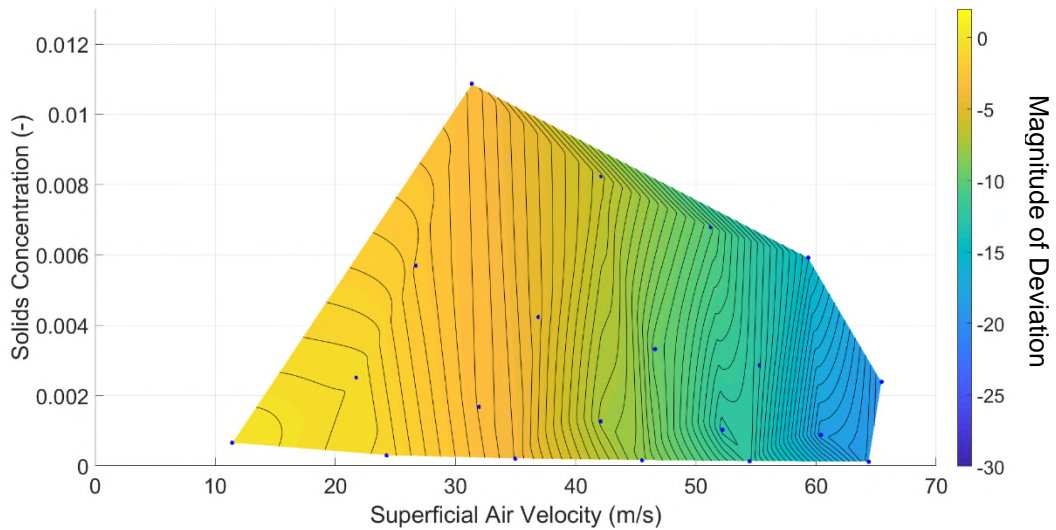


(d)

Figure 6 10: Particle attrition as measured by the magnitude of deviation in the 250 μm sieve for Carbolux SK type C for a (a) short radius bend and (b) a long radius bend; and for Carbolux SK Type B for a (c) short radius bend and (d) long radius bend

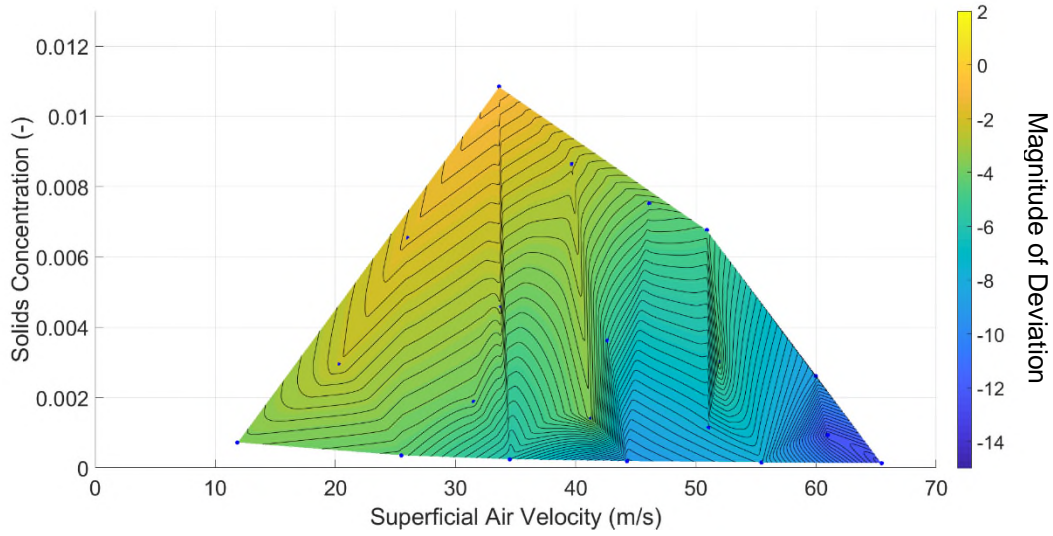


(a)

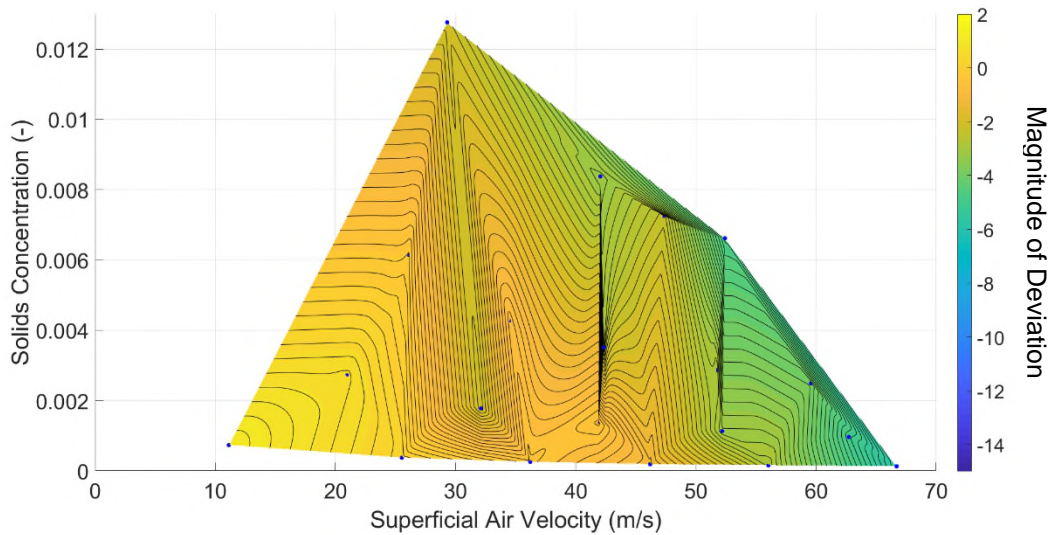


(b)

Figure 6-11: Particle attrition compared to superficial air velocity as measured by the magnitude of deviation in the 710 μm sieve for Carbolux SK type C for a (a) short radius bend and (b) a long radius bend; and magnitude of deviation in the 500 μm sieve for Carbolux SK Type B for a (c) short radius bend and (d) long radius bend



(c)



(d)

Figure 6 11: Particle attrition compared to superficial air velocity as measured by the magnitude of deviation in the 710 μm sieve for Carbolux SK type C for a (a) short radius bend and (b) a long radius bend; and magnitude of deviation in the 500 μm sieve for Carbolux SK Type B for a (c) short radius bend and (d) long radius bend

6.2.1 Influence of Particle Velocity on Measured Particle Attrition

As has been previously acknowledged (Section 2.4.4.1.1) particle velocity was expected to have the most significant influence over the magnitude of particle attrition measured for a given pipeline geometry. The range of pre-bend particle velocities considered were

from the transitional velocity (where particles start to fall out of the air stream and a moving particle bed was present on the pipe floor), up to 59 m/s which was the upper limit of the electrostatic particle velocity sensors positioned prior to the test bend.

It was observed that across all testing conditions, the amount of particle attrition increased with increasing pre-bend particle velocity, albeit to varying degrees. To consider the consequences of failing to measure particle velocity and to highlight the significance of slip velocity, Figure 6-11 implies that particles travel at much higher velocities than those presented in Figure 6-8 (if slip velocity was assumed to be negligible).

6.2.2 Influence of Particle Concentration

Particle concentration was found to have negligible effect on the level of particle attrition measured in some cases. This was exemplified by the vertical contour lines, indicating that the magnitude of particle attrition was approximately constant across the range of tested solids concentrations. Cases where this was particularly clear include Figure 6-8a, Figure 6-9c, and Figure 6-10a.

Some cases did not show a clear relationship between particle concentration and particle attrition (such as Figure 6-8d and Figure 6-9d) as there was too much noise in the data. These cases were more common in the results obtained from the Type B Carbolux SK. As concluded in Chapter 5, the smaller the particle size, the less likely it is to break for a given impact velocity. It is possible that this observation is due to the reduced span of the particle strength distribution was tested for the Type B material (in comparison to the type C material), however, this argument is negated in Section 6.2.4. In order to obtain results with greater clarity in their trends, the experiments should be repeated using pre-sieve particle size fractions (see Figure 5-6) and shall be left for further work.

Only one single case indicated the possible presence of a shielding effect – Figure 6-8c. This was shown by the non-vertical contour lines, with a positive gradient. The positive gradient indicated that the magnitude of particle attrition was equivalent for a low-velocity low-particle concentration condition, and a high-velocity high-particle concentration conveying condition.

After consideration of the data collected, it was evident that for homogeneous lean phase flow, particle concentration has negligible effect on the magnitude of particle attrition for a given pipeline geometry and superficial air velocity. Therefore, the observations presented by previous researchers regarding the 'shielding effect' must be the result of another phenomenon.

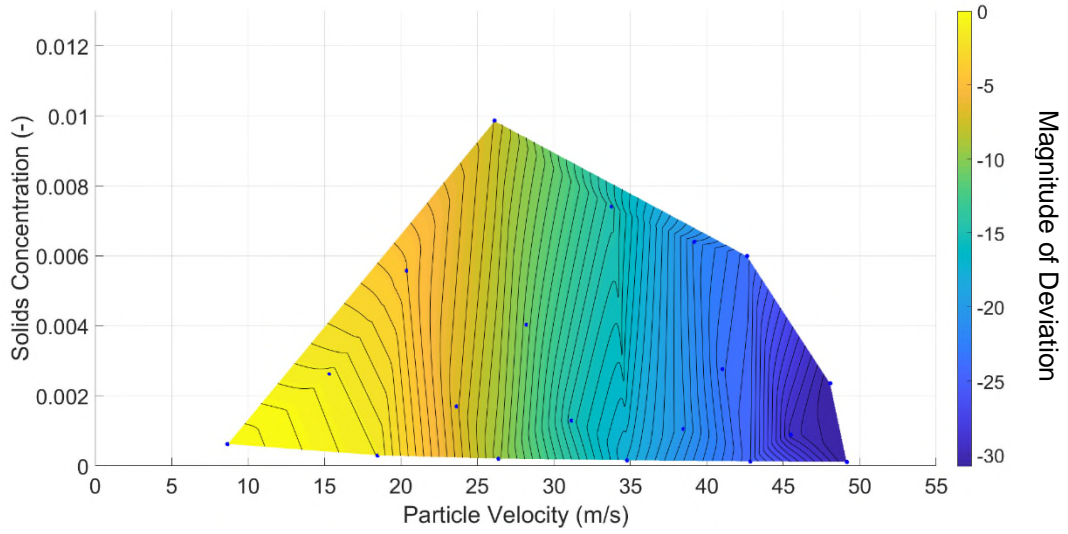
6.2.3 Influence of Bend Radius

Across all conveying conditions considered in this study, the magnitude of particle attrition manifested in a short radius bend was greater than that manifested in a long radius bend. A clear example of this relationship is in the comparison of Figure 6-8a and Figure 6-8b, where at the highest-velocity condition, the short radius bend inflicted 27.4% decrease in the 710-1000 μm compared to the 18.9% decrease in the long radius bend.

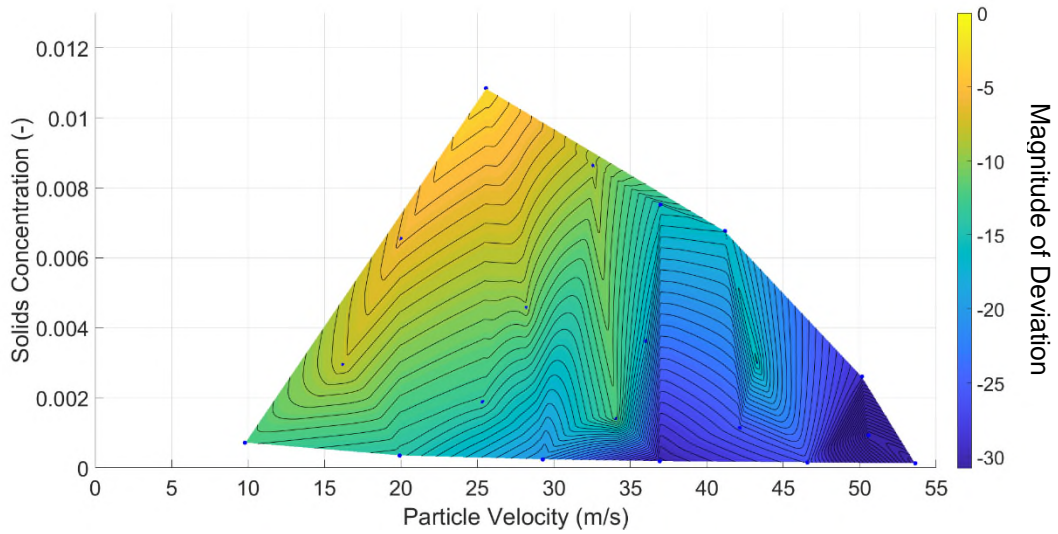
6.2.4 Influence of Particle Size Distribution

Figure 6-8 demonstrated that the magnitude of particle attrition (as measured by loss in a particular size fraction) was greater in the Type C compared to the Type B. This supports the results presented in Section 5.1.4.1 obtained from the Bench Scale Particle Attrition Tester. However, if the magnitude of deviation is taken as a percent of material retained in said size fraction (Percent Change Criterion, α) in the virgin particle size distribution (as described by Equation (6-1)), Figure 6-8a and Figure 6-8c become Figure 6-12a and Figure 6-12b respectively. This models a scenario where the entire sample resides within the primary size fraction.

$$\alpha = \frac{\Delta\%}{P_1} \times 100 \quad (6-1)$$



(a)



(b)

Figure 6-12: The weighted magnitude of deviation of the primary size fraction measured in a short radius bend for (a) Carbolux Type C, and (b) Carbolux Type B

The analysis undertaken in Figure 6-12 indicates that the amount of material removed from the primary size fraction of each material in a short radius bend is within the same order of magnitude.

6.2.5 Influence of Material Type (FCC catalyst)

In order to demonstrate the versatility of the apparatus and to provide some context with respect to the influence of material type in the Single Bend Attrition Tester, both types of Spent FCC catalyst were tested. The apparatus was modified to the straight-line conveying arrangement described in Section 6.1.1 to give the simplest basis for comparison and accommodated the small quantity of material available. The particle size distribution analysis was performed with the laser diffraction measurement technique.

The slip velocity profile was measured as part of this study, the results of which are presented in Figure 6-13. When compared to the slip velocity profile of both Carbolux SK materials, it can be concluded that the slip velocity of both types of Spent FCC Catalyst is significantly smaller in magnitude (i.e., the fully accelerated particle velocity is much closer to the superficial air velocity). In terms of particle size, this is in agreement with the trend observed in the two types of Carbolux SK; that the slip velocity of a material increases with increasing particle diameter.

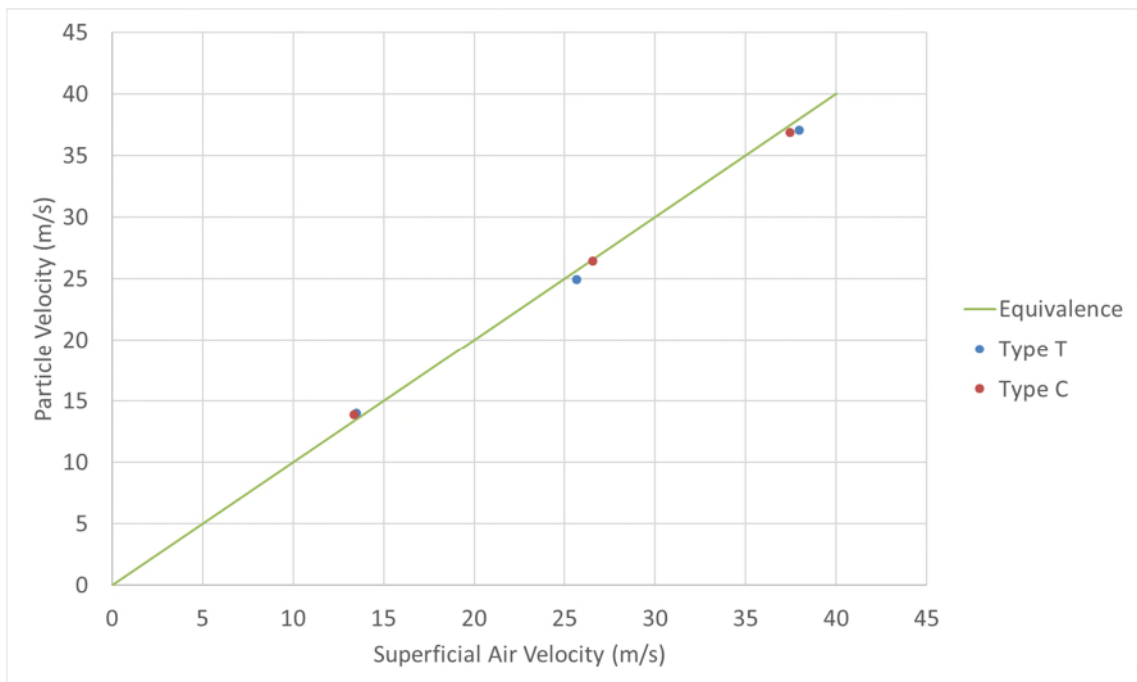


Figure 6-13: Particle velocity vs superficial air velocity for Spent FCC Catalyst

The particle attrition results are presented in Figure 6-14 for Type T material and in Figure 6-15 for Type C material. The magnitude of deviation is presented in non-decimal format. It was evident that, similar to the results obtained in Section 5.1.4.2, very small levels of particle attrition were detected. However, in contrast to the results obtained from the BSPAT tester, all of the results from the Single Bend Attrition Tester indicated the correct trends for particle attrition; no data sets implied particles were increasing in diameter. No clear relationship with particle velocity prior to the receiver could be discerned with respect the measured particle attrition levels.

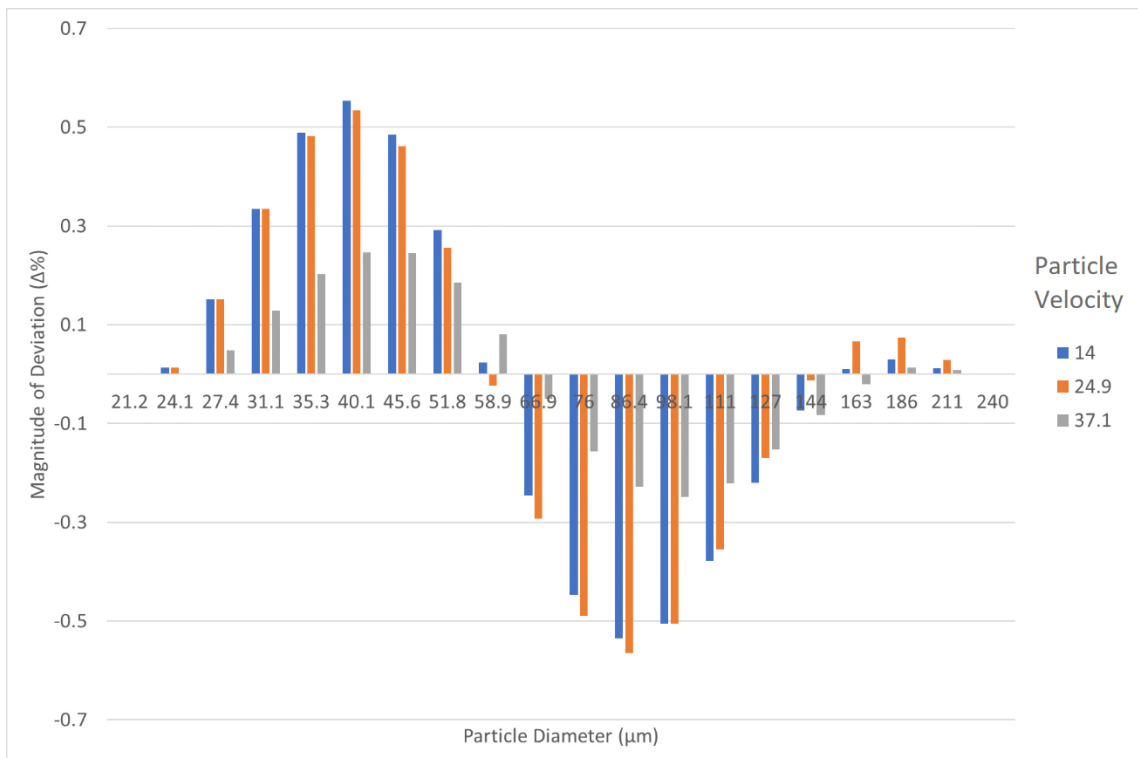


Figure 6-14: Particle attrition results for Spent FCC Catalyst Type T in the Single Bend Attrition Tester

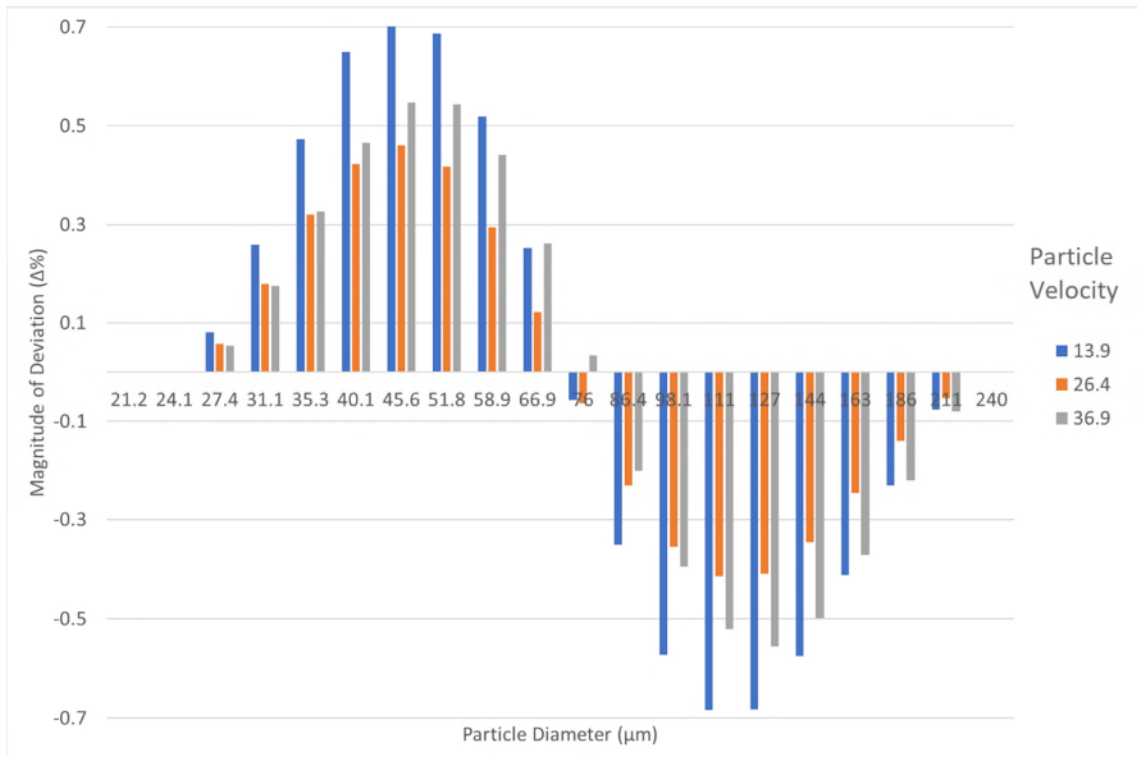


Figure 6-15: Particle attrition results for Spent FCC Catalyst Type C in the Single Bend Attrition Tester

It was evident from this study that the apparatus is most useful when studying particles that fail significantly after only a couple of impacts. The Spent FCC Catalyst did demonstrate some level of particle attrition; however, this was to a very small degree with unclear trends present in the data.

6.3 Conclusions

This chapter detailed the results and observations obtained from the Single Bend Attrition Tester. The geometrical and conveying conditions were systematically isolated and analysed with respect to their influence on the magnitude of particle attrition measured. Particle attrition was characterised through mass loss in a specific size fraction, and mass addition to a specific size fraction smaller than the virgin particles.

It was concluded that no clear, repeatable evidence could be found to support the existence of a 'shielding' effect (where particle attrition reduces with increasing particle concentration). To the contrary, multiple analyses indicated that the magnitude of measured particle attrition was largely unaffected by the particle concentration in the pipeline.

The slip velocity profile was measured for the Carbolux SK Type B and Type C materials, in addition to the Spent FCC Catalyst Type T and Type C. It was concluded that slip velocity reduces with reducing conveyed particle size. If the operator assumes that the slip velocity within a pneumatic conveying system is negligible, it was demonstrated that the magnitude of particle attrition predicted to occur in the pipeline will be grossly over-predicted.

CHAPTER 7: Results and Observations: Industrial Scale Pneumatic Conveying

This chapter shall present the results and observations obtained for industrial-scale pneumatic conveying systems. To avoid characterisation of a single pneumatic conveying pipeline geometry, two facilities were used for the industrial conveying experiments, and are described in detail in Section 4.4.3 and 4.4.4. The results and observations acquired from the test facility in the Wolfson Centre Testing Laboratory shall be presented first, followed by those acquired from the external test facility. The full set of results can be found in Appendix O.

7.1 Wolfson Centre Testing Facility

This section shall present the results obtained on the industrial-scale pneumatic conveying plant located in the Wolfson Centre Testing Laboratory (see Section 4.4.3 for description). In this programme of experimentation, three material types were tested: Carbolux SK Type B, Carbolux SK Type C, and Adipic Acid. The objective was to test a variety of conveying conditions, with respect to material type, particle size, superficial air velocity, and particle concentration as determined by the operator. Results are presented in terms of magnitude of deviation (see Section 5.1 for definition).

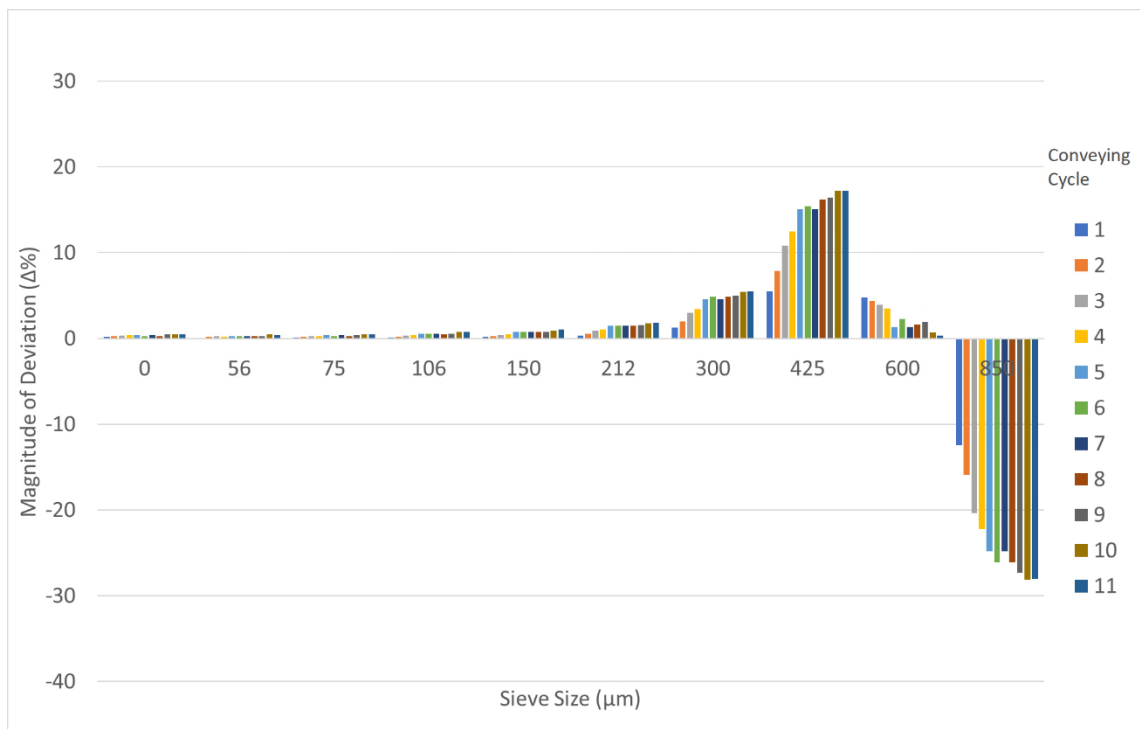
While the study of particle fatigue was not within the core scope of the work, the fatigue data was collected (under similar conveying conditions) due to the availability of a statistical sampler, and is intended to inform future studies. The full list of conveying conditions for each experiment are available in Appendix G).

7.1.1 Conveying of Carbolux SK Type C

The conveying conditions tested with the first cycle of each batch of Carbolux SK Type C are summarised in Table 7-1. Following this, the attrition results are presented in Figure 7-1a to Figure 7-1c for Batches A to C respectively.

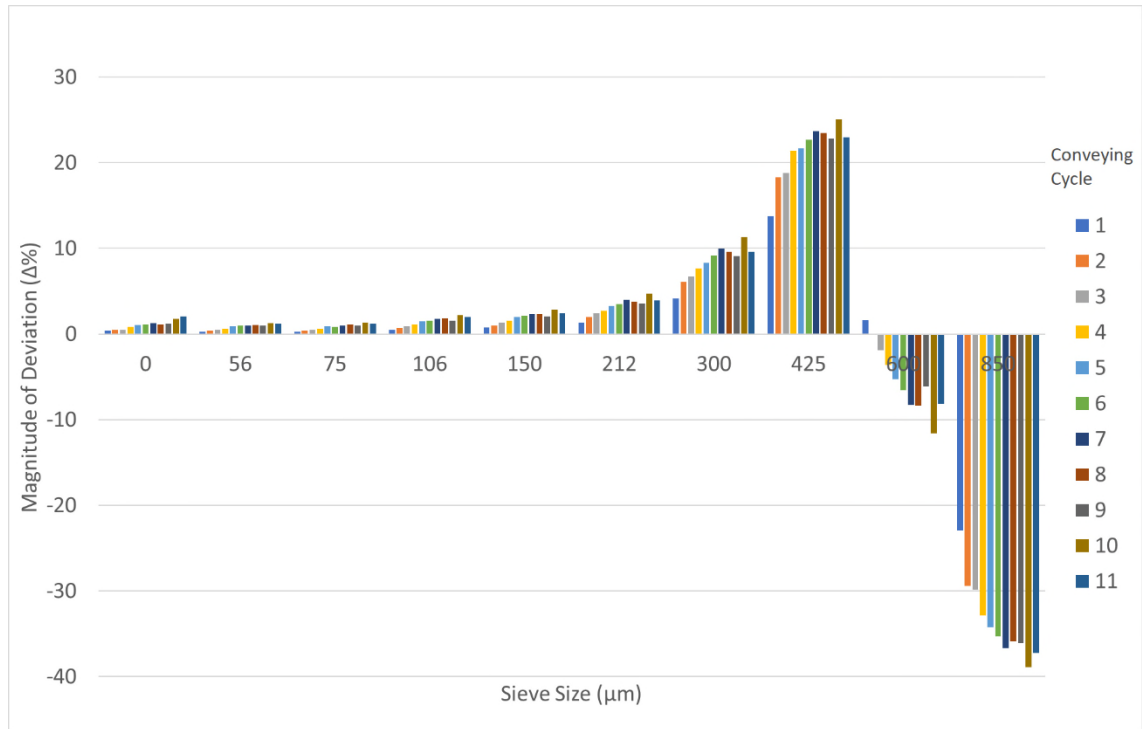
Table 7-1: Conveying conditions for Carbolux SK Type C in the Existing Industrial-Scale Pneumatic Conveying Plant for the first conveying cycle of each batch

Batch ID	Cycle Number	Averaged Superficial Air Velocity in Pipeline (m/s)		Solids Loading Ratio (kg/kg)
		Start	End	
A	1	24.70	28.0	0.44
B	1	29.90	36.7	0.80
C	1	23.03	30.5	4.28

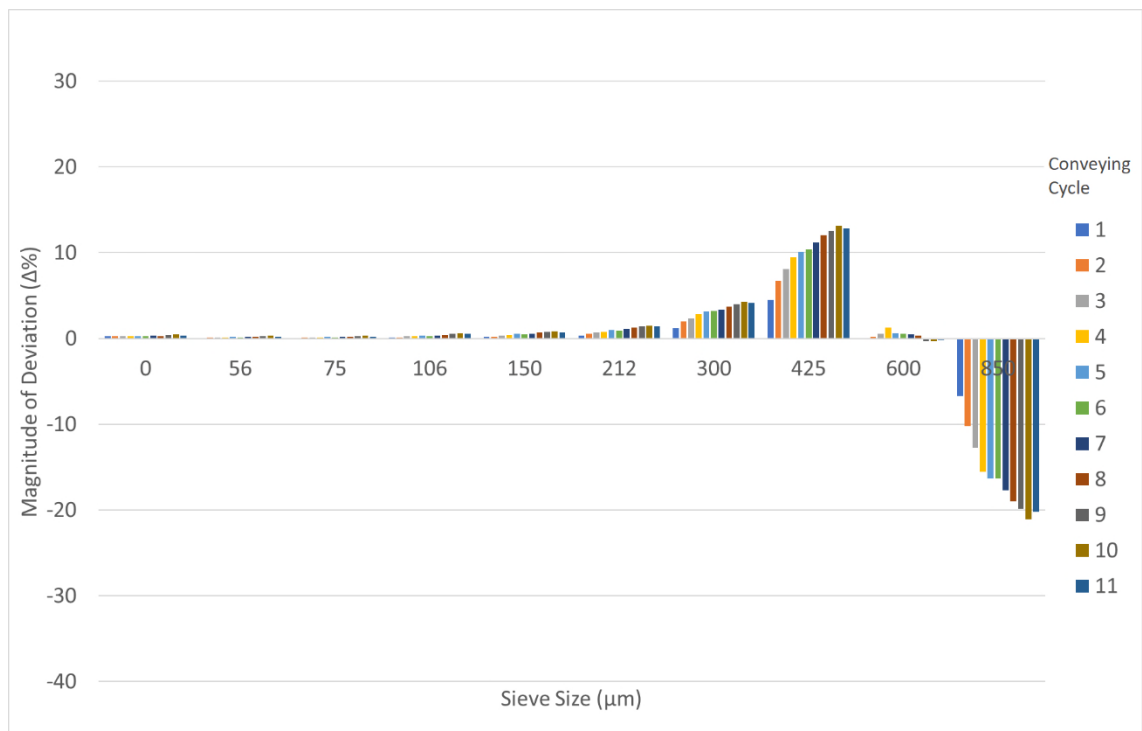


(a)

Figure 7-1: Particle size analysis results for each conveying cycle of Carbolux SK Type C for batches (a) A, (b) B, (c) C



(b)



(c)

Figure 7 1: Particle size analysis results for each conveying cycle of Carbolux SK Type C for batches (a) A, (b), B, (c) C

Across all conveyed batches, it was evident that the magnitude of particle attrition observed increased with increasing conveying cycles. Figure 7-2 arranges the batch in order of increasing superficial air velocity at the pipeline inlet (refer to Table 7-1: Conveying conditions for Carbolux SK Type C in the Existing Industrial-Scale Pneumatic Conveying Plant for the first conveying cycle of each batch). It was evident that for this material, inlet superficial air velocity has a clear influence on the magnitude of particle attrition measured.

Batch A and Batch C were conveyed at similar superficial air velocities, with a difference in solids loading ratio of approximately 4. Figure 7-2 indicates that after the first conveying cycle, Batch A has suffered nearly 100% more damage than Batch C. This difference in particle attrition is not as large as that observed for the influence of superficial air velocity (Batch A compared to Batch B).

To avoid attributing the above observation to a single conveying run, Figure 7-3 shows the full set of results for each of the conveying cycles, for the magnitude of deviation of the mass retained on the 850 μm sieve. The results of this analysis confirm the conclusions drawn from Figure 7-2. Whereby an increase in solids loading ratio (and hence particle concentration) in the pipeline, results in a reduced magnitude of particle attrition measured after conveying.

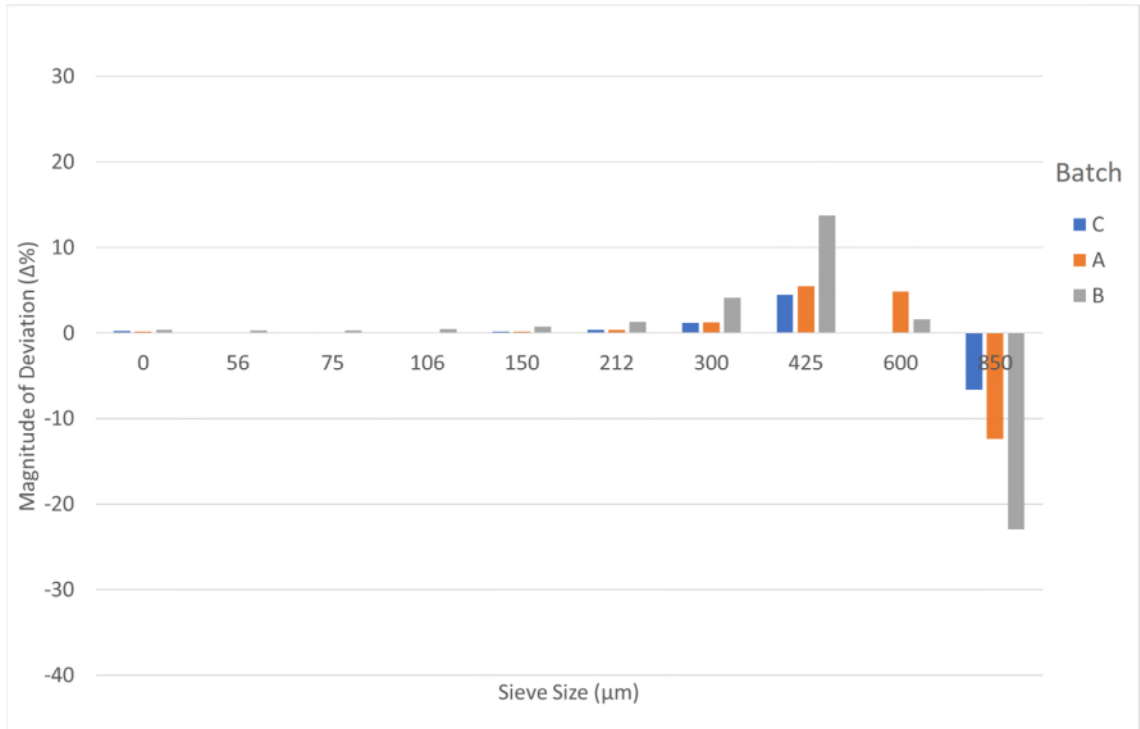


Figure 7-2: The particle attrition results of the first conveying cycle of each batch of Carbolux SK Type C

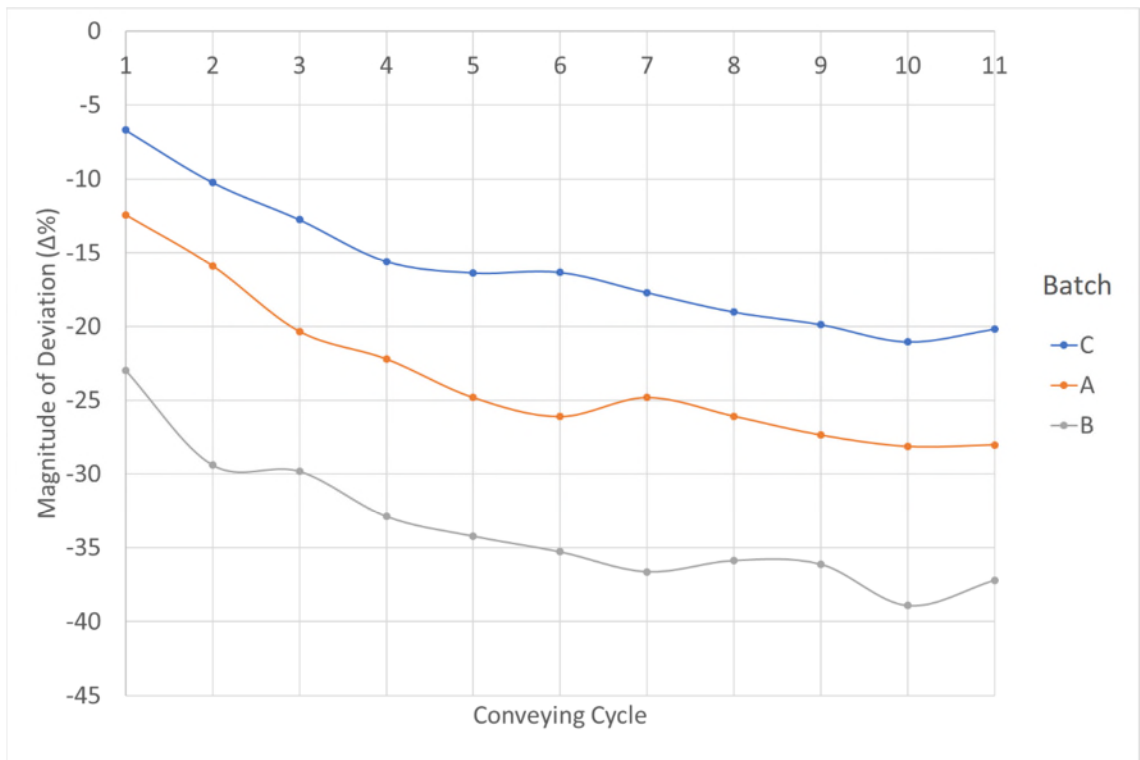


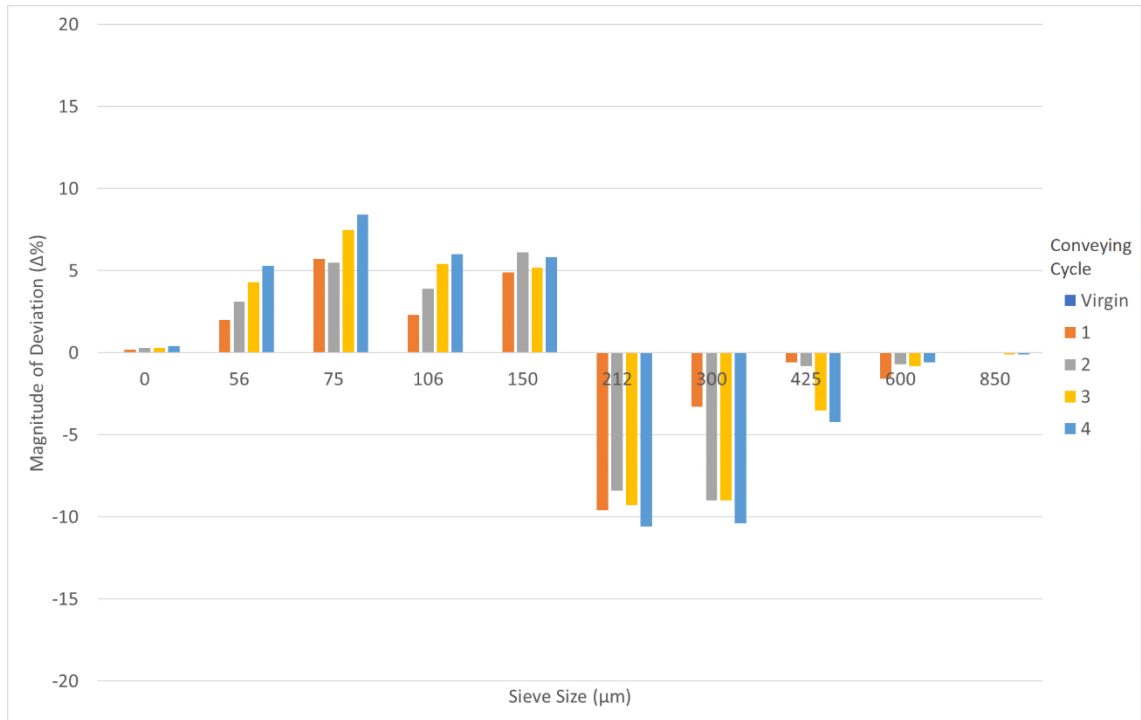
Figure 7-3: The magnitude of deviation measured for the mass retained on the 850 μm sieve across all conveying runs

7.1.2 Conveying of Adipic Acid

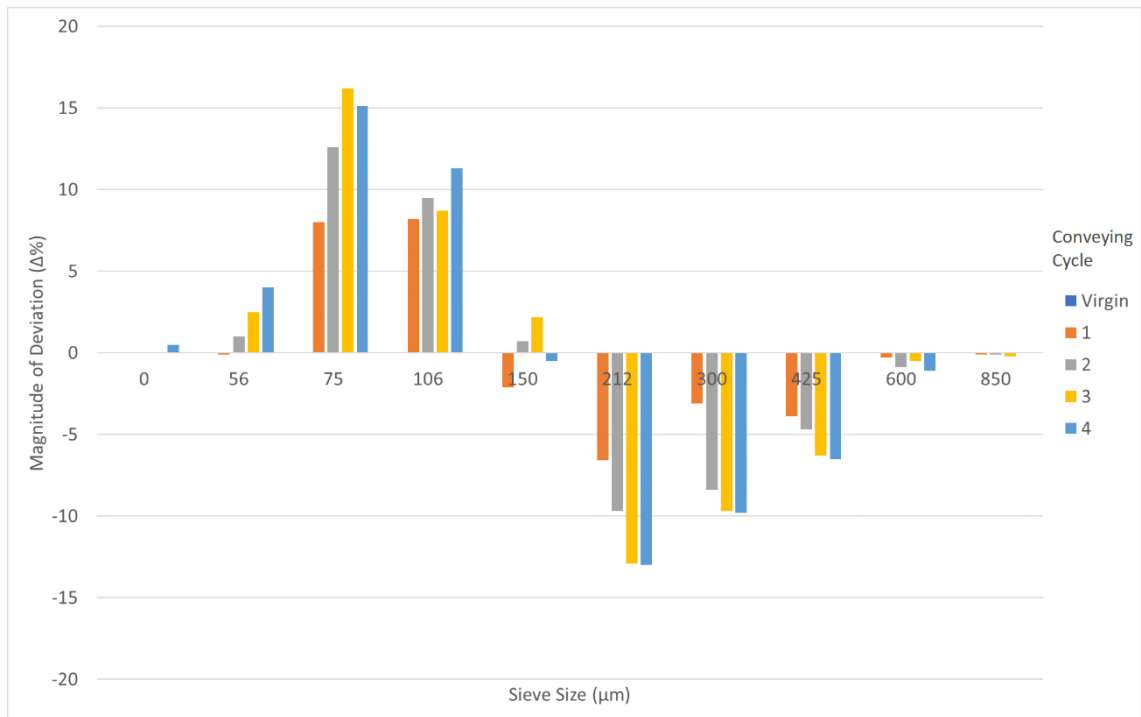
The conveying conditions tested with the first cycle of each batch of Adipic Acid are summarised in Table 7-2. Following this, the attrition results are presented in Figure 7-4a to Figure 7-4e for Batches B to F respectively.

Table 7-2: Conveying conditions for Adipic Acid in the Existing Industrial-Scale Pneumatic Conveying Plant for the first conveying cycle of each batch

Batch ID	Cycle Number	Averaged Superficial Air Velocity in Pipeline (m/s)		Solids Loading Ratio (kg/kg)
		Start	End	
B	1	16.74	28.0	5.22
C	1	20.04	36.9	3.26
D	1	22.99	34.1	2.25
E	1	18.55	38.1	5.78
F	1	19.45	25.7	0.64



(a)

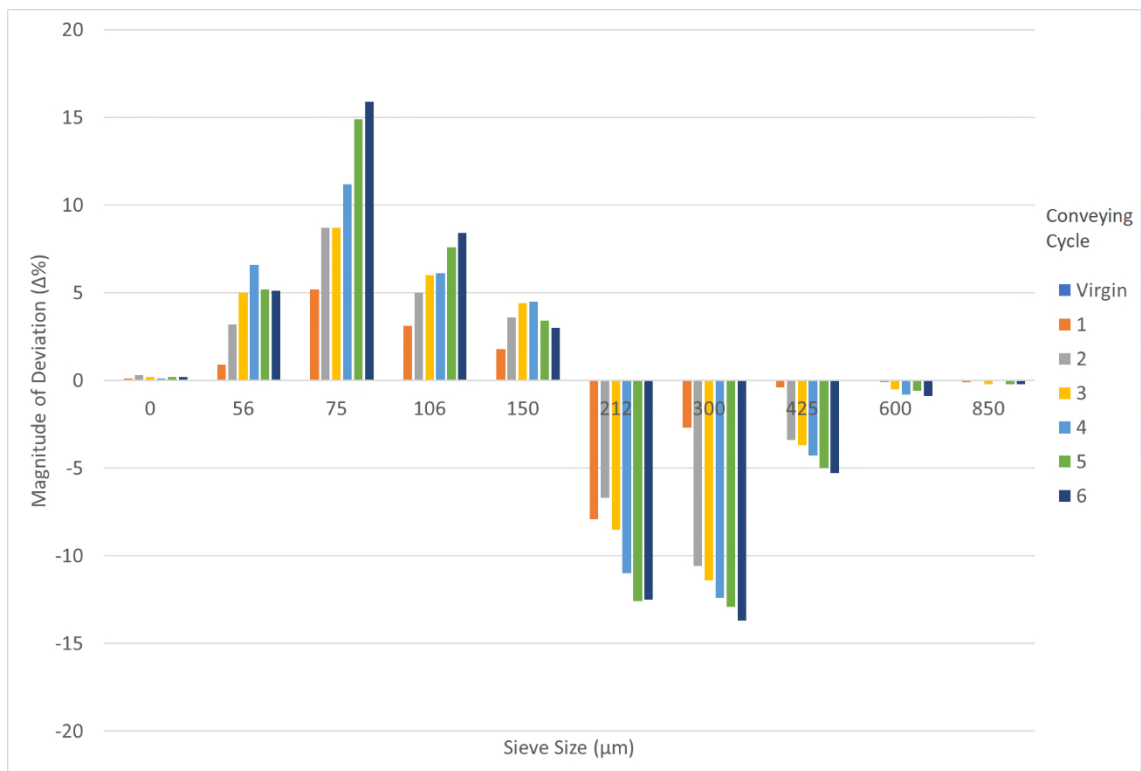


(b)

Figure 7-4: Particle size analysis results for each conveying cycle of Adipic Acid for batches (a) B, (b) C, (c) D, (d) E, and (e) F

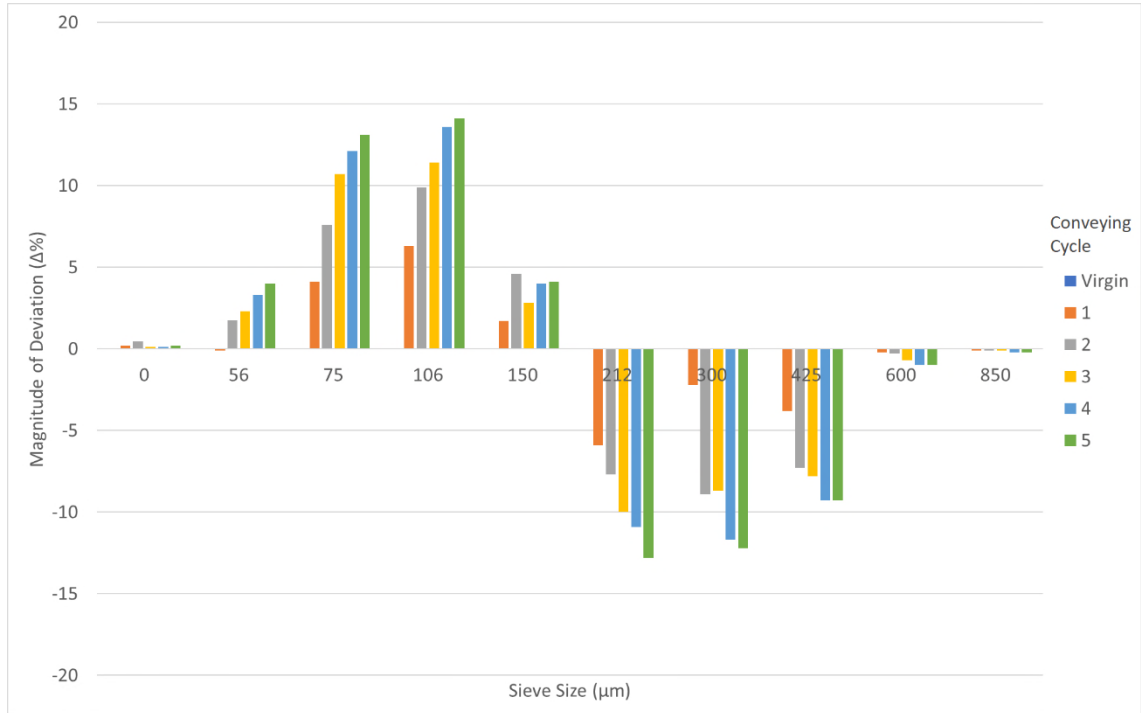


(c)



(d)

Figure 7 4: Particle size analysis results for each conveying cycle of Adipic Acid for batches (a) B, (b), C, (c) D, (d) E, and (e) F



(e)

Figure 7 4: Particle size analysis results for each conveying cycle of Adipic Acid for batches (a) B, (b), C, (c) D, (d) E, and (e) F

It is evident that the general effect of increasing the number of cycles (number of impact events) increased the measured amount of particle attrition. This is in agreement with the literature (Section 2.4.4.4). However, to examine the influence of superficial air velocity at the inlet to the conveying line, Figure 7-5 presents the results for the first cycle of each batch. These results have been re-arranged to show increase in velocity, where Batch B represents the lowest superficial air velocity condition, and Batch D represents the highest (refer to Table 7-2).

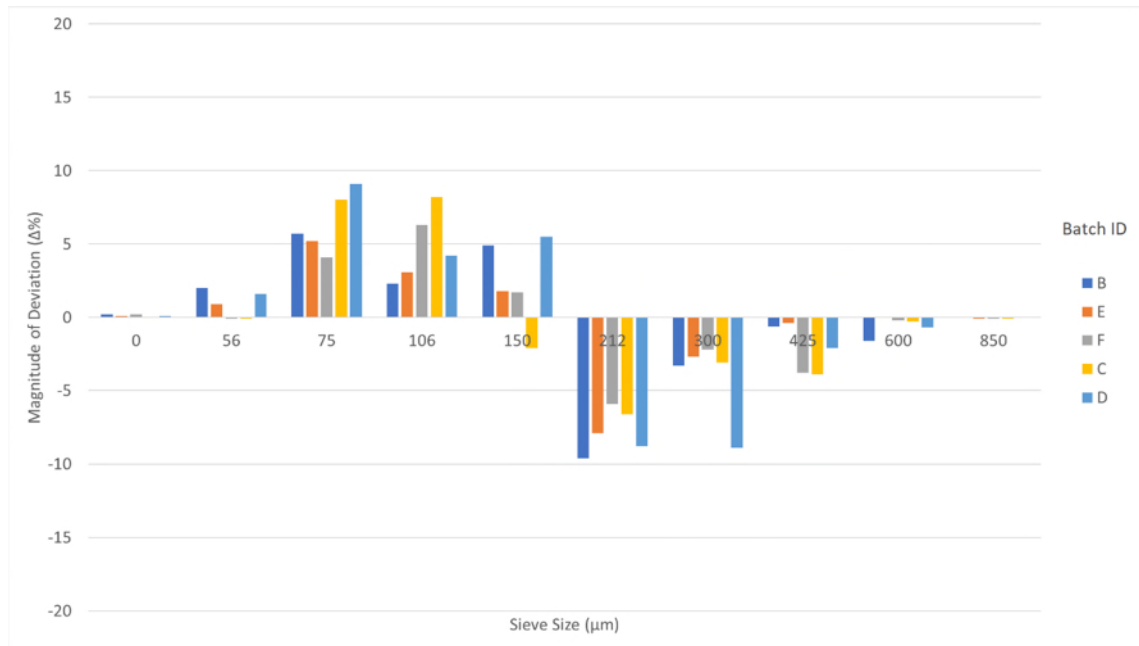


Figure 7-5: The particle attrition results of the first conveying cycle of each batch of Adipic Acid

Upon inspection of these results, it was evident that superficial air velocity at the pipeline inlet did not dictate the magnitude of particle breakage as strongly as was the particle velocity did in Chapter 5 and Chapter 6. However, as Adipic Acid did not form a part of the characterisation studies, this could be a material-dependent behaviour.

To determine the influence of solids loading ratio (and therefore, particle concentration) on the magnitude of particle attrition measured, Batch B shall be compared to Batch F for the material retained on the 425 μm sieve as they were conveyed with similar superficial air velocities, and a difference of approximately 4.6 between their solids loading ratios. This sieve was selected, as it was the largest size fraction that contained a significant amount (approximately 9%), and therefore child particles from breakage events involving particles from larger size fractions would not significantly influence the analysis.

By analysing the results in Figure 7-5, it can be seen that the low solids loading scenario, Batch F, suffers far more particle attrition than Batch B. The results for the 425 μm sieve was graphed across each of the conveying cycles to form Figure 7-6, and the same relationship between the batches remained. It was therefore reasonable to state for the adipic acid, that an increase in solids loading ratio (and hence particle concentration) correlated with a decrease in the magnitude of particle attrition measured.

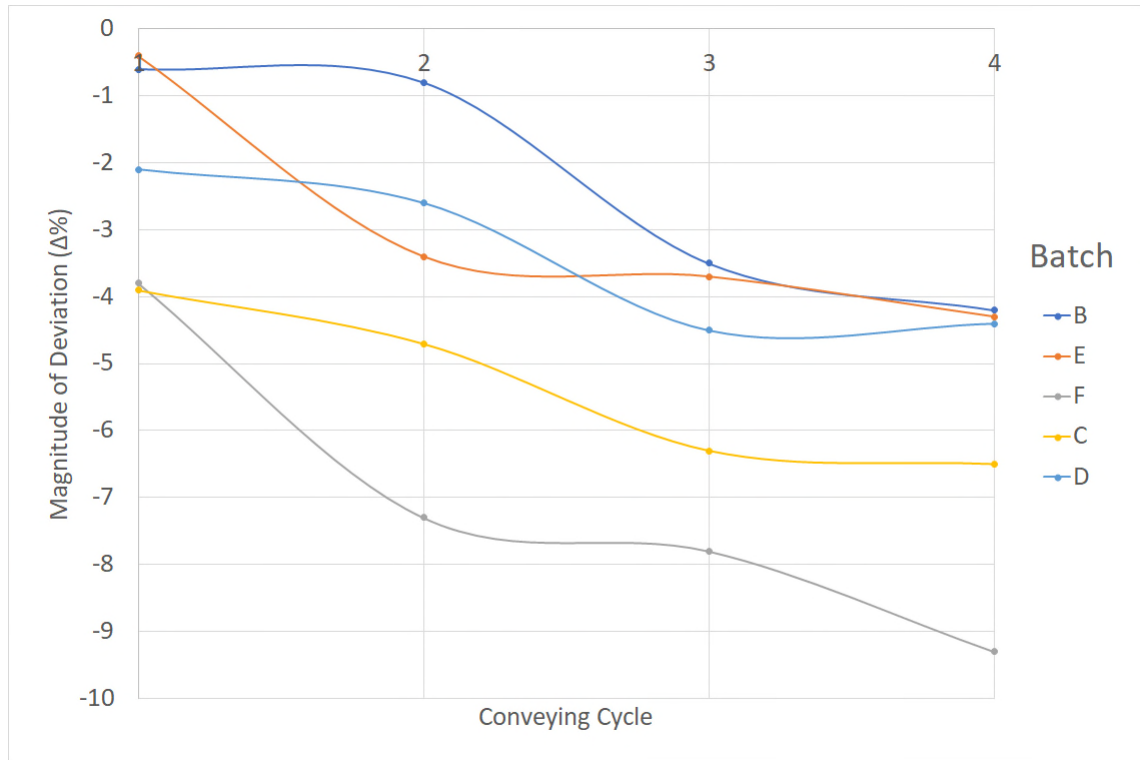
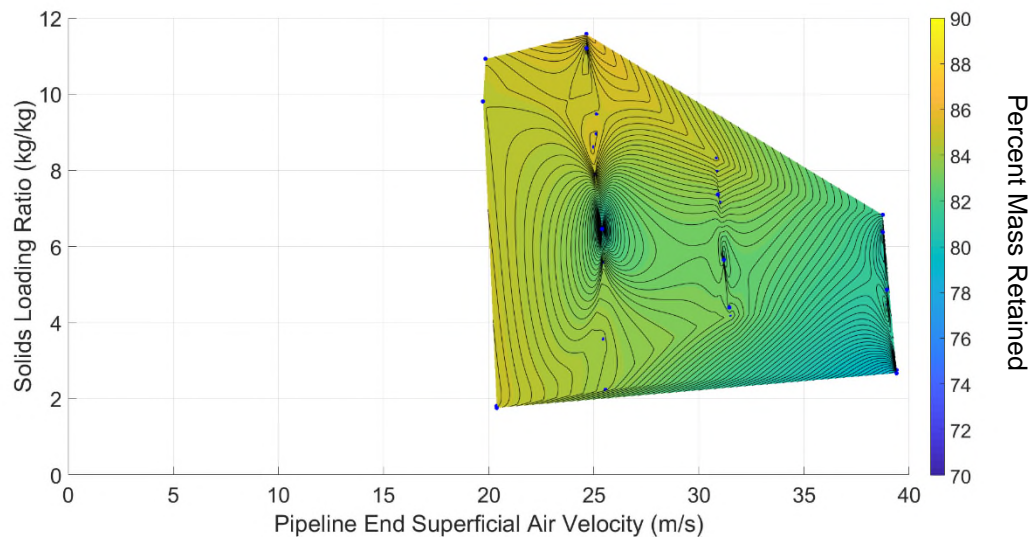


Figure 7-6: The magnitude of deviation measured for the mass retained on the 425 μm sieve across all conveying runs

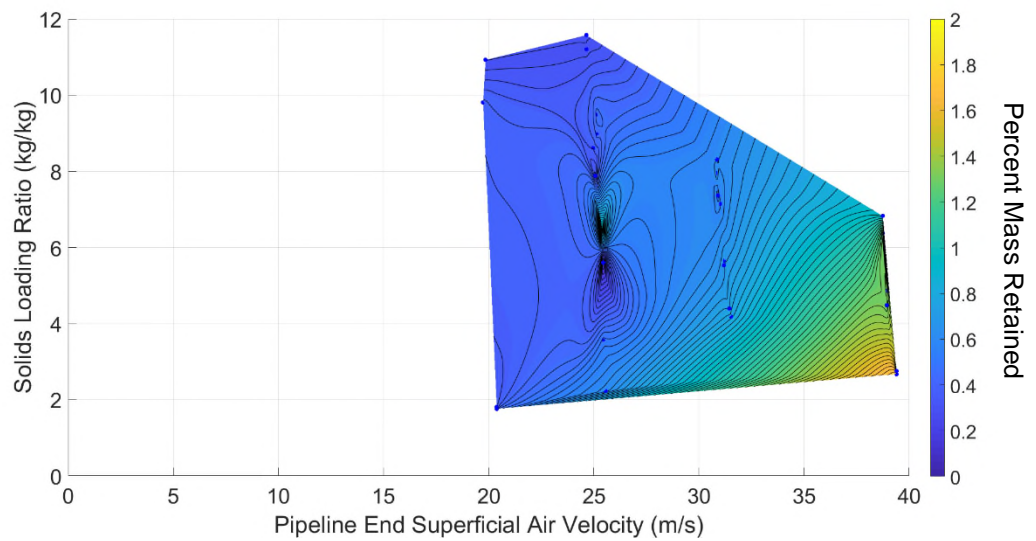
7.2 External Industrial-Scale Pneumatic Testing Facility

The results obtained from the external pneumatic conveying facility are presented in Figure 7-7 and Figure 7-8 in the form of breakage maps. All of the results obtained from this apparatus are for Carbolux Type C.

Figure 7-7 presents the data in terms of the percent of the tested sample material remaining on a specified sieve, and Figure 7-8 presents the data in terms of magnitude of deviation from the virgin particle size distribution. Note that the virgin particle size distribution was not obtained from each individual bag of virgin material, and therefore the averaged values of virgin particle size distribution obtained for the experimentation in Section 6.2 were used.

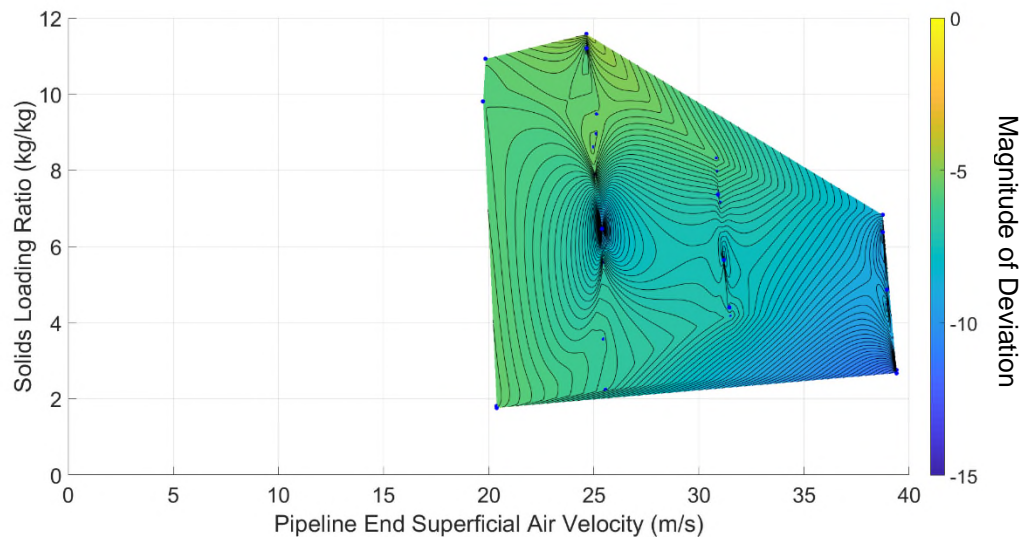


(a)

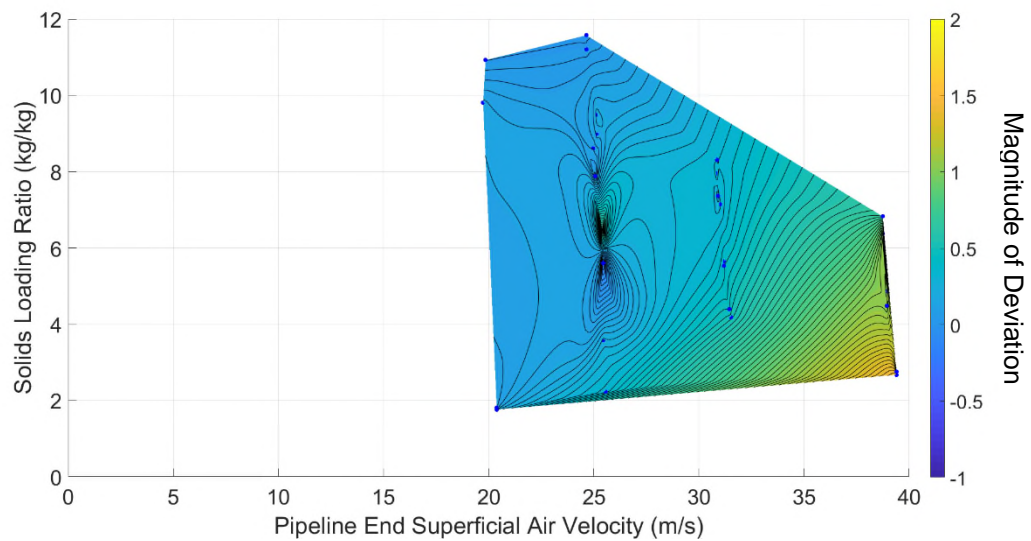


(b)

Figure 7-7: Percent mass retained on the (a) 700 μm , and (b) 355 μm sieve for Carbolux SK Type C across all testing conditions



(a)



(b)

Figure 7-8: Magnitude of deviation on the (a) 700 μm , and (b) 355 μm sieve for Carbolux SK Type C across all testing conditions

It was seen that a significant portion of the test region suggested reduced particle damage with increased solids loading ratio (indicated by contour lines with positive gradient values), across all forms of analysis. It should be noted that the sample was not pre-sieved prior to the testing to remove any large 'boulders' (particles greater than 2800 μm in diameter). Further analysis of these results shall be undertaken in Chapter 8.

7.3 Conclusions

Two different particle material types have been conveyed within two different industrial-scale lean phase pneumatic conveying systems. Particle attrition was measured on a mass loss basis (particles breaking and leaving a particular size fraction) and a mass gain basis (broken particles entering a smaller sieve size). It was determined that in all cases considered, that increasing the solids loading ratio used in the conveying system (and hence particle concentration) did correlate to a reduction in the magnitude of particle attrition measured. This finding contradicts the conclusions obtained from the Single Bend Attrition Tester (presented in Section 6.3), and shall be discussed further in Section 8.2.2.

CHAPTER 8: The Influence of Particle Concentration on Particle Attrition in Lean Phase Pneumatic Conveying Systems

This chapter shall discuss the results presented in Chapter 5 and Chapter 6 with respect to the influence of particle concentration on the magnitude of particle attrition measured under a range of impact conditions.

Firstly, the impact conditions shall be compared between the Bench Scale Particle Attrition Tester and the Single Bend Attrition Tester in terms of the range of particle mass flux that was achieved. Following this, commentary on the qualitative influence of particle concentration with each apparatus shall be given, and conclusions made in the context of the particle mass flux results.

To account for the results obtained within the Wolfson Centre Industrial-Scale Pneumatic Conveying System, the influence of conveying pipe diameter (Section 8.2.1.1) and particle morphology and size (Section 8.2.1.2) on the particle velocity distribution across the pipe cross-section shall be discussed with respect to the results published by other researchers. Similarly, the results obtained from the External Industrial-Scale Pneumatic Conveying System shall be discussed (Section 8.2.2) in terms of particle acceleration profile. Hypotheses are proposed on how the aforementioned conveying variables respond to changes in the particle concentration of the two-phase flow.

Finally, the conclusions shall summarise the key findings from this chapter.

8.1 Analysis of the Data collected from the BSPAT and the SBAT

It was evident in Chapter 5 and Chapter 6 that the influence of particle concentration within the BSPAT and SBAT respectively, was without a clear trend. In some cases, this influence was shown to be clearly negligible (see Figure 6-7a). To provide a clear definition of the particle-wall impact conditions across the full range of experiments conducted with Carbolux SK, Table 8-2 gives the particle mass flux ($\text{kg}/\text{m}^2/\text{s}$) at the impact surface. The values for the BSPAT were calculated according to Equation (8-1) from Deng et al. [213].

$$M_{flux} = \frac{M_f}{4\pi X_c [X_d \tan(\theta_d/2) + R_t]} \quad (8-1)$$

Where:

M_f	Mass feed rate of particles into test apparatus (kg/s)
M_{flux}	Mass flux of particles at target face (kg/m ² /s)
X_c	Distance from the accelerating disc centre to the centre of the target (m)
X_d	Flight distance of particles (m)
R_t	Radius of accelerating tube (m)
θ_d	Particle jet dispersion angle (degrees)

The dispersion half angle of the particle stream ($\theta_d/2$) was assumed to be 4 degrees based on the findings for Deng et al. [213] for glass beads.

For the SBAT apparatus, the surface area for primary particle impacts was considered to be the straight-line projection of the pipe cross-section into the bend. This assumes that particles are fully decoupled from the airstream upon entry to the bend, and hence travel in a straight line until impact. It is also assumed that the entire primary impact area is subjected to an equal value of particle mass flux, and therefore the value obtained was a numerical mean across the entire impact area.

The primary impact area was calculated through the use of 3D CAD modelling software, the results of which are given in Table 8-1. The particle mass flux was calculated using Equation (8-2).

Table 8-1: Projected impact areas for each bend type in the SBAT

Bend Type	Projected Impact Area (m ²)
Short Radius	0.0060526
Long Radius	0.0108685

$$M_{flux} = \frac{M_f}{A_p} \quad (8-2)$$

Where:

A_p Projected impact area of particle stream (m²)

Table 8-2: Particle mass flux (kg/m²/s) at the impact surface for various Carbolux SK types for the BSPAT and SBAT

Material	BSPAT	SBAT	
		Short Radius Bend	Long radius Bend
Carbolux SK Type B		2.734 - 108.327	1.521 - 60.298
Carbolux SK Type C		2.178 - 99.956	1.206 - 55.720
Carbolux SK 250-355	0.300		
Carbolux SK 355-500	0.265		
Carbolux SK 500-710	0.302		
Carbolux SK 710-1000	0.290		

It was evident from Table 8-2, that to equate the two apparatuses, the value of particle mass flux in the BSPAT would have to quadruple to achieve the lowest values obtained in the SBAT.

When the magnitude of particle attrition is compared between the two apparatuses, it was clear that from a qualitative perspective, the BSPAT inflicts comparable (or greater) particle attrition to the overall configuration of the SBAT (more detail in Chapter 9) at an impact angle of 20 degrees. This observation validates the BSPAT design decision made, where 20 degree impacts could be considered as representative of the impact conditions

occurring within a pneumatic conveying bend. One could suggest that this is due to the differences in particle mass flux at the target surface, however, when the results of the SBAT are examined across the full range of test conditions key conclusions can be drawn; the range of particle mass flux considered in the SBAT was many orders of magnitude greater than the discrepancy between the two apparatuses. It is therefore reasonable to assume that the difference in particle mass flux between the two apparatuses (considering the SBAT at the lowest particle mass flux condition) was negligible.

To now consider the SBAT data in isolation. As indicated in Section 6.2, most of the data maps provided no clear trend that supported the concept of particle ‘shielding’; none except Figure 6-7c, where contour lines of constant particle breakage displayed a positive gradient (noting that vertical contour lines indicated no influence of particle concentration on the magnitude of particle attrition measured). To the contrary, a clear example of where there is no influence of particle concentration on the magnitude of measured particle attrition was shown in Figure 6-7a and Figure 6-7b. It was therefore concluded, that the influence of particle concentration was negligible in the generation of particle attrition in homogeneous lean phase pneumatic conveying systems within the scope of this research.

8.2 Proposed Thought-Model of the Observed ‘Shielding Effect’

It was evident that the results presented in Chapter 7 indicated that as particle concentration was increased in the respective pipelines of the Industrial Scale Pneumatic Conveying Systems, particle attrition was (in some cases) reduced. This section shall propose explanations for these observations which conflict with the results obtained from the SBAT.

8.2.1 Geometrical Considerations of the Wolfson Centre Industrial Pneumatic Conveyor

A key difference between the pipe geometry of the SBAT and the Industrial Pneumatic Conveying System in the Wolfson Centre Laboratory, is that of pipe diameter. Figure 8-1 was captured during a conveying test on the system in a normal running case for a high

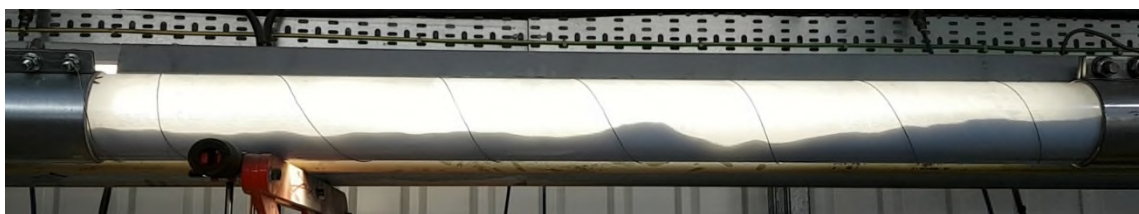
superficial air velocity; the event of a plug of material (due to an error in operation; particle attrition results from this test were discounted), the condition immediately after the plug had passed, the condition 10 seconds after the plug had passed, and the normal running conditions after the plug in a low superficial air velocity condition. It shows a distinct strand of material present on the floor of the pipeline. Periodically, this strand would be swept along the pipeline by a large accumulation of solids, and was therefore in an unsteady state. Under the majority of test conditions, the strand was mobile. There exists a sharp contrast between the homogeneous flow observed in the SBAT (Figure 6-4) and the flow observed in the Industrial Scale Pneumatic Conveying System.



(a)



(b)



(c)

Figure 8-1: Images of the sight glass in the Wolfson Centre Industrial Scale Pneumatic Conveying System, conveying Adipic Acid; for a high superficial air velocity (a) normal running case; and for a low superficial air velocity (b) plug of material, (c) immediately after the plug had passed, (d) 10 seconds after the plug had passed, and (e) the normal running condition.



(d)



(e)

Figure 8 1: Images of the sight glass in the Wolfson Centre Industrial Scale Pneumatic Conveying System, conveying Adipic Acid; for a high superficial air velocity (a) normal running case; and for a low superficial air velocity (b) plug of material, (c) immediately after the plug had passed, (d) 10 seconds after the plug had passed, and (e) the normal running condition.

Considering that the sight glass in this system was located at the midpoint between the preceding and successive bend, and that the length of the entire straight section was 27 m, some key conclusions can be inferred:

- Homogeneous lean phase pneumatic conveying was not achieved.
- The solids phase has had sufficient straight pipeline length to fully accelerate to steady-state flow (approximately 13.5 m)
- Therefore, the flow regime observed in the sight glass can be assumed to be representative of the flow condition prior to the ultimate bend in the system.
- Considering that the sight glass is positioned on the ultimate straight section of the system, the superficial air velocity is greater in this section compared to all other straight sections in the system. Therefore, if the homogeneous lean phase regime was achieved anywhere in the system, it should have been observed in the sight glass.
- It is therefore reasonable to conclude that the homogenous lean phase regime was not achieved (in a steady-state form) at any point throughout the system.

- Particles residing in the strand have a velocity much smaller than that of the gas phase, resulting in a very large slip velocity.

These conclusions have key impacts on the state of the two-phase flow at the entry point of a conveying bend. In the results obtained from the Wolfson Centre Industrial-Scale Pneumatic Conveying System, it was evident that the range of particle velocities across the pipe cross section was much larger than that observed in the SBAT. As was determined in the BSPAT, the particle velocity is significant in the determination of the magnitude of particle attrition manifested. Therefore, as the particle velocity distribution is reduced at the bend entry point, it follows that a reduced magnitude of particle attrition should result from the subsequent particle-wall impacts (for a set bend geometry).

Now, to inspect how the variation of particle concentration in the pipeline alters these flow dynamics. As was demonstrated by the work of McKee et al. [58] (Figure 8-2) and discussed in Section 2.3.2.3, as particle concentration is increased for any given pipe diameter (assuming constant superficial air velocity), the cross-sectional area of the subsequently formed particle strand is increased. The repercussion of this is that the particle velocity distribution of the conveyed material is skewed towards the lower velocities (see Section 8.2.1.1). This in turn, translates to lower average particle velocities upon entry to a pipe bend, and therefore lower particle attrition levels.

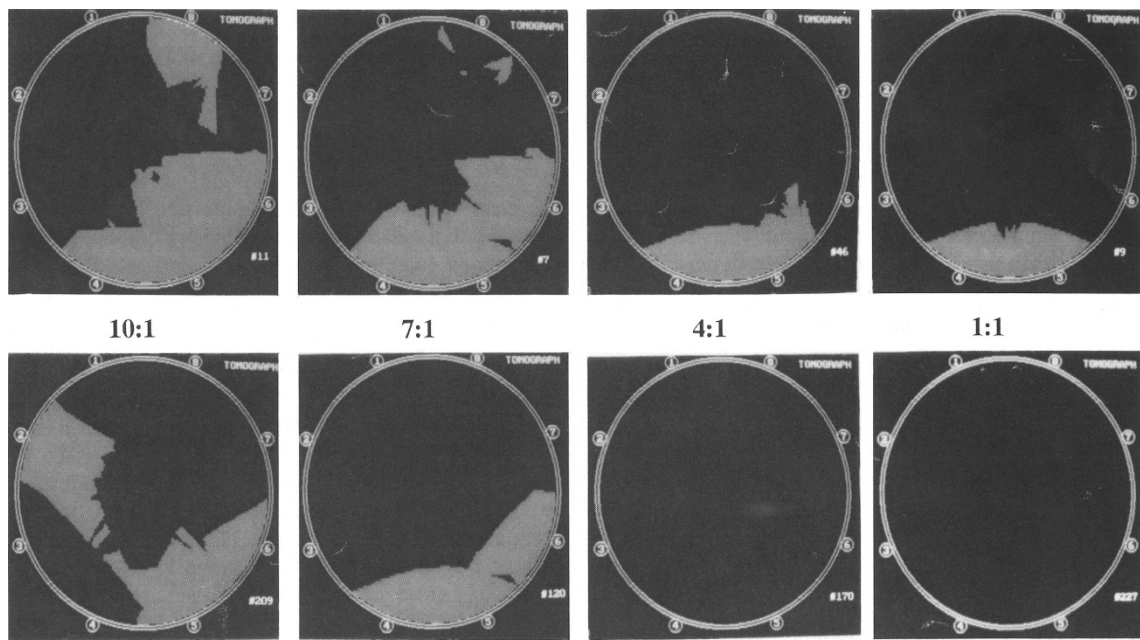


Figure 8-2: From the work of Mckee et al. [58] showing capacitance tomography images of the pneumatic conveying of sea salt at various solids loading ratios at a superficial air velocity of 28 m/s.

Deshmukh et al. [214] studied the particle velocity distribution of spherical glass particles through a rectangular channel. Their results are presented in Figure 8-3 for 465 μm mean diameter particles, and Figure 8-4 for 166 μm mean diameter particles. It is demonstrated in these figures that with increasing particle concentration (solids loading), that the mean particle velocity is reduced, and that skewedness of the cross-sectional particle velocity distribution is increasingly exaggerated. These effects are more prominent in the larger of the two particle sizes.

For the conditions under which this experimentation was conducted, the results cannot be directly applied to the present research due to the large difference in scale and range of operating conditions (the conveying channel was only 10 mm high and 40 mm wide, and mean particle velocities less than 6 m/s were tested). However, it is hypothesised that these findings apply, in principle, to the present research, and when considered in conjunction with the conclusions of Section 8.2.1.1 and 8.2.1.2, could account for the differences in pre-bend particle velocities that cause reduced magnitude of particle attrition with increase in particle concentration. It is necessary that further experimentation be conducted to verify this hypothesis.

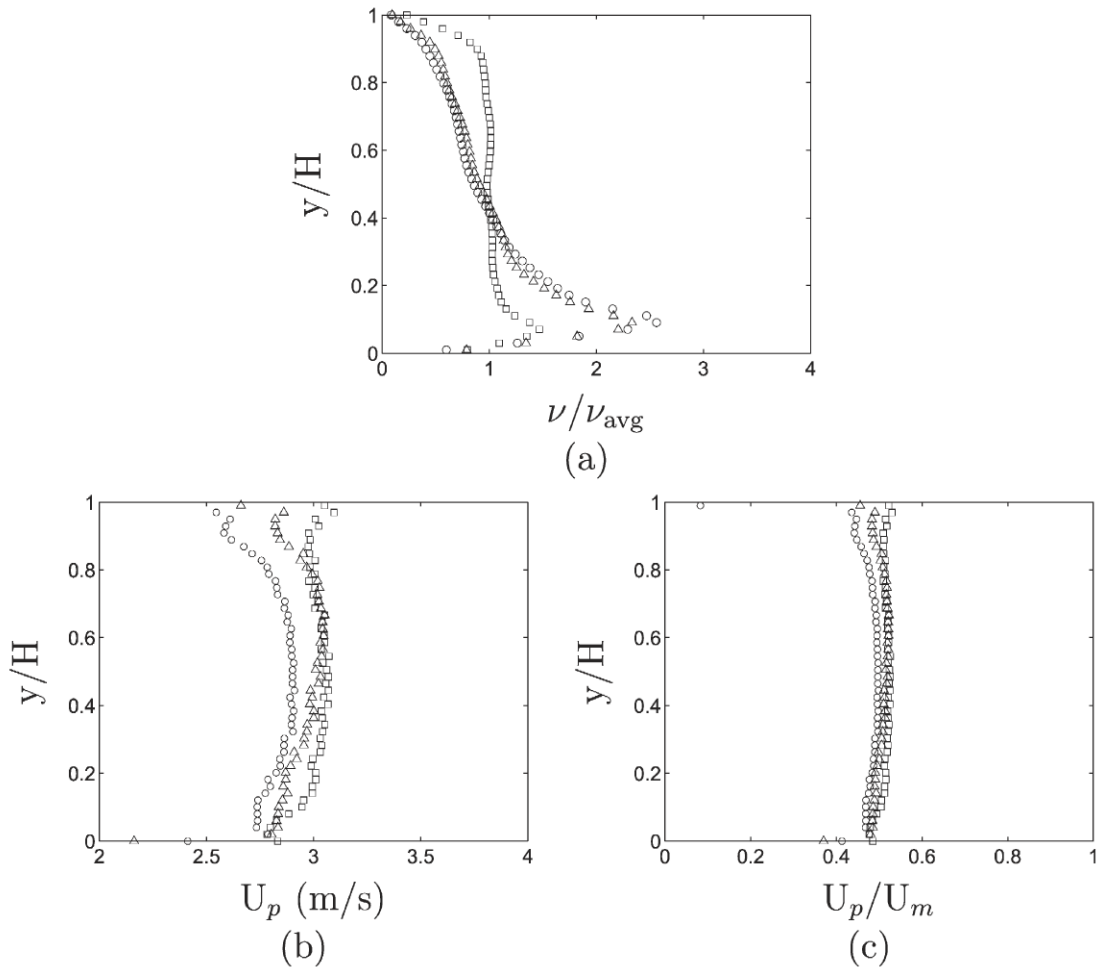


Figure 8-3: Data reported by Deshmukh et al [214], describing profiles for glass spheres of mean diameter $465 \mu\text{m}$ for (a) normalised volume fraction (ν/ν_{avg}), (b) mean solid velocity (U_p), and (c) normalised particle velocity (U_p/U_m), along the normalised channel height (y/H). Superficial gas velocity, $U_m = 5.84 \text{ m/s}$; mass loading ratios: 0.36 (squares), 1.0 (triangles), and 1.61 (circles)

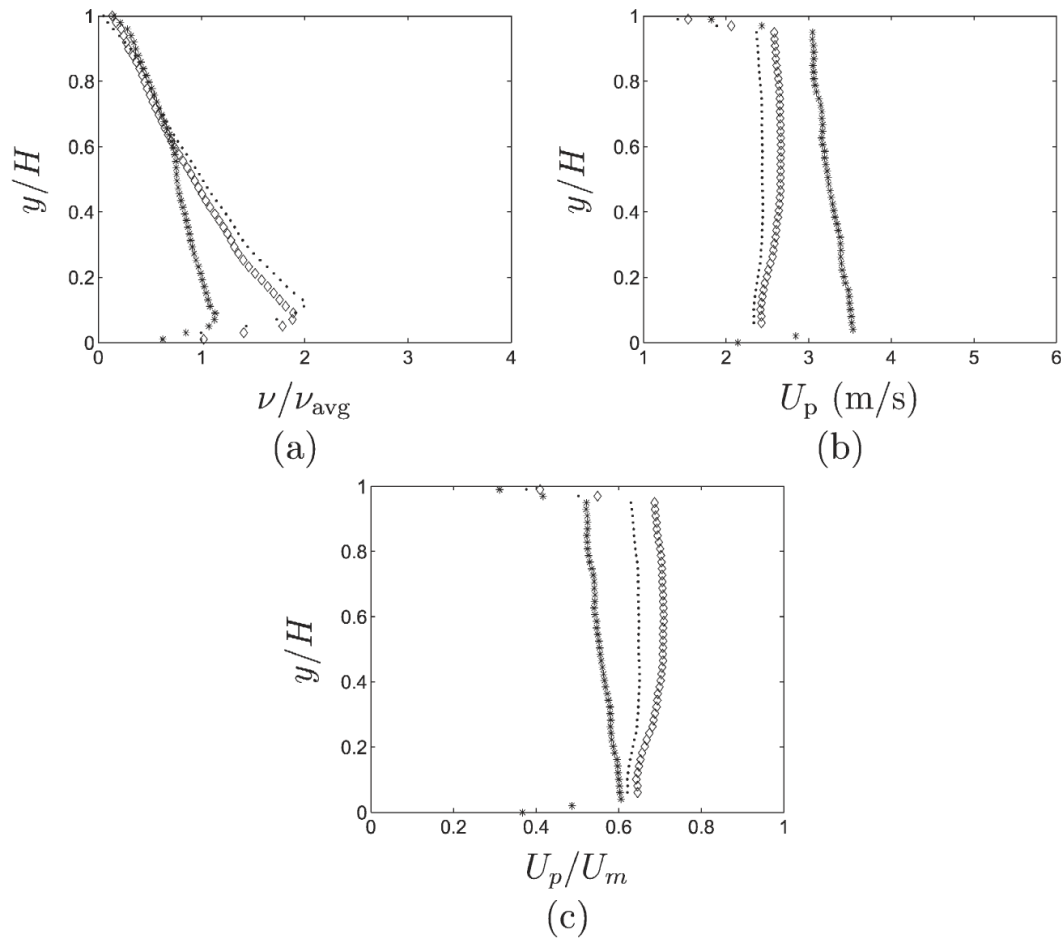


Figure 8-4: Data reported by Deshmukh et al [214], describing profiles for glass spheres of mean diameter $166 \mu\text{m}$ for (a) normalised volume fraction (ν/ν_{avg}), (b) mean solid velocity (U_p), and (c) normalised particle velocity (U_p/U_m), along the normalised channel height (y/H). Conditions: Superficial gas velocity, $U_m = 3.76 \text{ m/s}$, mass loading ratio $m = 1$ (diamonds); $U_m = 3.76 \text{ m/s}$, $m = 2.2$ (dots); and $U_m = 5.84$, $m = 1$ (stars).

8.2.1.1 Accounting for the Influence of Pipe Diameter

A key difference between the SBAT and the Wolfson Centre Industrial Scale Pneumatic Conveying System is that of pipe diameter. To understand how this influences the particle velocity profile across the pipe cross-section, the air-only condition shall be considered first.

The Reynolds numbers (Equation (8-3)) for internal flow in a circular pipe [215]) for a range of common pneumatic conveying systems is summarised in Figure 8-5.

$$Re = \frac{\rho V_{avg} D}{\mu} \quad (8-3)$$

Where:

Re Reynolds number of the fluid in the pipe (dimensionless)

ρ Density of the fluid (kg/m^3)

V_{avg} Average velocity of the fluid in the pipe (m/s)

D Diameter of the pipe (hydraulic diameter for non-circular pipes) (m)

μ Viscosity of the fluid (Pa·s)

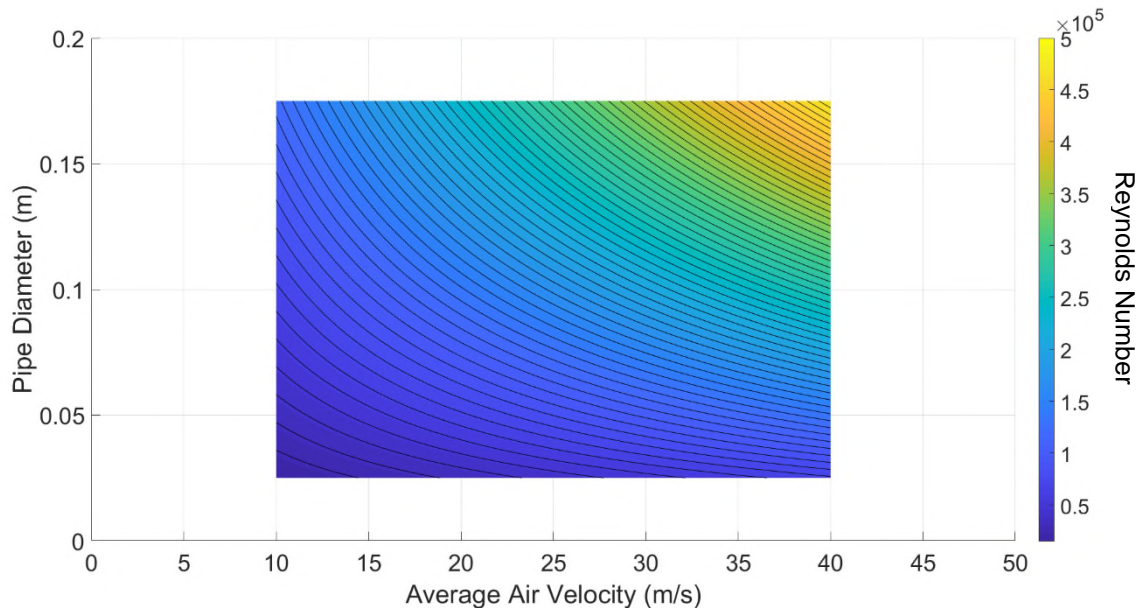


Figure 8-5: Reynolds number for a range of pneumatic conveying conditions assuming $\rho = 1.225 \text{ kg/m}^3$, and $\mu = 1.81 \times 10^{-5}$

Cengel and Cimbala [215] specify approximate boundaries separating laminar, transitional and turbulent flow. These boundaries are summarised in Table 8-3. The minimum Re number of the flow in Figure 8-5, corresponding to a pipe diameter of 0.025 m and an average air velocity of 10 m/s, was approximately 16920. It was therefore

considered acceptable to consider all pipeline flow, as conforming to the turbulent flow type.

Table 8-3: Flow types and their corresponding Reynolds numbers according to Cengel and Cimbala [215]

Reynolds Number	Flow Type
$Re \leq 2300$	Laminar Flow
$2300 \leq Re \leq 4000$	Transitional Flow
$Re \geq 4000$	Turbulent Flow

To now consider the fluid velocity profile across the pipeline section; the power-law velocity profile shown in Equation (8-4) [215] shall be used to approximate the fluid velocity as a function of radial distance from the pipe wall for turbulent fluid flow. The viscous sub layer is typically much less than 1% of the pipe diameter [215] and shall be deemed negligible in the scope of this analysis.

$$\frac{u}{u_{max}} = \left(\frac{y}{R}\right)^{1/n} \quad (8-4)$$

Where:

u	Velocity of the fluid at calculation position (m/s)
u_{max}	Maximum fluid velocity in pipe cross section (m/s)
y	Distance from pipe wall (m)
R	Radius of Pipe (m)
n	Constant (-)

The exponent, n , alters the velocity profile on approach to the pipe wall, however a value of 7 is accepted to approximate most flows [215]. To visualise the differences in turbulent fluid flow velocity profiles expected in the SBAT and Wolfson Centre Industrial Scale Pneumatic Conveying System, Figure 8-6 shows the profile in each pipeline (40.94 mm

and 100 mm pipe diameters respectively) for 'n' values of 7 and 8. A value of $n=8$ is also shown, as by increasing the value of 'n', the velocity profile represents that typical of higher Reynolds numbers. To quantify the difference in fluid-only velocity distribution attributed only to the difference in pipe diameter, Figure 8-7 shows the difference in magnitude for each value of 'n'.

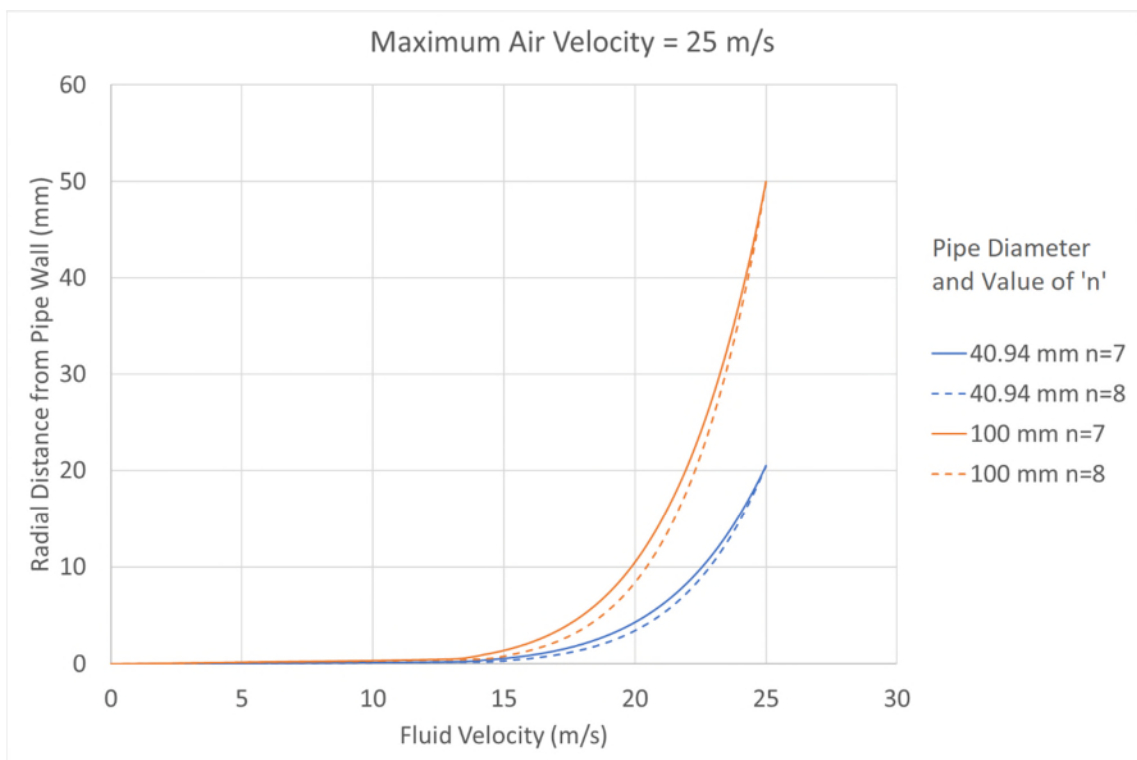


Figure 8-6: Fluid velocity profile by pipe diameter and value of coefficient 'n'

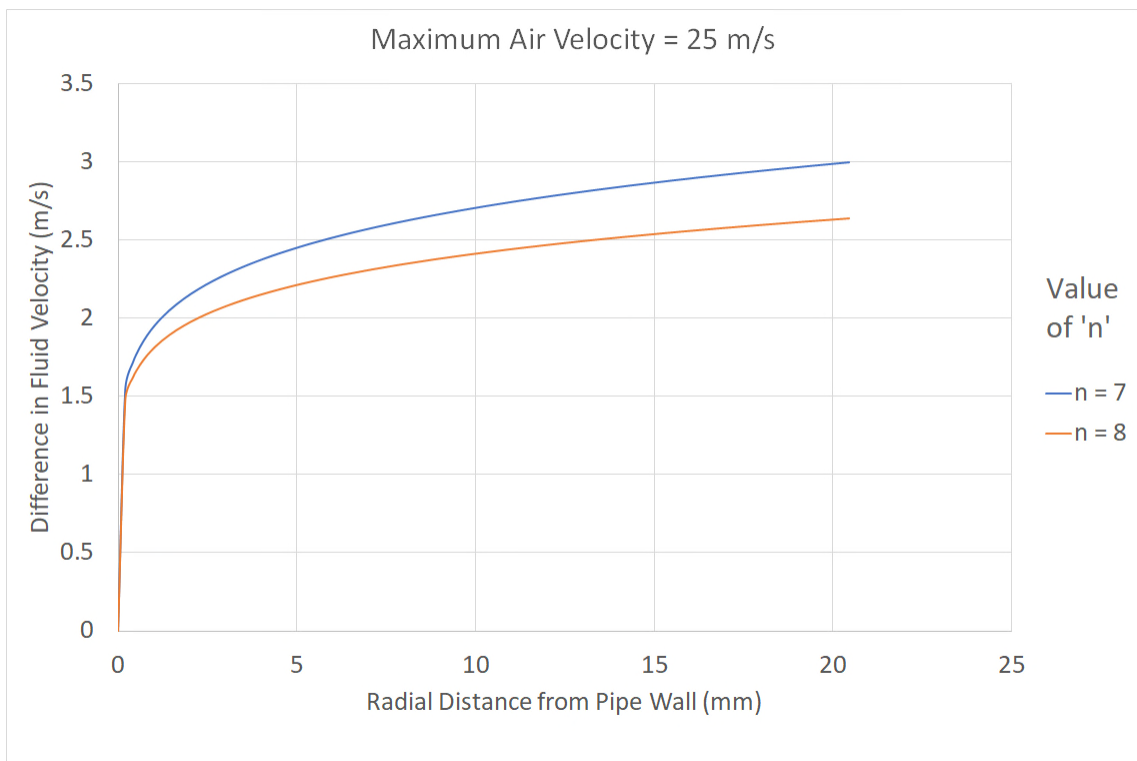


Figure 8-7: Difference in local fluid velocities for different values of 'n' for 100 mm diameter pipe subtracted from a 40.94 mm diameter pipe

Whilst the magnitude of difference in local fluid velocities is only small in comparison to the maximum air velocity (in the order of 10%), this could become significant should the local fluid velocity fall below the minimum conveying velocity. Such a scenario would contribute to the deposition of particles on the pipe floor, hence reducing the mean velocity of the solid phase. This would have a 'snowballing effect', whereby particles colliding with decelerated particles, would themselves decelerate and fall out of suspension. To better visualise the effect of the local air velocity alone, the state of flow shown in Figure 8-1e shall be considered. The height of the strand on the lower surface of the pipe is approximately 10% of the pipe diameter, obtained by image analysis. Figure 8-8 considers a scenario where 10 % of the pipe diameter (100 mm pipe diameter) experiences a local fluid velocity lower than the saltation velocity of the material (assumed to be 12 m/s). This is then compared with equivalent conditions in the 40.94 mm diameter pipe. As was revealed in the review of the literature (Section 2.3.1), recommended conveying conditions for the reduction of particle attrition was marginally above the saltation velocity of the solid phase. The average conveying velocity (representative of the measured superficial air velocity measured within industrial scale systems at the

location of a pressure measurement point – typically close to the material inlet to the line) for both pipelines in Figure 8-8 was approximately 13.1 m/s, with a maximum local velocity (at the pipe centreline) of 15.1 m/s. The difference in the height of the sub-saltation velocity zone is evident, noting that this is before the coupling with the solid phase is considered.

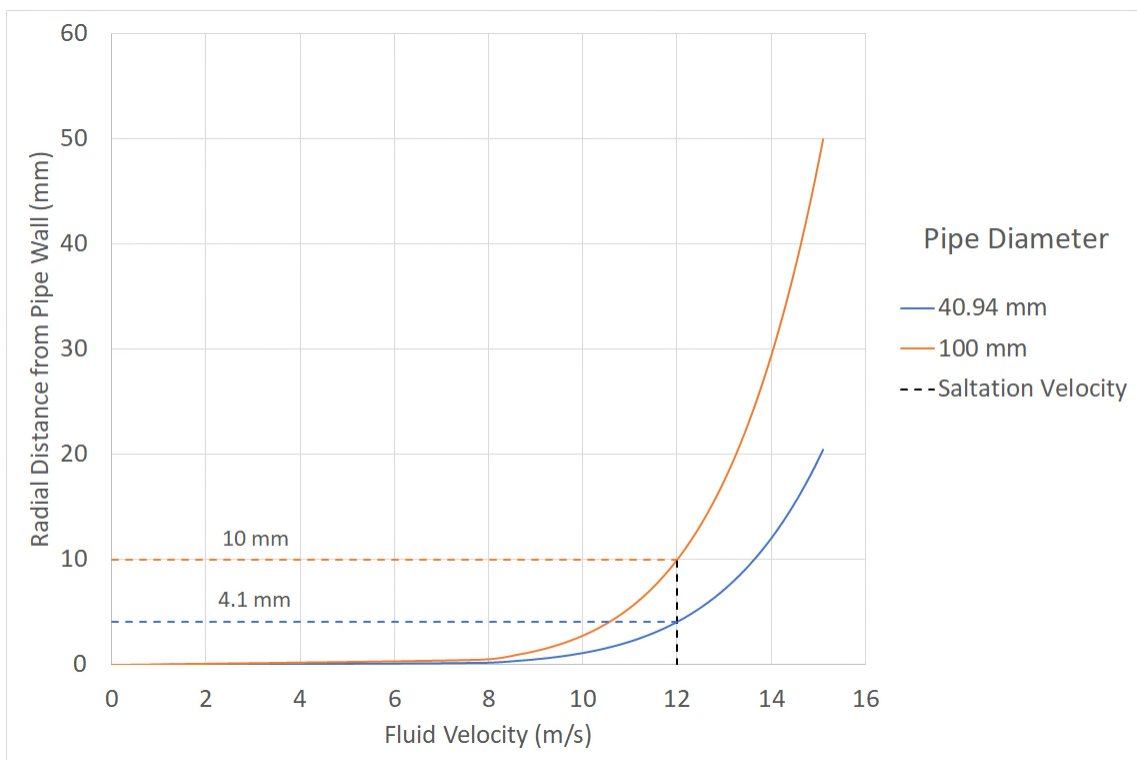


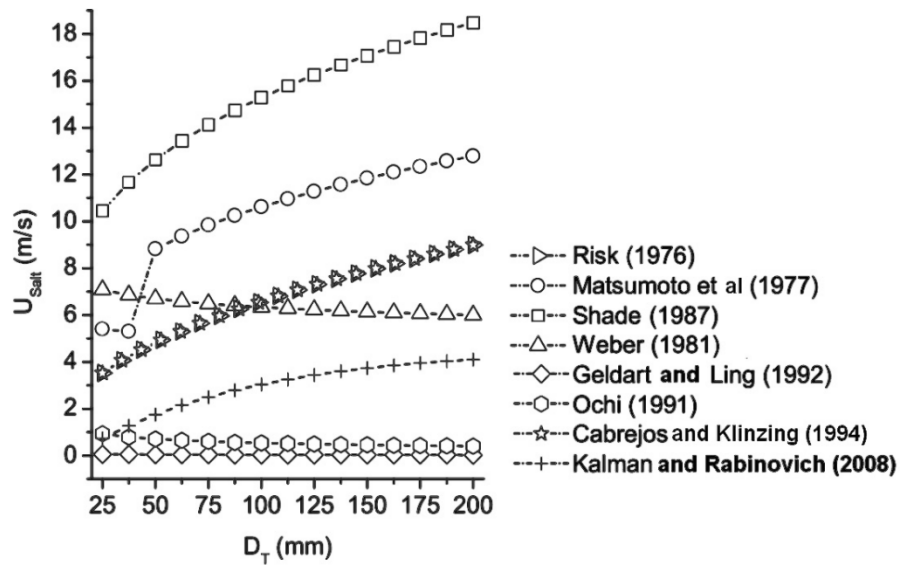
Figure 8-8: Height of the pipeline subjected to local air velocities below a theoretical saltation velocity of 12 m/s for $n=7$. Average air velocity = 13.1 m/s; maximum air velocity at pipe centreline = 15.1 m/s

To now consider the influence of the solid phase and how this alters the previously discussed fluid flow velocity profile. As indicated by Figure 8-1 and Figure 8-2, the presence of a strand of particles on the pipe floor effectively reduces the pipe diameter through which the fluid phase can flow. The logical consequence of this is for the fluid phase to increase in velocity. This higher fluid velocity has a greater propensity to re-entrain particles from the upper surface of the strand, an example of which is shown in Figure 8-9.

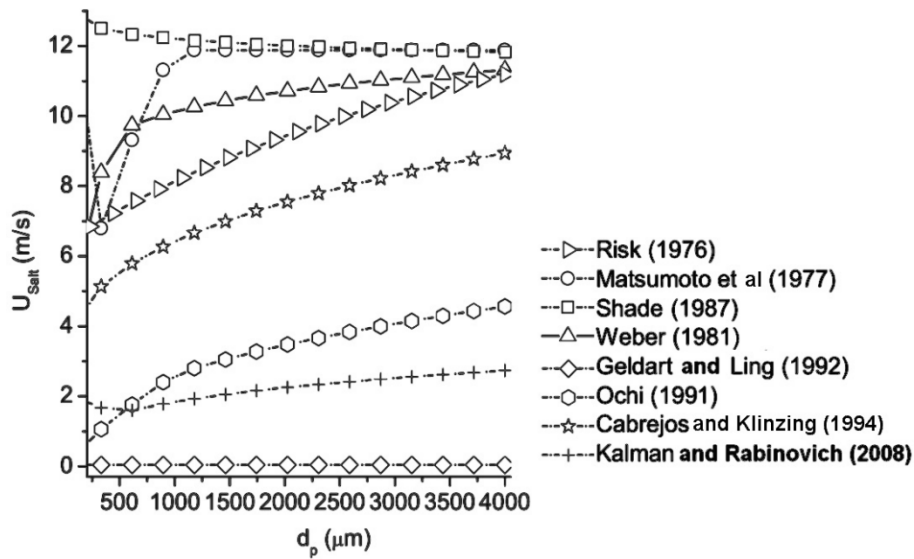


Figure 8-9: Image of sight glass showing particle pickup during a pneumatic conveying experiment

It therefore seems logical that both processes, particle deceleration and dis-entrainment, and subsequent particle reacceleration by localised high-velocity conveying medium, play a part in determining the average particle velocity along the pipeline. It does not however, seem logical to assume that the gas phase and the solid phase are travelling at the same velocity as suggested by other researchers in Section 2.3.1.1. The findings of this analysis are supported by the collated results reported by Gomes and Amarante Mesquita [216, 217] where comparisons of eight existing models concluded that as the internal diameter of the conveying pipe is increased, the pickup and saltation velocities are also increased. The same relationship was concluded for increases in the particle diameter and mass flow rate of the solid phase. These results are summarised in Figure 8-10 taken from Gomes and Amarante Mesquita [216]. Experimentation was also conducted into the influence of pipe diameter on the pickup velocity, the results of which are presented in Figure 8-11. Again, the trend shown in the data indicates that an increase in pipe diameter translates to an increase in the pickup velocity for all tested particle morphologies.

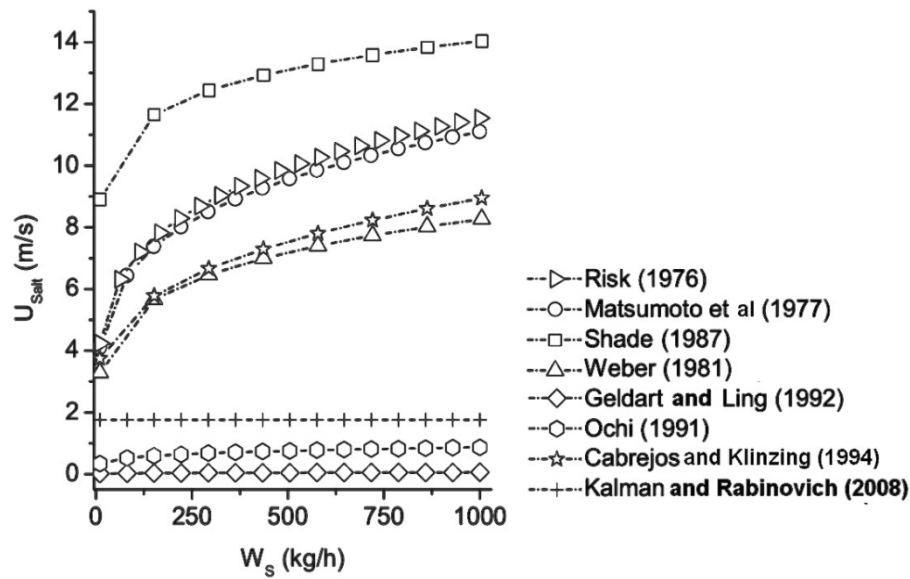


(a)



(b)

Figure 8-10: Results collated by Gomes and Amarante Mesquita [216], detailing the change of saltation velocity (U_{Salt}) with respect to changes in: (a) pipe diameter (D_T); (B) particle diameter (d_p); and mass flow rate of the solid phase (W_S). The references in the legends of the figures are as follows: Rizk [218]; Matsumoto et al. [219]; Shade [220]; Weber [221]; Geldart and Ling [222]; Ochi [223]; Cabrejos and Klinzing [224]; Kalman and Rabinovich [225].



(c)

Figure 8 10: Results collated by Gomes and Amarante Mesquita [214], detailing the change of saltation velocity (U_{Salt}) with respect to changes in: (a) pipe diameter (DT); (B) particle diameter (dP); and mass flow rate of the solid phase (WS). The references in the legends of the figures are as follows: Rizk [216]; Matsumoto et al. [217]; Shade [218]; Weber [219]; Geldart and Ling [220]; Ochi [221]; Cabrejos and Klinzing [222]; Kalman and Rabinovich [223].

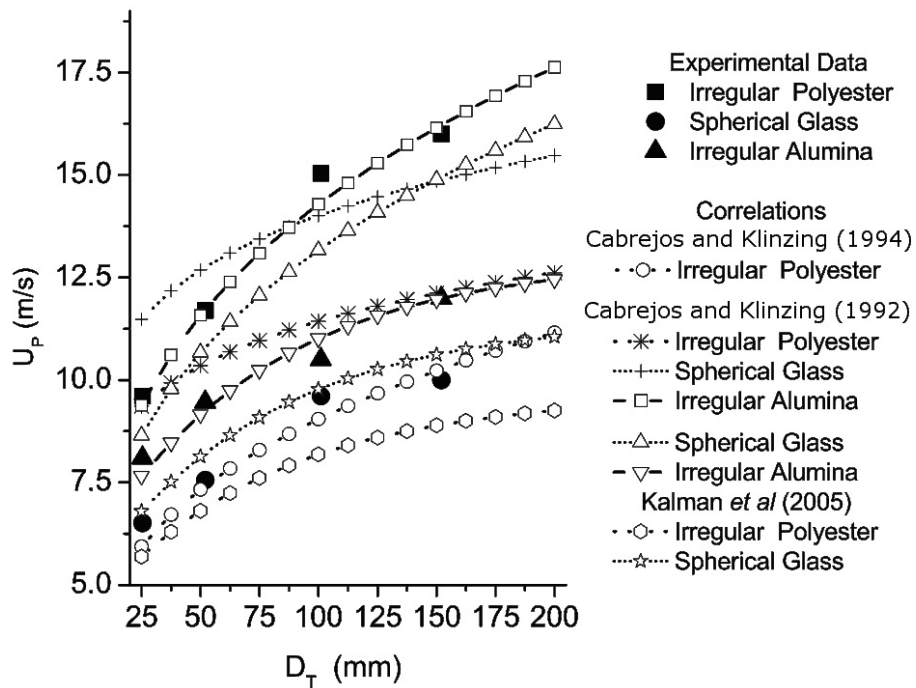


Figure 8-11: Results collated by Gomes and Amarante Mesquita [216], detailing the change of pickup velocity (U_P) with respect to change in pipe diameter (DT). References in the legend not detailed in Figure 8-10 are as follows: Cabrejos and Klinzing (1992) [226]; and Kalman et al. [227].

The increased cross-sectional area of the strand when conveying at a high solids loading ratio (particle concentration), which could be partially attributed to the reduced local fluid velocity at the pipe floor, potentially explains the observations of other researchers; where the decreased particle attrition observed at higher particle concentrations has been attributed to a 'shielding effect'. The results presented by this research propose that this is not due to particle 'cushioning' at the bends of the pipeline, but rather the reduced average particle velocity attributed to the increased size of the particle strand when conveying at higher particle concentrations.

8.2.1.2 Accounting for the Influence of Particle Morphology and Size

The information presented in Figure 8-10b concludes that the saltation velocity increases with increasing particle diameter. To now take a scenario that considers a model spherical particle in laminar flow; the drag force imposed by the relative motion of the fluid phase changes with respect to different particle diameters, Figure 8-12 was generated using Equation (8-5).

$$F_D = C_D A \frac{\rho V^2}{2} \quad (8-5)$$

Where:

F_D	Drag force (N)
C_D	Drag Coefficient (-)
A	Projected area of particle (m ²)
ρ	Density of the fluid (kg/m ³) (assumed to be 1.225 kg/m ³)
V	Fluid Velocity (m/s)

The coefficient of drag was adopted from the work of Mikhailov and Silva Freire [228] as described by Equation (8-6) for particle Reynolds Numbers: $1 < R_p < 100000$.

$$C_D = \frac{3808 \left[\left(\frac{1617933}{2030} \right) + \left(\frac{178861}{1063} \right) R_p + \left(\frac{1219}{1084} \right) R_p^2 \right]}{681 R_p \left[\left(\frac{77531}{422} \right) + \left(\frac{13529}{976} \right) R_p - \left(\frac{1}{71154} \right) R_p^2 \right]} \quad (8-6)$$

Where:

R_p Particle Reynolds Number (-)

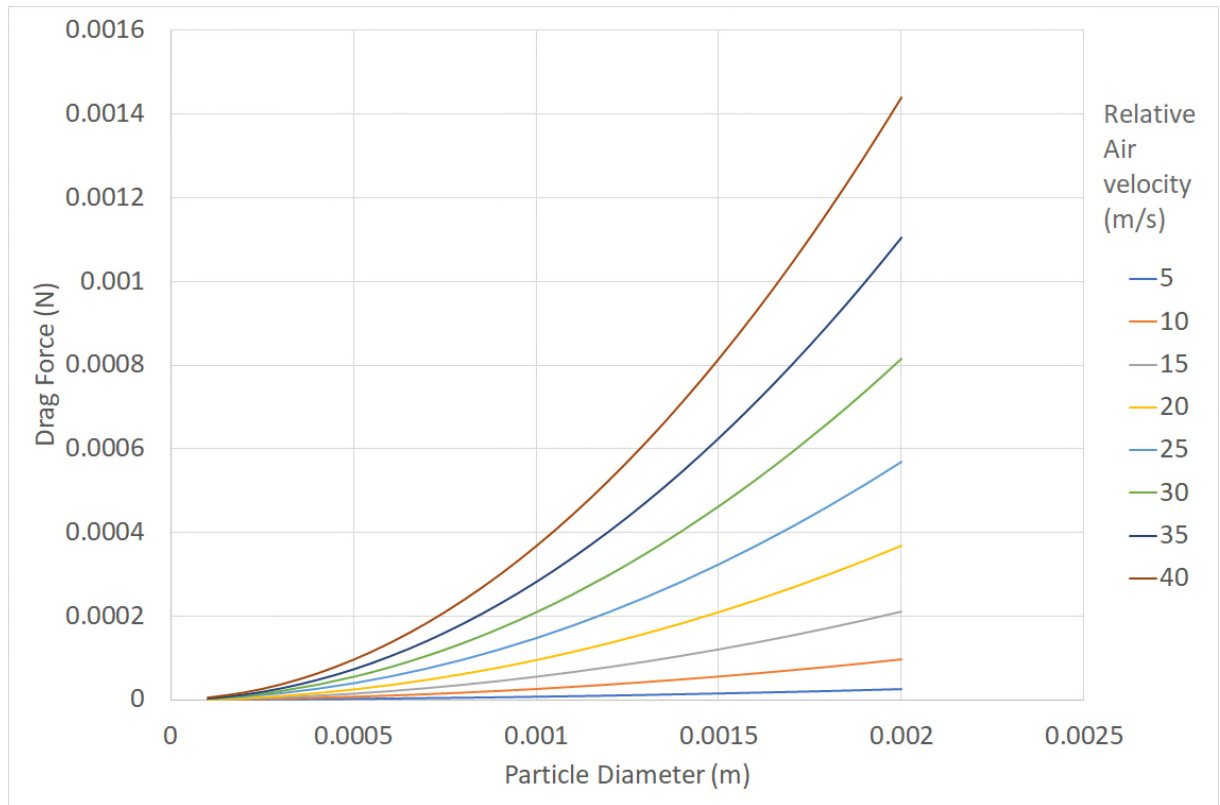


Figure 8-12: Drag force applied to spherical particles under laminar flow at various relative air velocities

It is clear that the force applied to larger particles is greater, and that as the relative air velocity increases, so too does this force. However, when applying this analysis to the conditions in the conveying pipeline, it is the acceleration of particles due to the local air

velocity that is of importance. Therefore, by taking these drag forces (analysis shown in Figure 8-12), and dividing these values by the mass of the respective particle, we obtain the specific particle force (N/kg); through application of Newton's first Law of Motion, this becomes the particle acceleration. Figure 8-13 shows the results of this calculation where a nominal particle density of 1800 kg/m^3 was adopted to represent an average particle density of Carbolux SK.

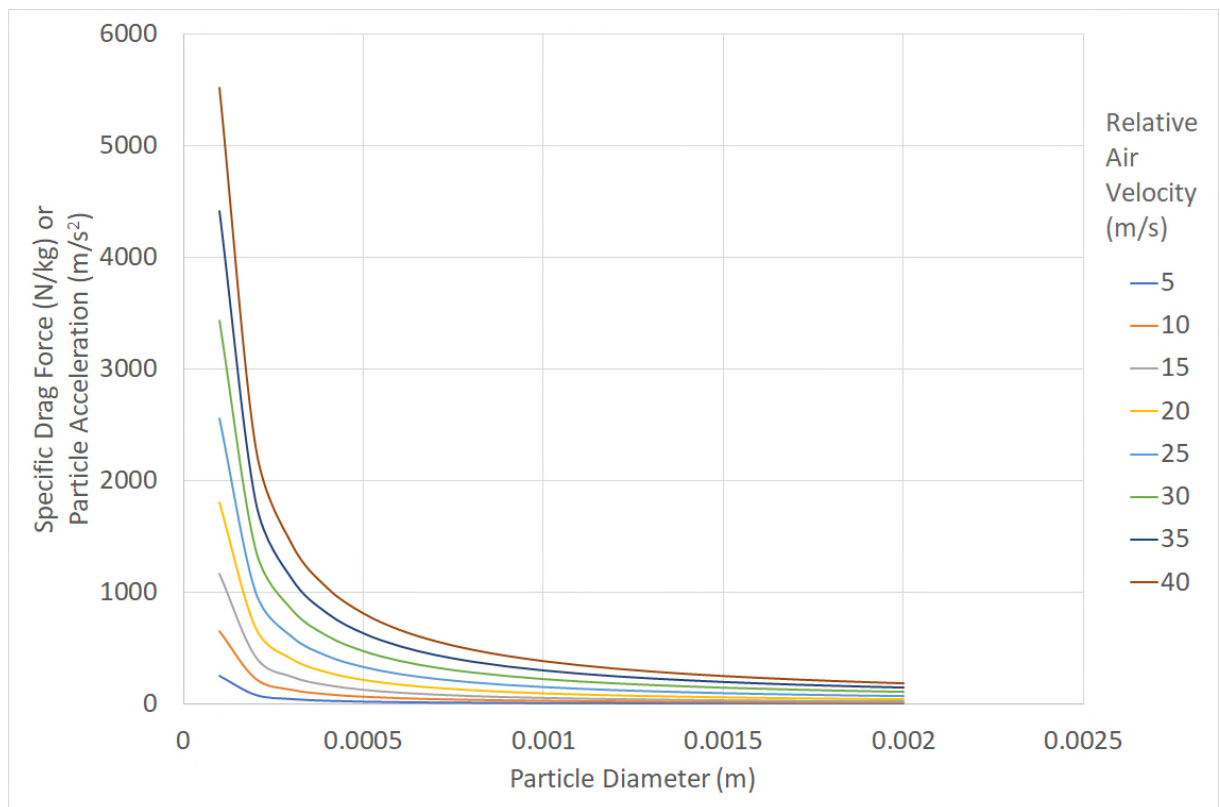
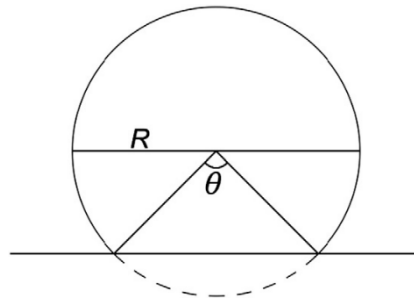


Figure 8-13: Acceleration of spherical particles under turbulent flow at various relative air velocities

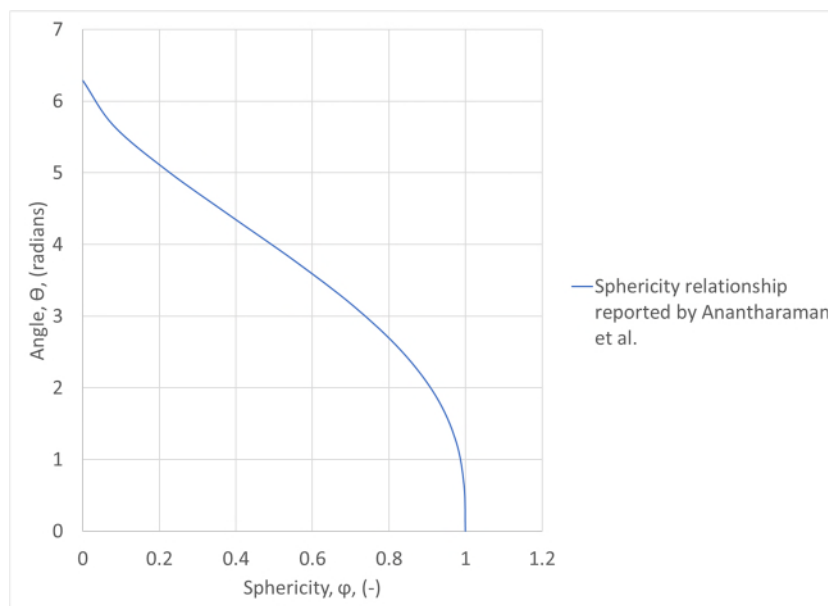
Through the analysis undertaken, it is logical that larger particles more readily fall out of suspension during pneumatic conveying, in agreement with the conclusions of Gomes and Amarante Mesquita [216]. These results also reflect the slip velocity characteristics of the Spent FCC Catalyst, and both types of Carbolux SK; the slip velocity was found to be greater for larger particle sizes. In the above analysis, coefficient of drag values were only determined for laminar fluid flow about a single particle in isolation. In future work, the coefficient of drag should be determined for turbulent flow, and for a system of

particles. The above analysis aimed to qualitatively determine at a simple level, the relationship between particle size and particle acceleration.

As has been previously acknowledged, not only the particle size, but also the particle morphology has an influence on the pickup and saltation velocities of the material. A number of researchers have modelled this relationship, one such example being that of Anantharaman et al. [229]. Many definitions of particle shape exist, with the approach adopted by Anantharaman et al. described in Figure 8-14 and Equation (8-7). Equation (8-8) subsequently describes the pickup velocity model, with the results of the model applied in Figure 8-15.



(a)



(b)

Figure 8-14: (a) the definition of the segment angle used to define particle sphericity; (b) the relationship between particle segment angle and particle sphericity as reported by Anantharaman et al. [229].

$$\varphi = \sqrt{1 - \frac{\theta}{2\pi} + \frac{\sin \theta}{2\pi}} \quad (8-7)$$

$$U_{pu,calculated} = \left[1 - \left(\frac{d_p}{D} \right)^{1.5} \right] \sqrt{\frac{\frac{2\pi}{3} f Ar \frac{\mu_f^2}{\rho} f_2(\theta)}{n C_D \rho d_p^2 f_1(\theta)}} \quad (8-8)$$

Where:

φ	Sphericity (-)
$U_{pu,calculated}$	Calculated minimum pickup velocity (m/s)
d_p	Particle diameter (m)
D	Pipe Diameter (m)
f	Coefficient of friction (-)
Ar	Archimedes number (-)
μ_f	Fluid viscosity (kg/m·s)
ρ	Fluid density (kg/m ³)
n	Coefficient to account for flow over a layer of particles (-)
C_D	Drag coefficient (-)

Where for brevity, $f_1(\theta)$ and $f_2(\theta)$ were defined as:

$$f_1(\theta) = (2\pi - \theta + \sin \theta) \quad (8-9)$$

$$f_2(\theta) = [4 + 6\cos(\theta/2) + 2\cos^3(\theta/2)]^{2/3} \quad (8-10)$$

And 'n' was empirically defined as:

$$n = 0.5759 \left(\frac{U_{pu}}{D} \sqrt{\frac{d_p}{g}} \right)^{0.3248} \quad (8-11)$$

Where:

g Acceleration due to gravity (m/s^2)

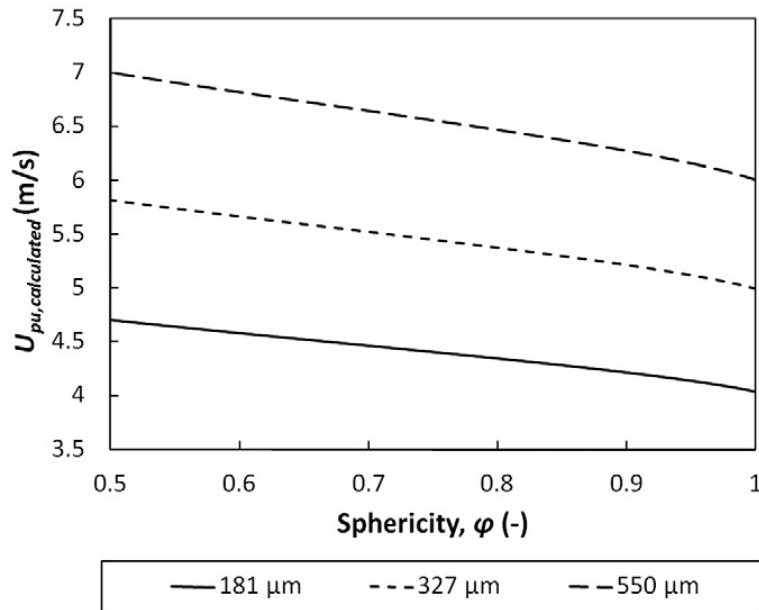


Figure 8-15: Results presented by Anantharaman et al. [229] modelling pickup velocity for particles of varying sphericity and diameter

From the results presented in Figure 8-15, it was clear that particle pickup velocity was expected to increase with decreasing particle sphericity and with increasing particle diameter. However, qualitatively comparing the influences of these two variables, it appeared that particle size has a greater influence on particle pickup velocity in comparison to the influence of particle sphericity. This could explain why the Spent FCC Catalyst displayed a much lower slip velocity compared to both types of Carbolux SK in the SBAT, even though the Catalyst has a much higher value of particle sphericity.

8.2.2 Geometrical Considerations of the External Industrial Pneumatic Conveyor

In the results obtained from the External Industrial-Scale Conveying System, there were clear zones indicating a reduction of the magnitude of measured particle attrition with increased particle concentration in the pipeline (for example, see Figure 7-5a). The analysis detailed in the previous section of this work highlighted the importance of pipe diameter in terms of the local fluid velocity; however, the internal pipe diameter in the External Conveying System was 47 mm. The difference of approximately 6 mm in the pipe diameters was considered negligible, and therefore further analysis was required to explain the observations.

Due to the reduced level of attrition observed, fully accelerated flow cannot be considered representative of the overall External Industrial-Scale Conveying System, and the relationships elucidated in the previous section shall be applied. In this comparison, the characteristics of the material tested in each apparatus (Carbolux SK Type C) shall be assumed to be equivalent. Therefore, any differences in the results between the two systems shall be considered to be due to the differences in pipeline geometry and flow conditions. To more closely examine the influence of pipeline geometry, Table 8-4 provides the isometric breakdown of the External Industrial-Scale Pneumatic Conveying System sections. The section length details the distances between the points in the line where the pipe transitions from straight section, to curved section (or vice-versa).

Table 8-4: Breakdown of section geometry for the External Industrial Scale Pneumatic Conveying System

Section Type	Section Length (mm)	Orientation H= Horizontal V = Vertical
Product Pickup - Funnel	N/A	N/A
Straight	3100	H
Bend (90°)	2000	H→V up
Straight	3600	V up
Bend (90°)	2000	V up → H
Straight	7200	H
Bend (90°)	2000	H → H
Straight	4500	H
Bend (90°)	2000	H → H
Straight	16000	H
Bend (90°)	2000	H → Inclined Down
Straight	1200	Inclined Down
Bend (90°)	2000	Inclined Down → H
Straight	2700	H
Bend (30°)	1300	H → H
Filter Receiver	N/A	N/A
Total Length	51.6 m	

It was evident that the geometry of the system described by Table 8-4 is far more complex than that of the SBAT. However, one key distinction should be made; the straight pipe sections of the External System were all less than that of the SBAT, except one. The pre-bend straight section of the SBAT was specifically designed to a length of 12 m to permit full

acceleration of the flow and achieve a steady state condition, for each of the operating conditions tested in the programme of experimentation. As 86% of the straight pipe sections in the External System were equal to, or less than 60% of the length of the pre-bend straight section of the SBAT, it was concluded that the flow was not fully accelerated throughout the majority of the system.

It was concluded that from the trends present in Figure 8-10c that an increase in the particle concentration corresponds to a higher saltation velocity of the conveyed material. In addition to this, it was shown in Figure 8-13 that large particles accelerate slower than smaller particles. This has been recently studied through experimentation by Tripathi et al. [230] by correlating the acceleration length of the solid phase with the Archimedes number (Ar), as presented in Figure 8-16. The solid line represents the fitted curve described in Equation (8-13). These results were obtained at low solids feed rates (of the order of 400 kg/hr or 0.11 kg/s), so little influence of the particle concentration on the acceleration length was to be expected. The authors of this work cited publications stating that acceleration length does not change with change in particle concentration / solids loading ratio (references: [231, 232]). The cited works are questionable in their findings due to the following:

- Pinho [231] reported the acceleration length of cork stoppers through measurement of pipeline pressure drop. This raises two main issues:
 - This is a low density, large cylindrical particle (see Table 8-5) reported to produce a fine dust that slicks the pipe wall (dramatically reducing particle-wall friction). The particle size of this material was orders of magnitude larger than the particle sizes discussed in the present research.
 - The measurement of pressure drop is an indirect measurement of particle velocity, and does not comprehensively describe the mean particle velocity or the particle velocity distribution at each pipeline position. More accurate results should be obtained from direct measurement of particle velocity.
 - Solids loading factors from 0.14 to 1.25 were considered (on a mass basis). This range is insufficient to inform the present research where testing was undertaken over solids loading factors from approximately 0.15 to 20.
- Marcus et al. [232] does provide commentary on an extensive test programme where Portland cement was conveyed [233]. Particle acceleration length was

measured by the pressure drop method. However, immediately after this, another piece of research was cited [234], noting that the acceleration length for fly ash increased with increasing solids loading ratio. The relationship proposed by Rose and Duckworth [235] (Equation (8-12)) was found to under-predict the acceleration length for Portland cement, and for large particles (10 to 40 mm in diameter). The research published by Marcus et al. [232] does not provide conclusive evidence that particle concentration (or solids loading ratio) has no influence on the particle acceleration length in a pneumatic conveying system.

$$L_{accel} = 6D \left[\frac{\dot{G}}{\rho g^{1/2} D^{5/2}} \cdot \left(\frac{D}{d} \cdot \frac{\rho}{\rho_p} \right)^{1/2} \right]^{1/3} \quad (8-12)$$

Where:

L_{accel}	Acceleration length of the solid phase (m)
D	Pipe diameter (m)
\dot{G}	Mass flow rate of solids (kg/s)
d	Particle diameter (m)
ρ_p	Particle density (kg/m ³)
ρ	Gas density (kg/m ³)
g	Acceleration due to gravity = 9.806 m/s ²

In light of the conflicting data available, the influence of particle concentration on the acceleration length of the solid phase remains unquantified and further research is required before further conclusions can be drawn. The analysis performed by Tripathi et al. [230] has been performed on the Carbolux SK Type C in Figure 8-17. It should be noted that the work by Tripathi et al. was performed on a pneumatic conveying line of internal pipe diameter 52.5 mm.

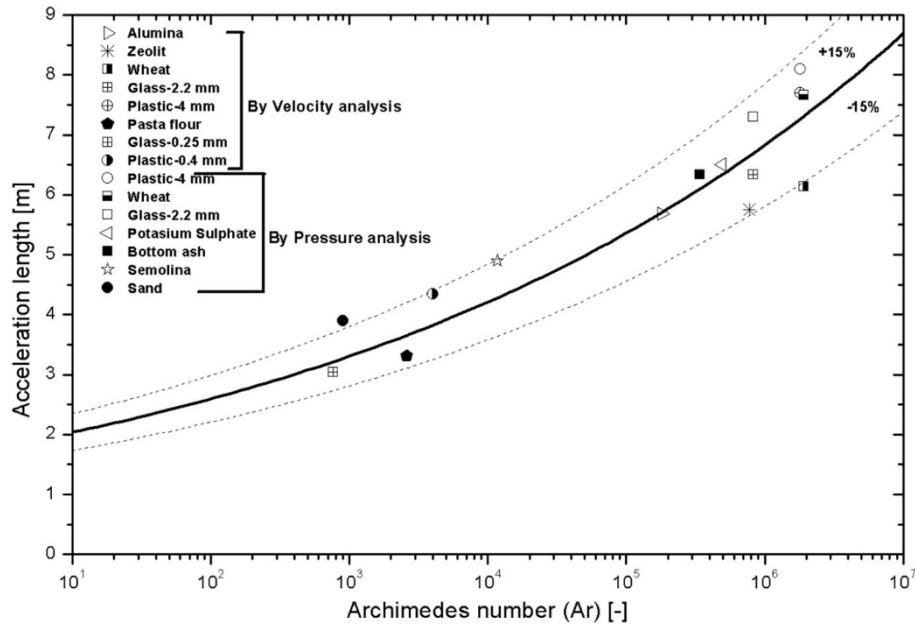


Figure 8-16: Results present by Tripathi et al. [230], correlating the solid phase acceleration length with the Archimedes number of the flow

$$L_{acc} = 1.6Ar^{0.1} \quad (8-13)$$

Where;

$$Ar = \frac{(\rho_p - \rho_f)g \cdot d^3}{v^2 \cdot \rho_f} \quad (8-14)$$

And:

L_{acc} Particle acceleration length (m)

ρ_p Particle density (kg/m³)

ρ_f Fluid density (kg/m³)

g Acceleration due to gravity (m/s²)

d Particle diameter (m)

v Kinematic viscosity of the fluid (m²/s)

Table 8-5: Cork stopper dimensions and density reported by Pinho [231]

Cork Stopper Size (length x diameter)	Density (kg/m ³)
27 x 20	195
38 x 22	219
38 x 24	198
45 x 24	177

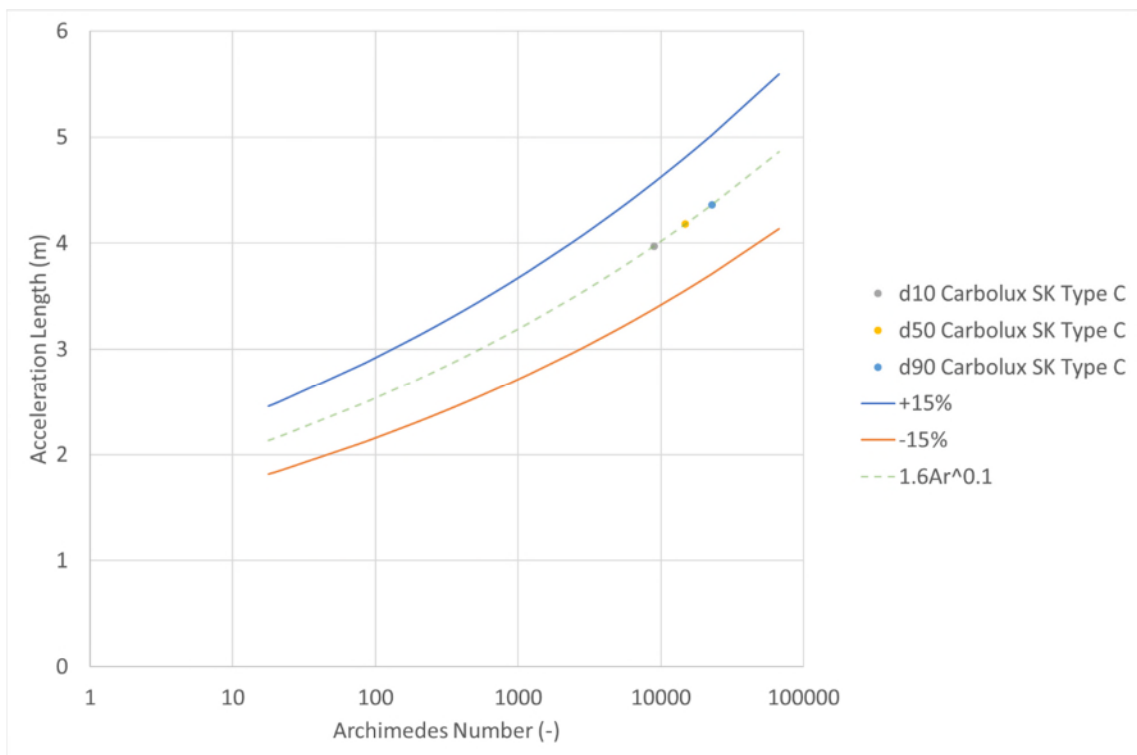


Figure 8-17: Acceleration lengths for the d10, d50 and d90 particle sizes of Carbolux SK Type C according to Equation (8-14); assuming $\rho_f = 1.177 \text{ kg/m}^3$, $g = 9.81 \text{ m/s}^2$, and $\nu = 1.48 \times 10^{-5} \text{ m}^2/\text{s}$

Upon inspection of Figure 8-17, it can be concluded that for this ideal scenario, the majority of the pipeline bends in the External System (4 out of 7 bends) were not subjected to fully accelerated flow. Another bend, Bend 4, has a preceding straight pipe length only marginally greater than the analysis shown in Figure 8-17, and therefore cannot be conclusively determined to be subjected to fully-accelerated flow. Furthermore, as the

particle concentration is increased, it is possible that the acceleration length increases; but this hypothesis requires further experimentation for validation.

8.3 Conclusions

This chapter has extensively discussed the observations and particle attrition results obtained across the full breadth of the experimental programme with respect to the 'shielding effect' proposed by other researchers. A broad spectrum of flow conditions, along with respective models proposed by other researchers, have been considered, and applied to the data obtained from the Bench Scale Particle Attrition Tester (BSPAT), Single Bend Attrition Test (SBAT), and the Wolfson and External Industrial Conveying Systems.

The discrepancies in the results across these different scales were attributed to material factors and process factors. The material factors identified were: particle diameter, particle morphology and particle density. The process factors identified were the length of straight pipe preceding a pipe bend, particle concentration in the pipeline, superficial air velocity, and pipe diameter. The resulting interaction between these two types of factors included the particle acceleration length, fluid velocity distribution across the pipeline cross-section, and particle slip velocity. The generalised relationships between these variables are summarised in Table 8-6.

Table 8-6: Summary of the inter-relationships between variables in a pneumatic conveying system

Increase in:	Saltation Velocity	Pickup Velocity	Particle Acceleration	Particle Acceleration Length
Particle Density	↑	↑	↓	↑
Particle Sphericity	-	↓	-	-
Particle Diameter	↑	↑	↓	↑
Pipe Diameter	↑	↑	-	-
Particle Concentration	↑	↑	-	-
Superficial Air Velocity*	N/A	N/A	↑	-

*Assume turbulent flow

- No information

It was clear from the results obtained on the BSPAT and the SBAT that particle attrition was not mitigated by increasing the particle concentration (and hence particle mass flux at the impact surface), for the range of values considered. However, the results from the two industrial-scale pneumatic conveying systems (Wolfson and External) did not show the same degree of disconnection with the SBAT.

- It was concluded that the pipe diameter of the Wolfson Centre Industrial Scale Pneumatic Conveyor was sufficiently large by comparison with the SBAT pipeline, to convey the Carbolux SK Type C particles below the slip ratio measured on the SBAT. This reduction is hypothesised to change with increasing particle concentration (or solids loading ratio), whereby the slip ratio decreases (slip velocity increases) with increasing pipe diameter, along with the formation of a low particle velocity region close to the pipeline floor. The size of this region is hypothesised to increase with decreasing superficial air velocity, and increasing particle concentration, for a given internal pipe diameter. The final result of the formation of this low particle velocity region is that the particle velocity distribution across the pipe cross section is not of the same form as the fluid phase. Rather,

the particle velocity distribution is skewed towards lower velocities close to the pipe floor.

- With respect to the analysis of the results obtained from the External Industrial Pneumatic Conveying System, the difference in pipe diameter was deemed negligible between this and the SBAT. However, it was demonstrated that the majority of straight sections between successive bends in the pipeline were too short to accelerate the particles to generate impacts under fully-accelerated conditions. This meant that the acceleration profile of the solid phase had a significant effect on the impact conditions in the pipe bends. Furthermore, it was demonstrated on a theoretical basis, that the higher the particle concentration in the pipeline, the greater the saltation and pickup velocities of the flow. It was hypothesised that, based on single particle analysis, that the acceleration length of the solid phase also increases with increasing particle concentration. Therefore, the 'shielding' results obtained in the External System are, in fact, hypothesised to be the result of under-accelerated flow conditions at the bends, and not that of a cushioning effect provided by inter-particle collisions.

CHAPTER 9: Optimisation of Particle Attrition Characterisation and Modelling

This Chapter aims to address two primary objectives: to develop a modelling approach which can be used to reconcile the variations of particle velocity and particle impact angle within the Bench Scale Particle Attrition Tester; and to develop a model to scale particle attrition measured in the BSPAT, with that measured in the Single Bend Attrition Tester.

The first of these objectives will address the fundamental relationship of particle velocity components normal to, and parallel to the impact surface. The result of this derivation shall then be applied to the particle attrition data reported by other researchers. Finally, the modelling approach shall be evaluated with respect to its accuracy and a method to incorporate further conservatism into the output for design purposes.

The second objective is to correlate the particle breakage behaviour in the BSPAT with that observed in the short radius, and long radius bends in the SBAT. This has been addressed by consideration of three different methods of determining the representative mean particle impact angle for each of the bend radii tested. Then, the particle breakage correlations obtained in the BSPAT were applied and evaluated with respect to the coefficient of determination achieved for the fit of second power polynomial, and exponential sigmoid relationships.

9.1 Optimisation of the Bench Scale Particle Attrition Test Programme

It was evident that from the heavy time and resource requirements consumed from the Bench Scale Particle Attrition Tester (BSPAT) experimentation, that such an approach would be impractical across the majority of real-world applications. In practice, such an approach would fail to meet deadline and budget constraints; therefore, a method to reduce the experimentation required to characterise a particulate material was sought.

The form of analysis considered in Chapter 5 to Chapter 8 considered how various impact conditions influence the measured magnitude of deviation ($\Delta\%$, see Equation (5-1) and Equation (5-2)). This, by definition, is an observation of how much a particular size fraction

has changed with respect to the sample mass. In order to consider each of the primary size fractions (specified in Figure 5-6) isolated from the influence of the shape of the remainder of the particle size distribution, in this Chapter the Percent Change Criterion (α) was used (Equation (9-1)). This measurement considered how much material mass was lost from a specific size fraction, as a percent of the material retained in that fraction in the virgin particle size distribution. In essence, this approach considered a scenario where the entire sample consisted purely of the size fraction under scrutiny. It is worth noting that the value of Percent Change for most conditions, was very similar to the value of Magnitude of Deviation. This was due to the narrow particle size distribution of each pre-prepared particle size fraction, where almost all material resided on a single sieve size. By using the Percent Change criterion, however, the largest size fraction of any material can be analysed regardless of the remainder of the particle size distribution.

$$\alpha = \frac{\Delta\%}{m_{sieve}} \quad (9-1)$$

The variables that could be modelled included: impact velocity, impact angle, and particle size. This analysis shall begin by considering the influence of particle impact angle. Figure 9-1 shows the particle attrition data for 710-1000 μm primary particle batch size, across all tested impact velocities and angles on the BSPAT.

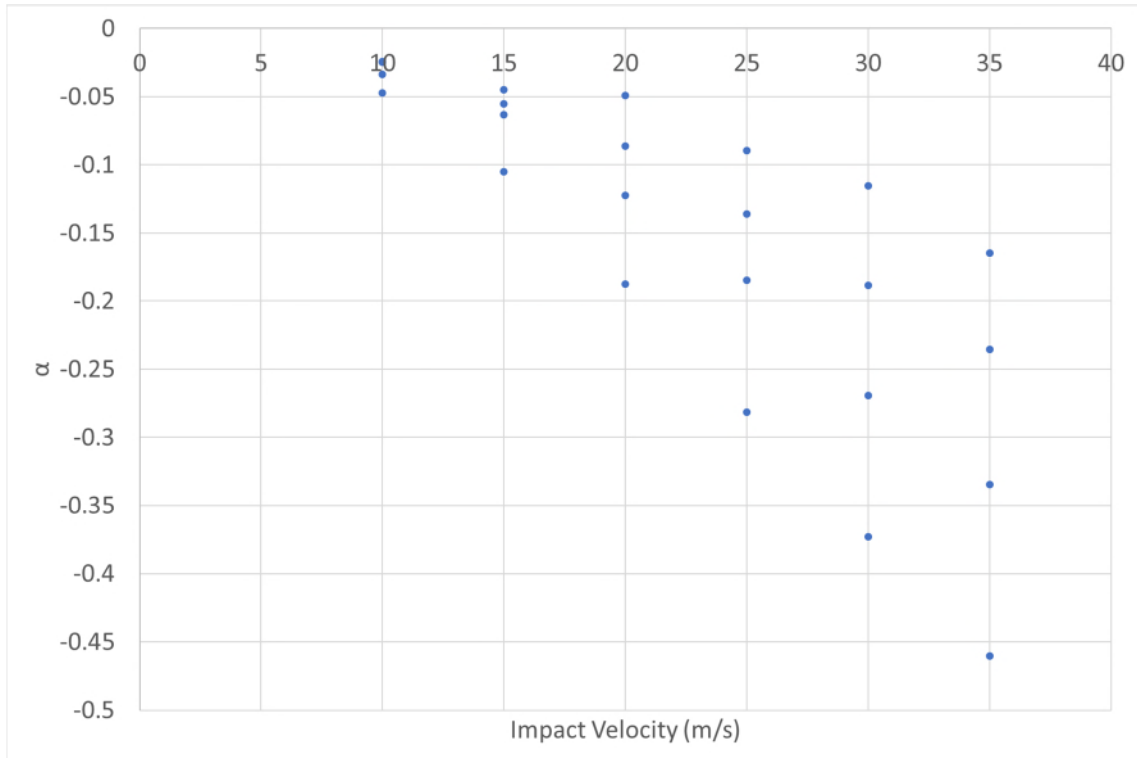


Figure 9-1: Raw data for 710-1000 μm primary batch size material on the BSPAT for all impact velocities and impact angles tested, as measured by the percent change criterion on the 710 μm sieve size.

The impact velocity can be separated into two components: the component normal to the impact surface (V_n); and the component parallel to the impact surface (V_t). These velocities are responsible for the manifestation of compressive and shear forces respectively, during an impact event. As was discussed in Section 2.4.4.1.2, the nature of the particle material can result in failure primarily to either one of these forces. However, at all impact angles non-normal to the impact surface, both normal and shear forces are applied. Therefore, the degree of particle attrition observed cannot be attributed solely to either the normal velocity component, or the parallel velocity component.

In order to account for both velocity components in the analysis of particle attrition data, a new approach was developed, the Velocity Combination Ratio (β), and defined by Equation (9-2) and Equation (9-3). The output of this modelling approach, V_m , is a theoretical velocity between the bounds of V_n and V_t . To visualise how V_m varies with β , Figure 9-2 graphs the full theoretical range of values that V_m can take. Through alteration

in the value of β , one can alter the influence of V_n and V_t on the way in which particle attrition data is analysed.

$$V_m = \beta V_n + \varepsilon V_t = V_p(\beta \sin \theta + \varepsilon \cos \theta) \quad (9-2)$$

Where:

$$\beta + \varepsilon = 1 \quad (9-3)$$

And:

V_m Model velocity (m/s)

V_p Particle velocity under experimental conditions (m/s)

θ Particle impact angle under experimental conditions, measured as the angle subtending the impact surface and the particle velocity vector (degrees)

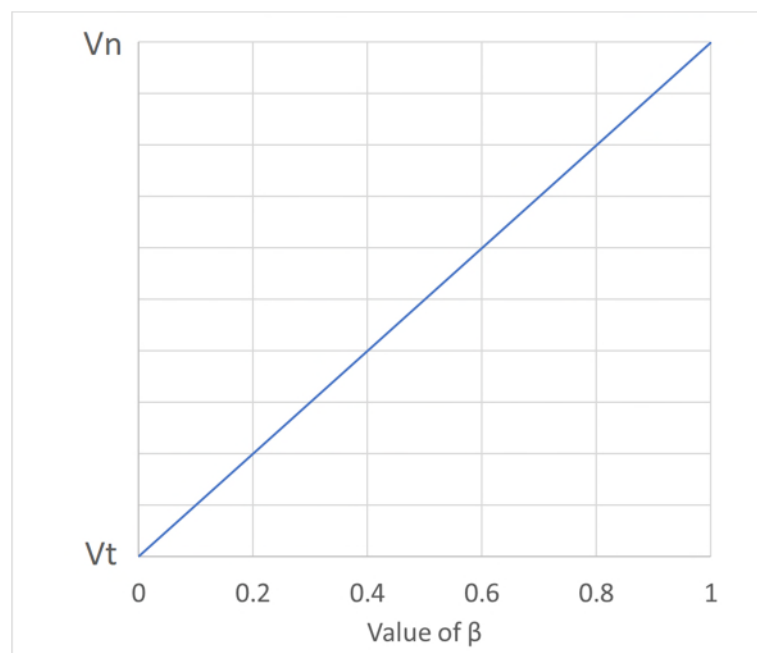
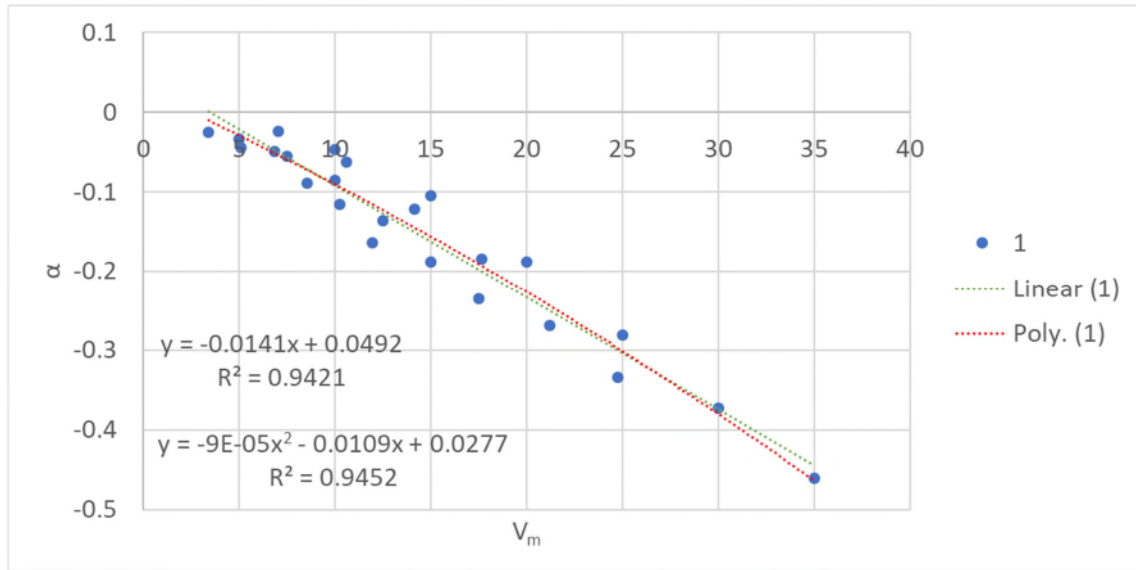
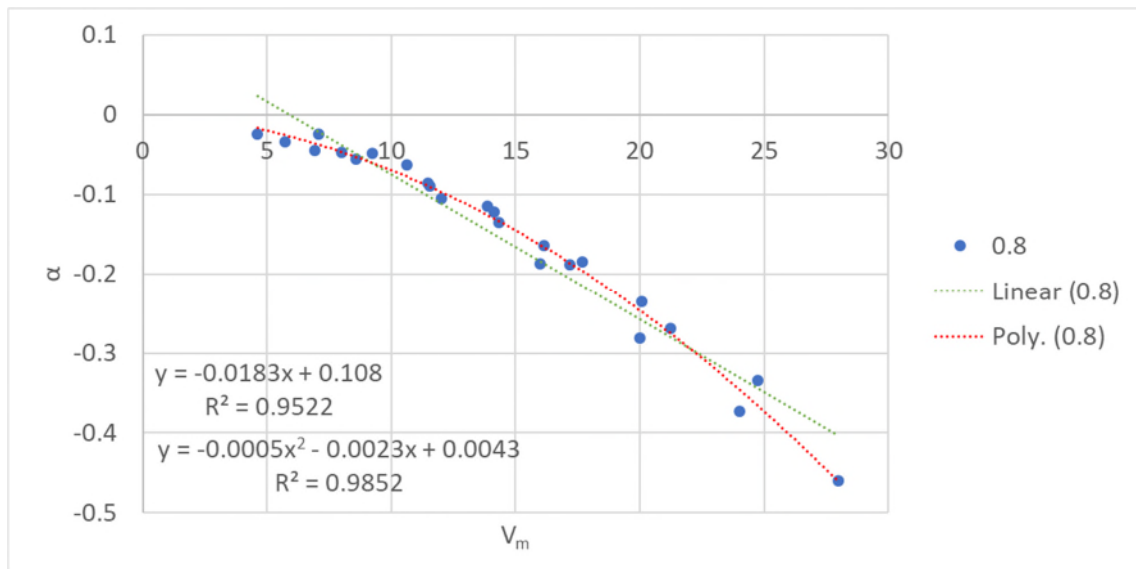


Figure 9-2: Variation of V_m with respect to variation in β

Now, to apply the Velocity Combination Ratio approach to the data presented in Figure 9-1. Figure 9-3a, Figure 9-3b, and Figure 9-3c show the data given in Figure 9-1 for β values of 1, 0.8, and 0.5 respectively, with the resulting V_m forming the x-axis. Additionally, two trendlines have been fit to each data set: one linear in nature, and the other a second-order polynomial. The criteria for fitting these trendlines was that the y-intercept must not be negative; there is no physical sense for the data-fit to yield breakage at an impact velocity of zero. In cases where this occurred, the y-intercept was forced through the origin. However, a positive x-intercept does yield valuable information into the nature of the strength of the particulate material. Such an occurrence approximates the impact velocity, below which, no particle breakage occurs.

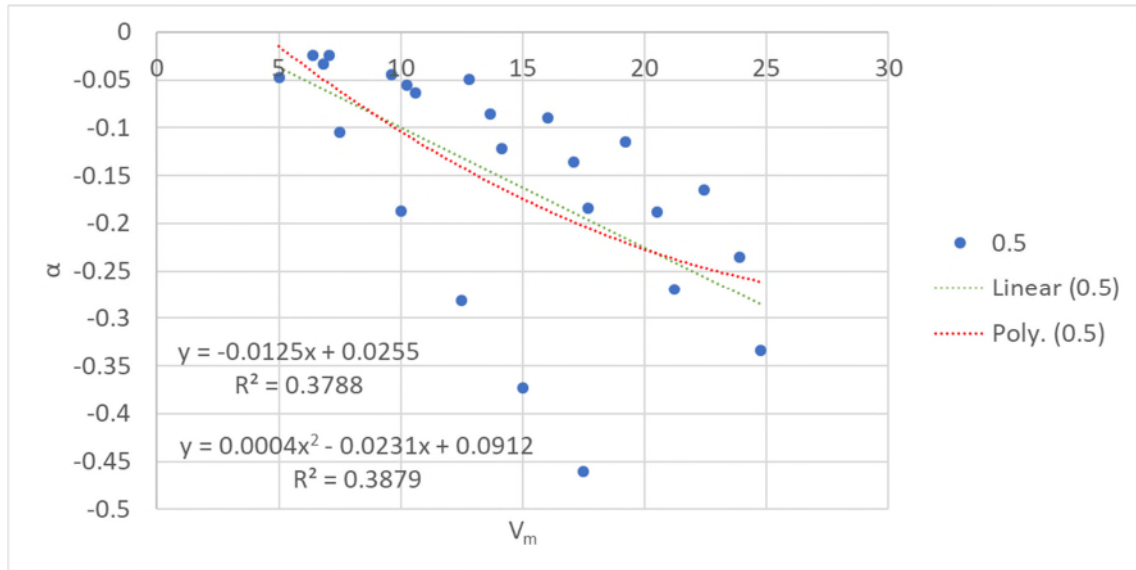


(a)



(b)

Figure 9-3: The data from Figure 9-1 graphed against V_m for values of β : (a) 1, (b) 0.8, and (c) 0.5



(c)

Figure 9 3: The data from Figure 9 1 graphed against V_m for values of β : (a) 1, (b) 0.8, and (c) 0.5

It is evident that in all cases, the polynomial trendline more closely fitted the data when considering the R^2 values. Additionally, the R^2 values of both the linear and polynomial trendlines are higher for the $\beta = 0.8$ condition in comparison to the other two conditions shown. This indicates that for this β value, the entire data set more closely resembles a polynomial trend. If the same analysis is completed for a with range of β values, with the same conditions for trendlines applied, the curves in Figure 9-4 are attained.

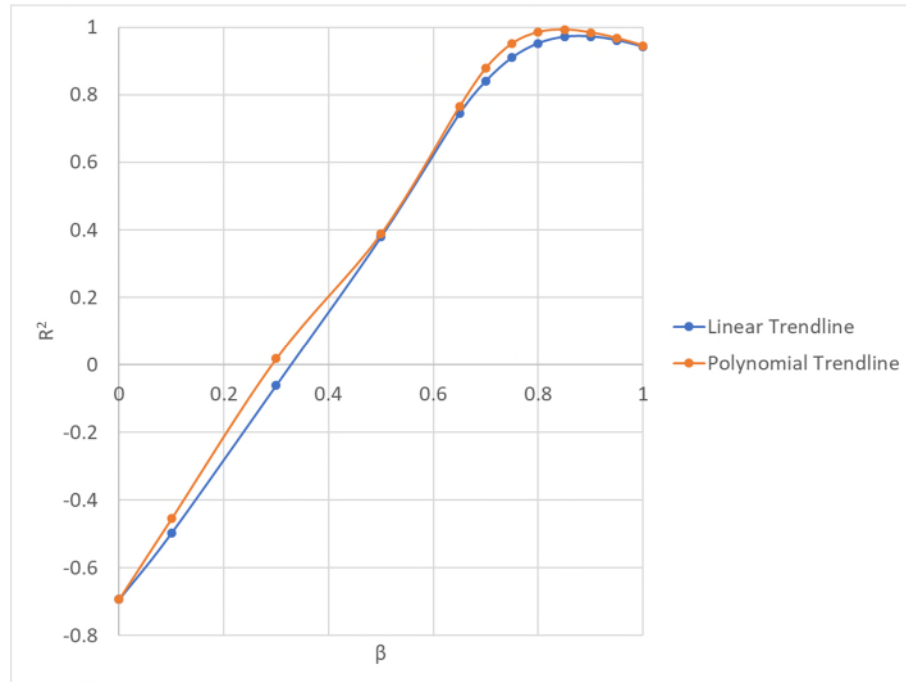


Figure 9-4: The R^2 results of fitting linear and polynomial trendlines to the Data graphed in Figure 9-1 for a wide range of values of β

Through qualitative observation of Figure 9-4, it is evident that there exists an 'optimum' value of β , for which the R^2 of the fitted trendlines is maximised. Of each of the values of β analysed, for the 710-1000 μm primary size fraction Carbolux SK material, the percent changed criterion (α) was best modelled at $\beta = 0.85$ with a second power polynomial fit. The results of this data point are shown in Figure 9-5, and the full set of graphs used to determine the optimum value are found in Appendix H.

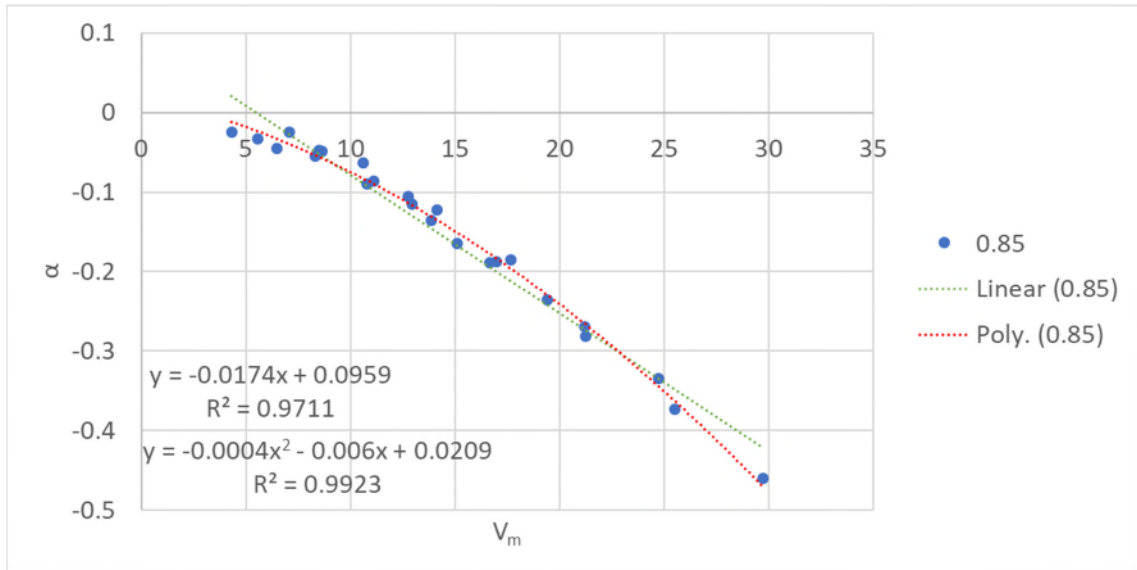
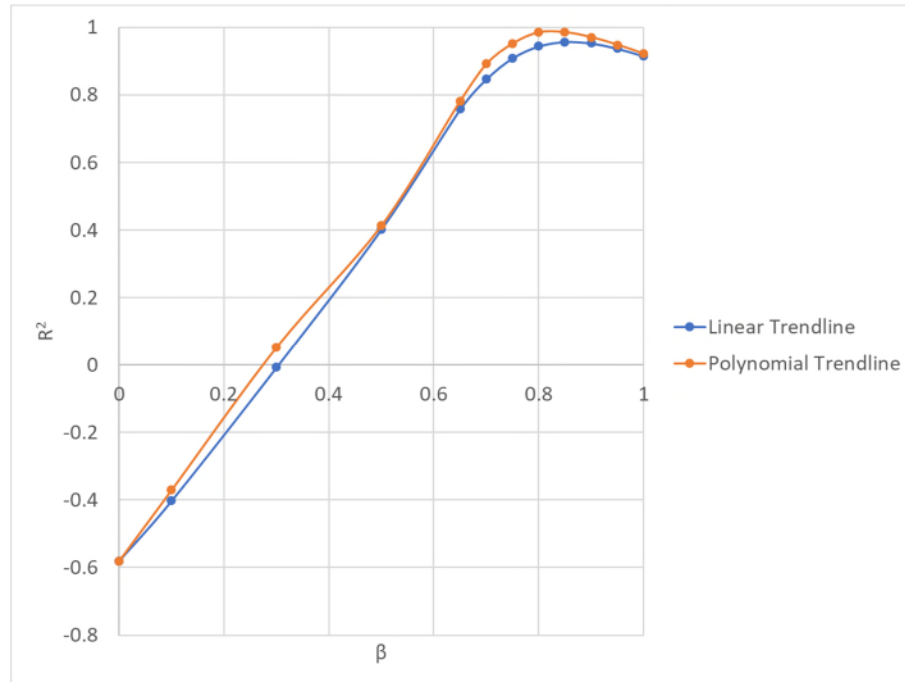


Figure 9-5: The data from Figure 9-1 graphed against V_m for $\beta=0.85$

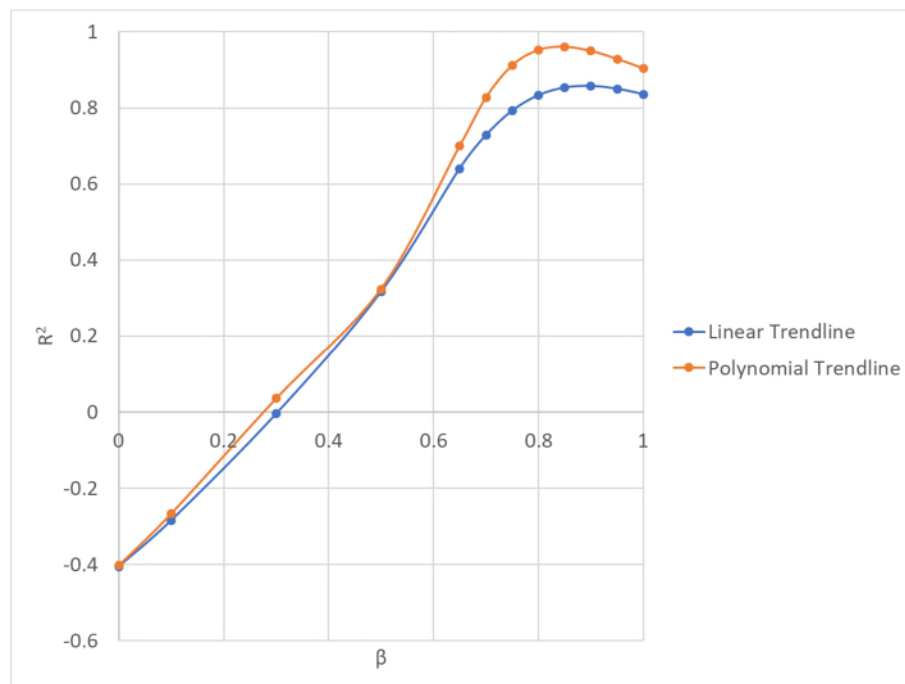
Comparing the form of the data between Figure 9-1 and Figure 9-5 shows a significant difference in the relationship between relative data points in terms of describing the material response to relative impact velocity vectors. Not only does this support the concept that the particle attrition behaviour of Carbolux SK cannot be described with the normal impact velocity vector alone, but also describes the proportional response to each velocity vector. Due to the conditions by which the trendlines apply, negative values of R^2 were obtained. This meant, that in order to achieve a relationship that made physical sense, the fitted relationship was worse than that of a horizontal line. It was clear through this analysis that the velocity vector parallel to the target surface was of secondary influence to the overall particle attrition behaviour, and the normal velocity vector was the primary influence.

In order to determine the applicability of this form of analysis across the full factorial data set previously acquired on the BSPAT for Carbolux SK,

Figure 9-6 shows the R^2 fitting results obtained for the 500-710 μm and 355-500 μm primary particle size fractions in terms of particle breakage.



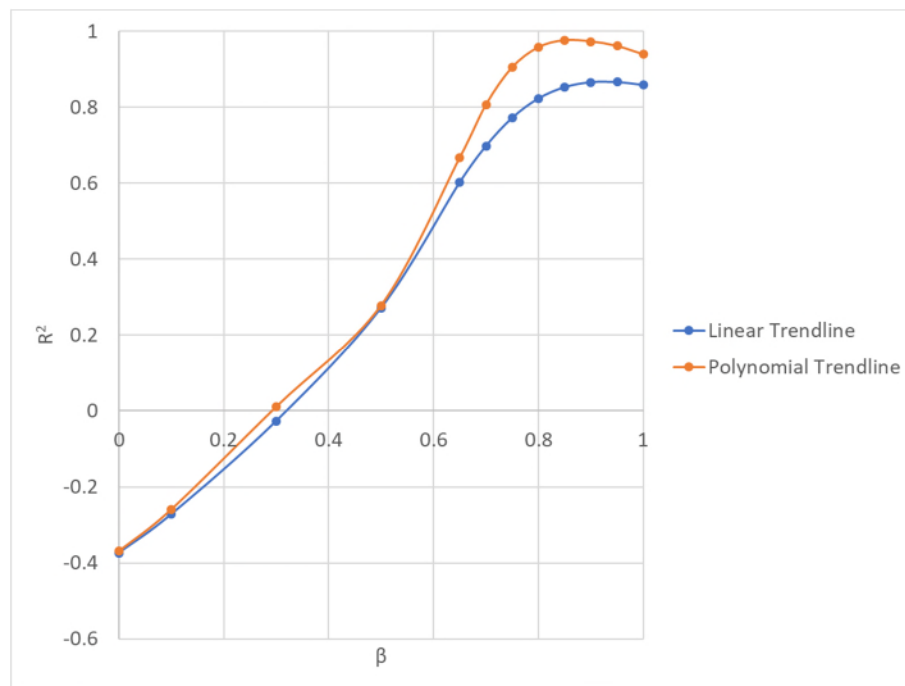
(a)



(b)

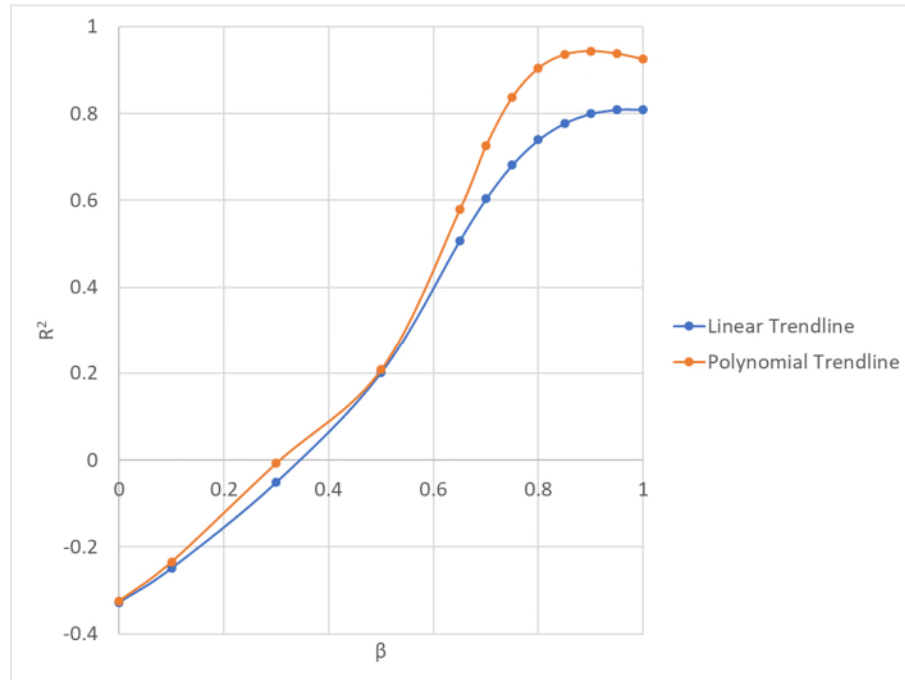
Figure 9-6: The R^2 results of fitting linear and polynomial trendlines to the data obtained from testing the (a) 500-710 μm and (b) 355-500 μm primary particle size fractions, then applying linear and polynomial trendlines for a wide range of values of β

For each of the Carbolux SK primary particle size fractions, the optimum value of β that was analysed equalled 0.85. It therefore implies that this parameter is not influenced by particle size, and that β reflected the nature of the material response to compressive and shear loads. This analysis has thus far only analysed the material lost from a given size fraction due to particle breakage. It shall be now applied to a size fraction where child particles or fragments enter as a result of a breakage event of a larger particle. The 180 μm was selected as no mass was retained on this sieve in the virgin particle size distributions for any of the primary particle size fraction batches. Equally, as this size fraction contained no mass in the virgin condition, the percent change criterion, α , could not be used. Therefore, the magnitude of deviation ($\Delta\%$) shall be used for this analysis. Figure 9-7 gives the R^2 analysis for each of the primary particle size fractions considered.

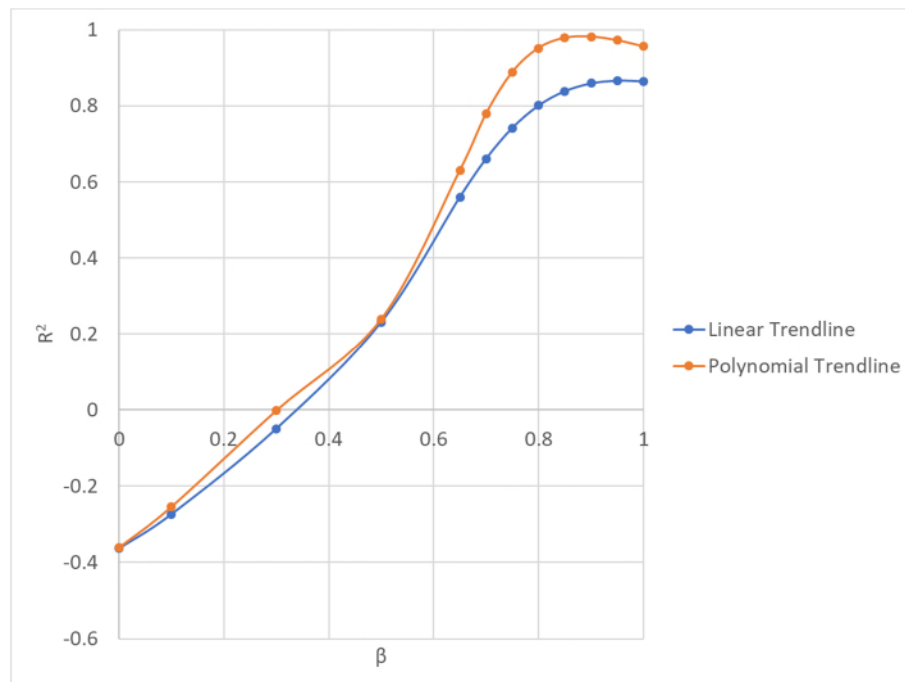


(a)

Figure 9-7: The R^2 results of fitting linear and polynomial trendlines to the data obtained from testing the (a) 710-1000 μm , (b) 500-710 μm and (c) 355-500 μm primary particle size fractions, then applying linear and polynomial trendlines for a wide range of values of β , with respect to the magnitude of deviation of material addition to the 180 μm sieve.



(b)



(c)

Figure 9 7: The R^2 results of fitting linear and polynomial trendlines to the data obtained from testing the (a) 710-1000 μm , (b) 500-710 μm and (c) 355-500 μm primary particle size fractions, then applying linear and polynomial trendlines for a wide range of values of β , with respect to the magnitude of deviation of material addition to the 180 μm sieve.

As was observed with the previous analysis on the sieve of the primary size fraction, the material addition to the 180 μm sieve conforms to the same type of relationship as shown in Figure 9-7. Again, a value of $\beta = 0.85$ resulted in the highest value of R^2 for the 710-1000 μm size fraction. However, for the 500-710 μm and 355-500 μm primary particle size fractions, a value of $\beta = 0.9$ resulted in the highest value of R^2 . In both of the latter cases, the difference between the R^2 values of the $\beta = 0.85$ and 0.95 data series was 0.0077 and 0.0033 respectively. Qualitatively, this difference is very small and in a pragmatic scenario, it is concluded that a value of $\beta = 0.85$ is appropriate for modelling each of the conditions previously described, regardless of virgin particle size or particle impact angle.

The generalised equation for the second power polynomial form of the model demonstrated in this research is given in Equation (9-4).

$$\alpha = bV_m^2 + cV_m + d \quad (9-4)$$

Substituting Equation (9-2) for V_m :

$$\alpha = b[V_p(\beta \sin \theta + \varepsilon \cos \theta)]^2 + c[V_p(\beta \sin \theta + \varepsilon \cos \theta)] + d \quad (9-5)$$

For:

$$\beta + \varepsilon = 1$$

$$d \geq 0 \quad \text{For particle breakage (mass leaving a size fraction)}$$

$$d \leq 0 \quad \text{For mass addition (entry of child particles into a size fraction)}$$

Where:

b , c , and d Material-specific, empirically-determined constants

These results are promising, as the number of tests required to characterise a material's particle attrition behaviour can be dramatically reduced. If the impact angle and impact velocity are known for any given impact event scenario, the previously described calibrated curve can be used to determine the magnitude of particle attrition to be expected. The reverse is also true for design purposes; the appropriate impact angle or impact velocity can be selected based on a desired magnitude of particle attrition due to the reversible nature of the calculation. Additionally, the impact velocity can be interpolated using the polynomial curves generated through this modelling approach.

The minimum amount of experimentation recommended for calibration of the model, considering a scenario of 4 particle size fractions, 4 impact angles, and 6 impact velocities, is 15 experiments, as follows:

- Using the first size fraction, undertake tests at 3 particle impact velocities and two different impact angles (preferably an upper, lower and middle particle velocity, and a maximum and minimum impact angle; totalling 6 experiments). The results from these experiments are used to obtain the optimum value of β .
- Then a further 3 experiments at each of the other (thus far untested) particle sizes, for the maximum, minimum and intermediate impact velocities (totalling 9 tests for the present scenario; 3 impact velocities for 3 untested particle sizes).

Now, having obtained the optimised value of β , and the equation of the percent change criterion curve (or magnitude of deviation curve for the material addition scenario) for each particle size, all information is present to predict the magnitude of mass change for any particular size fraction under known conditions. This scenario is compared to the full factorial approach, where the operator would be required to conduct 96 experiments; as was conducted in the present work. It is important to note however, that the more measurements the operator has used to calibrate the model, the better the model fit is expected to be.

The approach taken to develop this model results in two key limitations which need to be considered by the operator. The first is that the particulate material under investigation should not contain any large discontinuities in particle strength distribution. An example of such a discontinuity is in the case of materials which are manufactured under carefully

controlled conditions, resulting in a very narrow particle strength distribution. This would translate to a single impact condition, above which all of the particles would break, and below which, no particles would break. The second is the number of particles used for testing. The sample size should be of the order of tens of thousands of particles to obtain a statistically representative result for each impact condition. Very small test sample sizes could skew the results, thus misinforming the calibration of the model.

When using the model, it is recommended that the operator takes a conservative approach because each material type responds differently to variations in impact; velocity and angle, yet the proposed experimentation requires less than one sixth of the tests of a full factorial investigation. This approach is broadly defined within the present work, as adding a factor of safety which increases the predicted level of particle attrition for given conveying conditions. In the case of Carbolux SK where the breakage behaviour could be satisfactorily described with a negative quadratic, a possible approach is to develop a linear relationship coincident with the maximum and minimum model velocity points (see Figure 9-8). This should overpredict the magnitude of particle attrition to a reasonable degree, while retaining some relevance to the measured particle attrition behaviour.

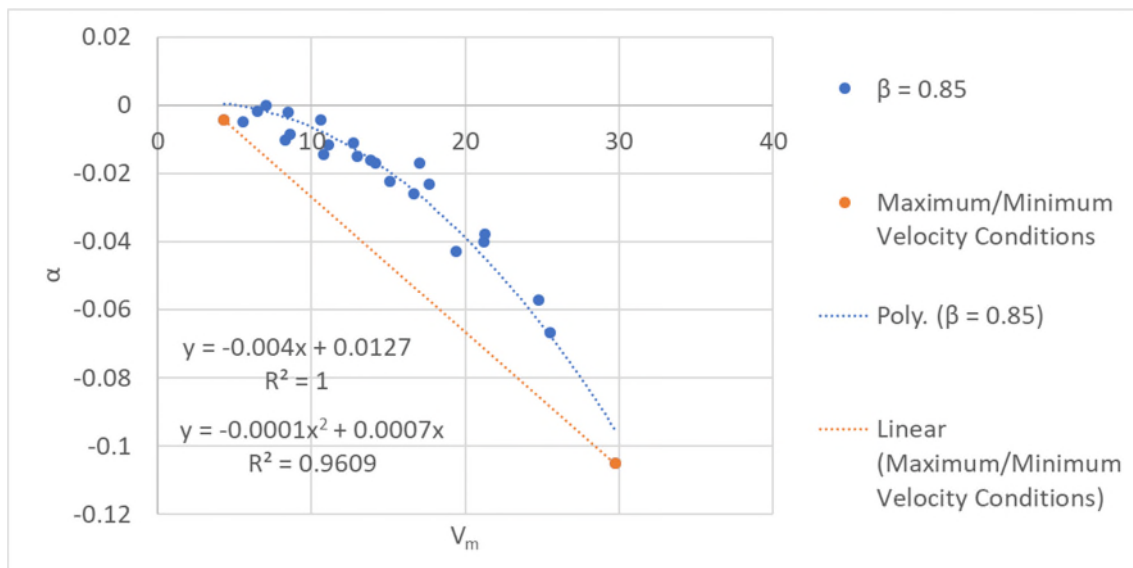


Figure 9-8: Percent Change criterion for the 355-500 μm primary size fraction material, and the application of a linear model (orange) subtending the maximum and minimum velocity conditions tested (orange)

It is not recommended to extrapolate the model outside of the velocity bounds tested; hence the recommendation of testing maximum and minimum particle velocities in the calibration phase of the model.

The same modelling approach proposed above for Carbolux SK shall now be applied to the experimental data reported by Salman et al [117]. Their research used a 'Continuous Flow Gas Gun' shown in Figure 9-9. Aluminium oxide spheres, 5.15 mm in diameter, were tested across a range of impact velocities and impact angles summarised in Table 9-1. Each test condition consisted of a sample size of 100 particles, for which the percent of unbroken particles was determined.

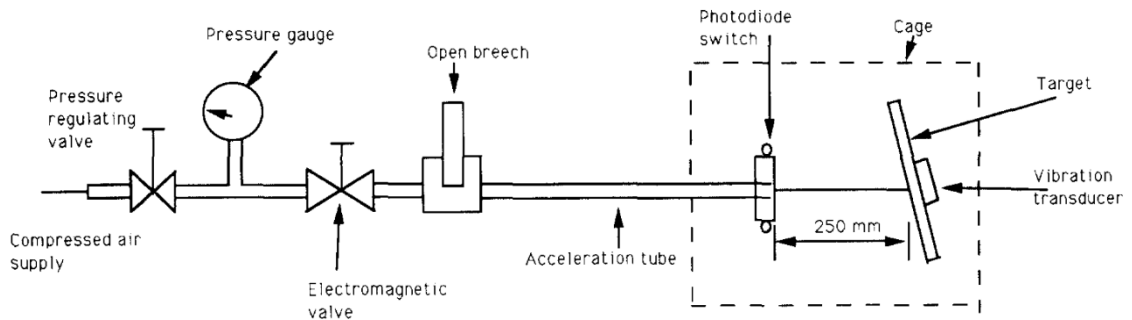


Figure 9-9: The Continuous Flow Gas Gun apparatus, taken from Salman et al. [117]

Table 9-1: Conditions tested by Salman et al. [117] on the Continuous Flow Gas Gun apparatus

Condition	Values Tested
Impact Velocity (m/s)	5 – 35 m/s (approx.)
Impact Angle (degrees)	90, 80, 70, 60, 50, 40, 35, 30, 20

The raw results have been collated into a single diagram, Figure 9-10, with each point representing 100 test particles. The results reported by Salman et al. [117] were recalculated to represent the magnitude of deviation for each data point. In this case, because all particles were of the same virgin size, the magnitude of deviation was equivalent to the percentage change criterion. Some inaccuracies are present in the data set in Figure 9-10, as the data was adapted from graphical sources.

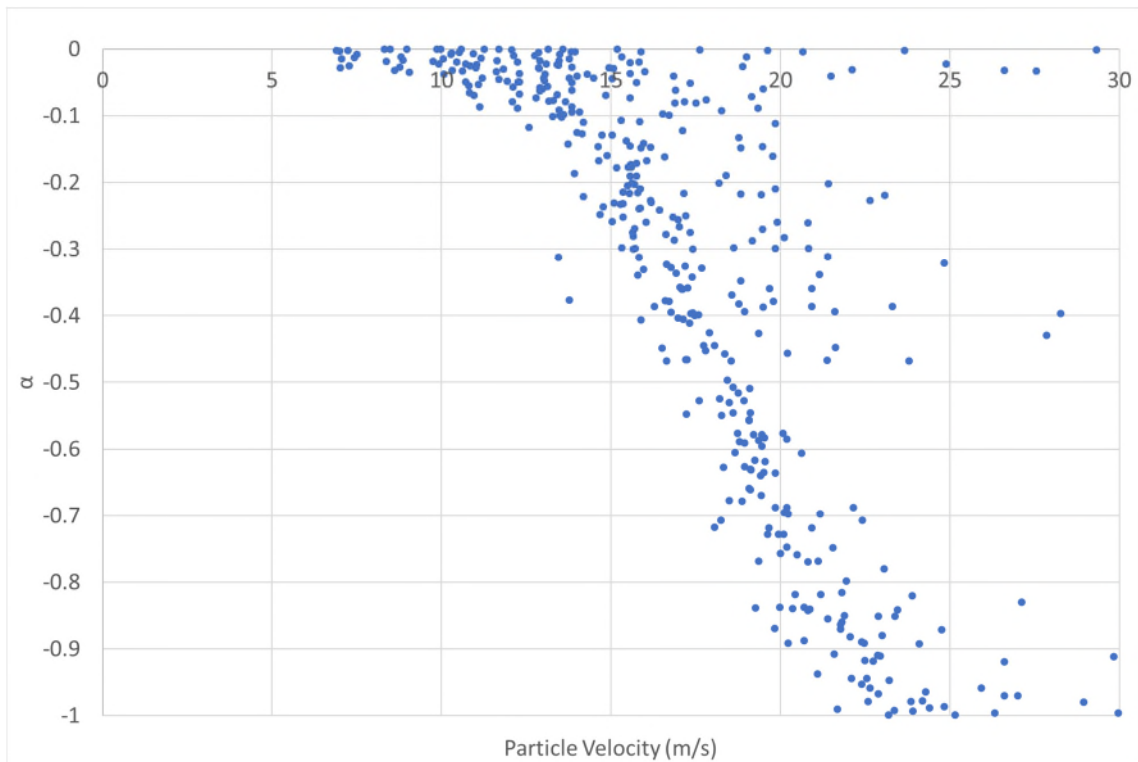


Figure 9-10: All collated data points presented by Salman et al. [117]

Through following the same steps as with the Carbolux SK, a polynomial trendline was fitted to the data for a wide range of values of β . The resulting R^2 values are given in Figure 9-11. The same general relationship between R^2 and β was observed for both Carbolux SK and the Aluminium Oxide material types. However, where the optimal value of β for Carbolux SK was 0.85, the optimum value for Aluminium Oxide spheres was 0.8. Qualitatively, this implies that the tangential component of the impact velocity contributes more to particle attrition in the Aluminium Oxide, in comparison to the Carbolux SK. In addition to this, the optimised value of β returns an R^2 value of 0.8549, as opposed to the values greater than 0.95 achieved for Carbolux SK. The value of R^2 achieved at the optimised values of β indicates the overall appropriateness of the model to the data set. This shall be further discussed in the proceeding paragraphs.

To better understand how the data sets are distributed, Figure 9-12 shows the $\beta = 0.8$ condition, with each of the impact angles distinguished by colour.

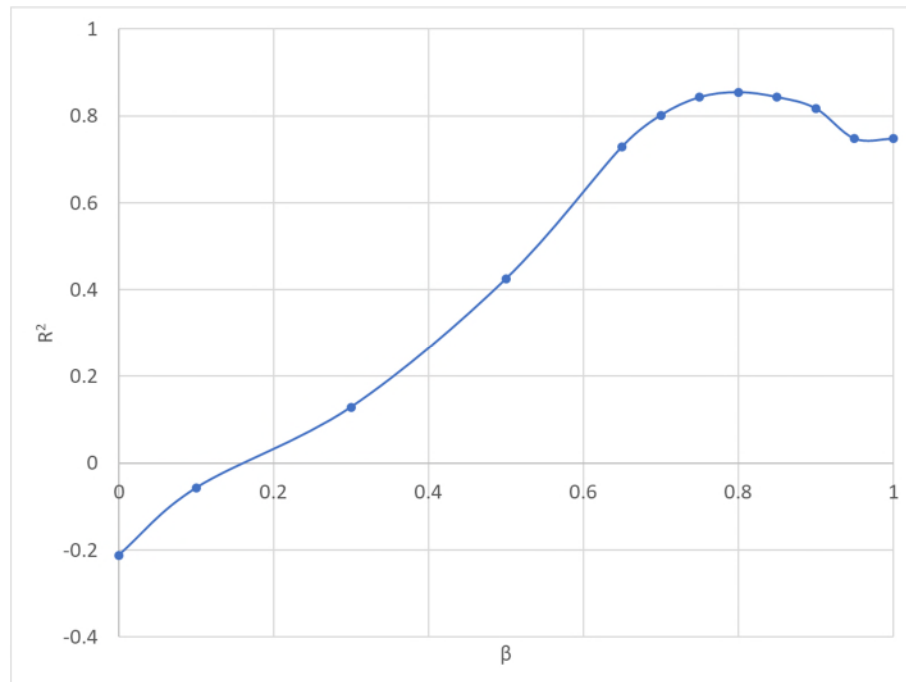


Figure 9-11: R^2 values to fitted polynomial trendlines to the data presented in Figure 9-10 for various values of β

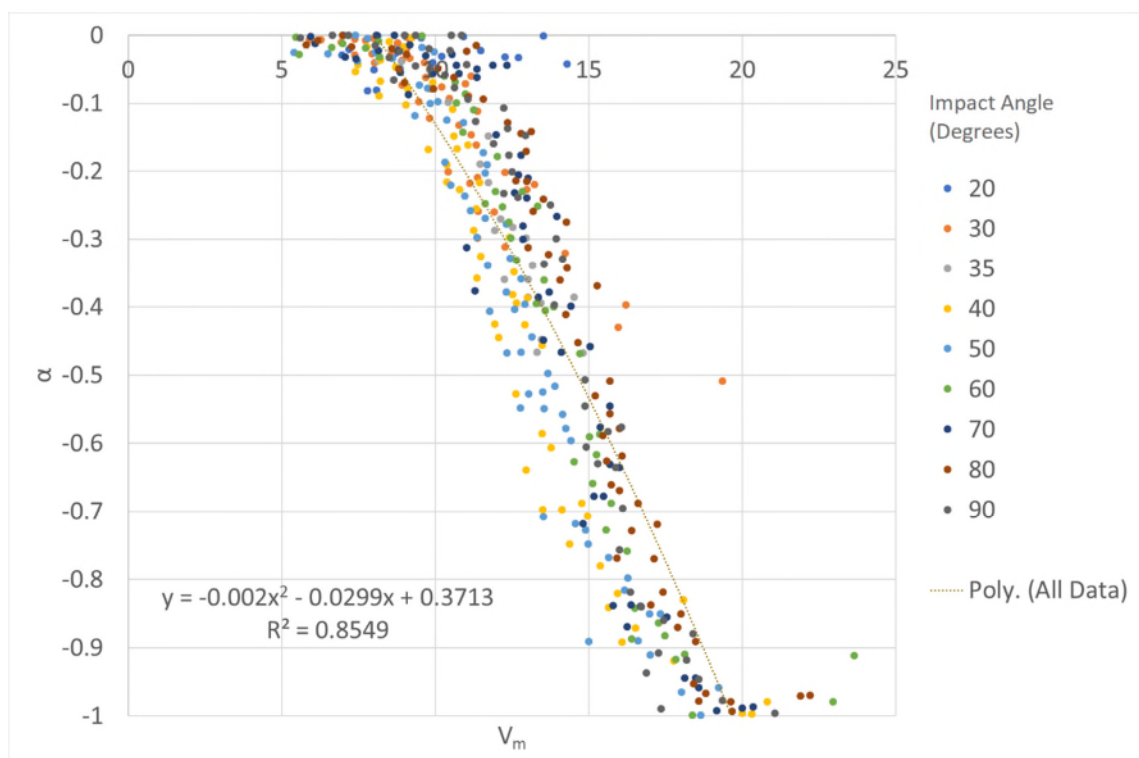


Figure 9-12: Full data set as presented by Salman et al. [117] modelled with a $\beta = 0.8$ condition, and data points coloured by impact angle.

While the spread of data points in Figure 9-12 is significantly narrower than that seen in Figure 9-10, there still appears to be a degree of data segregation based on impact angle. The lower impact angles form the majority of data to the right of the trend line (for example, see the 30 degree impact angle data set). The 40 degree and 50 degree impact angles clearly form a considerable proportion of data points to the left of the trendline. Other angles, such as the 90 and 80 degree data sets, appear to cross the trendline midway (around $\alpha = -0.5$). It is clear the proposed model is unable to fit the data to the same level of accuracy by comparison with the Carbolux SK material type.

There are some key considerations to be made when judging the appropriateness of the data reported by Salman et al. [117] to the proposed model. These are summarised as follows and contradict the recommendations for the application of the modelling method previously detailed:

1. The particle strength distribution demonstrated for the aluminium oxide is considerably narrower than that of the Carbolux SK. Reasons for this could include the considerable difference in virgin particle diameter (in the order of 10:1).
2. The sample size for each data point consisted of only 100 particles. This is contrasted with the estimated 170 thousand to 1.36 million particles that formed the sample size in the BSPAT experiments.
3. The criteria considered for breakage was qualitative, and subject to human error. Considering the small sample size, judgements made by the experimentalist could have had considerable effects on the results reported.

It should be noted that the results presented by Salman et al. [117] are not representative of the scale of particle attrition expected within industrial systems. If an operator's objective is to minimise the magnitude of particle attrition within a process, the processed particles should never be 100% broken. Typically, it is more useful to be able to predict the conditions required for an acceptable maximum magnitude of particle attrition, around which handling equipment can be designed.

Breakage of the entire particle sample was not achieved for the Carbolux SK, hence the rationale for applying a second power polynomial to the data. In the case of the aluminium oxide data, an exponential sigmoid would better agree with the data set. In this case, Equation (9-4) becomes Equation (9-6).

$$\alpha = \frac{b}{1 + e^{\left[\frac{-(V_m - c)}{d}\right]}} \quad (9-6)$$

Substituting Equation (9-2):

$$\alpha = \frac{b}{1 + e^{\left[\frac{-(V_p(\beta \sin \theta + \varepsilon \cos \theta) - c)}{d}\right]}} \quad (9-7)$$

For:

$b = -1$ For particle breakage (mass leaving a size fraction)

$b = 1$ For mass addition (entry of child particles into a size fraction)

Where:

e Euler's Number

c and d Material-specific, empirically-determined constants

To optimise the exponential sigmoid equation fit to the data of Salman et al. [117], a Matlab code was developed (see Appendix I), that tested a wide range of values of c and d against the resulting value of the coefficient of determination, R^2 (available in Appendix I). The results of this analysis are presented in Figure 9-13, for values of $c = 14.3$ and $d = 1.79$, achieving a coefficient of determination of $R^2 = 0.904$. This was a significant improvement over the fit of the previous second power polynomial.

To then compare the appropriateness of the sigmoid curve for Carbolux SK, the data from Figure 9-1 was processed with the aforementioned Matlab code, yielding the relationship shown in Figure 9-14. Optimised values of $c = 30$ and $d = 8.25$ resulted in a coefficient of determination of $R^2 = 0.978$. This fit was not as good as that achieved by the second power polynomial, however still sufficient for interpolative purposes.

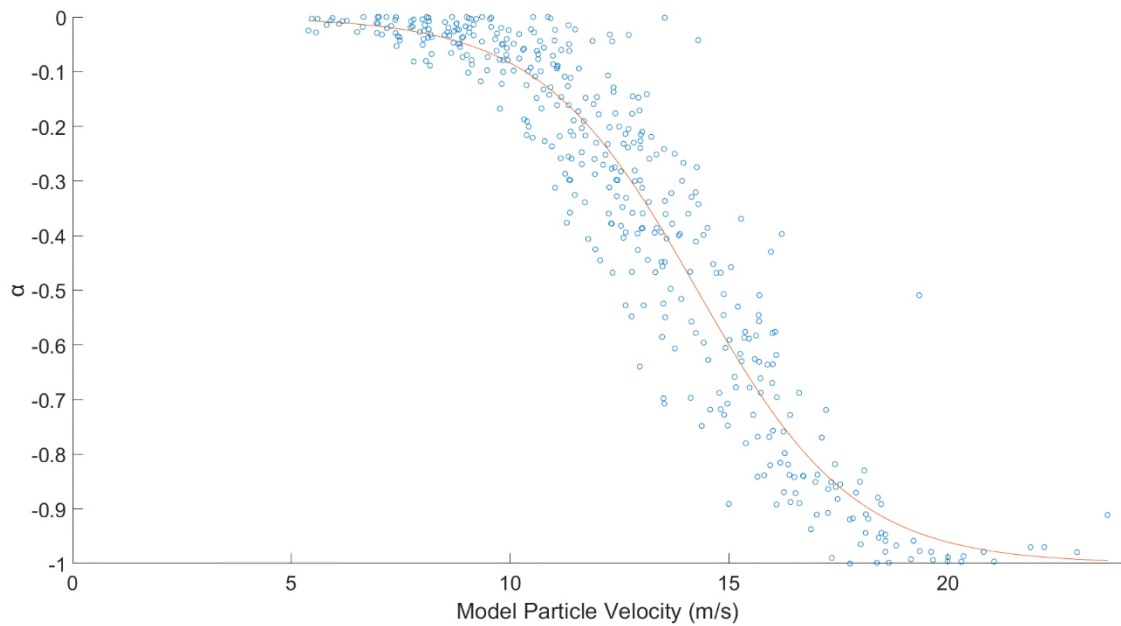


Figure 9-13: The optimised fit of an exponential sigmoid curve to the data reported by Salman et al. [117]

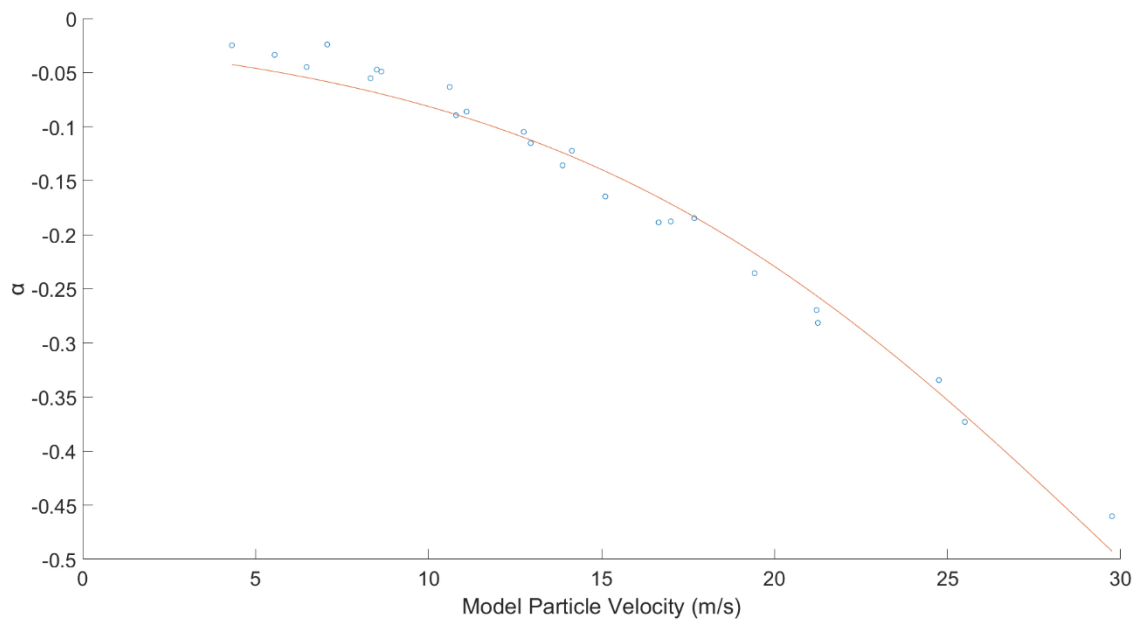


Figure 9-14: The optimised fit of an exponential sigmoid curve to the Carbolux SK breakage data from Figure 9-1.

It should be noted that the application of an exponential sigmoid curve has some repercussions as to the physical meaning behind the model approach. These issues can be summarised as follows:

1. The y-intercept will always be negative for particle breakage, and positive for mass addition (to smaller sieve sizes), as is the nature of this relationship. This means that particle breakage events will always be predicted for 0 m/s impact velocities.
2. In conjunction to the previous point, the model would be unable to predict the particle velocity at which no particle breakage occurs for any impact angle. The x-axis and the line $y = -1$, are asymptotes for the exponential sigmoid, and therefore cannot mathematically describe the 'no breakage' and 'total breakage' conditions.

Based on these observations, the exponential sigmoid approach appears to be applicable for determining the level of particle attrition for conditions where there is no breakage or total breakage. As shown in Figure 9-13 the exponential sigmoid approach achieved a better fit with the data set reported by Salman et al. [117], but was less appropriate for the data obtained for the Carbolux SK.

Finally, in light of the results of the application of the model to the aluminium oxide data, the previously recommended approach to adding a safety factor to the model must be revisited. This was previously defined by a linear relationship coincident with the maximum and minimum model velocity value data points (see Figure 9-8). For the case where a test condition is reached whereby all sample particles are broken ($\alpha = -1$), a linear relationship coincident with the lowest model velocity data point, and the data point which minimises the gradient of the resulting linear relationship. This recommendation, along with the previous recommendation are given visually in Figure 9-15.

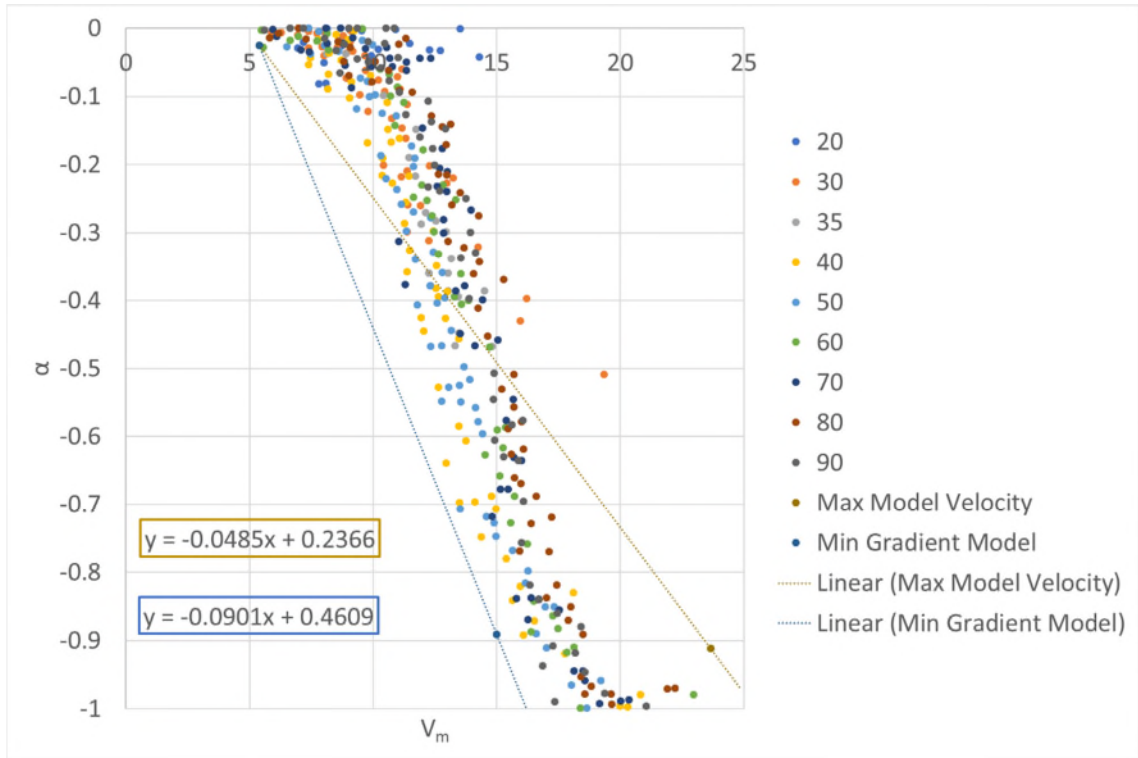


Figure 9-15: Application of different linear fitting models to add a conservative factor to particle attrition predictions in the event of inadequate data

It is evident from the qualitative relationships in Figure 9-15, that the minimum gradient approach delivers a more conservative response for materials where the total breakage scenario is achieved ($\alpha = -1$). The minimum gradient approach could be applied to all data sets, and in fact, returns the same trend in the Carbolux SK data. Therefore, in consideration of the applicability of the two models, the minimum gradient model described above is recommended above the maximum velocity model to determine the conservative particle breakage envelope to inform qualitative design conditions.

9.1.1 Conclusions

A modelling method has been proposed to interpolate the conditions tested on the Bench Scale Particle Attrition Tester for the Carbolux SK material type. With a fraction of the tests required to calibrate the model for a given material type in comparison to a full factorial approach, this model make particle attrition testing accessible for use within practical time and resource constraints.

The derivation of the modelling approach indicated that the particle failure due to impact at an angle other than normal to the target surface, was a combination of the applied compression and shear loads. Furthermore, this model gives a quantitative measure of the relative influences of the particle velocity components normal and parallel to the impact surface through the value of the Velocity Combination Ratio, β .

The modelling approach was then applied to the particle attrition data reported by Salman et al. [117] for aluminium oxide spheres. The relationship previously observed between the R^2 of a fitted polynomial curve and the value of β showed the same general form as that observed for the Carbolux SK. This was significant, as both materials indicated that there existed a single, optimum value of β : 0.85 for Carbolux SK and 0.8 for aluminium oxide spheres. The quality of the model fit was not as good as that achieved for the Carbolux SK, nonetheless, progress was made in terms of normalising the data set with respect to model velocity.

The Velocity Combination Ratio model proposed in this work has been demonstrated to provide promising relationships between particle velocity across the full spectrum of particle impact angles. Further work is required to widen the diversity of material types to determine the full extent of success this model has in reconciling particle attrition across different impact conditions.

9.2 Modelling the Relationship between Particle Attrition Behaviour in the BSPAT and the SBAT

The Single Bend Attrition Tester was designed with the intention of characterising the influence of particle concentration on the measured particle attrition behaviour. However, this apparatus was also a means of scaling the particle attrition behaviour characterised in the Bench Scale Particle Attrition Tester, to that observed in an intermediate-scale pneumatic conveyor. Whilst the mechanism causing particle attrition was equivalent between the testers, the distribution of impact velocities and impact angles was not.

The use of the electrostatic particle velocity sensor on the SBAT gave a mean particle velocity in the final 500 mm of the pre-bend straight pipeline. These velocity values were assumed to be representative of the particle velocity distribution in the entry condition to the pipe bend, and therefore used as the average particle impact velocity.

The particle impact angle however, presents a more difficult variable to define. This is due to the double curvature of the inside surface of the conveying pipe. Three approaches shall be taken to model this impact condition:

1. Angle of the pipe wall in the bend that is coincident with the central axis of the preceding straight pipe. This approach assumes that the particles are fully decoupled with the gas phase, and uses the centre of the impact zone (as viewed from the bend entry) as an approximation of the overall particle impact angle distribution.
2. The approach defined by Hanley [178], whereby the mean impact angle is calculated numerically by considering the straight-line trajectories of all particles assumed to be travelling parallel to the preceding straight-pipe section, and subsequently decouple with the gas-phase upon entry to the bend. This approach considers the full distribution of particle impact angles and results in a numerical mean.
3. The application of coupled CFD-DEM (Computational Fluid Dynamics – Discrete Element Method) modelling approaches to generate a particle impact angle distribution, from which the numerical mean can be derived. This does not assume that the solid and gas phases are decoupled upon entry to the bend.

Due to the clarity of the data obtained for the Carbolux SK Type C, and the breakage results of the 710-1000 μm primary size fraction in the BSPAT, these data sets shall be used to scale between the BSPAT and the SBAT. The raw data for all test conditions is presented in Figure 9-16.

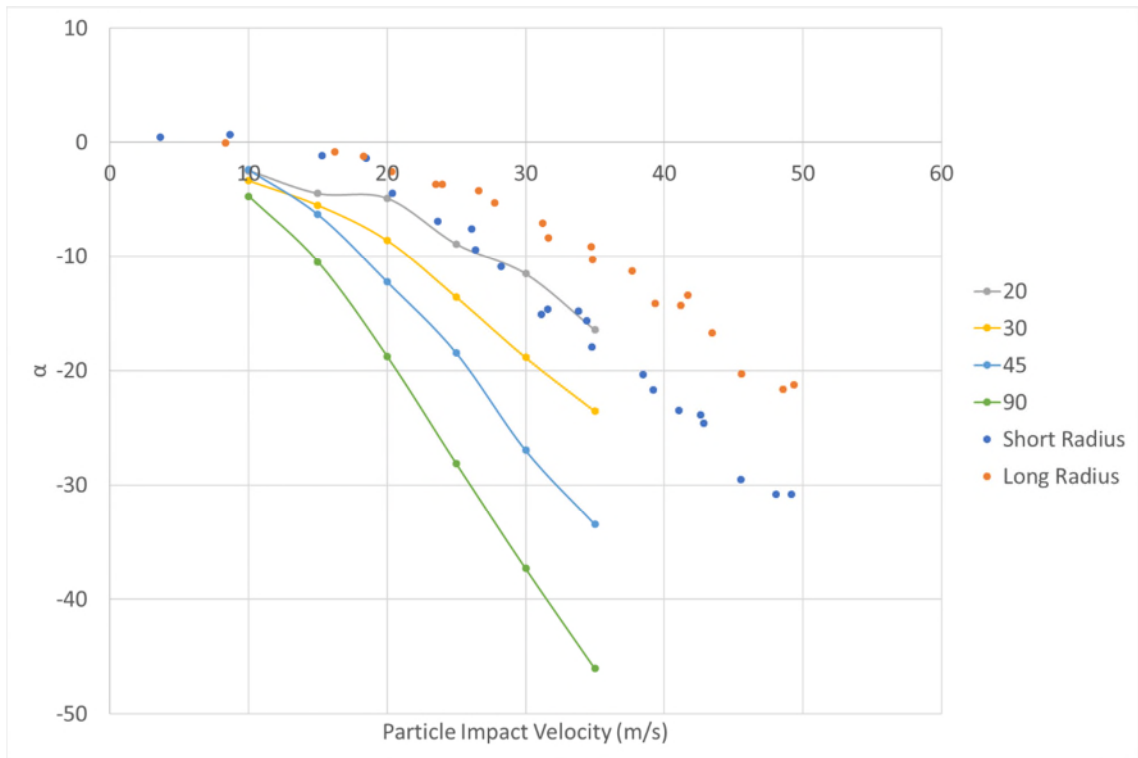


Figure 9-16: All data obtained for breakage of 710-1000 μm primary size fraction Carbolux SK in the BSPAT for specified impact angles (data points and lines); and data from the SBAT with specified bend radius (data points only)

The Velocity Combination Ratio (β) method was applied to the data sets shown in Figure 9-16. To maintain the physical meaning behind the method (as a fundamental descriptor of the material response to compressive and shear loads), $\beta = 0.85$ was used for all data sets.

9.2.1 Pipe Centreline Particle Impact Angle

This approach defines the simplest method within the present work to determine the mean particle impact angle within a pneumatic conveying bend. The approach is visualised in Figure 9-17 and the calculation is given in Equation (9-8). The results of this analysis for the short radius bend was a mean impact angle of 31.0 degrees; and for the long radius bend, a mean impact angle of 16.3 degrees.

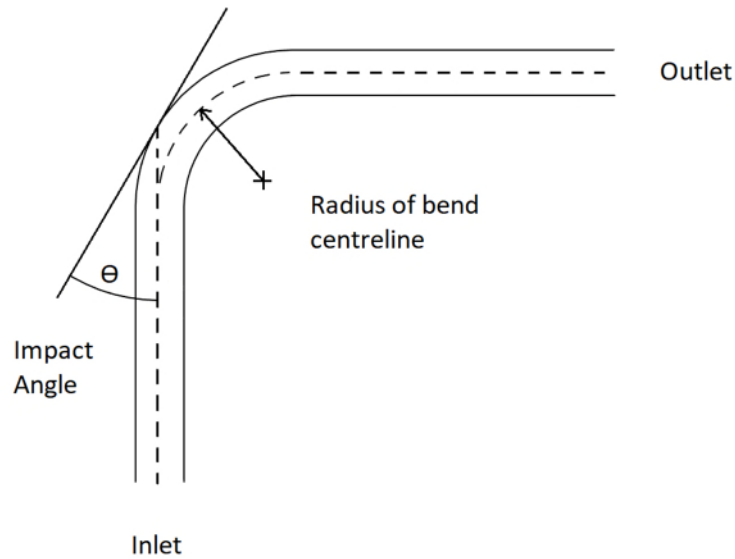


Figure 9-17: Schematic of the calculation of the mean particle impact angle through the intersection of the inlet pipe axis projected to the outer wall of the pipe bend

$$\theta_m = \frac{\pi}{2} - \sin^{-1} \left(\frac{r_b}{r_b + r_p} \right) \quad (9-8)$$

Where:

θ_m Pipe centreline impact angle (radians)

r_b Radius of the bend centreline (m)

r_p Internal radius of the pipe (m)

Through applying the Velocity Combination Ratio method, and using the previously specified mean particle impact angles for their respective bend types, Figure 9-18 was produced.

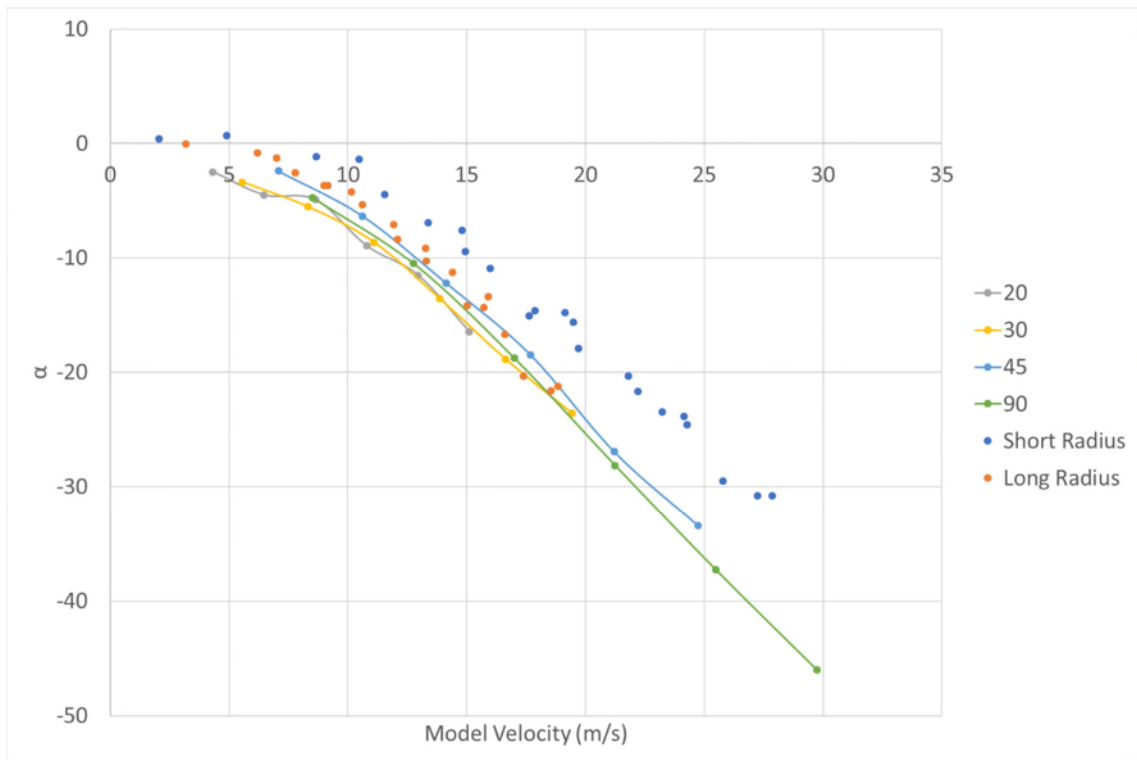


Figure 9-18: Results of the Velocity Combination Ratio method, as applied to the data in Figure 9-16, where $\beta = 0.85$, and the impact angles approximated for the long radius and short radius bends were 31.0 and 16.3 degrees respectively.

Upon inspection of Figure 9-18, it can be seen that the modelling approach provides a relatively close prediction of particle attrition in the long radius bend, albeit slightly conservative. However, when considering the fit of the model to the short radius bend, the model is very conservative, overpredicting breakage by a value of α of -14.9 for the same model velocity.

A potential reason for this is that by decoupling the particles from the gas phase upon entry to the pipe bend, the particles are expected (within the model) to impact the pipe wall at a higher impact angle than the real situation. As the particles enter the bend, the velocity vector of the gas phase begins changing in the direction of the bend outlet. As the gas phase undergoes this change of direction, the applied drag force on the solid

phase also undergoes the same transformation. In the short radius bend, the velocity vector of the gas phase is expected to change more rapidly (due to the reduced residence time in the short radius bend in comparison to the long radius bend), and therefore expected to apply a higher drag force component transverse to the pipe.

9.2.2 Straight Line Projection Mean Particle Impact Angle

This approach for defining the mean particle impact angle within each pipe bend type requires a numerical approach to integrate across the entire projected area of the inlet pipe as the impact surface. The equations required to calculate the probability density function of impact angle were described by Hanley [178], and are given in Equation (9-9), Equation (9-10), and Equation (9-11).

$$\theta_c = \cos^{-1} \left(\frac{1}{1 + \frac{R - r_p}{R_b}} \right) \quad (9-9)$$

$$\theta_{max} = \cos^{-1} \left(\frac{1 - \frac{R - r_p}{R_b}}{1 + \frac{R - r_p}{R_b}} \right) \quad (9-10)$$

$$P(\theta) = \frac{2 \sin \theta}{\pi (R - r_p)^2} \sqrt{[R - r_p - R_b + (R_b + R - r_p) \cos \theta](1 - \cos \theta)(R_b + R - r_p)^{\frac{3}{2}}} \quad (9-11)$$

For:

$$0 \leq \theta \leq \theta_{max}$$

Where:

θ	Particle impact angle (radians)
θ_c	Centreline impact angle (radians)
θ_{max}	Maximum impact angle (radians)
$P(\theta)$	Probability density function of impact angle
R	Pipe radius to outside surface (m)
r_p	Pipe thickness (m)
R_b	Bend Radius to pipe centreline (m)

Hanley concluded that through analysis of the results of the above equations, the mean impact angle correlated to a ratio of the centreline impact angle, described by Equation (9-12). This equation was used to determine the mean impact angles for the short and long radius bends, which resulted in angles of 29.9 degrees and 15.7 degrees respectively. Figure 9-19 shows the results of the Velocity Combination Ratio analysis on the experimental data of the present research.

$$\mu_{\theta} = 0.965\theta_c \quad (9-12)$$

Where:

μ_{θ}	Mean particle impact angle (radians)
----------------	--------------------------------------

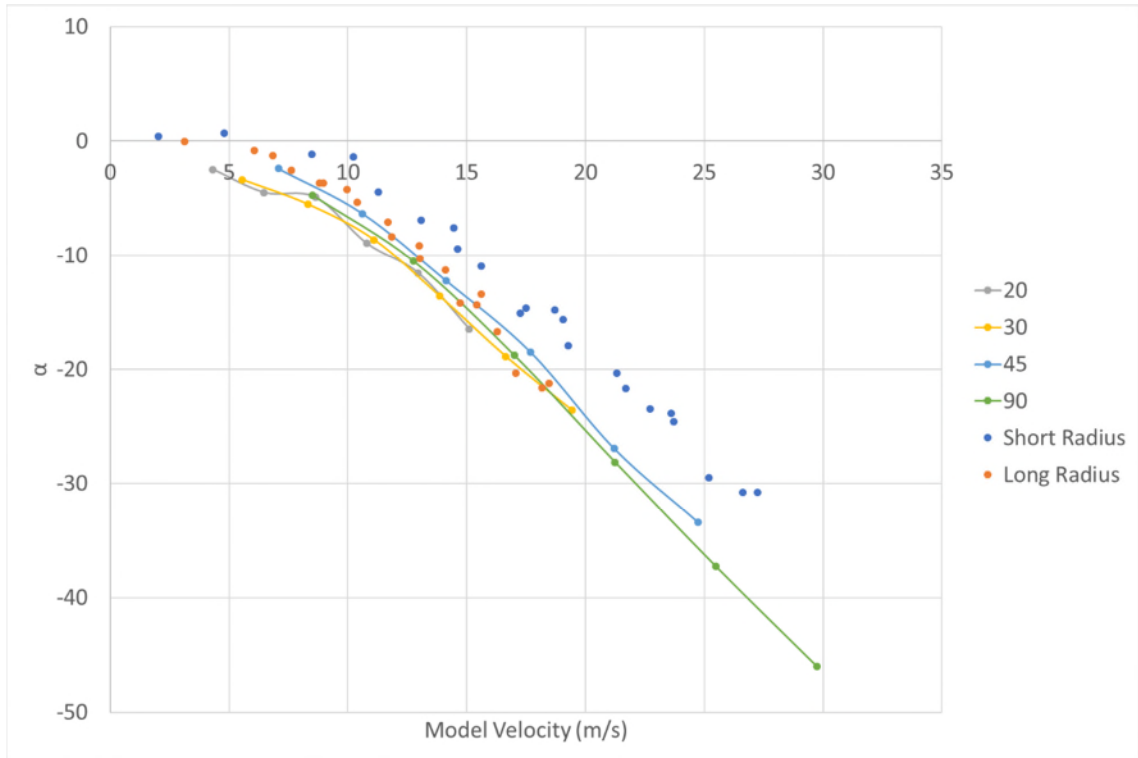


Figure 9-19: Results of the Velocity Combination Ratio method, as applied to the data in Figure 9-16, where $\beta = 0.85$, and the impact angles approximated for the long radius and short radius bends were 29.9 and 15.7 degrees respectively.

As was observed in the results given in Figure 9-18, the results obtained by using the mean particle impact angle, largely overpredict the amount of particle attrition in the SBAT for the short radius bend. The long radius bend results appear to be well approximated by the trends obtained from the BSPAT.

The explanations for the discrepancies in the short radius bend predictions made in Section 9.2.1, are also applicable to the current scenario. This is due to the assumed decoupling of the solid and gas phase upon entry to the bend section.

9.2.3 Definition of Particle Impact Angle Distribution by CFD-DEM Simulation

The third method for determination of the mean particle impact angle within each conveying bend type was the coupling of CFD and DEM simulations to model the primary impact angle distribution for a sample of conveyed particles (performed by Miguel Angel

Romero-Valle, BASF SE). The theory behind the simulation setup is available in the work of Kloss et al. [236] and Goniva et al. [237].

To reduce the computational expense of the simulation, the steady-state flow characteristics for the two-phase flow were determined by simulating a 1 m length of conveying pipe, where the particles loop from the output of the 1 m conveying length, back to the input of the simulated section. In this way, the conveying conditions at the end of the simulated section become the input conditions in a real-time scenario. This simulation was left to run until a steady-state flow condition was achieved. This steady-state flow condition was used as the input conditions for the inlet to the pipe test bend.

An example of the primary impact angle data of the simulations is summarised in Figure 9-20 for the short radius bend. The mean particle impact angle within the short radius bend was approximately 22 degrees, and 12 degrees for the long radius bend.

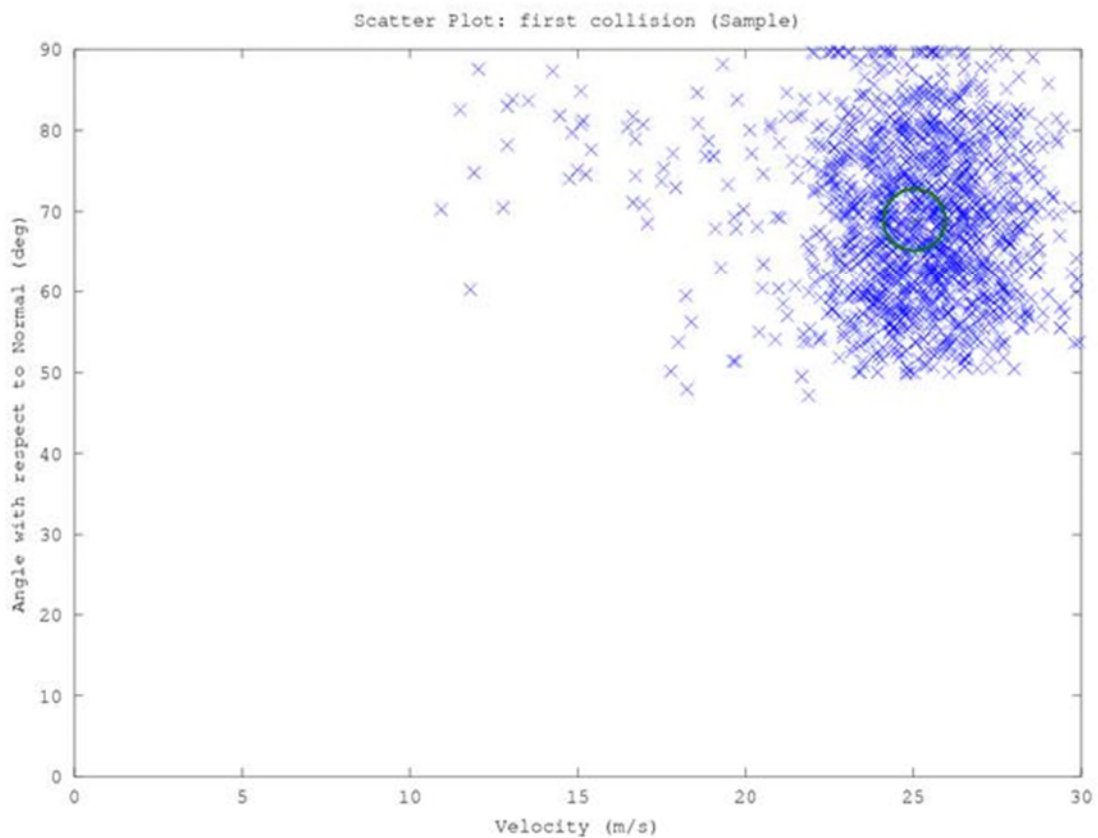


Figure 9-20: Particle impact angle data obtained from CFD-DEM simulations with a particle velocity of approximately 26 m/s and a solids concentration of 0.38 kg/m³

The Velocity Combination Ratio modelling method was applied with the mean particle impact angles obtained from the CFD-DEM simulations above, resulting in Figure 9-21.

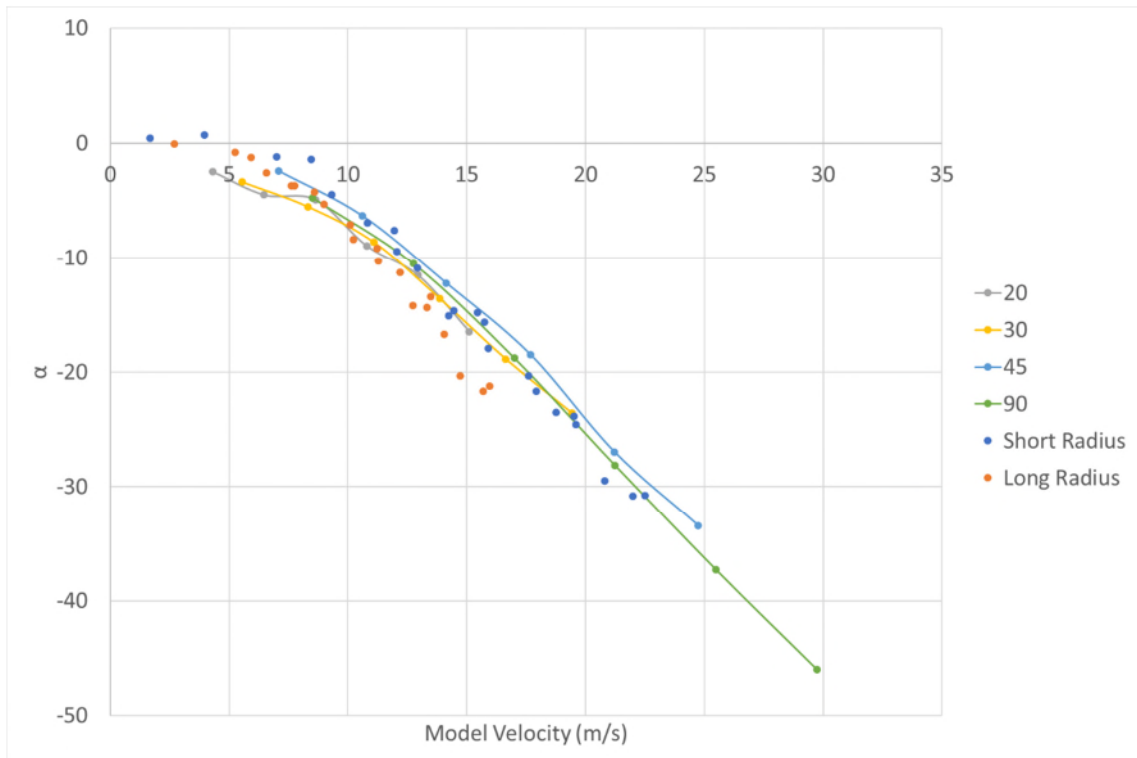


Figure 9-21: Results of the Velocity Combination Ratio method, as applied to the data in Figure 9-16, where $\beta = 0.85$, and the impact angles approximated for the long radius and short radius bends were 29.9 and 15.7 degrees respectively.

Upon inspection of the modelling results, the data for the short radius bend appears to fit the BSPAT data very well. In contrast to this, the results from the long radius bend are now under-predicted by the BSPAT data.

The primary particle-wall contact within the short radius bend was expected to dominate the magnitude of particle attrition measured in the SBAT results. This was due to a relatively rapid change in direction, where particles would be significantly slowed by the first impact; secondary and tertiary impacts would then be negligible in comparison. Considering that the CFD-DEM simulation only recorded the first particle-wall impact within the simulation, the mean simulated particle-wall impact angle is in very good agreement with the results.

This was not the case with the long radius bend. An explanation for this is that the primary particle-wall impact within the SBAT for the long radius bend did not cause the overwhelming majority of particle damage. Rather, secondary and tertiary impacts may have played a role in the particle attrition within the long radius bend. Such behaviour was not captured in the CFD-DEM simulation, nor the results from the BSPAT.

9.2.4 Conclusions on the Method of Determining the Mean Particle Impact Angle

An in-depth study has been undertaken into the appropriateness of second power polynomials, and exponential sigmoid curves to fit the breakage data obtained in the Single Bend Attrition Tester, based on the breakage characterisation obtained from the Bench Scale Particle Attrition Tester. Three different methods were presented and compared to determine the most appropriate approach for approximating the mean particle impact angle in a conveying pipeline bend. The optimised relationships obtained from the BSPAT data are presented in Table 9-2. The Coefficient of determination obtained by fitting the relevant curve to the data measured from the SBAT is presented in Table 9-3 for the short radius bend, and Table 9-4 for the long radius bend (the graphical representations of which are given in Appendix J). The highest value of the coefficient of determination for each scenario is shaded in grey.

Table 9-2: Optimised relationships obtained from breakage of 710-1000 μm primary size fraction Carbolux SK in the BSPAT

Function Type	Carbolux SK Breakage (from 710 μm sieve)	Carbolux SK Addition (into 180 μm sieve)
Polynomial (2 nd Power)	$\alpha = -0.0004V_m^2 - 0.006V_m + 0.0209$ $R^2 = 0.9923$	$\alpha = 0.00002V_m^2 - 0.0001V_m$ $R^2 = 0.9756$
Exponential Sigmoid	$\alpha = \frac{-1}{1 + e^{\left[\frac{-(V_m-30)}{8.25}\right]}}$ $R^2 = 0.978$	$\alpha = \frac{1}{1 + e^{\left[\frac{-(V_m-63.1)}{7.68}\right]}}$ $R^2 = 0.98$

Table 9-3: Coefficient of determination of SBAT data (Type C Carbolux SK) modelled with different mean impact angle calculations and nature of fitted relationships for the short radius bend

Method of Mean Impact Angle Determination	Carbolux SK Breakage (from 710 μm sieve)		Carbolux SK Addition (into 180 μm sieve)	
	Polynomial (2 nd Power)	Exponential Sigmoid	Polynomial (2 nd Power)	Exponential Sigmoid
Pipe Centreline	0.236	0.532	0.306	0.918
Pipe Projection	0.395	0.684	0.48	0.922
CFD-DEM Simulation	0.968	0.912	0.915	0.437

Table 9-4: Coefficient of determination of SBAT data (Type C Carbolux SK) modelled with different mean impact angle calculations and nature of fitted relationships for the long radius bend

Method of Mean Impact Angle Determination	Carbolux SK Breakage (from 710 μm sieve)		Carbolux SK Addition (into 180 μm sieve)	
	Polynomial (2 nd Power)	Exponential Sigmoid	Polynomial (2 nd Power)	Exponential Sigmoid
Pipe Centreline	0.83	0.826	0.91	0.704
Pipe Projection	0.87	0.833	0.939	0.662
CFD-DEM Simulation	0.909	0.741	0.809	0.352

Based on the values of the coefficient of determination across each of the conditions in the above tables, the short radius bend is best modelled with a polynomial fit using the CFD-DEM-determined value of the mean angle of particle impact. The long radius bend is best modelled using a polynomial fit, with the mean particle impact angle determined by the projection of the pipe cross-section.

CHAPTER 10: Conclusions and Further Work

This chapter shall summarise each of the findings and conclusions resulting from the present research. Subsequently, recommendations for areas requiring further research are outlined, and placed within the context of the present work.

A brief summary of the conclusions of this research is as follows, with each of the research objectives addressed in turn.

1. Particle concentration was found to have a negligible effect on the magnitude of particle attrition measured within homogeneous lean phase horizontal pneumatic conveying systems.
2. An improved apparatus was developed for the characterisation of particle attrition behaviour due to a single impact. Insight into the design philosophy of such apparatus was given.
3. Two models were proposed;
 - a. A thought-model to explain the apparent manifestation of a 'shielding effect' in industrial-scale pneumatic conveying systems, and lack of such observations in the Single Bend Attrition Tester
 - b. A Velocity Combination Ratio Model, which reconciled the breakage behaviours in the Bench Scale Particle Attrition Tester and the Single Bend Attrition Tester; requiring a considerably-reduced particle attrition characterisation test programme.

10.1 Conclusions of the Research

The conclusions of the present research shall be addressed in terms of the objectives described in Chapter 3.

The first objective of this research was to determine the influence of particle concentration on the magnitude of particle attrition measured in a homogeneous lean phase pneumatic conveying system. This was achieved through the development of a new test apparatus,

and subsequent application of existing research (as referenced in Chapter 8) to the phenomenon.

In order to determine the influence of particle concentration on the measured level of particle attrition in a homogeneous lean phase pneumatic conveying system, the Single Bend Attrition Tester was designed, built and commissioned. This apparatus was capable of measuring the pre-bend particle velocity, in addition to the air mass flow rate within the pipeline. Indirect measurements of the particle concentration at the bend inlet thus enabled the decoupling of particle velocity influences from particle concentration influences.

A full factorial set of single bend attrition tests were undertaken across the testable range of variables (controlling the mass flow rate of solids with orifice plates at the hopper outlet), for two different particle size distributions of Carbolux SK (Type B and type C). The data was analysed by mapping the magnitude of particle breakage with respect to the pre-bend particle concentration, and pre-bend mean particle velocity; subsequent annotation with contour lines specified locations with the same magnitude of particle breakage. In analysing the data obtained from this programme of experimentation, it was determined that particle concentration at the inlet to the bend of the pneumatic conveying line had negligible influence on the magnitude of particle attrition observed. This was true when particle attrition was measured in terms of the breakage of large particles (measured by loss in mass from a specified sieve), and in terms of the generation of smaller particles as a results from fragmentation events (measured by increase in particle mass retained on a specified sieve). The results obtained from the short radius bend more clearly demonstrated the lack of any influence of particle concentration on the magnitude of particle attrition in terms sample mass loss from the size fraction under scrutiny, in comparison to that observed from the long radius bend. However, both bend radii clearly demonstrated negligible influence of particle concentration on the magnitude of particle attrition measured in terms of material addition to 180 μm sieve.

It was noted that the single bend attrition tester (SBAT) was an ideal system where the conveying characteristics could be closely monitored. This was contrasted to the results obtained in two industrial-scale pneumatic conveying systems. Both industrial-scale systems displayed 'shielding-like' behaviour whereby increases in particle concentration resulted in decreased levels of particle attrition for similar superficial air velocity

conditions. An in-depth analysis of the two-phase flow conditions occurring in each pipeline was presented. The conclusions from this comparative study, was that the reduction in particle attrition within the industrial-scale systems could be attributed to differences in mean particle velocities. The Wolfson Centre System used a larger pipe diameter than what was tested in the SBAT; and the External Pneumatic Conveying System use shorter straight pipeline lengths to separate successive bends in comparison to that tested in the SBAT. Therefore, an exaggeration in particle velocity across the pipeline cross-section and non-fully accelerated particle velocities at the pipe bend inlets were proposed to explain the observations within the respective apparatuses.

The second objective of this research was to evaluate current particle attrition behaviour characterisation methods, and if required, develop a new/improved method. This objective was achieved through the development of an improved particle attrition characterisation tester, and a method was proposed to simplify the experimental programme required to characterise the particle attrition behaviour of any given sample.

An extensive review of the literature was conducted with respect to the existing methods of characterising particle attrition behaviour. It was determined that the centrifugal accelerator-style particle attrition tester was most suited for testing the particle attrition mechanism present in lean phase pneumatic conveyors. The rationale for this was that the centrifugal accelerator-style tester enabled the close control of particle impact velocity and particle impact angle; the most important variables in particle attrition by impact. Two such testers were pre-existing in the Wolfson Centre laboratory, and were compared on a quantitative basis. The Large Scale Particle Attrition Tester yielded results that were well in line with the expectations developed from the theory, however, due to the relatively large flight distance between the accelerating disc and the impact targets, and the fan-like design of the accelerating disc, there was significant scope for air current interaction manipulating the particle trajectory. In addition to the requirement for large sample sizes (not always appropriate when sample material is limited), this tester was deemed inadequate for the present research. The QPM particle degradation tester, was a small, bench-scale design requiring only small sample volumes for each test. However, after an extensive testing programme, it was determined that secondary particle impacts against the outer wall of the impact chamber were significantly altering the results, especially when shallow impact angles ($\Theta \leq 45^\circ$) were tested.

Informed from these results, the Bench Scale Particle Attrition Tester was designed, constructed and commissioned. This apparatus aimed to mitigate the majority of the drawbacks presented by the two previously-mentioned testers. Upon evaluation of a full factorial investigation, the BSPAT was concluded to have improved upon the design of the previous testers. These improvements include:

- Reduction of the influence of secondary and tertiary impacts within the impact chamber
- Improved ease of sample recollection, resulting in:
 - Repeatable measurements of sub 150 μm particles
 - Improved apparatus hygiene
 - High level of results sensitivity with respect to changes in particle impact angle and particle impact velocity
- Closed-loop control of the accelerating disc motor resulting in higher accuracy and consistency of particle impact velocities between tests, and throughout a single test.

Additionally, as shall be addressed in the proceeding paragraphs, the results obtained from the bench scale particle attrition tester (BSPAT) agree well with the single bend attrition test (SBAT) results.

The third primary objective of the research was to develop an empirically-informed model enabling the quantitative prediction of the magnitude of particle attrition inflicted by a homogenous lean phase pneumatic conveying system. This was addressed through the presentation of two components: a modelling method proposed to interpolate between the particle impact velocity and particle impact angle conditions within the bench scale particle attrition tester (BSPAT); and evaluation of appropriate mean particle impact angle attributed to a given pipe bend geometry with subsequent application of the aforementioned model to predict magnitude of particle attrition.

The predictive method proposed for the BSPAT particle attrition behaviour characterisation involved the optimisation of a Velocity Combination Ratio, β . The fundamental function of this ratio is to attribute the proportion of particle breakage due to the shear and compression forces applied to the particle upon impact. It was found that for the range of conditions tested within this research, the value of β did not change for the Carbolux SK across all impact angles and impact velocities tested. This included

particle breakage as measured for mass loss in the 710-1000 μm sieve, and mass addition to the 180 μm sieve (which contained negligible mass in the virgin particle size distribution). Once the value of β had been optimised, a second power polynomial and an exponential sigmoid was fitted to the data. It was concluded that the second power polynomial was more appropriate for modelling the no-breakage and total-breakage conditions in addition to the neighbouring impact conditions. However, for modelling the total particle attrition behaviour throughout the full range of impact conditions from no-breakage to total-breakage, the exponential sigmoid curve was concluded to be more appropriate. This modelling method was found to dramatically reduce the experimental programme required to characterise the particle attrition behaviour for a given material.

To apply the aforementioned modelling method to the data obtained from the single bend attrition test (SBAT), it was necessary to determine the most appropriate criteria to determine the representative particle impact angle for a given pipe bend type. Three different methods of determining this angle were considered the:

- angle subtending the projection of the central axis of the preceding straight pipe section and the tangent of the pipe wall where this projection intersects;
- mean of the impact angle as determined numerically by projecting the entire preceding straight pipe cross section to the internal surface of the bend; and
- mean impact angle as obtained by CFD-DEM simulation.

It was concluded that the best overall method for modelling the Carbolux SK Type C in the SBAT was dependant on the bend radius used. A polymeric fit was most appropriate in all cases. The best method to approximate the mean particle-wall impact angle within the short radius bend was the CFD-DEM approach, while the projection of the pipe cross-section was the best approach for the long radius bend. The proposed reason for this is that the particle attrition attributed to the short radius bend was attributed more to the primary impact (which was modelled by the CFD-DEM approach) than in the long radius bend (where secondary and tertiary impacts played more of a role).

This research has provided a physically sound explanation of the so-called 'shielding effect' where the mitigation of particle attrition in lean phase pneumatic conveying systems is not due to a particle 'cushioning' effect, but rather the alteration of the particle velocity profile across the pipe cross section, and in terms of the particles' ability to accelerate to steady-state conditions. This research has also provided a method whereby

particle characterisation tests can be interpolated for particle impact velocity and particle impact angle, drastically reducing the volume of experimentation required to characterise particle attrition behaviour. This was also extended to a small vacuum conveying system (SBAT) with good agreement, if the mean particle impact angle for the pipeline bend was calculated as described in the preceding paragraph.

The culmination of the findings of this research is believed to be a significant contribution to knowledge and understanding in the characterisation of particle attrition behaviours and their prediction in homogeneous lean phase pneumatic conveying systems.

10.2 Recommendations for Further Work

Throughout the course of the research programme, a considerable number of topics for further investigation were identified. This section shall concisely summarise how each would contribute to the research presented in this thesis.

There remain a large number of uncharacterised variables with respect to the geometry and conveying conditions on the Single Bend Attrition Tester (SBAT), many of which are also required to fully describe industrial-scale systems. The geometrical considerations include that of the pipe diameter. The SBAT is capable of accommodating a 2" and 3" NPS Schedule 40 pipe specification. These pipe diameters could enable the scaling of particle velocity distributions (and subsequently particle attrition behaviours) between the BSPAT and an Industrial-Scale lean phase pneumatic conveying system. With an appropriate sight glass prior to the bend, and a sufficiently high specification of slow motion camera, the particle velocity distribution across the pipe cross section for fully-accelerated flow could be characterised. Again, a wide range of materials would require testing for universally applicable results. It would also be possible with particle attrition testing at these larger pipe diameters, to determine the appropriate calculation for the mean particle impact angle in the bend (should it be any different to that presented in this work for 1.5" NPS Schedule 40 pipe). Finally, the influence of particle concentration on the particle velocity distribution across the pipe cross section, with respect to each of the previous variables could be elucidated, and compared with the hypothesis presented in Chapter 8 of this work. This avenue of further research is the most important in terms of making the present work more relevant to the manifestation particle attrition in industrial-sized pneumatic conveying systems. Once the influence of pipe diameter is ascertained, the mean impact condition for each bend within a given industrial-scale system can be characterised and tested for on the Bench Scale Particle Attrition Tester.

The literature review identified a wide range of particle failure types (such as crystalline, amorphous, and agglomerate failure mechanisms), however, it was not possible to investigate each failure mechanism within the present research programme. It is therefore recommended for further work to investigate further particle types and determine the particle attrition behaviour within the Bench Scale Particle Attrition Tester. This would

further inform the modelling method presented in Chapter 9, and quantify its validity across a range of particle types.

Further experimentation is required to quantify the influence of particle size on the level of attrition for a range of impact conditions. This could be achieved with the BSPAT, experimentation should include particles manufactured to a particular size (such as glass spheres) and particles sieved from a particle size distribution (such as that presented in this work). These two particle groups respectively represent virgin particles which have not been previously broken, and particles which could be child particles from previous breakage events (but also represented particles from a more realistic industrial scenario). The influence of particle size on the particle attrition behaviour of each aforementioned group of particles is key to understanding how particle size affects the magnitude and distribution of particle strengths within a sample of material.

Chapter 2 summarised some of the work by other researchers on the topic of particle fatigue behaviours. The present work should be coupled with an appropriate fatigue model to achieve a realistic prediction of the magnitude of particle attrition in a multi-bend homogeneous lean-phase pneumatic conveying system. As was noted in Chapter 5, the characterisation of particle attrition is specific to the characterisation tester geometry. Therefore, to inform the research presented in this document, fatigue studies should be carried out on the BSPAT.

The particle attrition behaviour as characterised by the BSPAT is not believed to be specific to homogeneous lean phase pneumatic conveying systems. Rather, the characterised behaviour should theoretically be applicable to any scenario where particle attrition is manifested through the impact attrition mechanism. Such scenarios could include the use of impact plates at transfer points between belt conveyors (or other conveyor types) and cyclones used for separation of the gas and solid phases at the end of a pneumatic conveying line. There could even be the possibility of correlating the particle attrition in the BSPAT to that observed in a hammer mill. It is evident that the BSPAT could theoretically be applied to a wide range of particle attrition scenarios, however each requires further work in terms of validation testing.

A final topic for further research is that of acceleration profiles for particulate materials within lean phase pneumatic conveying systems. With the creation of more electrostatic velocity sensors, and the facility to log the significantly larger volume of data, the

acceleration profile of particles along the initial straight pipe section of the SBAT could be measured to a high resolution. The variables of interest to this topic area include particle size, particle size distribution, particle concentration, superficial air velocity and pipe diameter. This would better inform the predictive modelling method presented in the present research, in terms of its application to lean phase pneumatic conveying systems which do not allow sufficient length of straight sections between successive bends in the system for fully-accelerated flow conditions to the proceeding bend inlet. Furthermore, such research would address the hypothesis presented in Chapter 8 regarding a theoretical increase in particle acceleration length for an increase in particle concentration.

CHAPTER 11: References

- [1] C. R. Bemrose and J. Bridgwater, "A review of attrition and attrition test methods," *Powder Technol.*, vol. 49, no. 2, pp. 97–126, Jan. 1987.
- [2] I. M. Hutchings, "Mechanisms of wear in powder technology: A review," *Powder Technol.*, vol. 76, no. 1, pp. 3–13, Jul. 1993.
- [3] G. K. Reynolds, J. S. Fu, Y. S. Cheong, M. J. Hounslow, and A. D. Salman, "Breakage in granulation: A review," *Chem. Eng. Sci.*, vol. 60, no. 14, pp. 3969–3992, Jul. 2005.
- [4] H. Kalman, "Attrition control by pneumatic conveying," *Powder Technol.*, vol. 104, no. 3, pp. 214–220, Oct. 1999.
- [5] H. Kalman, "Attrition of powders and granules at various bends during pneumatic conveying," *Powder Technol.*, vol. 112, no. 3, pp. 244–250, Oct. 2000.
- [6] K. J. Hanley, E. P. Byrne, K. Cronin, J. C. Oliveira, J. a. O'Mahony, and M. a. Fenelon, "Effect of pneumatic conveying parameters on physical quality characteristics of infant formula," *J. Food Eng.*, vol. 106, no. 3, pp. 236–244, Oct. 2011.
- [7] H. Akilli, E. . Levy, and B. Sahin, "Gas–solid flow behavior in a horizontal pipe after a 90° vertical-to-horizontal elbow," *Powder Technol.*, vol. 116, no. 1, pp. 43–52, May 2001.
- [8] W. Yang and B. Kuan, "Experimental investigation of dilute turbulent particulate flow inside a curved bend," *Chem. Eng. Sci.*, vol. 61, no. 11, pp. 3593–3601, Jun. 2006.
- [9] A. D. Salman, M. J. Hounslow, and A. Verba, "Particle fragmentation in dilute phase pneumatic conveying," *Powder Technol.*, vol. 126, no. 2, pp. 109–115, Jul. 2002.
- [10] H. Kalman and D. Goder, "Design criteria for particle attrition," *Adv. Powder Technol.*, vol. 9, no. 2, pp. 153–167, Jan. 1998.
- [11] H. Li and Y. Tomita, "Particle velocity and concentration characteristics in a horizontal dilute swirling flow pneumatic conveying," *Powder Technol.*, vol. 107, no. 1–2, pp. 144–152, Jan. 2000.

- [12] A. Rinoshika, F. Yan, and M. Kikuchi, "Experimental study on particle fluctuation velocity of a horizontal pneumatic conveying near the minimum conveying velocity," *Int. J. Multiph. Flow*, vol. 40, pp. 126–135, Apr. 2012.
- [13] D. G. Papadopoulos and M. Ghadiri, "Impact breakage of poly-methylmethacrylate (PMMA) extrudates: I. Chipping mechanism," *Adv. Powder Technol.*, vol. 7, no. 3, pp. 183–197, Jan. 1996.
- [14] K. R. Yuregir, M. Ghadiri, and R. Clift, "Observations on impact attrition of granular solids," *Powder Technol.*, vol. 49, no. 1, pp. 53–57, Dec. 1986.
- [15] L. Frye and W. Peukert, "Identification of material specific attrition mechanisms for polymers in dilute phase pneumatic conveying," *Chem. Eng. Process. Process Intensif.*, vol. 44, no. 2, pp. 175–185, Feb. 2005.
- [16] K. A. Aarseth, "Attrition of Feed Pellets during Pneumatic Conveying: the Influence of Velocity and Bend Radius," *Biosyst. Eng.*, vol. 89, no. 2, pp. 197–213, Oct. 2004.
- [17] A. . Salman, J. Fu, D. . Gorham, and M. . Hounslow, "Impact breakage of fertiliser granules," *Powder Technol.*, vol. 130, no. 1, pp. 359–366, 2003.
- [18] C. Xu, J. Li, and S. Wang, "A spatial filtering velocimeter for solid particle velocity measurement based on linear electrostatic sensor array," *Flow Meas. Instrum.*, vol. 26, pp. 68–78, 2012.
- [19] J. Li, C. Xu, and S. Wang, "Spatial filtering characteristics of electrostatic sensor matrix for local velocity measurement of pneumatically conveyed particles," *Measurement*, vol. 53, pp. 194–205, 2014.
- [20] Y. Tsuji and Y. Morikawa, "LDV measurements of an air-solid two-phase flow in a horizontal pipe," *J. Fluid Mech.*, vol. 120, pp. 385–409, 1982.
- [21] W. Wei, G. Qingliang, W. Yuxin, Y. Hairui, Z. Jiansheng, and L. Junfu, "Experimental study on the solid velocity in horizontal dilute phase pneumatic conveying of fine powders," *Powder Technol.*, vol. 212, no. 3, pp. 403–409, Oct. 2011.
- [22] I. . Barratt, Y. Yan, B. Byrne, and M. S. . Bradley, "Mass flow measurement of pneumatically conveyed solids using radiometric sensors," *Flow Meas. Instrum.*, vol. 11, no. 3, pp. 223–235, Sep. 2000.

- [23] Z. Chen, C. Jim Lim, and J. R. Grace, "Study of limestone particle impact attrition," *Chem. Eng. Sci.*, vol. 62, no. 3, pp. 867–877, Feb. 2007.
- [24] P. J. Mendies, J. N. Wheeldon, and J. C. Williams, "The Velocity of Granular Material Flowing in a Pneumatic Conveyor," in *Proceedings of Pneumotransport 2 : Second International Conference on the Pneumatic Transport of Solids in Pipes*, 1973.
- [25] M. S. A. Bradley, R. J. Farnish, L. M. Hyder, and A. R. Reed, *Handbook of Conveying and Handling of Particulate Solids*, vol. 10. Elsevier, 2001.
- [26] I. Bridle, "The Analysis of Particle Degradation in Pneumatic Conveyors Utilizing a Pilot-Sized Test Facility," University of Greenwich, 2000.
- [27] M. S. A. Bradley, "Prediction of Pressure Losses in Pneumatic Conveying Pipelines," Thames Polytechnic, 1990.
- [28] P. W. Wypych and P. C. Arnold, "On improving scale-up procedures for pneumatic conveying design," *Powder Technol.*, vol. 50, no. 3, pp. 281–294, May 1987.
- [29] P. W. Wypych, "Pneumatic Conveying of Bulk Solids," University of Wollongong, 1989.
- [30] C. Ratnayake, "A Comprehensive Scaling Up Technique for Pneumatic Transport Systems," The Norwegian University of Science and Technology, 2005.
- [31] N. Santo and H. Kalman, "Blinded T-bends flow patterns in pneumatic conveying systems," *Powder Technol.*, vol. 321, pp. 347–354, Nov. 2017.
- [32] Z. F. Tian, K. Inthavong, J. Y. Tu, and G. H. Yeoh, "Numerical investigation into the effects of wall roughness on a gas–particle flow in a 90° bend," *Int. J. Heat Mass Transf.*, vol. 51, no. 5–6, pp. 1238–1250, Mar. 2008.
- [33] M. Sommerfeld and J. Kussin, "Wall roughness effects on pneumatic conveying of spherical particles in a narrow horizontal channel," *Powder Technol.*, vol. 142, no. 2–3, pp. 180–192, Apr. 2004.
- [34] N. Zumaeta, E. P. Byrne, and J. J. Fitzpatrick, "Predicting precipitate breakage during turbulent flow through different flow geometries," *Colloids Surfaces A Physicochem. Eng. Asp.*, vol. 292, no. 2, pp. 251–263, 2007.

- [35] T. Deng, M. S. Bradley, and M. Bingley, "An investigation of particle dynamics within a centrifugal accelerator type erosion tester," *Wear*, vol. 247, no. 1, pp. 55–65, Jan. 2001.
- [36] Y. Zheng and Q. Liu, "Review of techniques for the mass flow rate measurement of pneumatically conveyed solids," *Measurement: Journal of the International Measurement Confederation*, vol. 44, no. 4. Elsevier, pp. 589–604, 01-May-2011.
- [37] Y. Yan, "Mass flow measurement of bulk solids in pneumatic pipelines," *Meas. Sci. Technol.*, vol. 7, no. 12, pp. 1687–1706, 1996.
- [38] A. Uzi, H. Kalman, and A. Levy, "A novel particle attrition model for conveying systems," *Powder Technol.*, vol. 298, pp. 30–41, Sep. 2016.
- [39] B. Kuan, W. Yang, and M. P. Schwarz, "Dilute gas–solid two-phase flows in a curved duct bend: CFD simulation with experimental validation," *Chem. Eng. Sci.*, vol. 62, no. 7, pp. 2068–2088, Apr. 2007.
- [40] D. Mills, M. G. Jones, and V. K. Agarwal, *Handbook of Pneumatic Conveying Engineering*. 2004.
- [41] R. Macchini, M. S. Bradley, and T. Deng, "Influence of particle size, density, particle concentration on bend erosive wear in pneumatic conveyors," *Wear*, vol. 303, no. 1–2, pp. 21–29, Jun. 2013.
- [42] J. Ma and Y. Yan, "Design and evaluation of electrostatic sensors for the measurement of velocity of pneumatically conveyed solids," *Flow Meas. Instrum.*, vol. 11, no. 3, pp. 195–204, 2000.
- [43] P. Chapelle, H. Abou-Chakra, N. Christakis, I. Bridle, M. K. Patel, J. Baxter, U. Tuzun, and M. Cross, "Numerical predictions of particle degradation in industrial-scale pneumatic conveyors," *Powder Technol.*, vol. 143–144, pp. 321–330, Jun. 2004.
- [44] T. Deng, A. R. Chaudhry, M. Patel, I. Hutchings, and M. S. A. Bradley, "Effect of particle concentration on erosion rate of mild steel bends in a pneumatic conveyor," in *Wear*, 2005, vol. 258, no. 1–4 SPEC. ISS., pp. 480–487.
- [45] H. L. Hu, T. M. Xu, S. E. Hui, and Q. L. Zhou, "A novel capacitive system for the concentration measurement of pneumatically conveyed pulverized fuel at power

- stations," *Flow Meas. Instrum.*, vol. 17, no. 2, pp. 87–92, Apr. 2006.
- [46] D. Yang and X. Xu, "Twin-array capacitance sensor for multi-parameter measurements of multiphase flow," *Particuology*, vol. 22, pp. 163–176, Oct. 2015.
- [47] J. Mennell, B. Byrne, and Y. Yan, "Appraisal of radiometric techniques to determine absolute solids fraction in pneumatic suspensions of particulate solids," *Flow Meas. Instrum.*, vol. 11, no. 3, pp. 213–221, Sep. 2000.
- [48] Y. Van, B. Byrne, and J. Coulthard, "Radiation attenuation of pulverised fuel in pneumatic conveying systems," *Trans. Inst. Meas. Control*, vol. 15, no. 3, pp. 98–103, 1993.
- [49] J. Mennell, B. Byrne, and Y. Yan, "Non-invasive two phase flow measurement using soft X-ray attenuation," *IEE Colloq.*, no. 92, p. 9/1-9/3, 1996.
- [50] X. Chen, W. Zhou, X. Cai, M. Su, and H. Liu, "In-line imaging measurements of particle size, velocity and concentration in a particulate two-phase flow," *Particuology*, vol. 13, no. 1, pp. 106–113, Apr. 2014.
- [51] K. Miyazaki, J. G. Chen Present address: Copros Company, F. Yamamoto, J. Ohta, Y. Murai, and K. Horii, "PIV measurement of particle motion in spiral gas solid two-phase flow," *Exp. Therm. Fluid Sci.*, vol. 19, no. 4, pp. 194–203, 1999.
- [52] A. J. Burnett, "The use of laboratory erosion tests for the prediction of wear in pneumatic conveying bends," University of Greenwich, 1996.
- [53] S. Laín and M. Sommerfeld, "Numerical calculation of pneumatic conveying in horizontal channels and pipes: Detailed analysis of conveying behaviour," *Int. J. Multiph. Flow*, vol. 39, pp. 105–120, Mar. 2012.
- [54] S. Fokeer, S. Kingman, I. Lowndes, and a Reynolds, "Characterisation of the cross sectional particle concentration distribution in horizontal dilute flow conveying—a review," *Chem. Eng. Process. Process Intensif.*, vol. 43, no. 6, pp. 677–691, Jun. 2004.
- [55] P. Middha, B. V. Balakin, L. Leirvaag, A. C. Hoffmann, and P. Kosinski, "PEPT — A novel tool for investigation of pneumatic conveying," *Powder Technol.*, vol. 237, pp. 87–96, Mar. 2013.

- [56] A. R. Chaudhry, "Prediction of Bend Pressure Losses in Horizontal Lean Phase Pneumatic Conveying," University of Greenwich, 2004.
- [57] Y. Ding, Z. Wang, D. Wen, M. Ghadiri, X. Fan, and D. Parker, "Solids behaviour in a dilute gas–solid two-phase mixture flowing through monolith channels," *Chem. Eng. Sci.*, vol. 61, no. 5, pp. 1561–1570, 2006.
- [58] S. L. McKee, T. Dyakowski, R. A. Williams, T. A. Bell, and T. Allen, "Solids flow imaging and attrition studies in a pneumatic conveyor," *Powder Technol.*, vol. 82, no. 1, pp. 105–113, 1995.
- [59] C. A. R. Duarte, F. J. de Souza, and V. F. dos Santos, "Mitigating elbow erosion with a vortex chamber," *Powder Technol.*, vol. 288, pp. 6–25, 2016.
- [60] D. R. Andrews and N. Horsfield, "Particle collisions in the vicinity of an eroding surface," *J. Phys. D. Appl. Phys.*, vol. 16, no. 4, pp. 525–538, Apr. 1983.
- [61] B. van Laarhoven, S. H. Schaafsma, and G. M. H. Meesters, "Toward a desktop attrition tester; validation with dilute phase pneumatic conveying," *Chem. Eng. Sci.*, vol. 73, pp. 321–328, May 2012.
- [62] T. Han, A. Levy, and H. Kalman, "DEM simulation for attrition of salt during dilute-phase pneumatic conveying," *Powder Technol.*, vol. 129, no. 1–3, pp. 92–100, Jan. 2003.
- [63] H. Kalman, M. Hubert, E. Grant, Y. Petukhov, and M. Haim, "Fatigue behavior of impact comminution and attrition units," *Powder Technol.*, vol. 146, no. 1–2, pp. 1–9, Aug. 2004.
- [64] M. Ghadiri and Z. Zhang, "Impact attrition of particulate solids. Part 1: A theoretical model of chipping," *Chem. Eng. Sci.*, vol. 57, no. 17, pp. 3659–3669, Sep. 2002.
- [65] E. N. Hiestand and C. B. Peot, "Tensile Strength of Compressed Powders and an Example of Incompatibility as End-Point on Shear Yield Locus," *J. Pharm. Sci.*, vol. 63, no. 4, pp. 605–612, Apr. 1974.
- [66] A. A. Griffith, "The Phenomena of Rupture and Flow in Solids," *Philos. Trans. R. Soc. London A Math. Phys. Eng. Sci.*, vol. 221, no. 582–593, pp. 163–198, Jan. 1921.

- [67] B. W. Darvell, "Uniaxial compression tests and the validity of indirect tensile strength," *J. Mater. Sci.*, vol. 25, no. 2 A, pp. 757–780, Feb-1990.
- [68] H. M. Pollock, D. Maugis, and M. Barquins, "CHARACTERIZATION OF SUBMICROMETRE SURFACE LAYERS BY INDENTATION.," *ASTM Spec. Tech. Publ.*, pp. 47–71, 1985.
- [69] D. G. Bika, M. Gentzler, and J. N. Michaels, "Mechanical properties of agglomerates," *Powder Technol.*, vol. 117, no. 1–2, pp. 98–112, Jun. 2001.
- [70] W. J. Beekman, G. M. H. Meesters, T. Becker, A. Gaertner, M. Gebert, and B. Scarlett, "Failure mechanism determination for industrial granules using a repeated compression test," in *Powder Technology*, 2003, vol. 130, no. 1–3, pp. 367–376.
- [71] S. M. Iveson and J. D. Litster, "Liquid-bound granule impact deformation and coefficient of restitution," *Powder Technol.*, vol. 99, no. 3, pp. 234–242, Oct. 1998.
- [72] J. B. Hawkyard, "A theory for the mushrooming of flat-ended projectiles impinging on a flat rigid anvil, using energy considerations," *Int. J. Mech. Sci.*, vol. 11, no. 3, pp. 313–333, Mar. 1969.
- [73] E. E. Gdoutos, "Fracture Mechanics: An Introduction," *Book*, vol. 123, p. 369, 2005.
- [74] ASMT E399-90, "Standard Test Method for Plane-Strain Fracture Toughness of Metallic Materials," *ASTM Int.*, pp. 1–31, 1997.
- [75] J. Subero and M. Ghadiri, "Breakage patterns of agglomerates," *Powder Technol.*, vol. 120, no. 3, pp. 232–243, Oct. 2001.
- [76] G. R. Irwin, "Analysis of Stresses and Strains Near the End of a Crack Traversing a Plate," *Journal of Applied Mechanics*, vol. 24, no. September, pp. 361–364, 1957.
- [77] N. Ouchiyama, J. J. Benbow, and J. Bridgwater, "On the fracture toughness of extrudates and its relationship to rates of bulk particle attrition," *Powder Technol.*, vol. 51, no. 1, pp. 103–114, Jun. 1987.
- [78] S. Antonyuk, J. Tomas, S. Heinrich, and L. Mörl, "Breakage behaviour of spherical granulates by compression," *Chem. Eng. Sci.*, vol. 60, no. 14, pp. 4031–4044, Jul. 2005.
- [79] B. . Mishra and C. Thornton, "Impact breakage of particle agglomerates," *Int. J.*

- Miner. Process.*, vol. 61, no. 4, pp. 225–239, Apr. 2001.
- [80] F. K. Wittel, H. a. Carmona, F. Kun, and H. J. Herrmann, “Mechanisms in impact fragmentation,” *Int. J. Fract.*, vol. 154, no. 1–2, pp. 105–117, Feb. 2009.
- [81] Z. B. Tong, R. Y. Yang, A. B. Yu, S. Adi, and H. K. Chan, “Numerical modelling of the breakage of loose agglomerates of fine particles,” *Powder Technol.*, vol. 196, no. 2, pp. 213–221, Dec. 2009.
- [82] K. . Kafui and C. Thornton, “Numerical simulations of impact breakage of a spherical crystalline agglomerate,” *Powder Technol.*, vol. 109, no. 1–3, pp. 113–132, Apr. 2000.
- [83] Z. Ning, R. Boerefijn, M. Ghadiri, and C. Thornton, “Distinct element simulation of impact breakage of lactose agglomerates,” *Adv. Powder Technol.*, vol. 8, no. 1, pp. 15–37, Jan. 1997.
- [84] A. . Salman, G. . Reynolds, J. . Fu, Y. . Cheong, C. . Biggs, M. . Adams, D. . Gorham, J. Lukenics, and M. . Hounslow, “Descriptive classification of the impact failure modes of spherical particles,” *Powder Technol.*, vol. 143–144, pp. 19–30, Jun. 2004.
- [85] M. Ghadiri, K. R. Yuregir, H. M. Pollock, J. D. J. Ross, and N. Rolfe, “Influence of processing conditions on attrition of NaCl crystals,” *Powder Technol.*, vol. 65, no. 1–3, pp. 311–320, Mar. 1991.
- [86] J. A. S. Cleaver, M. Ghadiri, and N. Rolfe, “Impact attrition of sodium carbonate monohydrate crystals,” *Powder Technol.*, vol. 76, no. 1, pp. 15–22, Jul. 1993.
- [87] M. Thomas and A. F. B. van der Poel, “Physical quality of pelleted animal feed 1. Criteria for pellet quality,” *Anim. Feed Sci. Technol.*, vol. 61, no. 1–4, pp. 89–112, Sep. 1996.
- [88] M. Thomas, D. J. van Zuilichem, and A. F. B. van der Poel, “Physical quality of pelleted animal feed. 2. contribution of processes and its conditions,” *Anim. Feed Sci. Technol.*, vol. 64, no. 2–4, pp. 173–192, Feb. 1997.
- [89] M. Thomas, T. van Vliet, and A. F. B. van der Poel, “Physical quality of pelleted animal feed 3. Contribution of feedstuff components,” *Anim. Feed Sci. Technol.*, vol. 70, no. 1–2, pp. 59–78, Jan. 1998.

- [90] R. Seifried, W. Schiehlen, and P. Eberhard, "Numerical and experimental evaluation of the coefficient of restitution for repeated impacts," *Int. J. Impact Eng.*, vol. 32, no. 1–4, pp. 508–524, Dec. 2005.
- [91] D. B. Hastie, "Experimental measurement of the coefficient of restitution of irregular shaped particles impacting on horizontal surfaces," *Chem. Eng. Sci.*, vol. 101, pp. 828–836, 2013.
- [92] J. Fu, M. J. Adams, G. K. Reynolds, A. D. Salman, and M. J. Hounslow, "Impact deformation and rebound of wet granules," *Powder Technol.*, vol. 140, no. 3, pp. 248–257, Feb. 2004.
- [93] C. Mangwandi, Y. S. Cheong, M. J. Adams, M. J. Hounslow, and A. D. Salman, "The coefficient of restitution of different representative types of granules," *Chem. Eng. Sci.*, vol. 62, no. 1–2, pp. 437–450, Jan. 2007.
- [94] M. Meier, E. John, D. Wieckhusen, W. Wirth, and W. Peukert, "Generally applicable breakage functions derived from single particle comminution data," *Powder Technol.*, vol. 194, no. 1–2, pp. 33–41, Aug. 2009.
- [95] M. Meier, E. John, D. Wieckhusen, W. Wirth, and W. Peukert, "Characterization of the grinding behaviour in a single particle impact device: studies on pharmaceutical powders.," *Eur. J. Pharm. Sci.*, vol. 34, no. 1, pp. 45–55, May 2008.
- [96] M. Meier, E. John, D. Wieckhusen, W. Wirth, and W. Peukert, "Influence of mechanical properties on impact fracture: Prediction of the milling behaviour of pharmaceutical powders by nanoindentation," *Powder Technol.*, vol. 188, no. 3, pp. 301–313, Jan. 2009.
- [97] Y. Rozenblat, D. Portnikov, A. Levy, H. Kalman, S. Aman, and J. Tomas, "Strength distribution of particles under compression," *Powder Technol.*, vol. 208, no. 1, pp. 215–224, 2011.
- [98] R. K. Soni, C. Eswaraiah, and B. K. Mishra, "A novel and direct approach for modeling and simulation of impact grinding," *Adv. Powder Technol.*, vol. 26, no. 3, pp. 1031–1039, May 2015.
- [99] R. P. King, *Modeling and Simulation of of Mineral Processing Systems*, 1st ed. Butterworth-Heinemann Publishers, 2001.

- [100] S. . Wu, K. . Chau, and T. . Yu, "Crushing and fragmentation of brittle spheres under double impact test," *Powder Technol.*, vol. 143–144, pp. 41–55, Jun. 2004.
- [101] J. Fu, G. K. Reynolds, M. J. Adams, M. J. Hounslow, and A. D. Salman, "An experimental study of the impact breakage of wet granules," *Chem. Eng. Sci.*, vol. 60, no. 14, pp. 4005–4018, Jul. 2005.
- [102] S. Z. Wu and K. T. Chau, "Dynamic response of an elastic sphere under diametral impacts," *Mech. Mater.*, vol. 38, no. 11, pp. 1039–1060, Nov. 2006.
- [103] L. Liu, K. D. Kafui, and C. Thornton, "Impact breakage of spherical, cuboidal and cylindrical agglomerates," *Powder Technol.*, vol. 199, no. 2, pp. 189–196, Apr. 2010.
- [104] Z. Zhang and M. Ghadiri, "Impact attrition of particulate solids. Part 2: Experimental work," *Chem. Eng. Sci.*, vol. 57, no. 17, pp. 3671–3686, Sep. 2002.
- [105] S. Antonyuk, S. Palis, and S. Heinrich, "Breakage behaviour of agglomerates and crystals by static loading and impact," *Powder Technol.*, vol. 206, no. 1–2, pp. 88–98, Jan. 2011.
- [106] S. Aman, J. Tomas, and H. Kalman, "Breakage probability of irregularly shaped particles," *Chem. Eng. Sci.*, vol. 65, no. 5, pp. 1503–1512, Mar. 2010.
- [107] H. Briesen, "Two-dimensional population balance modeling for shape dependent crystal attrition," *Chem. Eng. Sci.*, vol. 64, no. 4, pp. 661–672, 2009.
- [108] F. Shi and T. Kojovic, "Validation of a model for impact breakage incorporating particle size effect," *Int. J. Miner. Process.*, vol. 82, no. 3, pp. 156–163, Apr. 2007.
- [109] L. Vogel and W. Peukert, "Determination of material properties relevant to grinding by practicable lab-scale milling tests," *Int. J. Miner. Process.*, vol. 74, pp. S329–S338, Dec. 2004.
- [110] G. A. Banini, "An Integrated Description of Rock Breakage in Comminution Machines," The University of Queensland, 2002.
- [111] L. G. Austin, "The effect of damage on breakage kinetics," *Powder Technol.*, vol. 143–144, pp. 151–159, Jun. 2004.
- [112] W. Weibull, "A statistical theory of the strength of materials," *Royal Swedish*

Institute for Engineering Research, vol. 151. pp. 1–45, 1939.

- [113] K. J. Hanley, E. P. Byrne, and K. Cronin, “Probabilistic analysis of particle impact at a pipe bend in pneumatic conveying,” *Powder Technol.*, vol. 233, pp. 176–185, Jan. 2013.
- [114] K. A. Aarseth and E. Prestløyken, “Mechanical Properties of Feed Pellets: Weibull Analysis,” *Biosyst. Eng.*, vol. 84, no. 3, pp. 349–361, Mar. 2003.
- [115] A. Paluszny, X. Tang, M. Nejati, and R. W. Zimmerman, “A direct fragmentation method with Weibull function distribution of sizes based on finite- and discrete element simulations,” *Int. J. Solids Struct.*, vol. 80, pp. 38–51, Feb. 2016.
- [116] W. Weibull, “A statistical distribution function of wide applicability,” *Journal of applied mechanics*, vol. 18. pp. 293–297, 1951.
- [117] A. Salman, D. Gorham, and A. Verba, “A study of solid particle failure under normal and oblique impact,” *Wear*, vol. 187, pp. 92–98, 1995.
- [118] A. Johansen and T. Schafer, “Effects of interactions between powder particle size and binder viscosity on agglomerate growth mechanisms in a high shear mixer,” *Eur. J. Pharm. Sci.*, vol. 12, no. 3, pp. 297–309, 2000.
- [119] S. T. Keningley, P. C. Knight, and A. D. Marson, “An investigation into the effects of binder viscosity on agglomeration behaviour,” *Powder Technol.*, vol. 91, no. 2, pp. 95–103, May 1997.
- [120] K. Schönert, “Breakage of spheres and circular discs,” *Powder Technol.*, vol. 143–144, pp. 2–18, Jun. 2004.
- [121] B. R. Lawn and M. V. Swain, “Microfracture beneath point indentations in brittle solids,” *J. Mater. Sci.*, vol. 10, no. 1, pp. 113–122, Jan. 1975.
- [122] P. M. M. Vervoorn and L. G. Austin, “The analysis of repeated breakage events as an equivalent rate process,” *Powder Technol.*, vol. 63, no. 2, pp. 141–147, Nov. 1990.
- [123] R. Clift, J. R. Grace, and M. E. Weber, *Bubbles, Drops, and Particles*. London: Academic Press, Inc., 1978.
- [124] D. Portnikov, R. Peisakhov, G. O. Gabrieli, and H. Kalman, “Selection function of

- particles under impact loads: The effect of collision angle," *Part. Sci. Technol.*, vol. 0, no. ja, p. null, 2017.
- [125] Y. S. Cheong, A. D. Salman, and M. J. Hounslow, "Effect of impact angle and velocity on the fragment size distribution of glass spheres," *Powder Technol.*, vol. 138, no. 2–3, pp. 189–200, Dec. 2003.
- [126] A. Samimi, R. Moreno, and M. Ghadiri, "Analysis of impact damage of agglomerates: effect of impact angle," *Powder Technol.*, vol. 143–144, pp. 97–109, Jun. 2004.
- [127] R. Moreno, M. Ghadiri, and S. J. Antony, "Effect of the impact angle on the breakage of agglomerates: a numerical study using DEM," *Powder Technol.*, vol. 130, no. 1–3, pp. 132–137, Feb. 2003.
- [128] C. Subero-Couroyer, M. Ghadiri, N. Brunard, and F. Kolenda, "Weibull Analysis of Quasi-Static Crushing Strength of Catalyst Particles," *Chem. Eng. Res. Des.*, vol. 81, no. 8, pp. 953–962, 2003.
- [129] C. Couroyer, "Attrition of Alumina Catalyst Carrier Beads," University of Surrey, 2000.
- [130] K. T. Chau, X. X. Wei, R. H. C. Wong, and T. X. Yu, "Fragmentation of brittle spheres under static and dynamic compressions: experiments and analyses," *Mech. Mater.*, vol. 32, no. 9, pp. 543–554, Sep. 2000.
- [131] S. M. Iveson, N. W. Page, and J. D. Litster, "The importance of wet-powder dynamic mechanical properties in understanding granulation," *Powder Technol.*, vol. 130, no. 1–3, pp. 97–101, Feb. 2003.
- [132] D. . Gorham, A. . Salman, and M. . Pitt, "Static and dynamic failure of PMMA spheres," *Powder Technol.*, vol. 138, no. 2, pp. 229–238, 2003.
- [133] M. Ghadiri, Z. Ning, S. . Kenter, and E. Puik, "Attrition of granular solids in a shear cell," *Chem. Eng. Sci.*, vol. 55, no. 22, pp. 5445–5456, Nov. 2000.
- [134] C. E. D. Ouwerkerk, "A micro-mechanical connection between the single-particle strength and the bulk strength of random packings of spherical particles," *Powder Technol.*, vol. 65, no. 1–3, pp. 125–138, Mar. 1991.

- [135] A. U. Neil and J. Bridgwater, "Attrition of particulate solids under shear," *Powder Technol.*, vol. 80, no. 3, pp. 207–219, Sep. 1994.
- [136] C. Hare, M. Ghadiri, and R. Dennehy, "Prediction of attrition in agitated particle beds," *Chem. Eng. Sci.*, vol. 66, no. 20, pp. 4757–4770, Oct. 2011.
- [137] A. D6175-03, "Standard Test Method for Radial Crush Strength of Extruded Catalyst and Catalyst Carrier Particles," *ASTM Int.*, 2013.
- [138] M. . Chaudhri, "Impact breakage of semi-brittle spheres," *Powder Technol.*, vol. 143–144, pp. 31–40, Jun. 2004.
- [139] P. H. Shipway and I. M. Hutchings, "Attrition of brittle spheres by fracture under compression and impact loading," *Powder Technol.*, vol. 76, no. 1, pp. 23–30, Jul. 1993.
- [140] D. Goder, H. Kalman, and a Ullmann, "Fatigue characteristics of granular materials," *Powder Technol.*, vol. 122, no. 1, pp. 19–25, Jan. 2002.
- [141] D. Goder, O. Eskin, and H. Kalman, "Fatigue Characteristics of Granular Materials," in *The Third Israeli Conference for Conveying and Handling of Particulate Solids*, 2000, p. 3.32-3.38.
- [142] T. Han, H. Kalman, and A. Levy, "Theoretical and experimental study of multi-compression particle breakage," *Adv. Powder Technol.*, vol. 14, no. 5, pp. 605–620, Dec. 2003.
- [143] T. Han, H. Kalman, and A. Levy, "Theoretical and Experimental Study of Fatigue Strength of Particles," in *The Third Israeli Conference for Conveying and Handling of Particulate Solids*, 2000, p. 3.139-3.144.
- [144] T. Han, Y. Petukhov, A. Levy, and H. Kalman, "Theoretical and experimental study of multi-impact breakage of particles," *Adv. Powder Technol.*, vol. 17, no. 2, pp. 135–157, Feb. 2006.
- [145] Y. Rozenblat, A. Levy, H. Kalman, I. Peyron, and F. Ricard, "A model for particle fatigue due to impact loads," *Powder Technol.*, vol. 239, pp. 199–207, 2013.
- [146] L. . Tavares and R. . King, "Modeling of particle fracture by repeated impacts using continuum damage mechanics," *Powder Technol.*, vol. 123, no. 2–3, pp. 138–146,

Mar. 2002.

- [147] L. M. Tavares, "Analysis of particle fracture by repeated stressing as damage accumulation," *Powder Technol.*, vol. 190, no. 3, pp. 327–339, 2009.
- [148] ASTM G76 - 13, "Standard Test Method for Conducting Erosion Tests by Solid Particle Impingement Using Gas Jets," *ASTM Int.*, 2013.
- [149] DIN 50 332, "Solid particle erosion test; basic rules," *DIN*, 1989.
- [150] T. Deng, M. S. Bingley, M. S. a. Bradley, and S. R. De Silva, "A comparison of the gas-blast and centrifugal-accelerator erosion testers: The influence of particle dynamics," *Wear*, vol. 265, no. 7–8, pp. 945–955, Sep. 2008.
- [151] P. H. Shipway and I. M. Hutchings, "Influence of nozzle roughness on conditions in a gas-blast erosion rig," *Wear*, vol. 162–164, pp. 148–158, Apr. 1993.
- [152] GOST 23.201-78, "Products wear resistance assurance. Gas abrasive wear testing of materials and coatings with centrifugal accelerator," 1979.
- [153] B. A. Kotzur, M. S. A. Bradley, R. J. Berry, and R. J. Farnish, "Breakage Characteristics of Granulated Food Products for Prediction of Attrition during Lean-Phase Pneumatic Conveying," *Int. J. Food Eng.*, vol. 12, no. 9, pp. 835–850, 2016.
- [154] P. Chapelle, H. Abou-Chakra, N. Christakis, M. Patel, A. Abu-Nahar, U. Tüzün, and M. Cross, "Computational model for prediction of particle degradation during dilute-phase pneumatic conveying: the use of a laboratory-scale degradation tester for the determination of degradation propensity," *Adv. Powder Technol.*, vol. 15, no. 1, pp. 13–29, Jan. 2004.
- [155] A. J. Burnett, M. S. A. Bradley, D. J. O'Flynn, T. Deng, and M. S. Bingley, "Anomalies in the results obtained from rotating disc accelerator erosion testers: A discussion of possible causes," *Wear*, vol. 233–235, pp. 275–283, Dec. 1999.
- [156] A. J. Burnett, S. R. De Silva, and A. R. Reed, "Comparisons between 'sand blast' and 'centripetal effect accelerator' type erosion testers," *Wear*, vol. 186–187, pp. 168–178, Jul. 1995.
- [157] G. J. Brown, "A fractal description of the progeny of double impact single particle breakage," *Miner. Eng.*, vol. 10, no. 2, pp. 229–235, Feb. 1997.

- [158] D. . Weedon and F. Wilson, "Modelling iron ore degradation using a twin pendulum breakage device," *Int. J. Miner. Process.*, vol. 59, no. 3, pp. 195–213, 2000.
- [159] R. K. Sahoo, D. M. Weedon, and D. Roach, "Single-particle breakage tests of Gladstone Port Authority's coal by a twin pendulum apparatus," *Adv. Powder Technol.*, vol. 15, no. 2, pp. 263–280, Mar. 2004.
- [160] R. K. Sahoo, D. M. Weedon, and D. Roach, "Degradation model of Gladstone Port Authority's coal using a twin-pendulum apparatus," *Adv. Powder Technol.*, vol. 15, no. 4, pp. 459–475, Jul. 2004.
- [161] R. Sahoo, "Review: An investigation of single particle breakage tests for coal handling system of the gladstone port," *Powder Technol.*, vol. 161, no. 2, pp. 158–167, 2006.
- [162] S. R. Krogh, "Crushing characteristics," *Powder Technol.*, vol. 27, no. 2, pp. 171–181, Nov. 1980.
- [163] L. . Tavares and R. . King, "Single-particle fracture under impact loading," *Int. J. Miner. Process.*, vol. 54, no. 1, pp. 1–28, Jun. 1998.
- [164] L. M. Tavares, "Energy absorbed in breakage of single particles in drop weight testing," *Miner. Eng.*, vol. 12, no. 1, pp. 43–50, Jan. 1999.
- [165] L. M. Tavares and R. P. King, "Measurement of the load–deformation response from impact-breakage of particles," *Int. J. Miner. Process.*, vol. 74, pp. S267–S277, 2004.
- [166] G. J. Brown, N. J. Miles, and T. F. Jones, "A fractal description of the progeny of single impact single particle breakage," *Miner. Eng.*, vol. 9, no. 7, pp. 715–726, Jul. 1996.
- [167] B. Kotzur, M. S. Bradley, R. J. Berry, and R. J. Farnish, "Influence of Solids Loading Ratio on Particle Attrition within a New Centrifugal Accelerator Impact Tester," in *PARTEC International Congress on Particle Technology*, 2016.
- [168] S. Söderberg, S. Hogmark, U. Engman, and H. Swahn, "Erosion classification of materials using a centrifugal erosion tester," *Tribol. Int.*, vol. 14, no. 6, pp. 333–343, Dec. 1981.

- [169] K. Schönert and M. Marktscheffel, "Liberation of composite particles by single particle compression, shear and impact loading," in *6th European Symposium on Comminution*, 1986, pp. 29–45.
- [170] E. Oveisi, A. Lau, S. Sokhansanj, C. J. Lim, X. Bi, S. H. Larsson, and S. Melin, "Breakage behavior of wood pellets due to free fall," *Powder Technol.*, vol. 235, pp. 493–499, Feb. 2013.
- [171] Y. Petukhov and H. Kalman, "A New Apparatus for Particle Impact Tests," *Part. Part. Syst. Charact.*, vol. 20, no. 4, pp. 267–275, 2003.
- [172] The American Society of Agricultural and Biological Engineers, "Densified Products for Bulk Handling - Definitions and Method," *ASAE/ASABE S269.5*, pp. 1–8, 2012.
- [173] R. Pitchumani, S. A. Strien, G. M. H. Meesters, S. H. Schaafsma, and B. Scarlett, "Breakage of sodium benzoate granules under repeated impact conditions," in *Powder Technology*, 2004, vol. 140, no. 3, pp. 240–247.
- [174] M. Gentzler and J. N. Michaels, "Impact attrition of brittle structured particles at low velocities: rigorous use of a laboratory vibrational impact tester," *Chem. Eng. Sci.*, vol. 59, no. 24, pp. 5949–5958, Dec. 2004.
- [175] T. A. Bell, A. Boxman, and J. B. Jacobs, "Attrition of salt during pneumatic conveying," in *5th World Congress of Chemical Engineering*, 1996, pp. 238–243.
- [176] J. B. Jacobs, "Attrition and flow patterns in dilute phase pneumatic conveying of sodium chloride," Delft University of Technology, 1996.
- [177] D. G. Papadopoulos, C. S. Teo, and M. Ghadiri, "Attrition of common salt," in *3rd World Congress on Particle Technology*, 1998, p. Paper 156.
- [178] K. J. Hanley, "Experimental Quantification and Modelling of Attrition of Infant Formulae during Pneumatic Conveying," University College Cork, 2011.
- [179] K. J. Hanley, K. Cronin, and E. P. Byrne, "Dispersion in particle velocity resulting from random motion through a spatially-varying fluid velocity field in a pipe," *Powder Technol.*, vol. 245, pp. 255–264, Sep. 2013.
- [180] R. K. Roy, *Design of Experiments Using the Taguchi Approach*. New York: Wiley New York, 2001.

- [181] R. A. Fisher, "Statistical Methods for Research Workers," in *Breakthroughs in Statistics: Methodology and Distribution*, S. Kotz and N. L. Johnson, Eds. New York, NY: Springer New York, 1992, pp. 66–70.
- [182] T. Brosh, H. Kalman, and A. Levy, "Fragments spawning and interaction models for DEM breakage simulation," *Granul. Matter*, vol. 13, no. 6, pp. 765–776, Oct. 2011.
- [183] T. Brosh, H. Kalman, and A. Levy, "DEM simulation of particle attrition in dilute-phase pneumatic conveying," *Granul. Matter*, vol. 13, no. 2, pp. 175–181, Aug. 2011.
- [184] T. Brosh, H. Kalman, and A. Levy, "Accelerating CFD–DEM simulation of processes with wide particle size distributions," *Particuology*, vol. 12, pp. 113–121, Feb. 2014.
- [185] H. Kalman, V. Rodnianski, and M. Haim, "A new method to implement comminution functions into DEM simulation of a size reduction system due to particle-wall collisions," *Granul. Matter*, vol. 11, no. 4, pp. 253–266, 2009.
- [186] A. Levy, D. J. Mason, D. Levy-Hevroni, and I. Borde, "Drying of wet solid particles in a steady-state one-dimensional flow," *Powder Technol.*, vol. 95, no. 1, pp. 15–23, Jan. 1998.
- [187] A. D. Salman, D. A. Gorham, M. Szabó, and M. J. Hounslow, "Spherical particle movement in dilute pneumatic conveying," *Powder Technol.*, vol. 153, no. 1, pp. 43–50, May 2005.
- [188] C. Aked, D. Goder, H. Kalman, and A. Zvieli, "Attrition of very fine powders during pneumatic conveying," *Powder Handl. Process.*, vol. 9, no. 4, pp. 345–348, 1997.
- [189] I. Bridle, S. R. Woodhead, and A. R. Reed, "The analysis of particle degradation in pneumatic conveyors utilizing a pilot-sized test facility," *Proc. Inst. Mech. Eng. Part E J. Process Mech.*, vol. 213, no. 2, pp. 85–91, 1999.
- [190] L. Frye and W. Peukert, "Attrition of Bulk Solids in Pneumatic Conveying: Mechanisms and Material Properties," *Part. Sci. Technol.*, vol. 20, no. 4, pp. 267–282, Oct. 2002.
- [191] L. Frye and W. Peukert, "Transfer of fracture mechanical concepts to bulk solids attrition in pneumatic conveying," *Int. J. Miner. Process.*, vol. 74, pp. S279–S289, Dec. 2004.

- [192] L. Frye and W. Peukert, "Progress in the understanding of bulk solids attrition in dilute phase pneumatic conveying," *Powder Technol.*, vol. 143–144, pp. 308–320, Jun. 2004.
- [193] H. Abou-Chakra, U. Tüzün, I. Bridle, M. Leaper, M. S. a Bradley, and a R. Reed, "An investigation of particle degradation by impact within a centrifugal accelerator type degradation tester," *Proc. Inst. Mech. Eng. Part E J. Process Mech. Eng.*, vol. 217, no. 3, pp. 257–266, Jan. 2003.
- [194] P. Chapelle, N. Christakis, H. Abou-Chakra, I. Bridle, M. S. a. Bradley, M. Patel, and M. Cross, "Computational model for prediction of particle degradation during dilute-phase pneumatic conveying: modeling of dilute-phase pneumatic conveying," *Adv. Powder Technol.*, vol. 15, no. 1, pp. 31–49, Jan. 2004.
- [195] Y. Rozenblat, "Investigating Size Reduction Functions for DEM Applications," Ben-Gurion University of the Negev, 2010.
- [196] Y. Rozenblat, D. Portnikov, H. Kalman, S. Aman, and J. Tomas, "Strength of Particles under Compression," in *Conveying and Handling of Particulate Solids*, 2009.
- [197] A. Uzi and A. Levy, "Particles' degradation and dynamics in conveying systems," *Powder Technol.*, vol. 311, pp. 247–256, Apr. 2017.
- [198] P. Gy, *Sampling for Analytical Purposes*. John Wiley and Sons, 1998.
- [199] L. Petersen, P. Minkkinen, and K. H. Esbensen, "Representative sampling for reliable data analysis: Theory of Sampling," *Chemom. Intell. Lab. Syst.*, vol. 77, no. 1–2, pp. 261–277, May 2005.
- [200] H. Abou-Chakra, P. Chapelle, U. Tüzün, J. Baxter, M. Patel, M. Cross, I. Bridle, and M. S. A. Bradley, "Sampling Issues in Assessing Particle Degradation in Pneumatic Conveying Systems," *Part. Part. Syst. Charact.*, vol. 21, no. 1, pp. 39–46, 2004.
- [201] P. Gy, "Sampling of discrete materials—a new introduction to the theory of sampling," *Chemom. Intell. Lab. Syst.*, vol. 74, no. 1, pp. 7–24, Nov. 2004.
- [202] P. Gy, "Sampling of discrete materials," *Chemom. Intell. Lab. Syst.*, vol. 74, no. 1, pp. 25–38, Nov. 2004.

- [203] P. Gy, "Sampling of discrete materials," *Chemom. Intell. Lab. Syst.*, vol. 74, no. 1, pp. 39–47, Nov. 2004.
- [204] L. Petersen, C. K. Dahl, and K. H. Esbensen, "Representative mass reduction in sampling—a critical survey of techniques and hardware," *Chemom. Intell. Lab. Syst.*, vol. 74, no. 1, pp. 95–114, Nov. 2004.
- [205] P. Kulkarni, "Development of Bench-Scale Die Filling Tester for Free Flowing Particulates," University of Greenwich, 2012.
- [206] A. Jillavenkatesa, S. J. Dapkunas, and L. H. Lum, *Particle Size Characterization*. Washington, D.C.: U.S. Department of Commerce, National Institute of Standards and Technology, 2001.
- [207] M. Li, D. Wilkinson, and K. Patchigolla, "Comparison of Particle Size Distributions Measured Using Different Techniques," *Part. Sci. Technol.*, vol. 23, no. 3, pp. 265–284, Jul. 2005.
- [208] P. Bowen, "Particle Size Distribution Measurement from Millimeters to Nanometers and from Rods to Platelets," *J. Dispers. Sci. Technol.*, vol. 23, no. 5, pp. 631–662, Jan. 2002.
- [209] Y. Petukhov and H. Kalman, "Empirical breakage ratio of particles due to impact," *Powder Technol.*, vol. 143–144, pp. 160–169, Jun. 2004.
- [210] J. Yao, C.-H. Wang, E. Wee Chuan Lim, and J. Bridgwater, "Granular attrition in a rotary valve: Attrition product size and shape," *Chem. Eng. Sci.*, vol. 61, no. 11, pp. 3435–3451, Jun. 2006.
- [211] T. Hussain, W. Kaialy, T. Deng, M. S. A. Bradley, A. Nokhodchi, and D. Armour-Chélu, "A novel sensing technique for measurement of magnitude and polarity of electrostatic charge distribution across individual particles," *Int. J. Pharm.*, vol. 441, no. 1, pp. 781–789, 2013.
- [212] L. M. Hyder, "The Effect of Particle Size and Density on Pressure Gradients in Horizontal Pipelines in Lean Phase Pneumatic Conveying," University of Greenwich, 2000.
- [213] T. Deng, M. . Bingley, and M. S. . Bradley, "Influence of particle dynamics on erosion test conditions within the centrifugal accelerator type erosion tester," *Wear*,

- vol. 249, no. 12, pp. 1059–1069, Dec. 2001.
- [214] A. Deshmukh, V. Vasava, A. Patankar, and M. Bose, “Particle velocity distribution in a flow of gas-solid mixture through a horizontal channel,” *Powder Technol.*, vol. 298, pp. 119–129, Sep. 2016.
- [215] Y. A. Cengel and J. M. Cimbala, *Fluid Mechanics: Fundamentals and Applications*. New York: McGraw-Hill, 2010.
- [216] L. M. Gomes and A. L. A. Mesquita, “On the prediction of pickup and saltation velocities in pneumatic conveying,” *Brazilian J. Chem. Eng.*, vol. 31, no. 1, pp. 35–46, 2014.
- [217] L. M. Gomes and A. L. A. Mesquita, “Effect of particle size and sphericity on the pickup velocity in horizontal pneumatic conveying,” *Chem. Eng. Sci.*, vol. 104, pp. 780–789, Dec. 2013.
- [218] F. Rizk, “Pneumatic conveying at optimal operation conditions and a solution of Bath’s equation,” *Proc Pneumotransp.*, vol. 3, pp. 443–458, 1976.
- [219] S. MATSUMOTO, M. KARA, S. SAITO, and S. MAEDA, “Minimum Transport Velocity for Horizontal Pneumatic Conveying,” *J. Chem. Eng. Japan*, vol. 7, no. 6, pp. 425–430, 1975.
- [220] B. Schade, “Zum Übergang Sprung-Strähnenförderung bei der Horizontalen Pneumatischen Feststoffförderung,” University of Karlsruhe, 1987.
- [221] M. Weber, “Principles of hydraulic and pneumatic conveying in pipes,” *Bulk Solids Handl.*, vol. 1, no. 1, pp. 57–63, 1981.
- [222] D. Geldart and S. J. Ling, “Saltation velocities in high pressure conveying of fine coal,” *Powder Technol.*, vol. 69, no. 2, pp. 157–162, 1992.
- [223] M. Ochi, “Saltation Velocity of the Gas-Solid Two-Phase Flow in a Horizontal Pipe.” in *The First ASME-JSME Fluids Engineering Conference*, 1991, vol. FED-121, pp. 163–166.
- [224] F. J. Cabrejos and G. E. Klinzing, “Pickup and saltation mechanisms of solid particles in horizontal pneumatic transport,” *Powder Technol.*, vol. 79, no. 2, pp. 173–186, May 1994.

- [225] E. Rabinovich and H. Kalman, "Boundary saltation and minimum pressure velocities in particle-gas systems," *Powder Technol.*, vol. 185, no. 1, pp. 67–79, Jun. 2008.
- [226] F. J. Cabrejos and G. E. Klinzing, "Incipient motion of solid particles in horizontal pneumatic conveying," *Powder Technol.*, vol. 72, no. 1, pp. 51–61, Oct. 1992.
- [227] H. Kalman, A. Satran, D. Meir, and E. Rabinovich, "Pickup (critical) velocity of particles," *Powder Technol.*, vol. 160, no. 2, pp. 103–113, Dec. 2005.
- [228] M. D. Mikhailov and A. P. S. Freire, "The drag coefficient of a sphere: An approximation using Shanks transform," *Powder Technol.*, vol. 237, pp. 432–435, 2013.
- [229] A. Anantharaman, A. Cahyadi, K. Hadinoto, and J. W. Chew, "Impact of particle diameter, density and sphericity on minimum pickup velocity of binary mixtures in gas-solid pneumatic conveying," *Powder Technol.*, vol. 297, pp. 311–319, 2016.
- [230] N. M. Tripathi, A. Levy, and H. Kalman, "Acceleration pressure drop analysis in horizontal dilute phase pneumatic conveying system," *Powder Technol.*, vol. 327, pp. 43–56, Mar. 2018.
- [231] C. Pinho, "Horizontal Pneumatic Conveying of Cork Stoppers," in *16th BRAZILIAN CONGRESS OF MECHANICAL ENGINEERING*, 2001, pp. 21–29.
- [232] R. D. Marcus, J. D. Hilbert Jr., and G. E. Klinzing, "FLOW THROUGH BENDS IN PNEUMATIC CONVEYING SYSTEMS.," *J. pipelines*, vol. 4, no. 2, pp. 103–112, 1984.
- [233] R. D. Marcus, "An Investigation into the Influence of Pressure Pulsations on the Flow Characteristics of Solid Gaseous Suspensions," University of the Witwatersrand, 1978.
- [234] G. M. Gordon, "An Investigation into Horizontal Dilute Phase Pneumatic Conveying," University of the Witwatersrand, 1984.
- [235] R. A. Duckworth and H. E. Rose, "Transport of solid particles in liquid and gases," *Eng.*, vol. March, p. 392, 1969.
- [236] C. Kloss, C. Goniva, A. Hager, S. Amberger, and S. Pirker, "Models, algorithms and

- validation for opensource DEM and CFD-DEM,” *Prog. Comput. Fluid Dyn. An Int. J.*, vol. 12, no. 2/3, p. 140, 2012.
- [237] C. Goniva, C. Kloss, N. G. Deen, J. A. M. Kuipers, and S. Pirker, “Influence of rolling friction on single spout fluidized bed simulation,” *Particuology*, vol. 10, no. 5, pp. 582–591, 2012.